Epifadin – A New Antimicrobial Peptide Polyene from the Human Microbiome and Chemical Total Syntheses to Study Lugdunin and Epifadin Motifs

Dissertation

der Mathematisch-Naturwissenschaftlichen Fakultät
der Eberhard Karls Universität Tübingen
zur Erlangung des Grades eines
Doktors der Naturwissenschaften
(Dr. rer. nat.)

vorgelegt von
Taulant Dema
aus Leonberg

Tübingen
2025

Gedruckt mit Genehmigung der Mathematisch-Naturwissenschaftlichen Fakultät der Eberhard Karls Universität Tübingen.

Tag der mündlichen Qualifikation:	26.09.2025
Dekan:	Prof. Dr. Thilo Stehle
1. Berichterstatter:	Prof. Dr. Stephanie Grond
2. Berichterstatter:	Prof. Dr. Dirk Schwarzer

Die vorliegende Arbeit wurde im Institut für Organische Chemie der Eberhard Karls Universität Tübingen von November 2019 bis September 2024 unter der Anleitung von Prof. Dr. Stephanie Grond durchgeführt.

EIGENSTÄNDIGKEITSERKLÄRUNG

Ich, Taulant Dema, geboren am 15.11.1993 in Leonberg, erkläre hiermit an Eides statt:

- Ich habe die eingereichte Dissertation eigenständig verfasst und ausschließlich die angegebenen Quellen und Hilfsmittel verwendet. Alle wörtlich oder sinngemäß aus fremden Quellen übernommenen Texte, Ideen, Konzepte, Grafiken etc. habe ich kenntlich gemacht und mit vollständigen Quellenangaben versehen.
- Generative KI-Tools habe ich ausschließlich genutzt, um die englische Sprache sowie die Formulierungen meiner eigenen Texte zu optimieren. Der gestalterische Einfluss dieser Arbeit liegt jedoch vollständig bei mir.
- Diese Arbeit wurde bislang weder im Inland noch im Ausland in gleicher oder ähnlicher Form bei einer anderen Prüfungsbehörde eingereicht.

Ich bin mir bewusst, dass ein Verstoß gegen die oben genannten Punkte prüfungsrechtliche Konsequenzen nach sich ziehen kann. Dies umfasst insbesondere die Bewertung der Prüfungsleistung mit „nicht ausreichend“ oder „nicht bestanden“. Bei mehrfachen oder schwerwiegenden Täuschungsversuchen können zudem eine Exmatrikulation erfolgen oder ein Verfahren zur Aberkennung eines verliehenen akademischen Titels eingeleitet werden.

Tübingen, den 17.01.2025 _____(Taulant Dema)

Declaration of Personal Contributions

Some of the data in this thesis have already been published in the following publications:

"Commensal production of a broad-spectrum and short-lived antimicrobial peptide polyene eliminates nasal *Staphylococcus aureus*", B. O. Torres Salazar, **T. Dema**, N. A. Schilling, D. Janek, J. Bornikoel, A. Berscheid, A. M. A. Elsherbini, S. Krauss, S. J. Jaag, M. Lämmerhofer, M. Li, N. Alqahtani, M. J. Horsburgh, T. Weber, J. M. Beltrán-Beleña, H. Brötz-Oesterhelt, S. Grond, B. Krismer, A. Peschel, *Nat. Microbiol.*, **2024**, *9*, 200–213.

"Structure of *Staphylococcus aureus* ClpP Bound to the Covalent Active-Site Inhibitor Cystargolide A", A. Illigmann, M.-T. Vielberg, M. Lakemeyer, F. Wolf, **T. Dema**, P. Stange, W. Kuttenlochner, E. Liebhart, A. Kulik, N. D. Staudt, I. Malik, S. Grond, S. A. Sieber, L. Kaysser, M. Groll, H. Brötz-Oesterhelt, *Angew. Chem. Int. Ed.*, **2024**, *63*, e202314028.

"The antimicrobial fibupeptide lugdunin forms water-filled channel structures in lipid membranes", D. Ruppelt, M. F. W. Trollmann, **T. Dema**, S. N. Wirtz, H. Flegel, S. Mönnikes, S. Grond, R. A. Böckmann, C. Steinem, *Nat. Commun.*, **2024**, *15*, 3521.

Personal contributions to the data presented in this thesis, some of which are also part of the publications mentioned above:
I optimized the isolation and purification procedures for epifadin and its natural peptide amide. NMR, HR-MS and UV spectra interpretations were done by me. I contributed ideas to the biosynthesis of epifadin and for the separation of enantiomers of the peptide amides. I planned and performed chemical syntheses and purification, including characterization of synthesized compounds by NMR and HRMS.
I was supervised by Prof. Dr. Stephanie Grond throughout my work.

Acknowledgements

I would like to express my deepest gratitude to my supervisor, Prof. Dr. STEPHANIE GROND, for trusting me with the opportunity to work on such exciting and diverse topics. Thank you for the many constructive discussions and the freedom I experienced in conducting research within the GROND group.

Many thanks also go to my second supervisor, Prof. Dr. DIRK SCHWARZER, for taking on the role of second examiner and for his valuable feedback.

Special appreciation is extended to MARKUS KRAMER, head of the NMR department, and his team, PRISKA KOLB and DOMINIK BRZECKI, for their fruitful advice on NMR experiments. I am equally grateful to NORBERT GRZEGORZEK, head of the MS department, for his expertise in mass spectrometry and chiral separations using HPLC.

I would like to thank STEPHAN BAMANN for his excellent support with chemical orders and shipments, as well as GABRIELA WIDMANN for her assistance with bureaucratic matters.

A special thanks to BERNHARD KRISMER, BENJAMIN ORLANDO TORRES SALAZAR, ANDREAS PESCHEL, ASTRID ILLIGMANN, HEIKE BRÖTZ-OESTERHELT, SIMON JAAG, MICHAEL LÄMMERHOFER, DOMINIK RUPPELT, and CLAUDIA STEINEM for the outstanding collaborations and the jointly published results.

Of course, I would also like to thank the entire GROND group for the amazing and unforgettable time we shared! Many thanks to NADINE, KLAUS, PATRIK, both JULIANS, PASCAL, SEBASTIAN, LARISSA, HEIKO, MONA, RHENA, and TIMM. TIMM, we've had a long journey together, and it was always great working with you! Thank you all for the discussions during coffee breaks, which often sparked great ideas. Thank you for your support, for sharing frustrations, and for celebrating successes together.

I also extend my gratitude to CHEMA for maintaining all technical devices and for his expertise with the MaXis, and to MICHAELA, with whom I could always talk openly.

Many thanks to all my interns and student assistants, EDWARD PERWUCHIN, FOTIOS FOTAKIS, IRINI GRIGORIADOU, MIHNEA MLAK-MARGINEAN, LUCAS JÄNSCH, and ISMAIL SOROUR for their dedicated work.

Finally, I want to thank my family for supporting me throughout my studies and my doctoral journey. I am deeply grateful to my parents and brothers for their understanding and patience during this chapter of my life.

A big thank you goes to ANN-MARIE PATRICIA PFLÜGER for walking this challenging path with me, for always supporting me through setbacks and celebrating achievements. I am profoundly grateful for everything you have done for me.

Index

A. THEORETICAL PART

1. Introduction

1.1. The need for antibiotics and danger of antibiotic resistance

The discovery of penicillin (**1**) by SIR ALEXANDER FLEMING in 1928 is probably one of the most pivotal events in the history of medicine. Penicillin (**1**) enabled the effective treatment of infected wounds, inflammations, and numerous bacterial diseases. Although discovered in 1928, penicillin (**1**) was first used in the 1940s to successfully treat serious bacterial infections. The intensive use of penicillins during the second world war led to the emergence of penicillin-resistant bacteria by the 1950s. In response, new antibiotics were discovered and developed throughout the 20th century, such as tetracycline (**2**), methicillin (**3**), ceftazidime (**4**) and levofloxacin (**5**). Alongside the development of these new antibiotic compounds, resistant bacteria were also reported (Figure 1).[1]

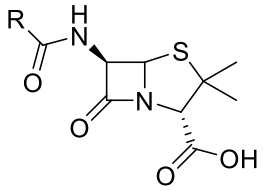

penicillin (**1**) **1928**

penicillin-resistant
S. aureus **1940**

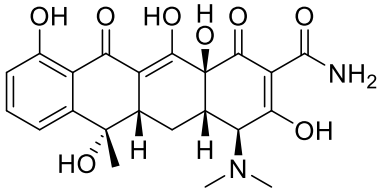

tetracycline (**2**) **1950**

tetracyline-resistant
Shigella **1959**

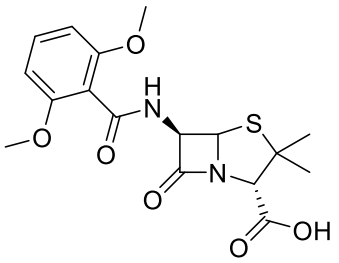

methicillin (**3**) **1960**

methicillin-resistant
S. aureus **1962**

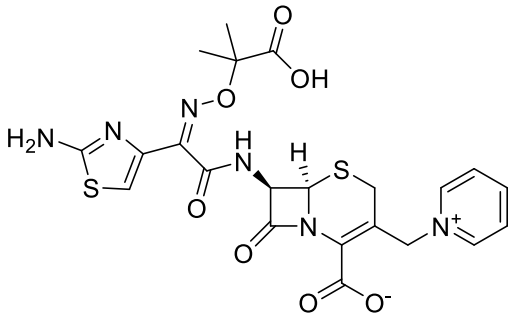

ceftazidime (**4**) **1985**

ceftazidime-resistant
Enterobacteriaceae **1987**

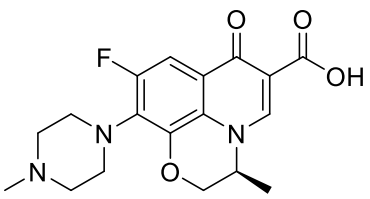

levofloxacin (**5**) **1996**

levofloxacin-resistant
pneumococcus **1996**

Figure 1: Selected set of antibiotics, their year of discovery and the reported resistant strain. R = benzyl for penicillin G, R = pent-2-enyl for penicillin F, R = *p*-hydroxybenzyl for penicillin X, R = heptyl for penicillin K.

Analyzing the mechanisms of action of antibiotics has enhanced our understanding of how bacteria develop their resistances towards antibiotics. Antibiotic compounds are categorized into classes based on their chemical structure, which results in the well-known classes of antibiotics.[2] Grouping antibiotics according to their mechanism of action, four main target sites can be identified: cell wall synthesis, protein biosynthesis, DNA synthesis and RNA synthesis.[3]

The β-Lactam antibiotics (penicillins, cephalosporins and carbapenems) inhibit cell wall synthesis by competitively inhibiting the peptidoglycan transpeptidase. Due to their highly reactive β-lactam structure the active site of the transpeptidase is irreversibly acylated, rendering the enzyme inactive.[4, 5] A compromised cell wall structure results in lyses and death of the bacterial cells. As peptidoglycan is found in both Gram-positive and Gram-negative bacteria, β-lactam antibiotics can be used against a broad spectrum of bacteria. Mammalian cells lack cell walls and peptidoglycan, therefore, β-lactam antibiotics can be used to target bacterial cells without greatly harming human cells.[5]

Tetracyclines consist of a linear fused tetracyclic core to which various functional groups are bound (Figure 1). Tetracyclines exhibit bacteriostatic rather than bactericidal properties and are effective against multiplying microorganisms. It is well known that tetracyclines inhibit protein biosynthesis by reversibly binding to the aminoacyl-tRNA in the ribosomal 30S unit, preventing the association of aminoacyl-tRNA with the bacterial ribosome. Like β-lactams, tetracyclines are also effective against a broad spectrum of Gram-positive and Gram-negative bacteria.[6]

Fluoroquinolones (e.g. see **5**) interfere with bacterial DNA synthesis, by entering bacteria through porin channels and inhibiting two DNA enzymes, the DNA gyrase and the topoisomerase IV. DNA gyrase is responsible for reducing topological strain in the process of DNA replication and topoisomerase IV decatenates replicated DNA. The inhibition of these enzymes leads in cleavage of bacterial DNA, which then inevitably results in the death of bacterial cells.[7, 8]

Bacteria develop resistance to antibiotics through various mechanisms. In a report from 2019 the U.S. CENTERS FOR DISEASE CONTROL AND PREVENTION has described antibiotic resistance as follows[9]:

"Antibiotic resistance is when germs (bacteria, fungi) develop the ability to defeat the antibiotics designed to kill them."

The key factors promoting antibiotic resistance are overuse, inappropriate prescribing, and extensive use of antibiotics in agriculture. By eliminating drug-sensitive competitors, resistant bacteria can reproduce through natural selection. These resistant bacteria can then share their resistance genes via plasmids. This is known as horizontal gene transfer, which can lead to the transfer of antibiotic resistance among different bacterial species.[1]

Since all antibiotics must be taken up by bacteria to unfold their bactericidal effects, the simplest defense mechanism is to prevent accumulation of antibiotics inside the cells. Fewer porin channels, which are responsible for the diffusion of molecules up to 5000 Da into and out of the cell, were found in resistant bacteria. A decreased number of such channels leads to a decreased uptake of drug molecules and thus to a lower susceptibility to antibiotics.[3] In contrast, an increased number of efflux pumps can be found in resistant bacteria. Efflux pumps are membrane proteins in the cytoplasmic membrane that are capable to transport a large variety of different compounds out of the cell and thus significantly contributing to multidrug resistant organisms.[3]

Additionally, spontaneous mutations in bacterial genes can alter antibiotic targets, preventing antibiotic binding. Typical reported modifications include changes in the ribosomes that prevent binding of antibiotics in the 30S or 50S subunits[10, 11] or modifications in the peptidoglycan transpeptidase that reduces β-lactams affinity.[12] Mutations in resistant bacteria have also led to altered DNA gyrase and topoisomerase IV, resulting in a reduced binding affinity of quinolones, which in turn leads to the development of resistance to them.[13]

Bacteria also use specialized enzymes like β-lactamases to inactivate antibiotics. These enzymes provide multi-resistance to the class of β-lactam antibiotics by hydrolyzing the amide bond of the four-membered β-lactam ring (Figure 2).[14] To this day, there have been identified more than 8000 different β-lactamases (www.bldb.eu[15]) with narrow or broad substrate spectra. This clearly shows that resistance to new β-lactam antibiotics is only a matter of time.

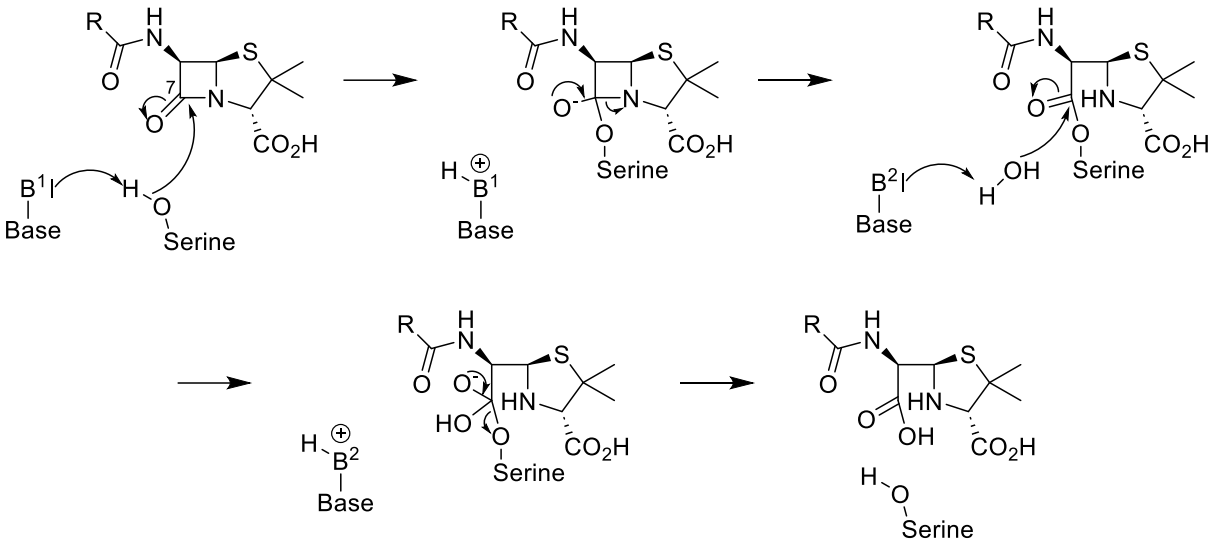

Figure 2: Hydrolysis of a generic penicillin substrate by a serine β-lactamase. Base B^1 activates serine for nucleophilic attack on amide carbonyl carbon C-7. Base B^2 activates a water molecule for nucleophilic attack on the acylenzyme carbonyl liberating penicilloate. Adapted from[14].

Antibiotic or antimicrobial resistance has serious consequences. Untreated diseases caused by bacteria can lead to severe, life-threatening conditions and ultimately lead to death. In 2016 the British economist JIM O'NEILL published a review on global antimicrobial resistance, estimating that by the year 2050, antimicrobial resistance could kill 10 million people per year.[16, 17] A group of Antimicrobial Resistance Collaborators systematically analyzed this major threat. They estimated that 4.95 million deaths were associated globally with bacterial antimicrobial resistance in 2019, with six leading pathogens (*Escherichia coli*, *Staphylococcus aureus*, *Klebsiella pneumoniae*, *Acinetobacter baumanii, Pseudomonas aeruginosa* and *Streptococcus pneumoniae,* five of these mentioned are part of ESKAPEE pathogens[18]) responsible for 3.57 million deaths.[19] Addressing the dissemination of resistant bacteria is an urgent global health issue.

1.2. Human microbiome – A source for new antimicrobials

Streptomycetes are well known for their ability to produce a variety of natural products, driven by the competitive soil environment that favors bacteria that produce compounds to outcompete other bacteria. Since the 1940s, these soil bacteria have been successfully cultivated and harvested using manifold strategies, such as the OSMAC (One Strain-Many Compounds).[20] These strategies have led to the discovery of natural products with interesting properties for medical applications such as antibacterial[21, 22], antifungal[23-25], and immunosuppressants.[26, 27] Since the golden age of antibiotics, there has been a steady decline in the discovery and approval of new antibiotics, leading to the so-called discovery void (Figure 3), which has persisted from the late 1980s to the present day. During this time, only a limited number of new lead structures have been innovative.[28-30]

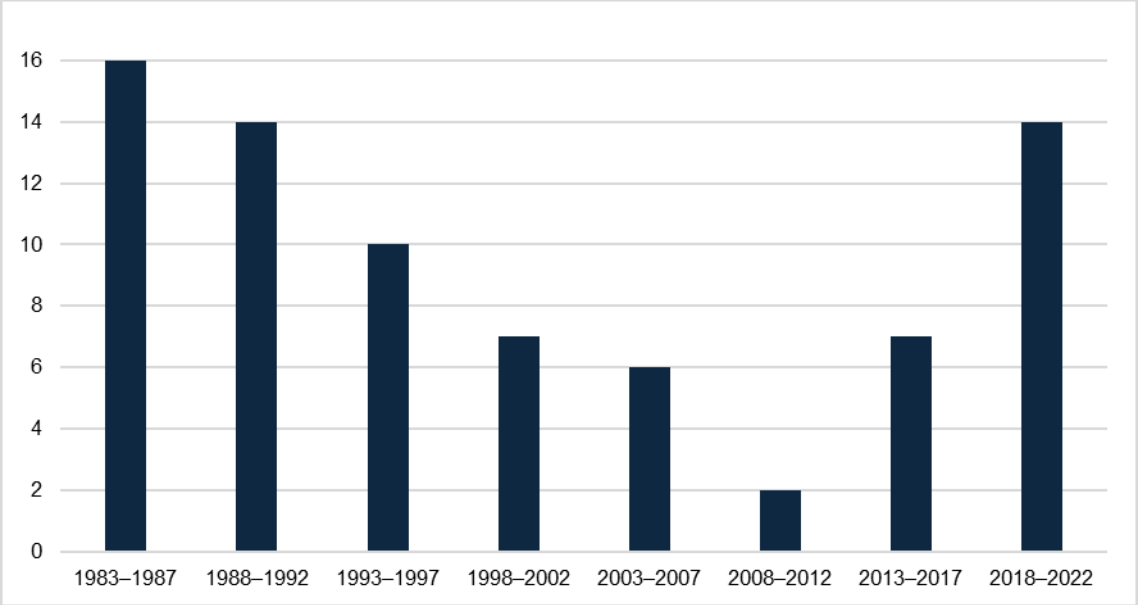

Figure 3: Approvals of new antibiotics from 1983 to 2023 by FDA. Adapted from[30].

While soil bacteria have been extensively explored as a source of new antibiotic lead compounds, recent research efforts to discover new antibiotics have shifted towards other bacterial groups such as the human microbiota.[31-35]

The average male human body harbors many microorganisms of which an estimated $3.8 \cdot 10^{13}$ are bacterial cells. The ratio of nucleated human cells ($0.3 \cdot 10^{13}$) to bacterial cells in the human body is estimated to be 1:10.[36] In the last decades, it has been highlighted that these microbes not only are even to or outnumber our cells, but also have an enormous influence on our physiology in many ways and are therefore referred to as “the hidden organ”.[37-39] Moreover, the human microbiota contributes

significantly to the gene pool of the human microbiome and harbors many biologically active natural products that remain undiscovered.[37, 38]

Recent studies have demonstrated that members of the human microbiota produce antimicrobial compounds, which allow to displace or even outcompete pathogens.[33] These compounds exhibit complex and diverse structures and modes of action. There have been reported non-ribosomal peptide synthase (NRPS) products like lugdunin (**6**), a protonophore[32, 40], or quorum-quenching lipopeptides such as fengycins.[41, 42] Additionally, the polyketide synthase (PKS)-NRPS hybrid compound like reutericyclin (**7**), another protonophore, is produced by *Lactobacillus reuteri* to achieve colonization advantages in the oral microbial habitat.[43, 44] Notably, the probiotic strain *Streptococcus salivarius* K12 produces salivabactin A/B (**8**) an antimicrobial compound with potent activity against several clinically relevant Gram-positive pathogens, including resistant strains such as *S. aureus* (MRSA: 2 μg·mL^{-1}) and *E. faecalis* (VRE: 2 μg·mL^{-1}).[45]

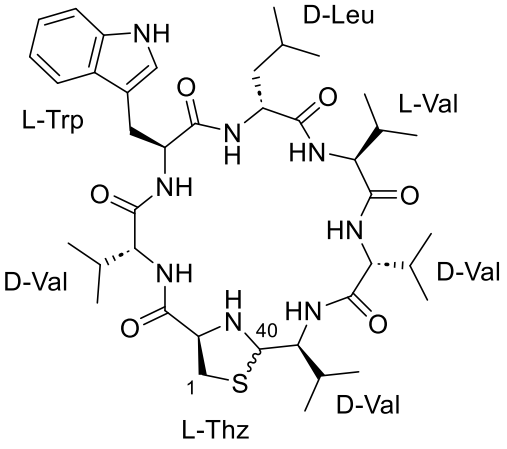

lugdunin (**6**)

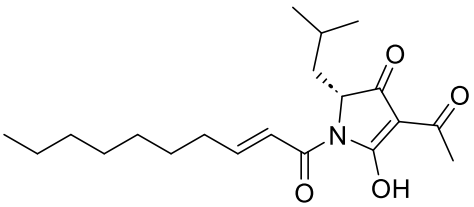

reutericyclin (**7**)

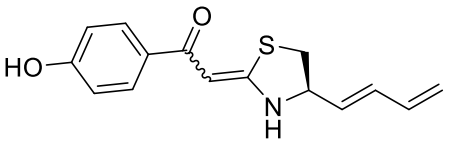

salivabactin A/B (**8**)

During a screening approach using human bacterial nasal isolates, *S. lugdunensis* has been found to strongly inhibit *S. aureus* growth, and that *S. lugdunensis* carriers have a significantly reduced *S. aureus* carriage rate. *S. lugdunensis* produces lugdunin (**6**), a cyclic antimicrobial heptapeptide comprising an unusual thiazolidine heterocycle and five amino acids with alternating stereo configuration. Lugdunin (**6**) is the first NRPS product from the human nose microbiome with antimicrobial activity, establishing a new class of fibupeptide antimicrobials.[32] It exists as two diastereomers in equilibrium with an (*R*)- or (*S*)-configuration in position 40, indicated by the wavy bond. It exhibits potent antimicrobial activity against a broad spectrum of Gram-positive bacteria, including resistant strains like *S. aureus* (MRSA: 1.5 μg·mL^{-1}, Glycopeptide resistant *S. aureus* (GISA): 3 μg·mL^{-1}) and *Enterococcus* isolates (VRE: 3–12 μg·mL^{-1}).

Importantly, development of resistance was not observed for *S. aureus*.[32] After establishing the solid-phase peptide synthesis (SPPS) of lugdunin (**6**), comprehensive structure-activity relationship studies were carried out, which revealed essential structural motifs for antimicrobial activity and proton translocation. Furthermore, it was found that the enantiomer of lugdunin (**6**) showed identical antimicrobial activity as **6**.[40, 46] However, the precise mode of action of lugdunin (**6**) has demanded further investigation.

1.3. Designing antibiotics for inhibition of Gram-negative bacteria

Most bacteria are classified into two major groups: Gram-positive and Gram-negative bacteria.[47] Gram-positive bacteria have a cell membrane surrounded by peptidoglycan layers (30–100 nm) composed of glycan strands, anionic teichoic acids and surface proteins that facilitate the transport of small molecules, sugars, and iron chelators (Figure 4).[48]

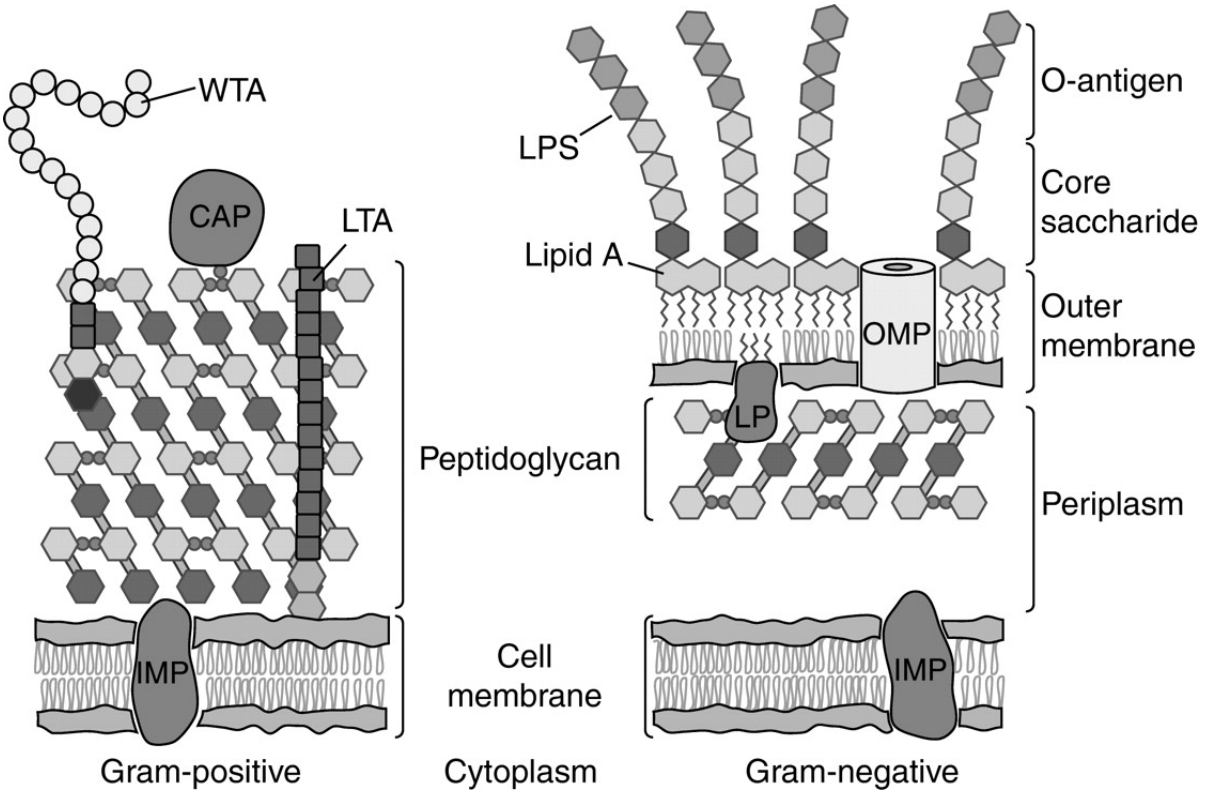

Figure 4: Gram-positive and Gram-negative cell envelopes are shown. LP: lipoprotein, LPS: lipopolysaccharide, LTA and WTA: teichoic acids, CAP: covalently attached protein, IMP: integral membrane protein, OMP: outer membrane protein. Adapted from[48].

In contrast, Gram-negative bacteria possess a thin peptidoglycan cell wall, surrounded by an outer membrane (OM) carrying lipopolysaccharides (LPS). The OM features various proteins, such as lipoproteins or β-barrel proteins, which mediate the diffusion

of small molecules, siderophores, and vitamins. LPS consist of lipid A, a core saccharide, and an O-antigen, which can be used to classify bacteria (Figure 4).[48] Bivalent cations like Mg^{2+}-ions, form bridges between the negatively charged phosphate groups in the lipid A moiety, creating a very effective barrier for hydrophobic small molecules (Figure 5).[49]

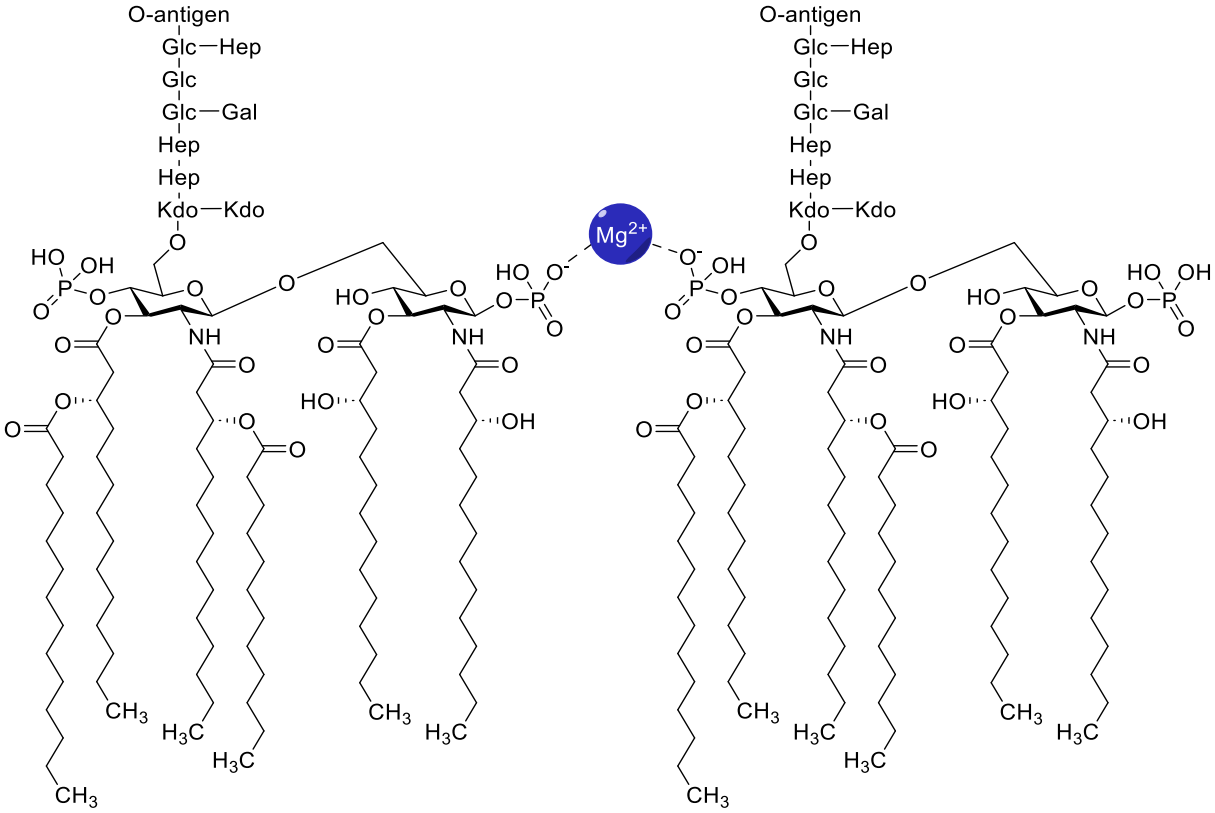

Figure 5: Chemical structure of the *E. coli* LPS. Glc: D-glucose, Hep: L-*glycero*-D-*manno*-heptose, Gal: D-galactose, Kdo: 3-deoxy-D-*manno*-oct-2-ulosonic acid. Adapted from[49].

Most Gram-positive-only antibacterials cannot traverse the OM of Gram-negative bacteria and therefore do not accumulate in the cell and do not reach their targets. It has been shown that increasing the polarity of small molecules facilitates their passage through the OM of Gram-negative bacteria. For instance, ampicillin (**9**), a broad-spectrum antibiotic, differs from penicillin G (**1**), a Gram-positive-only antibiotic, by an additional amino group. This increased polarity resulted in favorable minimum inhibitory concentrations (MICs) against various Gram-positive and Gram-negative bacteria.[50]

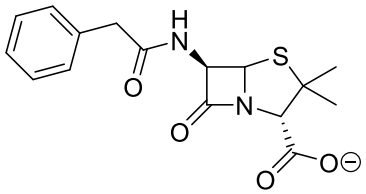

penicillin G (**1**)

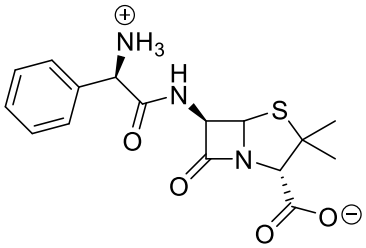

ampicillin (**9**)

Additional structure optimization studies have been conducted to develop broad-spectrum antibiotics. The structure of the streptomyces derived natural product arylomycin A (**10**) was optimized in terms of rigidity and polarity by generating a new compound (see **11**) with an amide with 2-aminoacetonitrile, replacing the *N*-terminal lipopeptide tail with a more rigid motif, and introducing primary amino groups to the phenolic oxygen atoms. This optimization led to G0775 (**11**), an antibiotic with potent activity against a variety of multidrug-resistant Gram-positive and Gram-negative bacteria (Figure 6).[51]

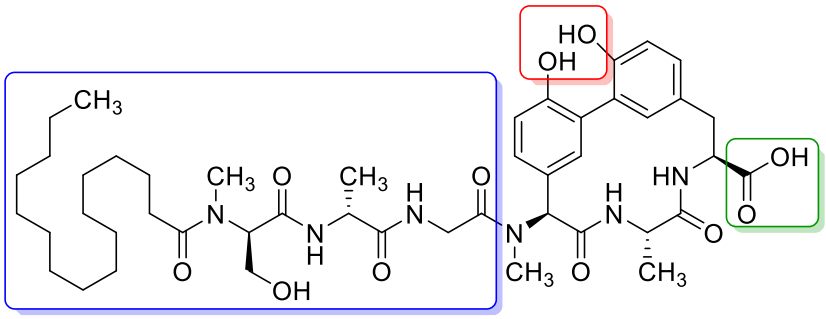

arylomycin (**10**)

Optimization

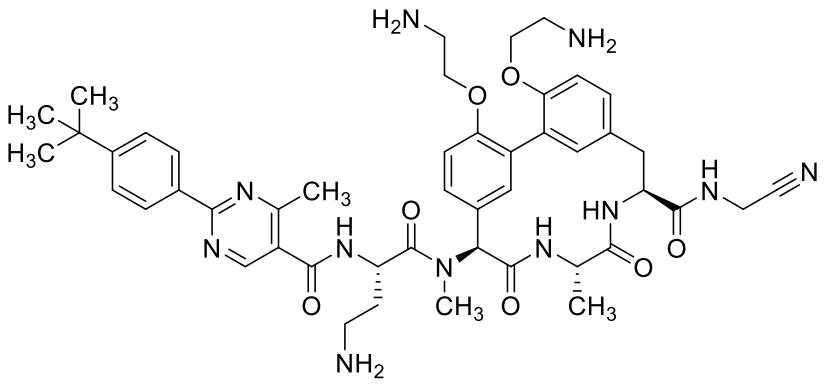

G0775 (**11**)

Figure 6: Optimization of arylomycin (**10**) leads to G0755 (**11**). Blue square indicates modifications in *N*-terminal lipopeptide tail, red square indicates modifications in phenolic oxygens, green square indicates modification in carboxylic acid moiety.

Over 180 small molecules with the ability to accumulate in *E. coli* were further investigated, leading to the establishment of the e**NTR**y rules by HERGENROTHER and colleagues. It was found that compounds are most likely to accumulate in *E. coli* if they have a non-sterically encumbered ionizable **N**itrogen, low **T**hree-dimensionality, and are relatively **R**igid (rotatable bonds ≤ 5).[52] Over the last decade, HERGENROTHER and colleagues have demonstrated that Gram-positive-only antibiotics can be converted into broad-spectrum antibiotics by implementing the eNTRy rules (Figure 7, see **12**–**17**).[53-55]

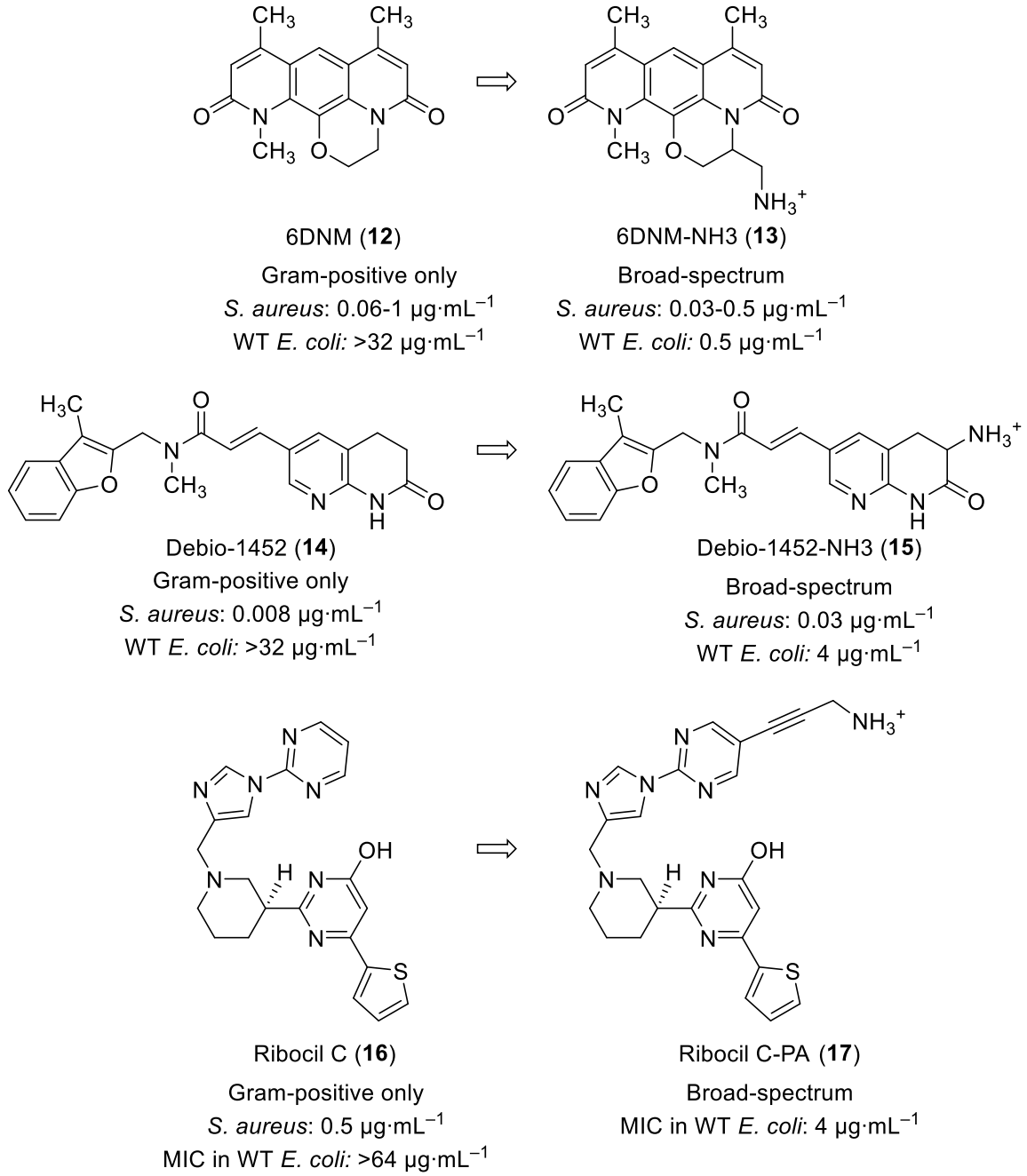

Figure 7: Selected set of Gram-positive-only antibiotics, which are converted into broad-spectrum antibiotics by implementing the eNTRy rules. WT = wild type.

Compounds **12**, **14** and **16** show significant antibiotic activity against Gram-positive strains (Figure 7) and exhibit suitable properties in terms of rigidity and three-dimensionality.[53-56] The introduction of a primary amine at a position that does not interfere with the mechanism of action, converts these compounds into broad-spectrum antibiotics with potent activity (Figure 7, see **13**, **15**, **17**).[57]

In a comprehensive study, the effect of other positively-charged, nitrogen-containing functional groups was investigated, concluding that guanidinium or pyridinium scaffolds should also be considered in developing Gram-negative antibiotics.[58] However, the mere addition of a primary amine on an antibiotic is not always sufficient to overcome the OM of Gram-negative bacteria. As previously mentioned, shape and rigidity parameters should not be neglected when it comes to developing Gram-negative antibiotics from Gram-positive-only antibiotics.[52]

1.4. Hybrid peptide-polyketide natural products

Natural products are compounds produced by living organisms, classified into primary and secondary metabolites and are molecules of relative small molecular weight.[59] Primary metabolites are required for growth and survival, whereas secondary metabolites, although not necessary for growth and survival under ideal conditions, provide advantages in environmental interaction.[60] Two large groups of secondary metabolites are polyketides and non-ribosomal peptides, which are produced by bacteria and fungi, among others, through megaenzymes known as polyketide synthases and non-ribosomal peptide synthases. The structures and formation mechanisms of secondary metabolites of these enzymes are well-understood.[61-65] Consequently, software tools for predicting these structures from the corresponding biosynthetic gene clusters (BGCs) are given more attention in structure elucidation.[66-69]

Non-ribosomal peptide synthase domains and their reactions

It has been shown that NRPSs have modular structures, and each module completes a peptide elongation cycle by biosynthetically adding an amino acid to the peptide chain in an assembly line-like fashion. An NRPS module consists of various domains, which have specific functions such as adenylation (A-domain), thiolation (PCP-domain), epimerization (E-domain), and condensation (C-domain). The A-domain activates an amino acid through ATP-hydrolysis, which then can be linked to a peptidyl-carrier-protein (PCP)-domain to form a thioester. The C-domain catalyzes the condensation reaction to form an amide bond between two amino acid thioesters. An E-domain in the modules can convert L-amino acids to the corresponding D-amino acids (Figure 8).[63]

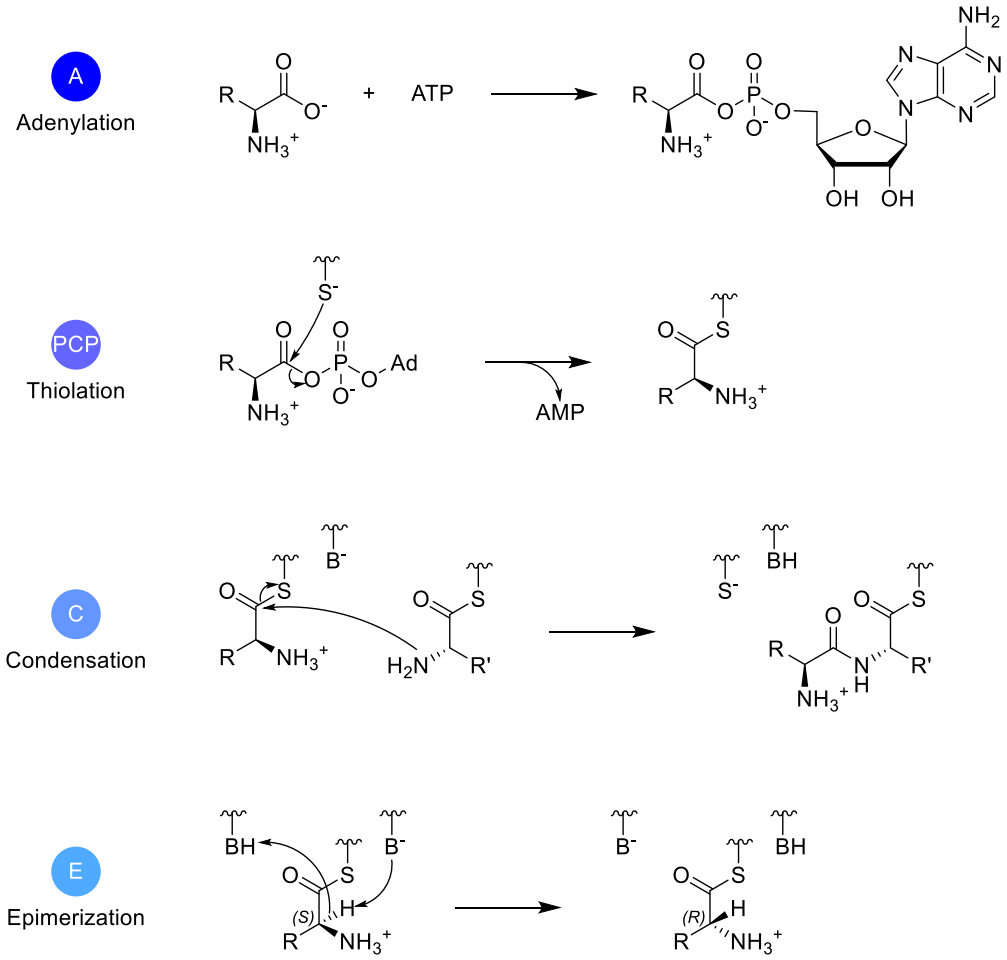

Figure 8: Reactions catalyzed by different domains in NRPS megaenzymes adapted from[63]. R = amino acid side chain, ATP = adenosine triphosphate, AMP = adenosine monophosphate, B = base.

Unlike ribosomal peptide synthesis, NRPSs also employ non-proteinogenic amino acids, such as ornithine[70] or pipecolic acid.[71] The peptide intermediates remain attached to the PCP-domain throughout the entire elongation process, and a thio-esterase (TE) domain typically cleaves off the peptide product from the enzyme.[62, 63] Various TE-mediated release mechanisms, such as hydrolysis for linear peptides, or macrolactamization[72] for macrocyclic structures, contribute significantly to the structural diversity of non-ribosomal peptides.[62]

Polyketide synthase domains and their reactions

Polyketides, like non-ribosomal peptides, are assembled sequentially from small building blocks, such as acetate (starter unit), malonate or alkyl malonate (extender units) compounds. PKS modules include at least a ketosynthase (KS), an acyltransferase (AT), and a thiolation (ACP)-domain. Additional accessory domains like ketoreductase (KR), dehydratase (DH), or enoylreductase (ER) further diversify polyketide structures. First an activated precursor (acyl-CoA) is transferred by the AT-domain to the acyl carrier protein (ACP)-domain (Figure 9A). Then a C-C bond formation between the upstream acyl thioester and the downstream acyl acceptor is catalyzed by the KS-module in a decarboxylative, CLAISEN-like fashion (Figure 9B). In Type I PKSs, the polyketide chain is transferred from one ACP-domain to the next during this reaction, while in Type II PKSs, the polyketide chain remains attached to the same ACP-domain. The β-ketoacyl intermediate undergoes further processing, leading to hydroxy functionalities, double bonds, or alkyl chains, depending on the contained domains (Figure 9C).[61, 62, 65]

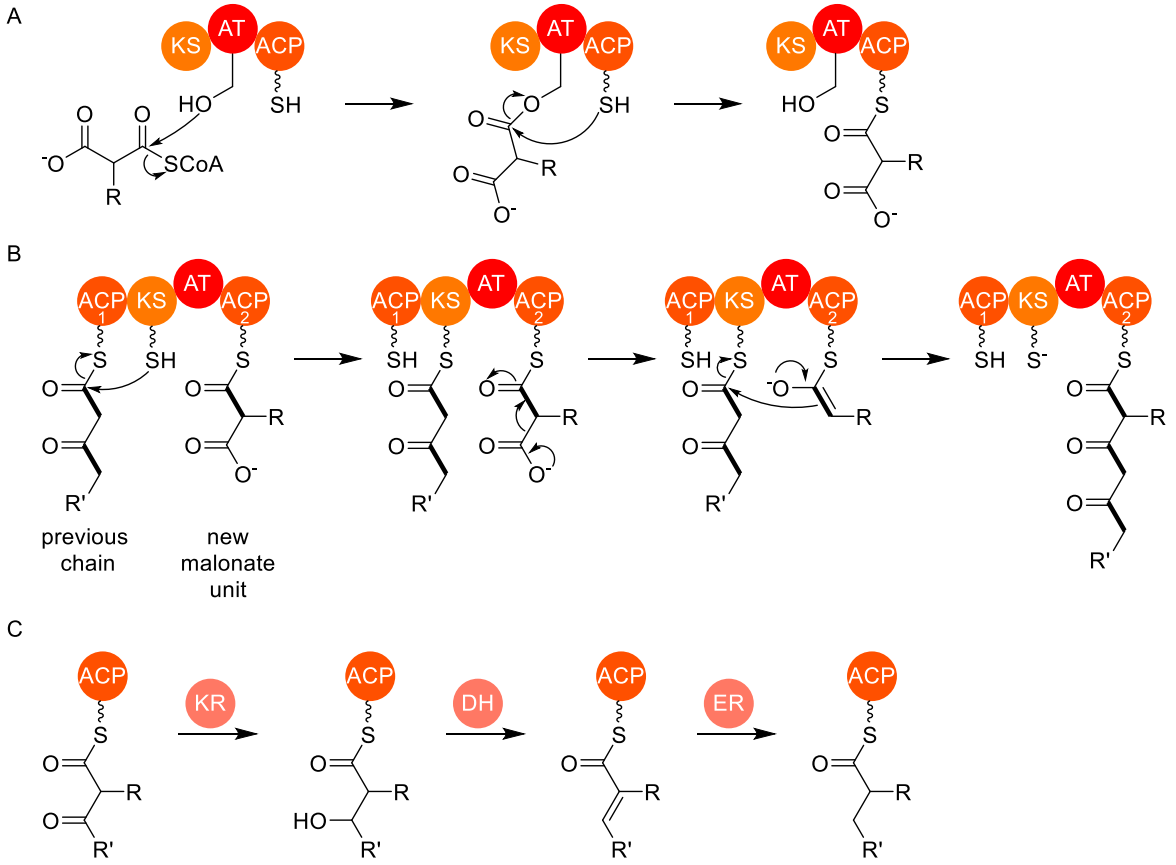

Figure 9: Mechanistic insights into the PKS machinery. A) Transfer of an acyl-CoA substrate to the ACP-domain. B) Elongation step catalyzed by KS in a decarboxylative, CLAISEN-like fashion. C) Further processing of the β-ketoacyl intermediate by KR, DH and ER. CoA = Coenzyme A, R = H or alkyl, R' = growing polyketide chain, bold bonds indicate starter and extender units. Adapted from[61].

PKSs are categorized into two major classes, the Type I PKSs and the Type II PKSs based on domain organization. Type I PKSs have multi-modular structures with their thiolation domain fused in *cis* to these modules, which means the domains are covalently bound to each other (Figure 10A). In Type II PKSs the domains are organized in *trans*, implying they are not covalently bound to each other (Figure 10B).

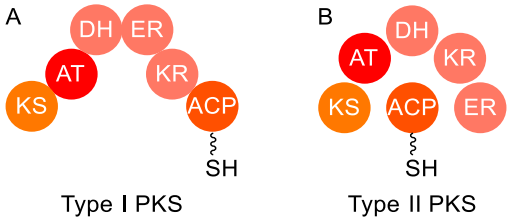

Figure 10: Comparison of Type I and Type II PKSs. A) Domains are covalently bound to each other (*cis*). B) Protein domains interacting in *trans*. KS = ketosynthase, AT = acyltransferase, DH = dehydratase, ER = enoylreductase, KR = ketoreductase, ACP = acyl carrier protein (thiolation domain). Adapted from[61].

NRPS and PKS hybrid compounds

These two biosynthetic pathways are as well used in combination to produce secondary metabolites, resulting in NRPS-PKS hybrid compounds with remarkable structural diversity and a wide range of biological activities.[64] Bacillaene (**18**) and salivabactin A/B (**8**) are antimicrobially potent NRPS-PKS hybrids produced by bacteria.[45, 73]

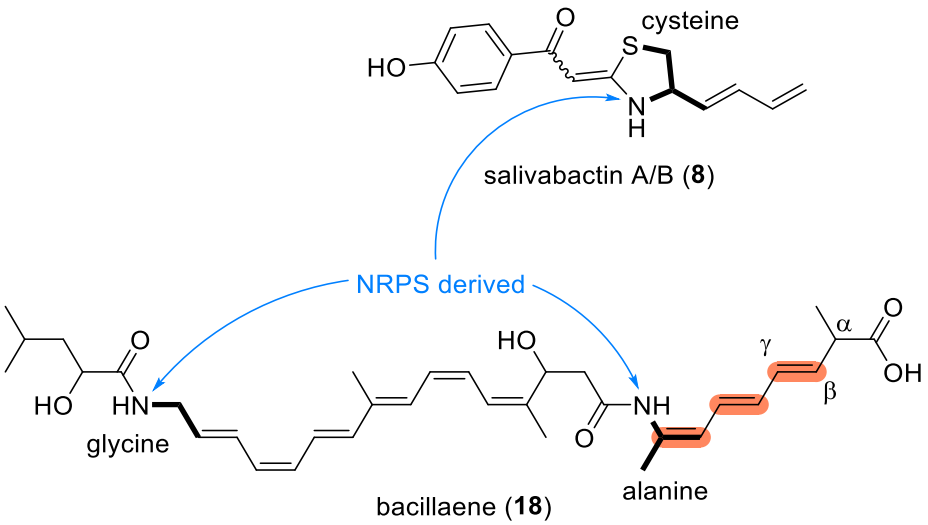

Figure 11: Structures of salivabactin A/B (**8**) and bacillaene (**18**). NRPS-derived moieties are indicated by blue arrows and bold bonds. Unusual β,γ-double bonds in bacillaene (**18**) are highlighted in orange.

Bacillaene (**18**) comprises two NRPS-derived amides and two polyene cores (hexaene and triene), with unusual β,γ-double bonds, which are introduced directly by PKS domains (Figure 11).[65, 74] Salivabactin A/B (**8**) features an aromatic moiety connected to a thiazolidine-ene ring and a diene moiety (Figure 11).[45]

Additionally, fungi and bacteria produce 3-acyltetramic acids using the NRPS-PKS machinery. 3-Acyltetramic acids exhibit characteristic tautomerism (Figure 12A), and in some cases form metal complexes.[75, 76] Their structures range from simple 3-acyltetramic acids[43, 77, 78] (see **19**) to more complex forms such as 3-polyenoyltetramic acids[79, 80] (see **20**, **21**), 3-decalinoyltetramic acids[81, 82] (see **22**) and macrocyclic tetramic acids[83] (see **23**) (Figure 12B).[84]

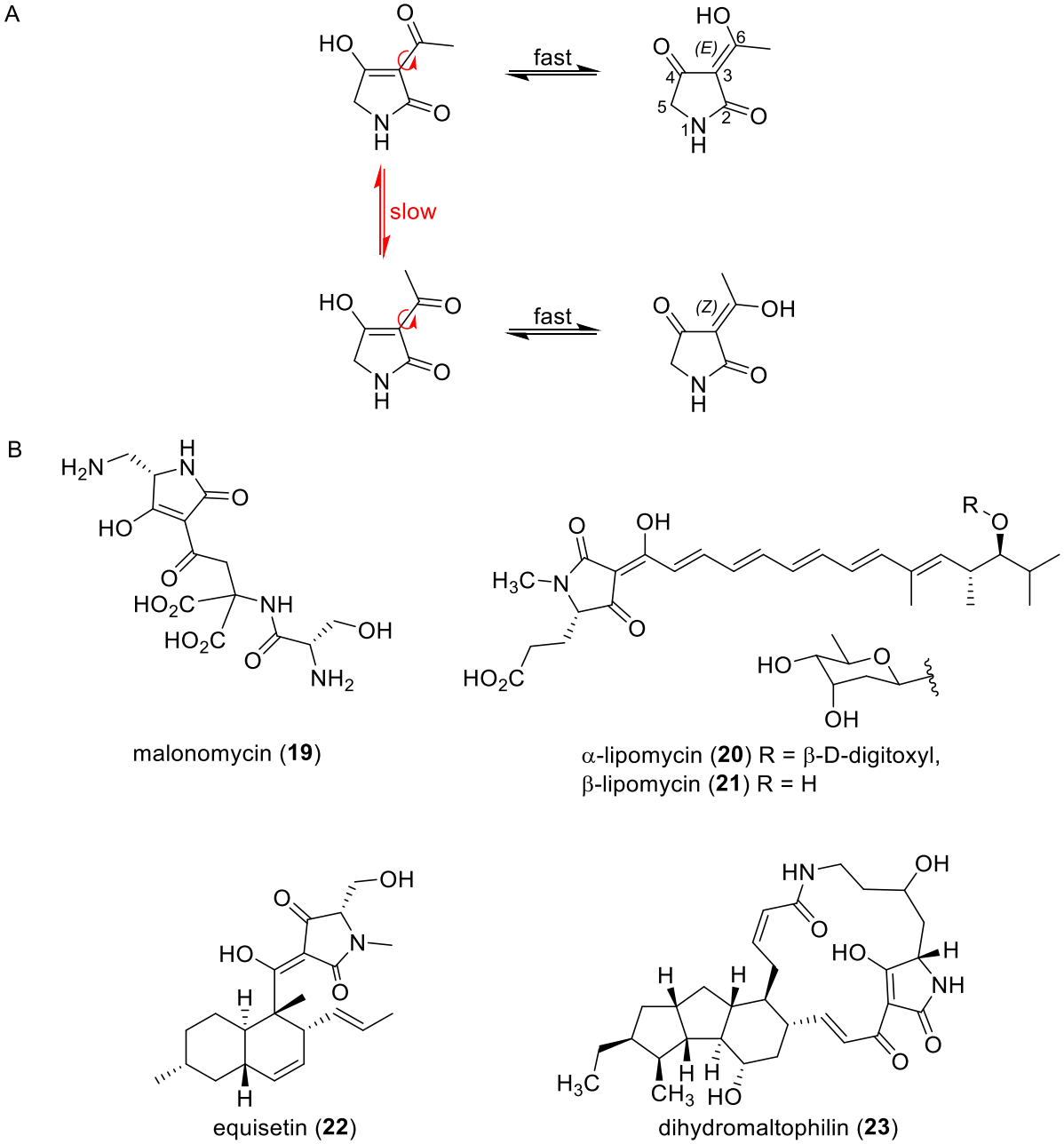

Figure 12: A) The four possible tautomers and rotamers for 3-acyltetramic acids. Bond rotation (red) is slow in NMR time scale and in contrast *enol*-formation is fast in NMR time scale in protic NMR solvents. B) selected examples of tetramic acids: 3-acyltetramic acid **19**, 3-polyenoyltetramic acids **20** and **21**, 3-decalinoyltetramic acid **22** and macrocyclic tetramic acid **23**.

The biological activities of tetramic acids are just as diverse as their structures. Malonomycin (**19**), produced by *Streptomyces rimosus paromomycinus*, exhibits antibacterial, antifungal, and antiprotozoal activity.[78, 85, 86] The lipomycins **20** and **21**, produced by *Streptomyces aurefaciens*, inhibit the growth of Gram-positive bacteria.[79] The macrocyclic dihydromaltophilin (**23**), also known as heat-stable antifungal factor (HSAF), produced by *Lysobacter enzymogenes*, shows antifungal activities against a broad spectrum of fungi.[87]

2. Scope of this work

2.1. Chemical analysis of epifadin (**24**) and syntheses to study epifadin motifs

In cooperation with the biology department of the University of Tübingen (Research Group KRISMER and PESCHEL), NADINE SCHILLING (Research group GROND, University of Tübingen) successfully detected a bioactive compound produced by *S. epidermidis* IVK83. This compound, named epifadin (**24**), exhibits potent activity against a wide range of targets, including MRSA strains. However, due to the high instability of epifadin (**24**), complete structure elucidation remained elusive. Analysis of its degradation products resulted in the identification of the NRPS moiety **25** from epifadin (**24**) using solid-phase peptide synthesis (SPPS) and HPLC high resolution mass spectrometry (Figure 13).[88]

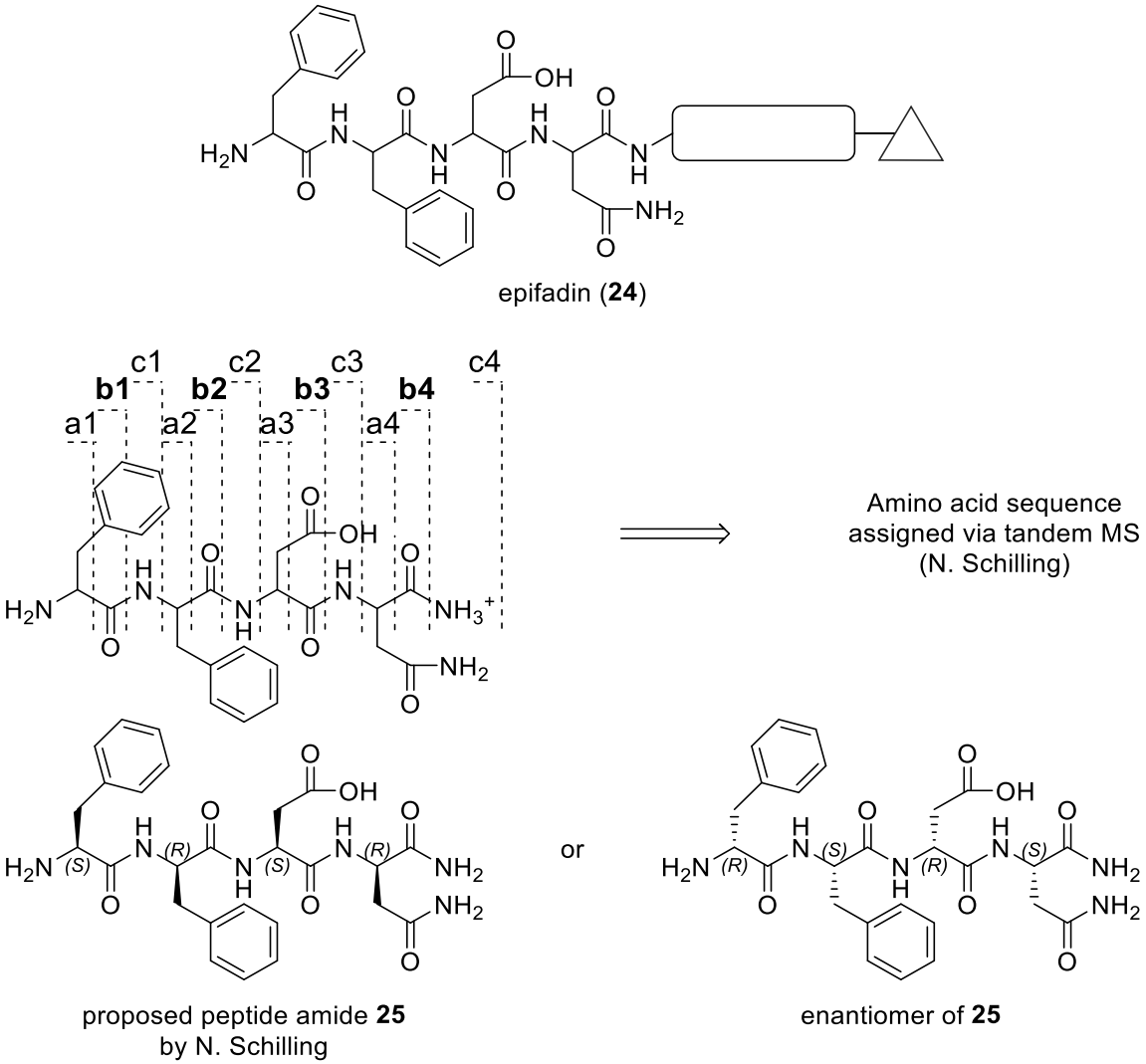

Figure 13: Structure of epifadin (**24**) with unknown structural elements depicted as geometrical objects. Assigned amino acid sequence via tandem MS (N. SCHILLING) and proposed absolute stereoconfiguration of peptide amide **25**.

The primary goal of this work is to fully elucidate the structure of epifadin (**24**). To achieve this, it is crucial to optimize extraction and chromatographic methods to increase the yield of isolated epifadin (**24**). With substantial amount of epifadin (**24**), comprehensive NMR spectroscopic and mass spectrometric experiments will be carried out. To unambiguously assign the stereoconfiguration of the peptide moiety **25** and conduct a chromatography study of such amides all 16 possible stereoisomers are synthesized using SPPS and analyzed via chiral HPLC-MS methods (in collaboration with research group LÄMMERHOFER). Additionally, efforts will focus on the synthesis of the PKS-NRPS moiety, which has not yet been structurally elucidated by NMR. These studies of chemical synthesis methods will contribute towards the total synthesis of epifadin analogues.

2.2. New lugdunin-like fibupeptides

The second part of this work focuses on synthesizing lugdunin-like fibupeptides to further investigate its mode of action. In collaboration with DOMINIK RUPPELT (Research group STEINEM, Georg-August-Universität Göttingen), the question of whether lugdunin (**6**) is a carrier ionophore (e.g. valinomycin[89]) or a channel-forming ionophore (e.g. nystatin[90]) will be tackled (Figure 14). To this end, *N*-methylated analogues of lugdunin (**6**) will be produced and further analyzed using biophysical methods. *N*-methylation would block β-sheet formation, thus preventing channel formation, and a consequent loss of bioactivity would indicate that lugdunin (**6**) is a channel-forming ionophore.

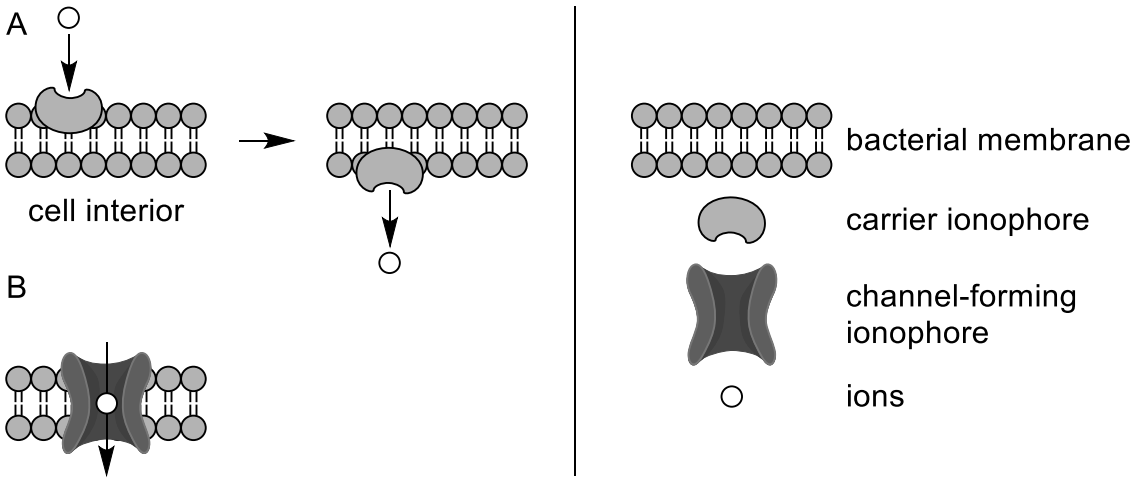

Figure 14: Depiction of different types of ionophores. A) Carrier ionophores bind ions and carry them through cell membranes. B) Channel-forming ionophores create channels within membranes to facilitate ion transport.

Given that lugdunin (**6**) is a Gram-positive-only antimicrobial, the concept of the HERGENROTHER eNTRy rules will be applied to lugdunin (**6**) to convert it into a broad-spectrum antimicrobial. Amino acid positions 2 and 5 in lugdunin (**6**) are amenable to substitution with other amino acids, enabling the preparation of lugdunin-like fibupeptides with a primary amino group in these positions.[40, 46] Non-proteinogenic amino acids, such as ornithine and 4-aminophenylalanine, are considered for these modifications. Moreover, the lugdunin analogues will be biologically profiled in cooperation with the medical microbiology (KRISMER, PESCHEL) of the University of Tübingen.

3. Results and discussion

3.1. Chemical analysis of epifadin (**24**) and syntheses to study epifadin motifs

Colonization of the human body's surface by pathogenic microorganisms poses a significant risk. Approximately one-third of the population is colonized by *Staphylococcus aureus*. As a preventive measure, *S. aureus* can be eradicated to minimize associated risks.[91] A study conducted by KRISMER investigated bacterial colonization of the nasal cavity, with the key question being which bacteria are capable of surviving in the nutrient-poor environment of the nose and whether these bacteria produce bacteriocins[33] – antimicrobial compounds – that could eliminate *S. aureus*. The study revealed that the strain *Staphylococcus epidermidis* IVK83 exhibited activity against several Gram-positive bacteria, including MRSA.[92]

Staphylococcus epidermidis IVK83 was successfully cultivated in tryptic soy broth (TSB) medium. The culture was grown for 44 hours in TSB at 30°C, and the supernatant was sterile-filtered. The culture filtrates exhibited antibacterial activity, but initial isolation attempts using common extraction methods with methanol, *n*-butanol, ethyl acetate, and halogenated solvents such as chloroform and dichloromethane, followed by chromatographic techniques, resulted in a loss of activity, likely due to the degradation of the active component epifadin (**24**).[88, 93] Treatment of the culture filtrate with hydrochloric acid (pH 2) at 4°C produced a precipitate, which was subsequently freeze-dried. The active component was then successfully dissolved from the precipitate using DMSO, enabling the first biological tests to be conducted. Using HPLC-UV, the UV spectrum of epifadin (**24**) was recorded, showing a UV maximum at 383 nm.[88] Based on its unique UV spectrum, it was hypothesized that epifadin (**24**) contains a polyene structure, which can be protected from degradation by antioxidants. By adding an antioxidant such as palmitoyl ascorbate (**26**) and storing the extract in the dark at –80°C, the antibacterial activity of the extract was preserved for the first time.[94]

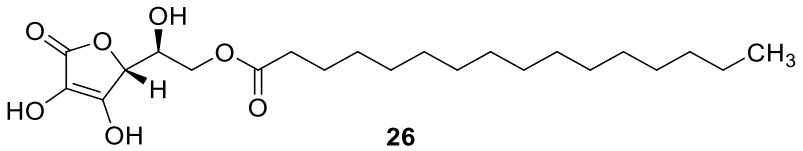

26

A comparison between *Staphylococcus epidermidis* IVK83 and its knockout mutant, which no longer produces epifadin (**24**), revealed through HPLC-MS analysis that the *S. epidermidis* IVK83 strain contains the peptide amide **25**. However, this compound

does not exhibit bioactivity, suggesting that it is a fragment of epifadin (**24**), likely formed during its degradation.[88]

Moreover, the genes encoding for epifadin (**24**) were analyzed to obtain further information about potential biosynthetic building blocks. With the epifadin-deficient mutant in hand, localization of the BGC in the wild type was achieved by direct comparison of genes. The BGC was localized on a plasmid and was confirmed by restoring the antibacterial activity in the mutant via complementation (medical microbiology department University of Tübingen, Research group KRISMER, PESCHEL).[94] Subsequently, the BGC composition was analyzed using AntiSMASH 5.0 (bacterial settings)[69], which revealed the domain organization of the NRPS I-PKS-NRPS II gene cluster (Figure 15).[94]

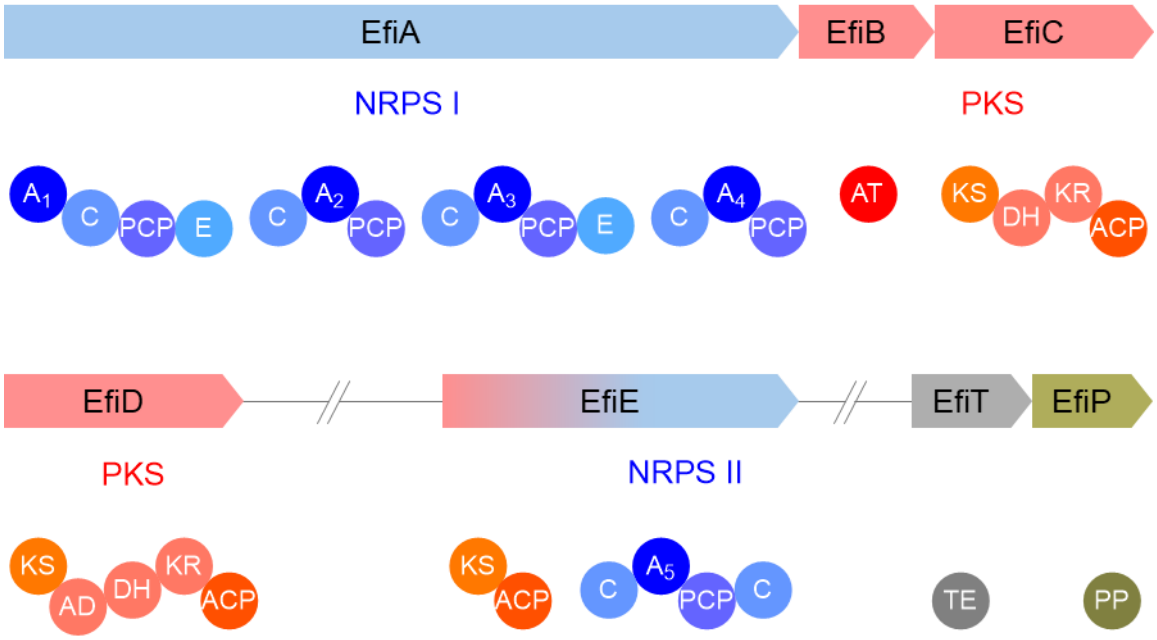

Figure 15: Domain organization of the NRPS and PKS involved in epifadin (**24**) biosynthesis. A_x = adenylation domain for a specific amino acid, AD = *trans*-AT docking, TE = thioesterase, PP = 4'-phosphopantetheinyl transferase.

3.1.1. Optimization of epifadin (**24**) isolation and purification strategies

In collaboration with the medical microbiology (KRISMER, PESCHEL) of Tübingen, N. SCHILLING developed a purification strategy for epifadin (**24**), which led to its isolation for the first time (Figure 16).[88] Despite this breakthrough, only 6 mg of epifadin (**24**) were isolated from over 100 L of *S. epidermidis* IVK83 culture supernatant. A careful comparison of the bioactivity potential of purified epifadin (**24**) and the DMSO extract of the precipitate indicated that the epifadin (**24**) content should be significantly higher than obtained after HPLC purification using method A (Experimental section 6.1.1.).

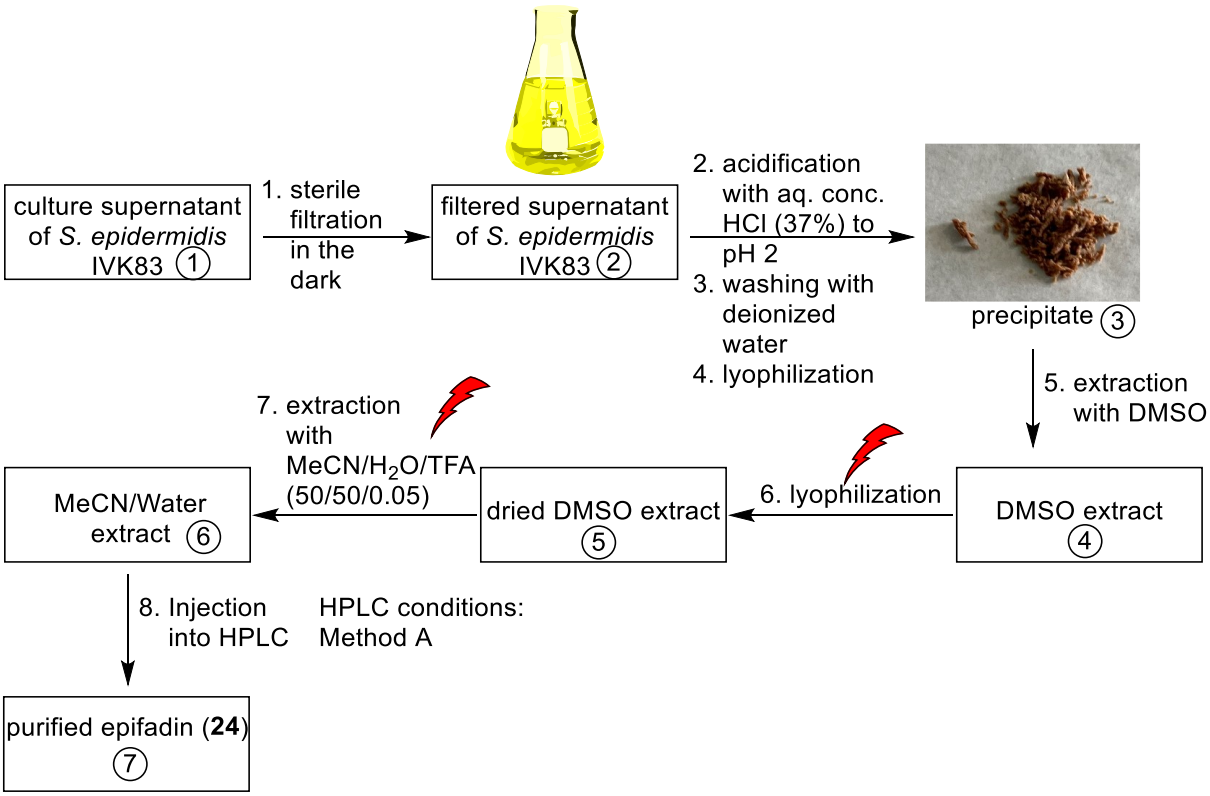

Figure 16: Purification steps developed by N. SCHILLING in cooperation with the medical microbiology of the University of Tübingen. Products after every process are marked with circled digits. Critical steps where decomposition of epifadin (**24**) can occur or where extraction is insufficient are marked with red thunder symbols.

The culture supernatant ① was sterile filtered, followed by adjustment of the pH value to pH 2. The mixture is left to sit for two hours at 4°C in the dark. The resulting precipitate ③ was then separated from the supernatant by centrifugation, washed several times with deionized water and lyophilized. Subsequent extraction with dimethyl sulfoxide (DMSO), lyophilization, and an additional extraction with the HPLC solvent mixture (acetonitrile/water/trifluoroacetic acid, 50/50/0.05) prior to injection into a HPLC system yielded purified epifadin (**24**) using method A (Experimental section 6.1.1.).[88]

The poor yield (6 mg out of 100 L of culture broth) could be attributed to the high instability of epifadin (**24**), which decomposes at prolonged light exposure, basic conditions, and in certain solvents like methanol.[88] In-depth biological and chemical analyses of each individual step of the purification strategy revealed that there are two critical steps where epifadin (**24**) decomposition or insufficient extraction might occur (Figure 16). During the freeze-drying process (Figure 16, step 6.), the frozen DMSO extract ④ thawed, causing the extract to evaporate at room temperature rather than sublimating at –40°C, potentially leading to decomposition of the highly instable epifadin (**24**). Moreover, the extraction solvent used for HPLC could be insufficient (Figure 16, Step 7), leaving most of the epifadin (**24**) in the residue ⑤ and resulting in poor yields after HPLC purification.

In a biological activity guided approach, different steps of the purification protocol were examined to determine whether biological activity is lost due to decomposition or insufficient extraction (Figure 17).

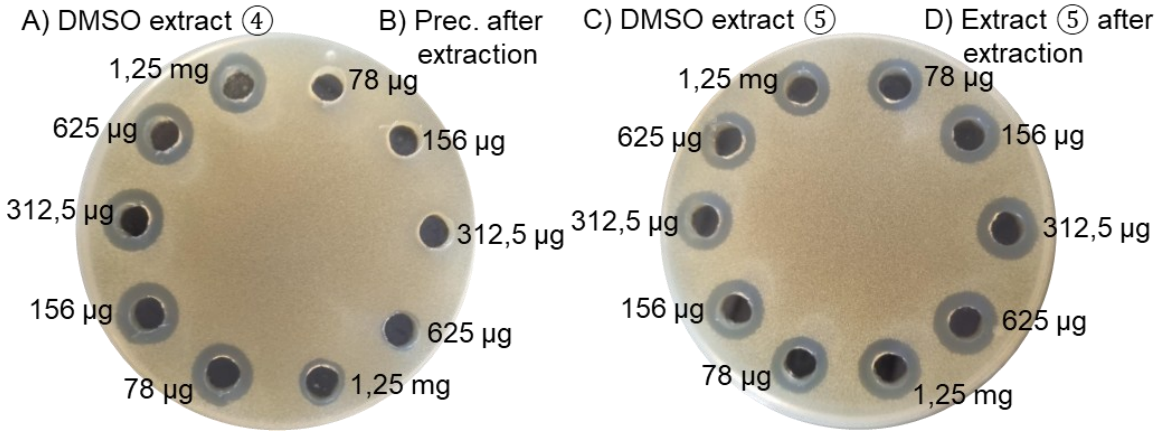

Figure 17: Agar diffusion assays of different samples at different steps of the purification protocol. Samples were prepared by extracting 10 mg of each sample with 400 µL of DMSO (25 mg·mL^{-1}). A) Dilution series for DMSO extract ④. B) Dilution series for precipitate (prec.) after extraction with DMSO. C) Dilution series for dried DMSO extract ⑤. D) Dilution series for extract ⑤ after extraction with MeCN/water/TFA (50/50/0.05) and subsequent lyophilization.

DMSO extracts ④ of the precipitate displayed large inhibition zones in agar diffusion assays, while the residue from this extraction step showed only a tiny inhibition zone or none (Figure 17A and 17B), depending on the amount of DMSO added to the assay. Dissolving the dried DMSO extract ⑤ with DMSO and testing by agar diffusion assay, revealed that no reduction in the size of the inhibition zones was observed (Figure 17C). This indicates that decomposition of epifadin (**24**) during the freeze-drying process is rather minimal and that DMSO can be used to efficiently extract epifadin (**24**). However, after extraction of the dried DMSO extract ⑤ with acetonitrile

water and TFA the residue of ⑤ displayed no reduction in size of inhibition zones after lyophilization and subsequent DMSO extraction for agar diffusion assay (Figure 17D). This clearly indicates that the solvent mixture used for HPLC injection insufficiently dissolves epifadin (**24**) and most of it remains in the residue, which in turn leads to poor yields after HPLC.

To optimize extraction of epifadin (**24**) for purification purposes on HPLC, samples of the precipitate were extracted using acetonitrile-water-TFA with varying DMSO contents. The obtained supernatants were then injected into an analytical HPLC system and chromatograms were recorded at multiple wavelengths using method D (Experimental section 6.1.1.).[88, 94] For each sample, 10 mg of the precipitate was first treated with the corresponding amount (0–40 µL) of DMSO and then 160 µL of acetonitrile-water-TFA (80/20/0.05) were added. The samples were vortexed, centrifuged, and 10 µL of the supernatant was injected into an analytical HPLC system.

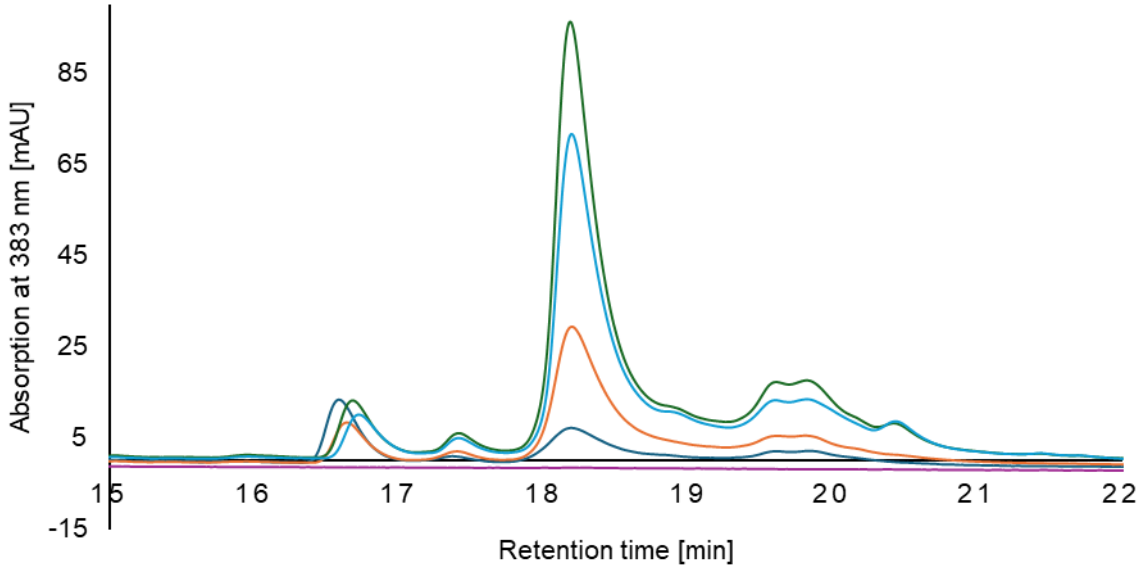

Figure 18: Method D (Experimental section 6.1.1.) was used for chromatography. Zoomed area of overlayed chromatograms at 383 nm is shown. Blank sample (purple): acetonitrile-water-TFA mixture (80/20/0.05). Dark blue: 0 µL DMSO (0 %DMSO), orange: 8 µL DMSO (5% DMSO), dark green: 32 µL DMSO (17%), turquoise: 40 µL DMSO (20% DMSO).

The comparison of chromatograms at the absorption maximum of epifadin (**24**, 383 nm), showed that the area of the epifadin peaks at 18.3 min increased significantly with a higher DMSO content in the extraction solvent and reached its maximum with 17% DMSO (Figure 18). Given that the amount of acetonitrile-water-TFA remained constant and only the amount of DMSO was increased, it can be assumed that the decrease in peak area with 20% DMSO constitutes a dilution effect.

Additionally, the stability of epifadin (**24**) in the solvent used for HPLC purification was investigated. Two samples were prepared by extracting the dried DMSO extract ⑤ with acetonitrile/water/TFA, (50/50/0.05) and exposing one to ambient light, while the other sample is stored in the dark at room temperature. Chromatograms at 383 nm were then recorded at specific time intervals using HPLC (Method B, experimental section 6.1.1.). The peak area of the epifadin signal was then determined and plotted against time (Figure 19). The sample exposed to light is assumed to undergo faster decomposition than the sample stored in the dark as our working hypothesis.

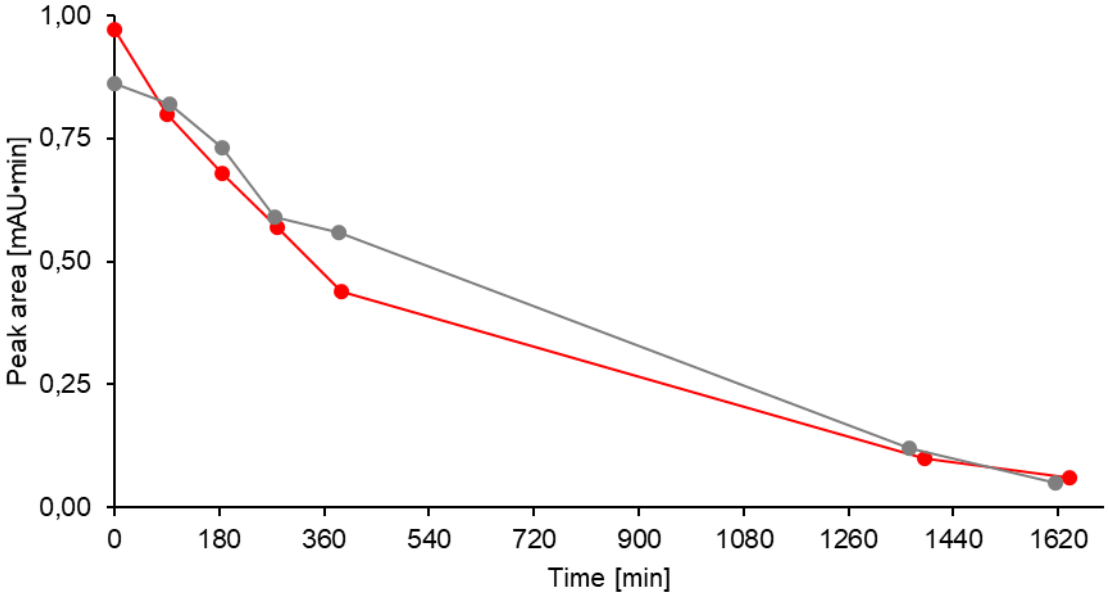

Figure 19: Peak areas of epifadin peak in correlation of time. Chromatograms were recorded on a semi-preparative HPLC system using method B (Experimental section 6.1.1.). Samples were prepared using acetonitrile-water-TFA (50/50/0.05). One is exposed to light (red), while the other sample is stored in the dark (grey) at room temperature.

Figure 19 revealed that epifadin (**24**) decomposes similarly in both light-exposed and dark-stored samples, with peak areas halving after 3 hours. This indicated that the solvent system acetonitrile-water-TFA was not suitable for long storage of epifadin-containing samples. However, the advantage of this solvent system over methanol is that mixtures of acetonitrile and water can be freeze-dried, whereas methanol-water mixtures thaw using a freeze-dryer. Since epifadin (**24**) is a highly unstable compound, the mild freeze-drying process is mandatory. Further solvent tests with nitrobenzene, methanol with trifluoroacetic acid, and dimethyl sulfoxide with and without trifluoroacetic acid showed that epifadin (**24**) was the most stable in DMSO, with a half-life of about four days (Figure 20). In this case, however, all samples were stored in the dark at room temperature throughout the entire experiment.

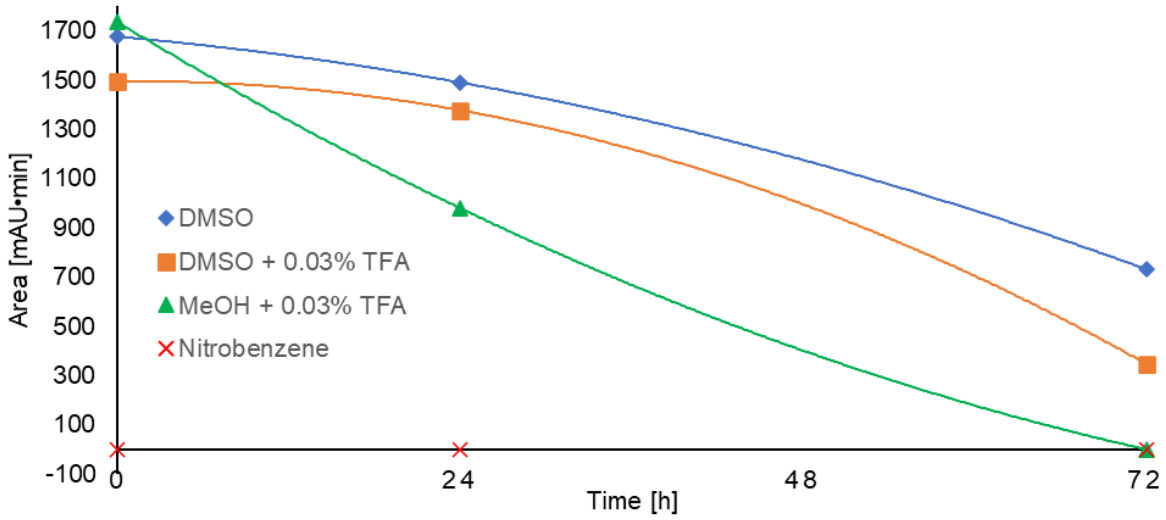

Figure 20: Stability of epifadin (**24**) in selected solvents used for extraction of precipitate. Chromatograms were recorded on an analytical HPLC system using method E (Experimental section 6.1.1.). The concentration was adjusted to 20 mg precipitate per mL solvent. Trendlines in corresponding colors were generated with Microsoft Excel.

Adding acid to the solvents accelerated decomposition of epifadin (**24**). Nitrobenzene does not dissolve epifadin (**24**). This experiment shows that epifadin (**24**) is best stored and handled with dimethyl sulfoxide as a solvent. In this case, palmitoyl ascorbate (**26**) was omitted as an antioxidant because it coeluted with epifadin (**24**) during HPLC purification (Figure 21).

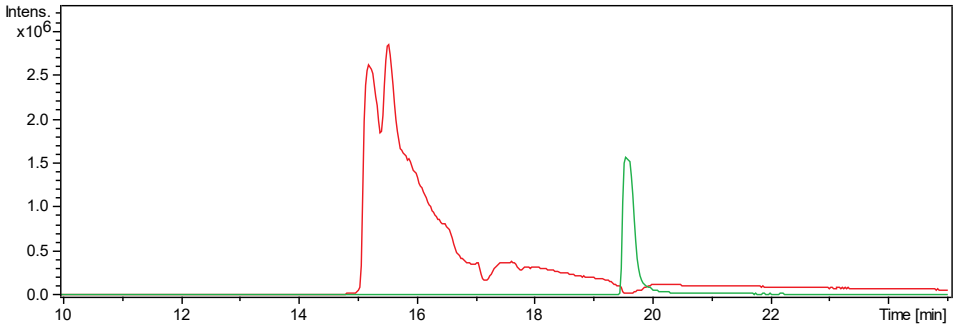

Figure 21: Epifadin (**24**) sample analyzed via HPLC-ESI-HRMS (Experimental section 6.1.4.) after purification via HPLC using method A.[88] EIC of epifadin (**24**, $C_{51}H_{62}N_7O_{12}^+$, 964.4451±0.01) is shown in red, EIC of palmitoyl ascorbate (**26**, $C_{22}H_{39}O_7^+$, 415.2690±0.01) is shown in green.

In addition, additives for solvents in HPLC were tested and HPLC was performed using ammonium acetate buffer (pH 5) as an additive. Under these conditions, however, no epifadin-characteristic signal at 383 nm could be observed. By replacing TFA (0.05%) with the much more environmentally friendly formic acid (FA, 0.1%)[95], no significant change in elution time for epifadin (**24**) was observed and has been rendered suitable. Since epifadin (**24**) dissolves best in DMSO and is most stable in it, DMSO must be used as the extraction solvent and injected into the HPLC.

Direct injection of the DMSO extract into HPLC resulted in a prominent DMSO signal at 220 nm in the chromatogram (Figure 25), which overlapped with the epifadin-signal due to tailing when method A (experimental section 6.1.1.) was applied. The most effective gradient was a step gradient of acetonitrile/water/FA (40/60/0.1) for 20 minutes, followed by acetonitrile/water/FA (50/50/0.1) for 20 minutes. Chromatography was performed on a Kromasil C18 column, and this method successfully eliminated overlap between the DMSO and epifadin signals in the chromatogram. Furthermore, washing of the precipitate with acetonitrile resulted in the removal of nonpolar compounds, such as fatty acids and derivatives thereof, while epifadin (**24**) is not soluble in acetonitrile. This was demonstrated by HPLC-HRMS (Figure 22).

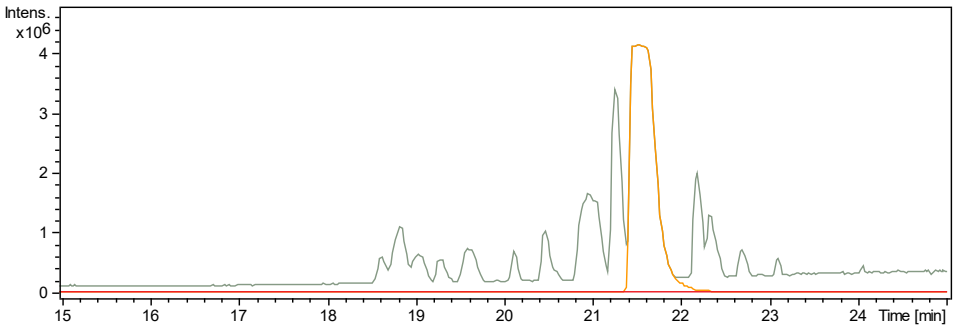

Figure 22: Acetonitrile used for washing of the precipitate was analyzed via HPLC-HRMS (Experimental section 6.1.4.). EIC of epifadin (**24**, $C_{51}H_{62}N_7O_{12}^+$, 964.4451±0.01) is shown in red, EIC of oleamide (**27**, $C_{18}H_{36}NO^+$, 282.2791±0.01) is shown in orange.

HPLC-HRMS analysis of the acetonitrile wash (Figure 22) revealed the presence of oleamide (**27**), with no detectable peptide amide **25** and epifadin-signal. This indicates that epifadin (**24**) is not soluble in pure acetonitrile.

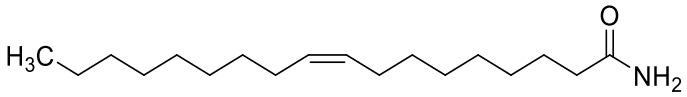

27

Considering that unwanted components can be washed from the precipitate using acetonitrile, that methanol cannot be used due to the low stability of epifadin (**24**) in methanol, and that DMSO is the most suitable solvent, a new purification protocol was developed accordingly (Figure 23).

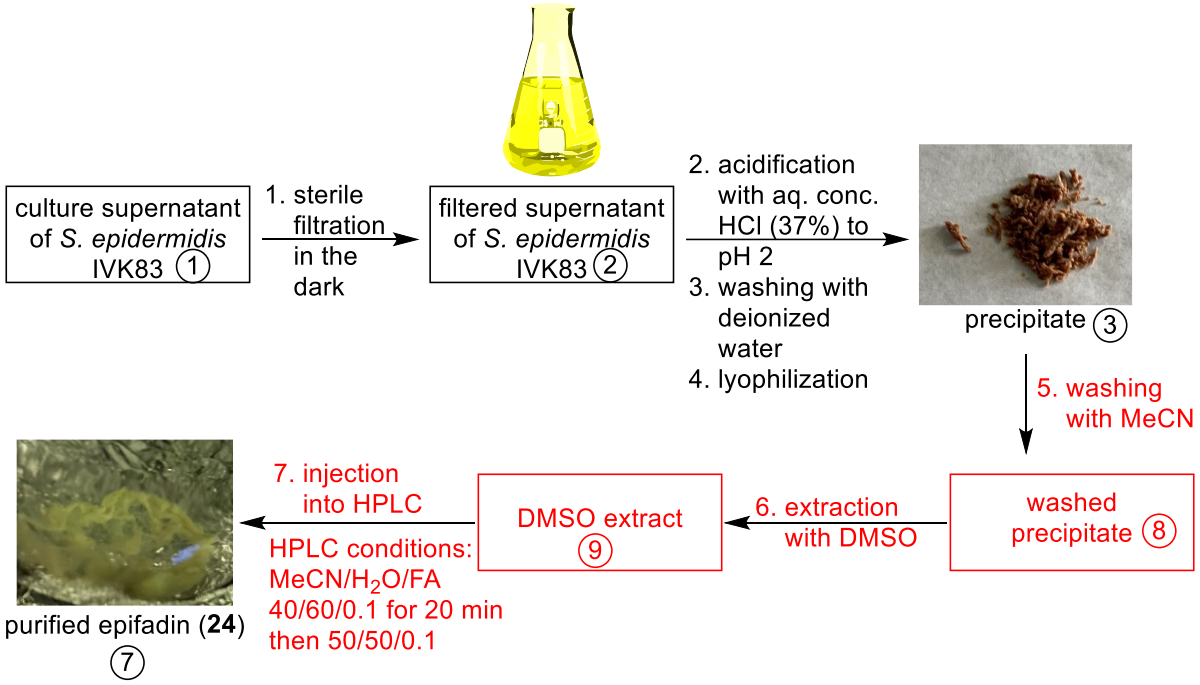

Figure 23: New purification protocol. Modifications are highlighted in red.

The steps to produce the precipitate remain unchanged. Precipitate ③ is washed with acetonitrile, centrifuged, and the supernatant is discarded. The residue is then extracted with DMSO to produce extract ⑨. Instead of evaporating the DMSO and subsequently re-extracting with the HPLC solvent, the extract ⑨ is injected directly into a preparative HPLC system. This minimizes decomposition of epifadin (**24**) from the prolonged exposure to room temperature in DMSO. Decomposition was further prevented by manually collecting epifadin-containing fractions in the dark at –80°C. This was realized by utilizing a fixed 500 mL round-bottom flask covered in aluminum foil and immersed in an isopropyl alcohol-liquid nitrogen cooling bath. The temperature of the cooling bath was continuously monitored using a low-temperature thermometer and adjusted to –80°C with liquid nitrogen as needed. In addition, a balloon filled with argon gas and a septum was used to maintain argon atmosphere in the collecting flask throughout the purification process (Figure 24).

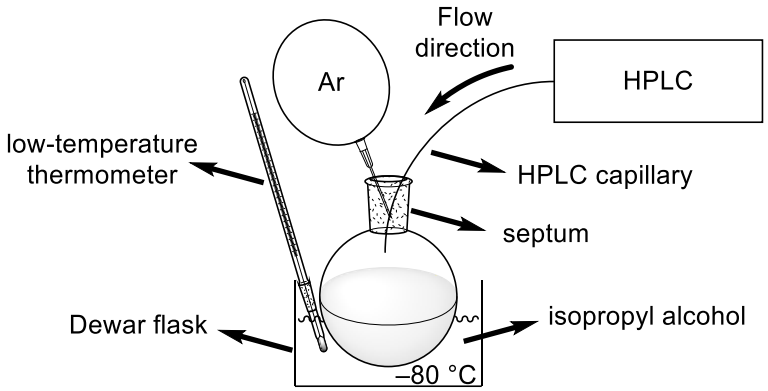

Figure 24: Instrumental set-up for collecting epifadin-containing fractions at –80°C.

Moreover, TFA was replaced by FA, making the method more environmentally friendly. Chromatograms for the new method showed clear separation of epifadin and DMSO signals (383 nm and 214 nm, respectively, Figure 25).

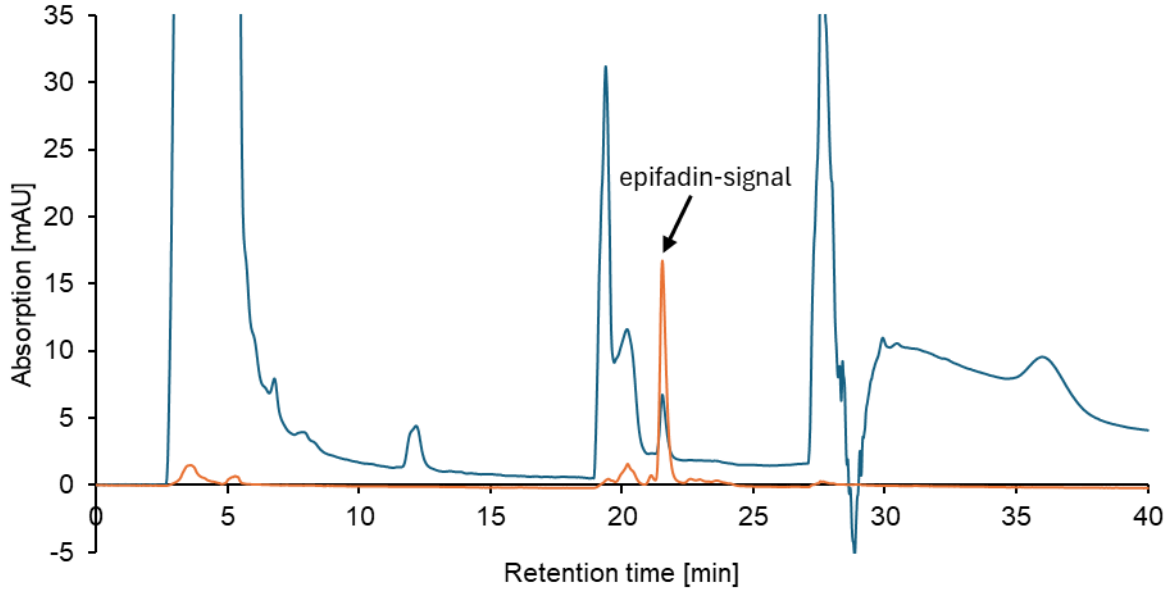

Figure 25: HPLC chromatograms of new chromatographic method C at 214 nm (blue) and 383 nm (orange). Signal of epifadin (**24**) at 21.5 min, signal of DMSO at 5 min.

With the optimized method at hand 1.2 g of precipitate were generated from 5 L of *S. epidermidis* IVK83 culture supernatant. Following washing with acetonitrile and extraction of the washed precipitate ⑧ with DMSO, the extract ⑨ was purified via HPLC (Method C experimental section 6.1.1.), yielding 3.5 mg of purified epifadin (**24**) as a voluminous yellow powder after lyophilization in the dark.[94] Using the new purification protocol, the yield of epifadin (**24**) was increased 12-fold compared to the 100 L approach with method A (experimental section 6.1.1.) which facilitates chemical analyses and biological assays.

3.1.2. Structure elucidation of the new peptide polyene tetramic acid **24**

Following preparative HPLC purification, a sample of epifadin (**24**, 0.2 mg·mL^{-1} in acetonitrile/water/TFA, 50/50/0.05) was subjected to HPLC-ESI-MS (high performance liquid chromatography electrospray ionization mass spectrometry) equipped with a DAD (diode array detector) to confirm its chemical formula and the UV spectrum, as previously determined and measured by N. SCHILLING.[88] For this purpose, a standard gradient on core-shell RP-C_{18} column material was used (see experimental section 6.1.4.). After purification, HPLC-MS analysis revealed that the sample contained epifadin (**24**), its decomposition product **25**, and unidentified impurities (Figure 26).[94]

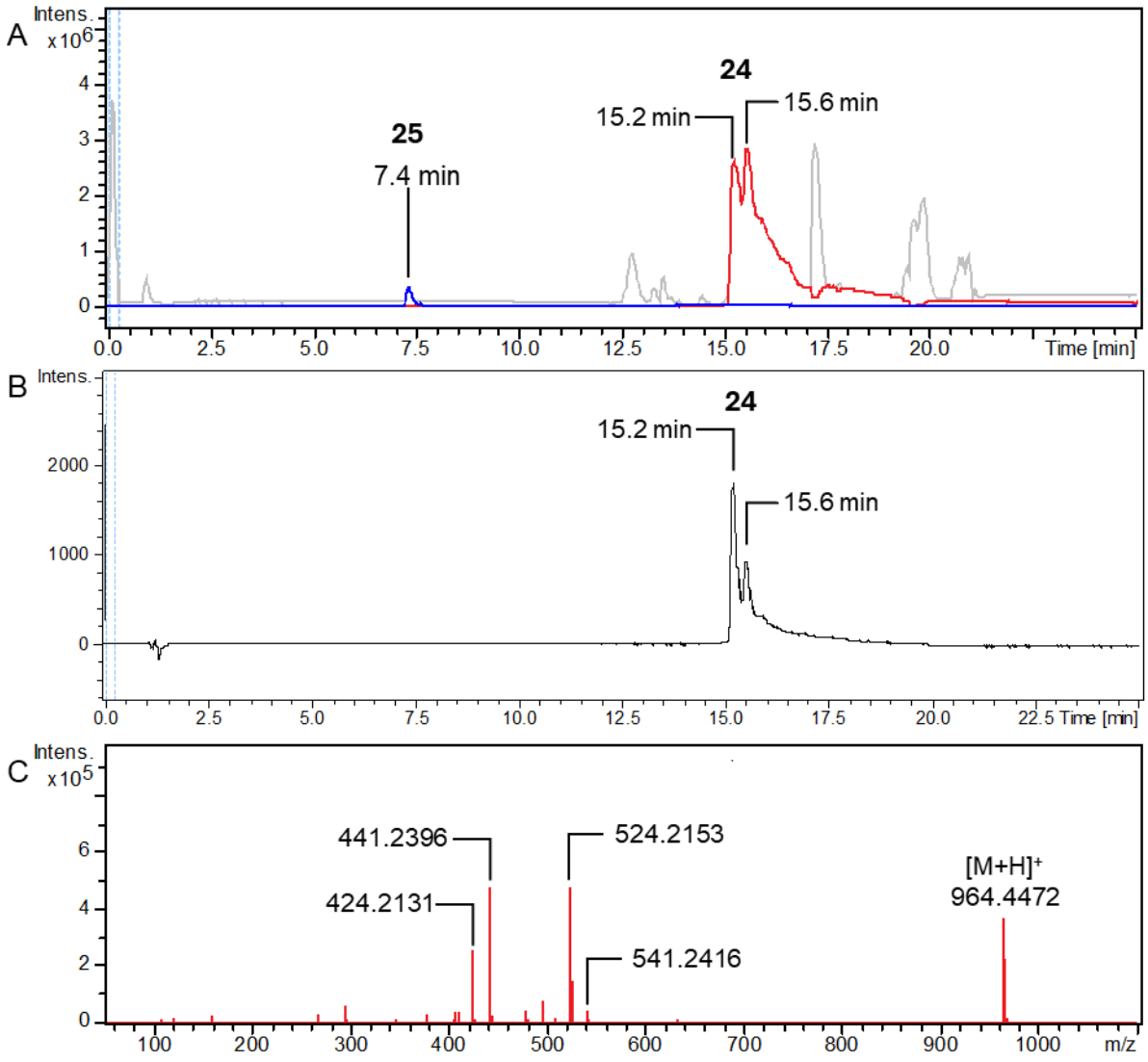

Figure 26: A) HPLC-MS analysis (Experimental section 6.1.4.) of purified epifadin-sample in acetonitrile/water/TFA, 50/50/0.05, containing 0.2 mg·mL^{-1} epifadin (**24**). Base peak chromatogram (BPC, grey), EIC of epifadin (**24**) (red, $C_{51}H_{61}N_7O_{12}$ $[M+H]^+$, *m/z* 964.4451±0.005 Da) and EIC of peptide amide **25** (blue, $C_{26}H_{32}N_6O_7$ $[M+H]^+$, *m/z* 541.2405±0.005 Da). B) UV chromatogram (black, 381-385 nm) C) Tandem MS (MS^2) spectrum of epifadin (**24**). $[M+H]^+$ signal and *m/z*-values of selected signals highlighted.

The impurities observed at a retention time of 17.2 minutes have *m/z*-values of 712.8983 and 950.1952 (Figure 27A). For single positively charged molecules, the ion mass corresponds directly to the measured *m/z*-value, resulting in an isotopic peak spacing of 1 Da. In the case of multiple positively charged molecules, the spacing between isotopic peaks is 1/*z* (where *z* represents the charge). This allows the determination of the ion's charge based on the measured *m/z*-values.

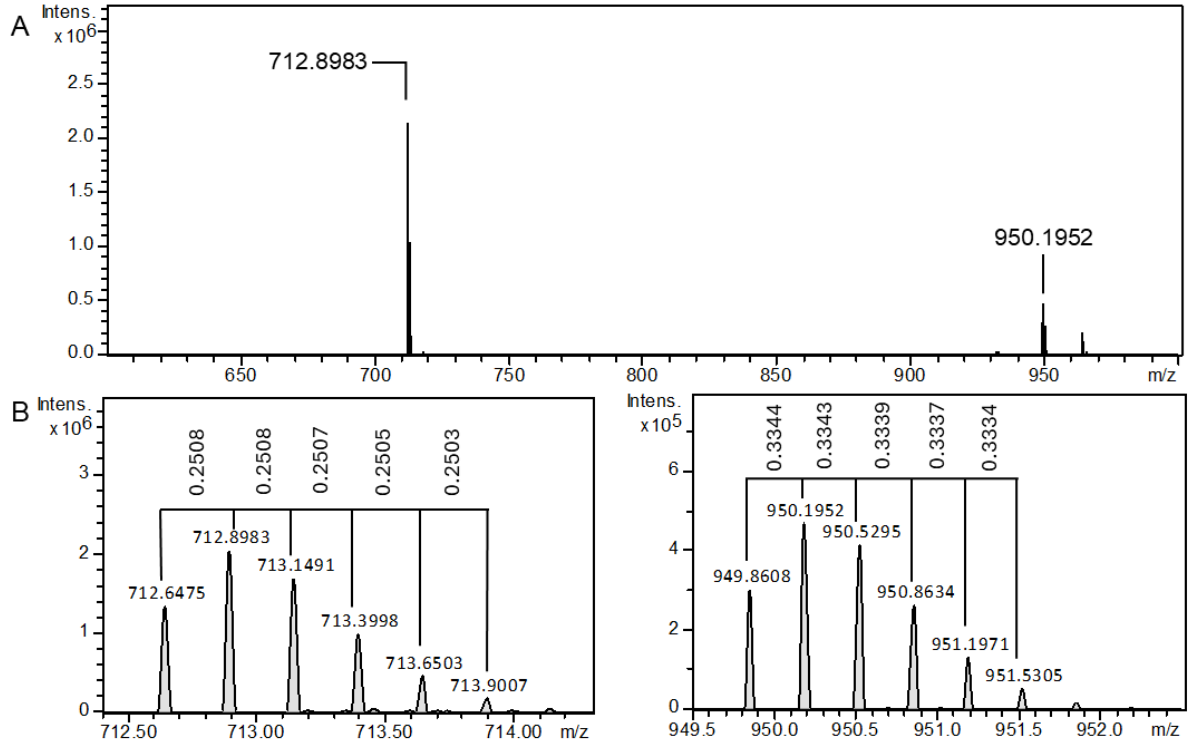

Figure 27: A) Mass spectrum of impurities at 17.2 minutes from HPLC-MS analysis (Experimental section 6.1.4.). B) Spacing of 712.9 and 950.2-signal.

The spacing between the monoisotopic peaks is 0.25 and 0.33, respectively (Figure 27B), indicating that the 712.9 signal is quadruple positively charged, while the 950.2 signal is triple positively charged.

Using the SmartFormula tool within DataAnalysis software (Version 4.2), the sum formulae for these signals were calculated (Table 1).

Table 1: Selected calculated sum formulae for 712.9 and 950.2-signal. Calculated with SmartFormula tool within DataAnalysis software (Version 4.2).

Measured *m/z*	Calc. ion formula	Measured *m/z*	Calc. ion formula
712.8983	$C_{69}H_{133}N_{23}O_{96}S^{4+}$	950.1952	$C_{69}H_{132}N_{23}O_{96}S^{3+}$
712.8983	$C_{67}H_{121}N_{37}O_{86}S^{4+}$	950.1952	$C_{76}H_{197}N_{82}O_{35}S^{3+}$
712.8983	$C_{65}H_{109}N_{51}O_{76}S^{4+}$	950.1952	$C_{82}H_{124}N_{25}O_{85}S^{3+}$

The calculated sum formulae show high nitrogen contents, suggesting these compounds may be composed of amino acids, with the presence of sulfur likely indicating a cysteine residue. Given their high *m/z*-values and corresponding sum formulae, these impurities are presumed to be larger peptides.

The peptide amide **25** is formed from chemical decomposition and therefore its signal with a *m/z*-value of 541.2416 is a reliable indicator for the decomposition of epifadin (**24**). In Figure 26A only a small signal of **25** is observed in the recorded chromatograms, indicating that the sample contained mainly intact epifadin (**24**). This finding is further supported by the UV chromatogram (Figure 26B), which shows absorption peaks at 381–385 nm. Five signals with relatively high intensity are observed in the tandem MS spectrum (Figure 26C). The signal with the *m/z*-value of 541.2416 can be assigned to the peptide amide **25**. Chemical formulae were determined using the SmartFormula tool within DataAnalysis software (Version 4.2). Analysis of the determined formulae and the corresponding *m/z*-values revealed two main fragments of epifadin (**24**). One fragment is proposed to be the acyl cation (**24-Frag 1**) of the peptide residue, and the other fragment is an amine (**24-Frag 2**) with the chemical formula $C_{25}H_{33}N_2O_5^+$ (Figure 28).

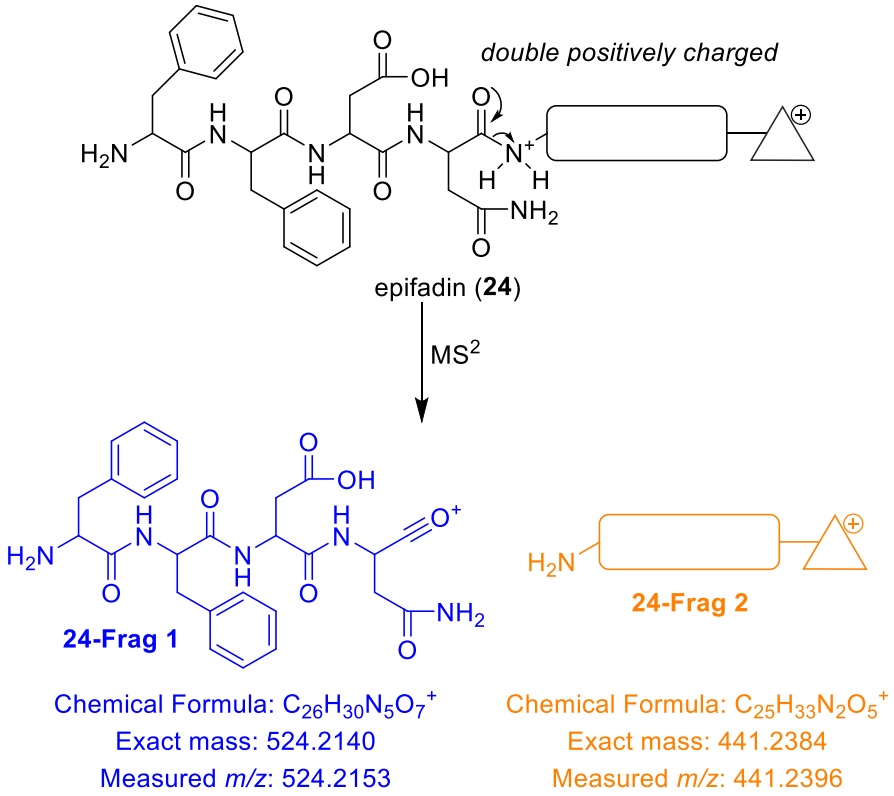

Figure 28: Two main fragments of epifadin (**24**), resulting from tandem MS fragmentation. The peptide bond in **24** is broken to form **24-Frag 1** and the amine **24-Frag 2** with the chemical formula $C_{25}H_{33}N_2O_5^+$.

The fragmentation of the peptide amide **25** is known from N. SCHILLING's work[88] (Figure 13) and was confirmed by finding further specific signals in the tandem mass spectrum of epifadin (**24**, Figure 29).

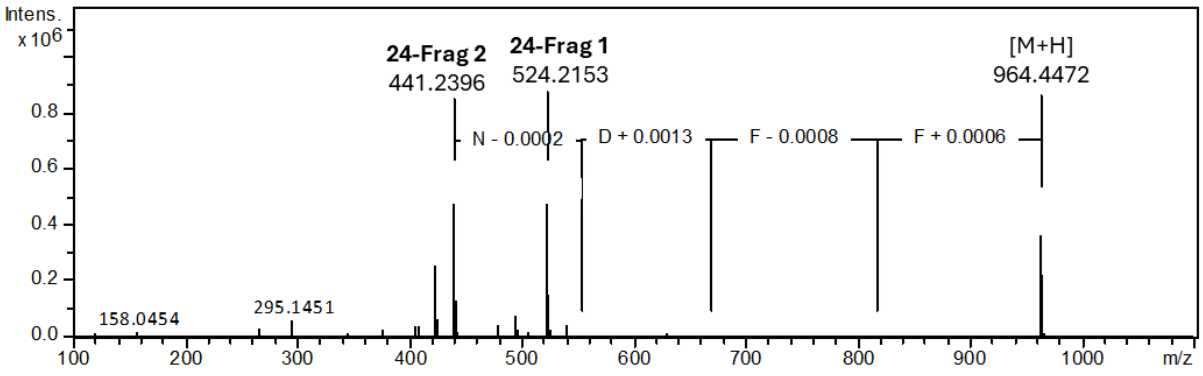

Figure 29: Tandem MS spectrum of epifadin (**24**, positive mode experimental section 6.1.4.). One-letter code was used for amino acids. N = asparagine, D = aspartate, F = phenylalanine.

Fragmentation of the protonated adduct of epifadin (**24**) reveals the amino acid sequence within the peptide moiety. Initially, two phenylalanine residues are cleaved, followed by the sequential loss of one aspartate and one asparagine residue, resulting in the base peak **24-Frag 2** in the tandem MS spectrum. However, the ion intensities for each amino acid loss are relatively low (Figure 29).

*UV-spectrum of epifadin (**24**)*

The chemical formula given for the eastern part of epifadin (**24**) indicates that the structure contains at least one amino acid derived functionality, and the ratio of carbon to hydrogen implies a highly unsaturated structure, such as a polyene. Polyenes often exhibit characteristic absorptions, which are dependent on the length of the polyene system. The higher the number of conjugated double bonds, the more absorption maxima shift to longer wavelengths.[96] In addition, various residues that are directly or indirectly attached to a polyene system can significantly influence the UV absorption by shifting absorption bathochromically (towards longer wavelengths) or hypsochromically (towards shorter wavelengths).[96] Since mass spectrometric data did not provide further structural insights for **24-Frag 2**, the UV spectrum of epifadin (**24**) was analyzed in more detail. Given that the peptide amide **25** does not exhibit any absorption above 280 nm, the higher wavelengths of the UV spectrum of epifadin (**24**) provide information about the chromophore of **24-Frag 2**. For this purpose, reference substances were measured to facilitate a comparison with the UV spectrum of epifadin (**24**). The reference substances used included militarinone C (**28**), amphotericin B (**29**), and the synthetically produced MCA17-1 (**30**).

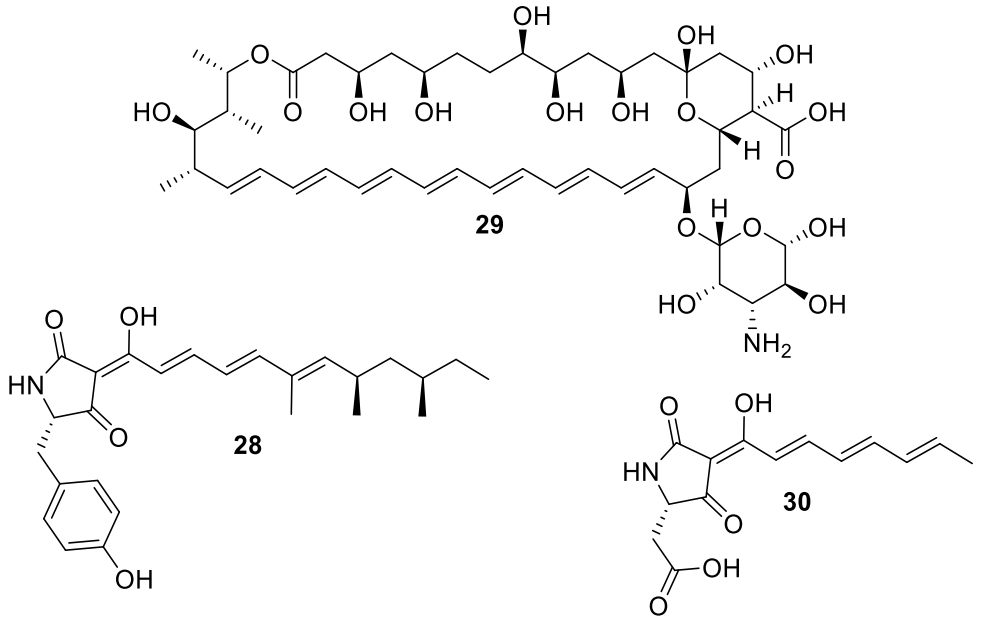

The UV spectra of epifadin (**24**), militarinone C(**28**)[1], amphotericin B (**29**) and synthetic MCA17-1 (**30**) were recorded using a HPLC-ESI-MS equipped with a DAD (Experimental section 6.1.4.) (Figure 30).

[1] We thank Prof. Dr. M. HAMBURGER for an authentic sample of militarinone C

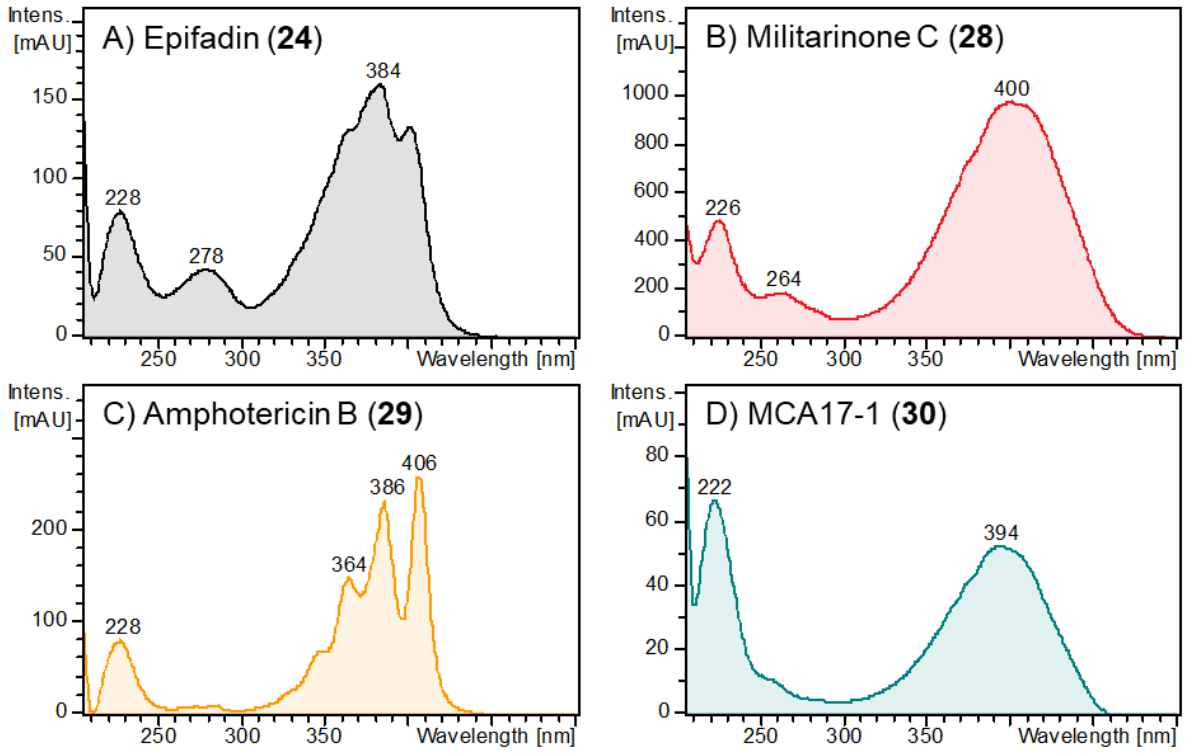

Figure 30: UV spectra (λ = 205 nm to 500 nm) of A) epifadin (**24**, grey), B) militarinone C (**28**, red), C) amphotericin B (**29**, orange) and D) MCA17-1 (**30**, green) are shown.

A comparison of the UV spectra (Figure 30) shows that all four compounds exhibit similar absorption spectra. However, the heptaene **29** displays distinctly sharper UV absorption bands between 350 nm and 450 nm (Figure 30C) compared to epifadin (**24**) and the 3-polyenoyltetramic acids **28** and **30**. The tetramic acids militarinone C (**28**) and MCA17-1 (**30**), each display one broad absorption band between 350 nm and 450 nm, whereas epifadin (**24**) shows a broad band with resolved tips within this range. Furthermore, epifadin (**24**) and militarinone C (**28**) display an absorption maximum between 260 nm and 280 nm, which is absent in the UV spectra of amphotericin B (**29**) and MCA17-1 (**30**). The presence of this maximum in epifadin (**24**) is likely due to its two phenylalanine residues, as determined from the peptide amide **25** structure, while militarinone C (**28**) exhibits a similar feature due to its tyrosine residue.[97]

Given that the heptaene **29**, with its seven conjugated double bonds, shows absorption maxima above 400 nm, it is likely that epifadin (**24**) has fewer than seven double bonds, as it does not exhibit this specific absorption feature. The UV spectra of tetramic acids **28** and **30** each display one broad peak between 340 and 450 nm, with maximum absorption around 400 nm. The broad absorption above 300 nm in the UV spectrum of epifadin (**24**), with distinct peaks within this region, may suggest a structure combining polyene and 3-polyenoyltetramic acid moieties. Epifadin's maximum

absorption occurs at 384 nm, suggesting fewer conjugated double bonds than **29** in the polyene moiety but likely at least two to three double bonds within its tetramic acid moiety. In conclusion, **24-Frag 2** likely contains less than seven conjugated double bonds in its polyene moiety and two to three conjugated double bonds in its tetramic acid moiety.

*Biosynthetic gene cluster (BGC) of epifadin (**24**)*

In recent years, software tools such as AntiSMASH have been increasingly used to identify and characterize new compounds by interpreting BGCs[98], an approach also applied in this work to interpret the BGC of epifadin (**24**, Figure 15) by the KRISMER/PESCHEL group.

It is known that the peptide amide **25** forms after decomposition of epifadin (**24**) and its amino acid sequence agrees with the prediction of AntiSMASH. However, the A_1-domain is responsible for the iterative incorporation of two phenylalanine residues in L- and D-configuration, respectively (Figure 15). Furthermore, the A_4-domain is predicted to be specific for the adenylation of a small amino acid with a hydrophobic side chain, such as glycine, alanine, or valine (Figure 15). Since the chemical decomposition of epifadin (**24**) leads to the formation of peptide amide **25** and no specific fragmentation pattern for a fifth amino acid is found in tandem MS, the fifth amino acid of NRPS I is assumed to be altered in the PKS assembly line. In the NRPS II, the A_5-domain is predicted to incorporate aspartate, which is presumed to be in the L-configuration due to the absence of an epimerase (Figure 15). The PKS modules contain KR- and DH-domains, which together are responsible for the introduction of double bonds. This again indicates that the eastern part of epifadin (**24**) likely contains a highly unsaturated structure. The PKS domain organization suggests that only two malonyl-CoA extender units are incorporated (Figure 15). Each malonyl-CoA unit extends the PKS chain by two carbon atoms (Figure 9B). Given that **24-Frag 2** (*m/z* = 441.2396, given formula: $C_{25}H_{33}N_2O_5^+$) incorporates at least two amino acids, one being aspartate ($C_4H_7NO_4$) and the other likely a small hydrophobic amino acid such as alanine ($C_3H_7NO_2$), the PKS chain length can be approximated by subtracting the number of carbon atoms contributed by these amino acids, resulting in a formula with 18 C atoms. This suggests that the PKS may incorporate up to nine malonyl-CoA extender units. This phenomenon of PKS is already known as stuttering, where the same module is used iteratively in biosynthesis.[99] Additionally, an unusual

C-domain (Figure 15) in the hybrid PKS-NRPS II gene EfiE suggests potential for macrocyclization or DIECKMANN condensation reactions. These reactions could lead to the formation of a tetramic acid (5-membered ring), similar to the biosynthesis of malonomycin (**19**), or to a pyridone moiety (6-membered ring), as observed in kirromycin (**31**) (Figure 31).[78, 94, 100]

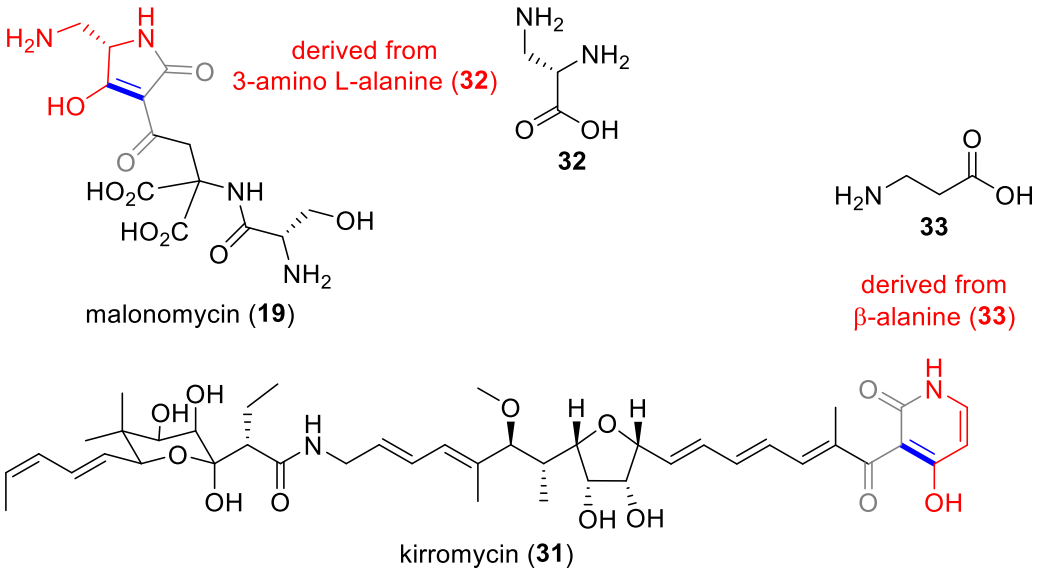

Figure 31: Structures of malonomycin (**19**), kirromycin (**31**), 3-amino L-alanine (**32**) and β-alanine (**33**). Amino acids incorporated in biosynthesis are highlighted in red, β-ketoamide moieties from PKS are highlighted in grey, bold blue bonds indicate C-C bond formed after DIECKMANN condensation reactions.

In malonomycin (**19**) biosynthesis the C-domain catalyzes a DIECKMANN condensation reaction between 3-amino L-alanine (**32**) and the β-ketoamide moiety of the PKS product, forming a 5-membered ring.[78] In contrast, in kirromycin (**31**) biosynthesis the C-domain facilitates a DIECKMANN condensation reaction that results in a 6-membered ring due to the incorporation of a β-amino acid rather than a α-amino acid.[100]

To gain deeper insights into the formation of the tetramic acid moiety catalyzed by the unusual C domain (Figure 15), a comprehensive MS-fragmentation analysis of epifadin (**24**) was conducted. Particular attention was given to the **24-Frag 2** ion (*m/z* = 441.2396), which provides critical information about the structural features of the molecule. Tandem mass spectra (Figure 32) of epifadin (**24**) were recorded using high-performance liquid chromatography coupled with electrospray ionization mass spectrometry (HPLC-ESI-MS). The experimental setup and conditions are detailed in section 6.1.4. These results are fundamental to elucidating the chemical structure of the eastern fragment **24-Frag 2** and to propose a biosynthetic pathway of epifadin (**24**).

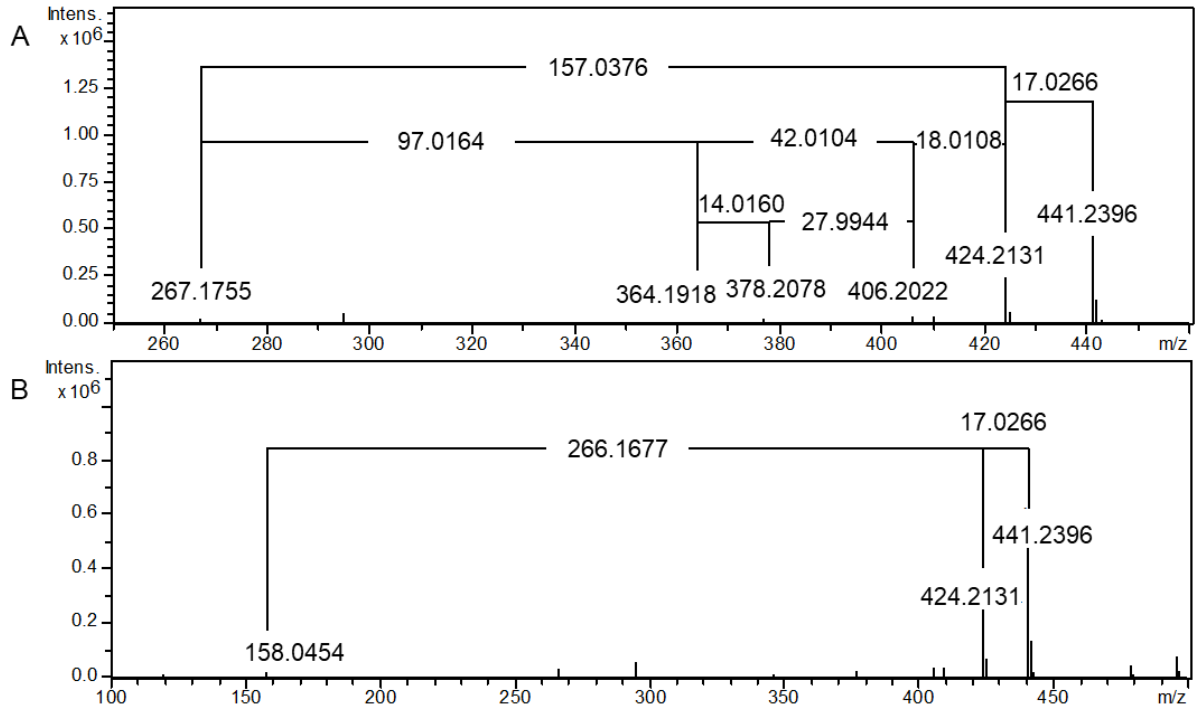

Figure 32: Tandem mass spectra of epifadin (**24**, *m/z* 964.4472) were acquired using HPLC-ESI-MS (positive mode, experimental section 6.1.4.). Selected *m/z* values were highlighted. A) Neutral losses resulting in the daughter ion with *m/z* = 267.1755. B) Neutral losses leading to daughter ion with *m/z* = 158.0454.

A detailed analysis of the tandem mass spectrum suggests that the initial fragmentation likely involves the neutral loss of an ammonia molecule (17.0266 Da), resulting in a fragment ion with *m/z* = 424.2131 (Figures 32A and 32B). Alternatively, epifadin (**24**) may fragment into the peptide amide **25** and a fragment with *m/z* = 424.2131, corresponding to the calculated sum formula $C_{25}H_{30}NO_5^+$ (Figure 33). Subsequent neutral losses of water (18.0108 Da) and carbon monoxide (27.9944 Da) suggest the presence of a carboxyl group (Figure 32A). A potential neutral loss of a carbene group (CH_2, 14.0157 Da) was observed, indicating cleavage of a CH_2 moiety. However, assuming a tetramic acid structure, this fragmentation could alternatively correspond to the neutral loss of ketene (C_2H_2O, 42.0106 Da), leading to a daughter ion with *m/z* = 364.1918. Based on this observation, a plausible fragmentation pathway can be proposed (Figure 33).

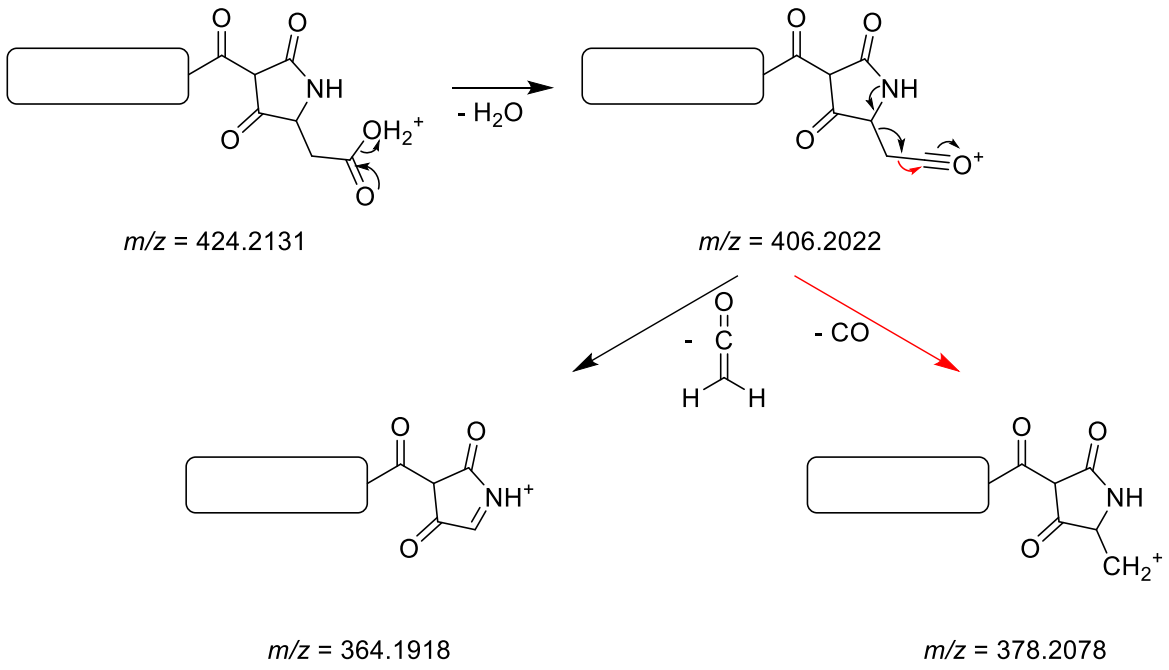

Figure 33: Proposed fragmentation pathway of the eastern part of epifadin (**24**) derived from tandem mass spectra obtained using HPLC-ESI-MS (experimental section 6.1.4.). The rectangle with rounded corners represents the PKS part of epifadin (**24**).

The tandem mass spectrum (Figure 32A) reveals a neutral loss of 5-hydroxy-3*H*-pyrrol-3-one (97.0164 Da), resulting in a daughter ion **24-Frag 3** with an *m/z* value of 267.1755. The calculated sum formula for this ion ($C_{19}H_{23}O^+$) further indicates a highly unsaturated structure due to its low carbon-to-hydrogen ratio (Figure 34).

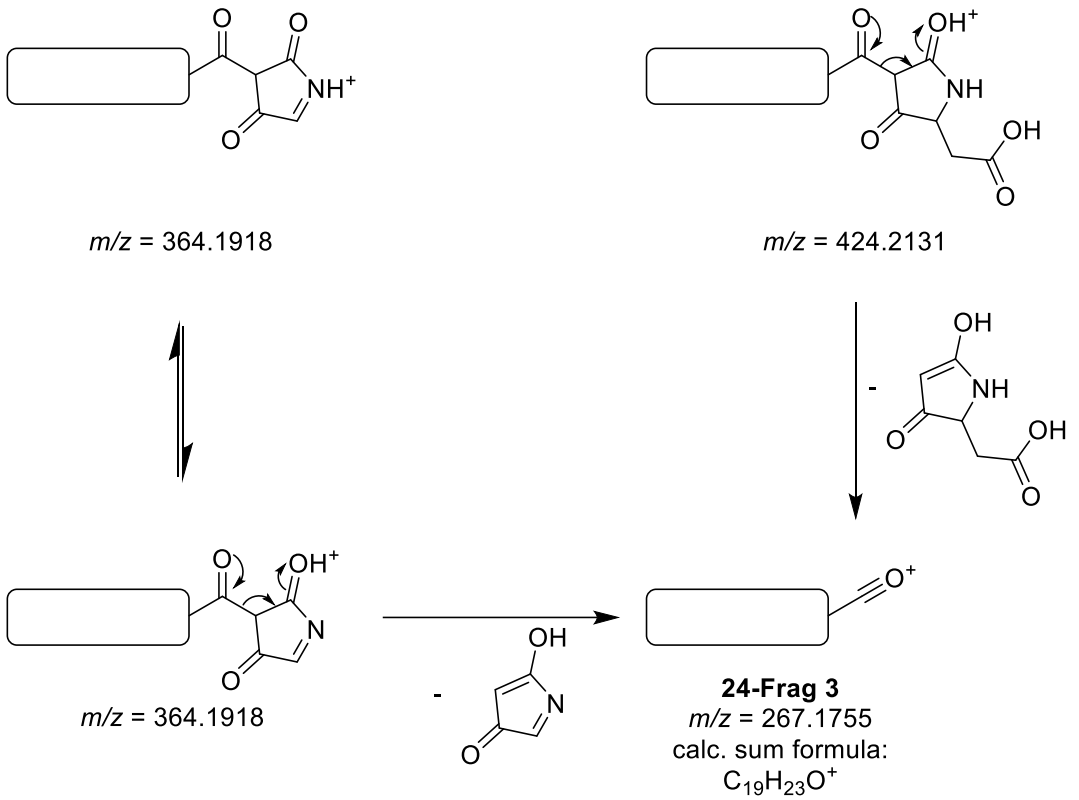

Figure 34: Proposed fragmentation pathways of fragment with *m/z* 364.1918 leading to the formation of the daughter ion **24-Frag 3** with an *m/z* value of 267.1755. The rectangle with rounded corners represents the PKS part of epifadin (**24**).

Additionally, the tandem mass spectrum (Figure 32A) reveals the potential for a neutral loss of 2-(5-hydroxy-3-oxo-2,3-dihydro-1*H*-pyrrol-2-yl)acetic acid (157.0376 Da), which would directly yield the daughter ion **24-Frag 3** with an *m/z* value of 267.1755. The proposed fragmentation pathways are depicted in Figure 34.

This observation would not have been detected without the use of a high-resolution mass spectrometer. A distinct peak at *m/z* = 267.1502, exhibiting greater intensity, was observed, likely due to the longer ion lifetime. In the absence of high-resolution mass spectrometry, this peak would have been indistinguishable from the signal at *m/z* = 267.1755. The ion with *m/z* = 267.1502 is attributed to a daughter ion generated during the fragmentation of the peptide moiety in epifadin (**24**) (Figure 35).

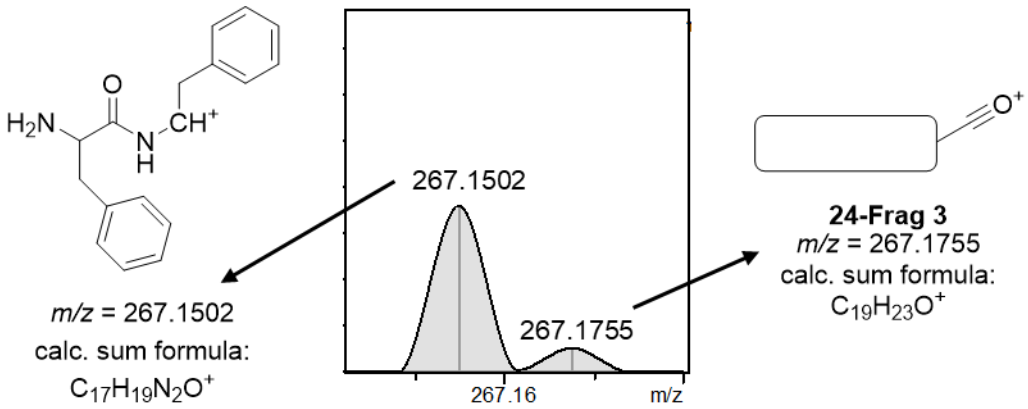

Figure 35: Distinction between the signals at *m/z* = 267.1502 and *m/z* = 267.1755 in the tandem mass spectrum of epifadin (**24**).

Furthermore, a neutral loss of **24-Frag 3** (266.1677 Da) is observed in the tandem MS spectrum (Figure 32B), yielding the daughter ion **24-Frag 4** (*m/z* = 158.0454). The UV spectra (Figure 30), which suggested a polyenoyl tetramic acid moiety in epifadin (**24**), imply that at least two or three (*enol*-form) conjugated double bonds are present in the tetramic acid moiety. Based on this information, the following fragmentation pathway can be proposed (Figure 36).

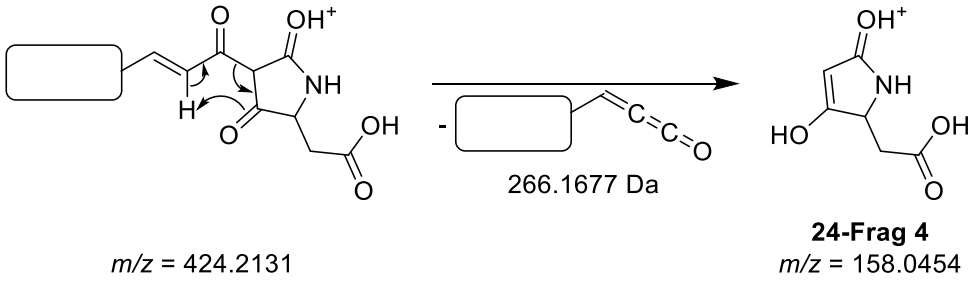

Figure 36: Proposed fragmentation pathway of *m/z* 424.2131 leading to the formation of the daughter ion **24-Frag 4** with an *m/z* value of 158.0454.

In the HPLC-ESI-MS analysis conducted in negative ionization mode (see experimental section 6.1.4), further evidence supporting this observation was obtained. A doubly negatively charged ion corresponding to epifadin (**24**) was detected in the mass spectrum (Figures 37A and 37B), which can be attributed to the presence of two carboxylic acid groups: one in the peptide moiety from the aspartate residue and the other in the tetramic acid moiety. Additionally, a signal with *m/z* = 156.0299 was identified, corresponding to the negatively charged **24-Frag 4** ion, along with a signal at *m/z* = 439.2235, which corresponds to the negatively charged **24-Frag 2** ion (Figure 37C).

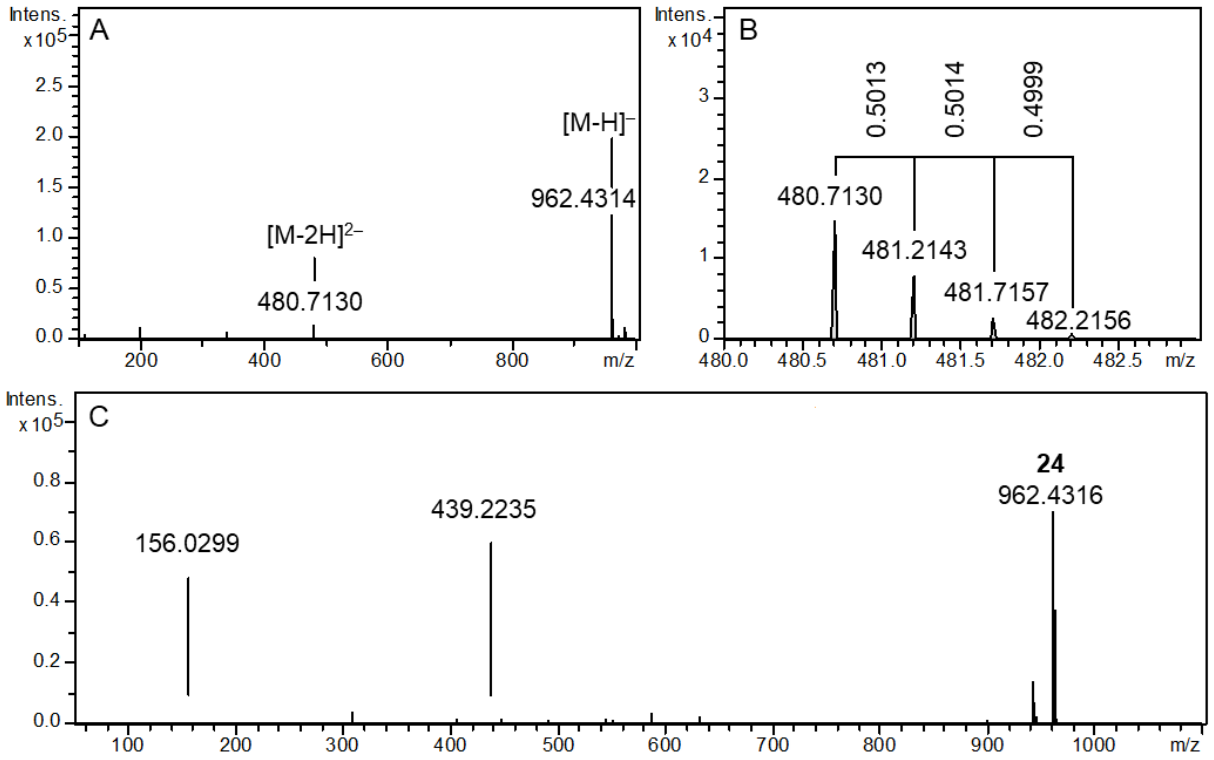

Figure 37: A) Mass spectrum of epifadin (**24**, experimental section 6.1.4., ESI negative mode). Quasimolecular ions of epifadin (**24**) are highlighted. B) Spacing of 480.7130 signal. C) Tandem mass spectrum of epifadin (**24**, experimental section 6.1.4., ESI negative mode).

In conclusion, the detailed MS analysis suggests that epifadin (**24**) likely contains a tetramic acid moiety. We hypothesize that it is biosynthetically formed via a DIECKMANN condensation reaction, presumably catalyzed by the atypical C-domain (Figure 38). This key structural feature is consistent with the proposed biosynthetic pathway, where the unusual C-domain facilitates the cyclization reaction to form the tetramic acid scaffold. Given the absence of an epimerase domain within the BGC, the incorporated aspartate is likely in the L-configuration.[94]

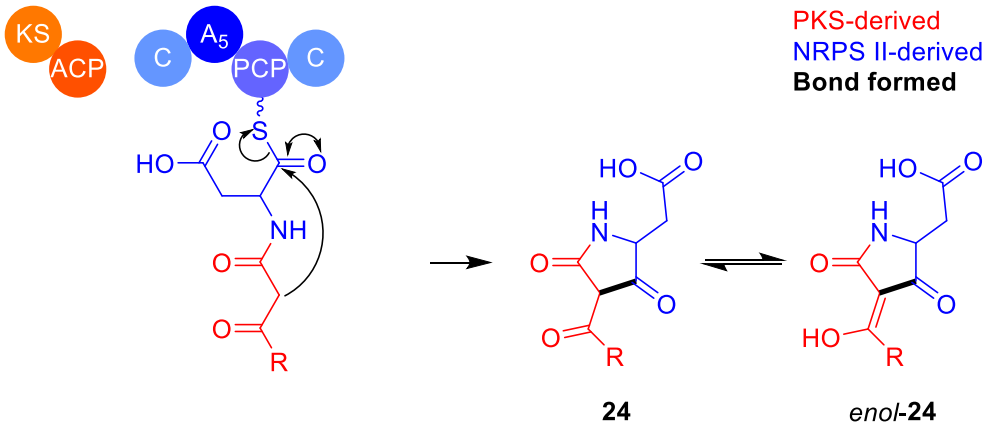

Figure 38: Possible formation of tetramic acid moiety in epifadin (**24**) via DIECKMANN condensation reaction and subsequent *keto-enol* tautomerism. R = NRPS I and PKS residue.

NMR spectroscopic characterization and analysis

Nuclear Magnetic Resonance (NMR) spectroscopy is a non-destructive analytical technique that enables the correlation of NMR-active nuclei with their chemical environment. The resulting spectral data facilitate precise structural elucidation. Both one-dimensional and two-dimensional NMR experiments can be employed, allowing for in-depth structural characterization and comprehensive analysis of molecular architectures. Due to the instability of epifadin (**24**), specific precautions are required to minimize or prevent its decomposition. To achieve this, inert deuterated DMSO and argon as protective gas were employed. Following purification and freeze-drying, the obtained voluminous yellow powder was immediately transferred to a glovebox with argon atmosphere[2], where it was dissolved in absolute deuterated DMSO and subsequently transferred into a J. YOUNG NMR tube. This setup ensured oxygen- and moisture-free conditions for the acquisition of NMR spectra. This allowed comprehensive 1D- and 2D-NMR studies which, together with previous NMR recordings, revealed the challenging structure of the new antimicrobial peptide polyene epifadin (**24**).[94]

The ^{1}H NMR spectrum (Figure 39) exhibits distinct chemical shift regions corresponding to various protons within the molecule: peptide backbone protons (9.10–6.60 ppm), aromatic protons (7.30–6.90 ppm), olefinic protons (6.80–5.70 ppm), H^{α} protons (4.90–3.90 ppm) and aliphatic protons (3.00–0.80 ppm).

[2] We thank Prof. Dr. IVANA FLEISCHER for providing us access to the glovebox.

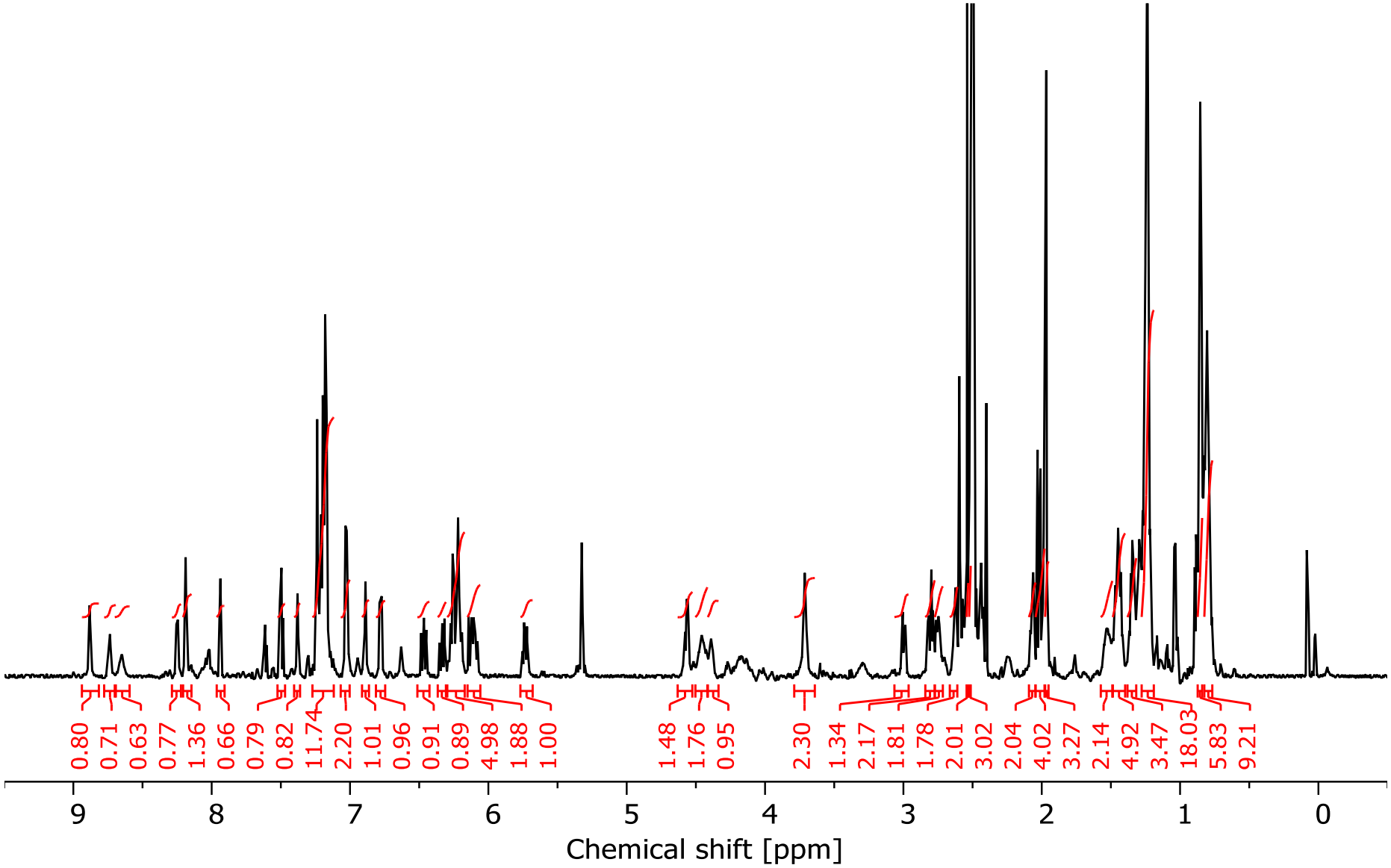

Figure 39: ^{1}H NMR spectrum of epifadin (**24**) in DMSO-d_6 (700 MHz, 30°C). Integrals of signals are depicted in red. The assignment is shown in Table 3 and 4.

*NMR signal assignment for the peptide moiety in epifadin (**24**)*

Initially, the peptide amide **25** was synthesized via SPPS, and its NMR spectra were recorded. Peptide backbone and aromatic protons were assigned first by comparing the chemical shifts of epifadin (**24**) with those of peptide amide **25** through spectral overlay (Figure 40).[94]

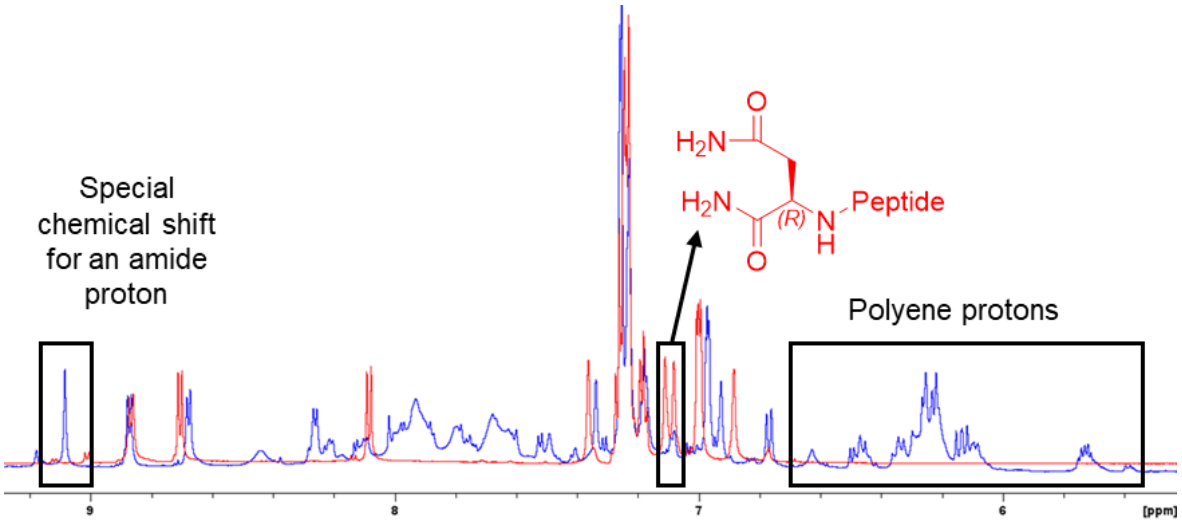

Figure 40: Overlay of ^{1}H NMR spectra (DMSO-d$_6$, 700 MHz, 30°C) of epifadin (**24**, blue) and peptide amide **25** (red) in the region of 9.20–5.40 ppm, with key differences highlighted.

The spectral overlay highlights features observable in the ^{1}H NMR spectrum of epifadin (**24**). These include a distinct chemical shift for an amide proton at 9.08 ppm, the absence of two singlet signals corresponding to amide protons in the asparagine amide moiety, and signals attributed to olefinic protons within the range of 6.70–5.60 ppm. MS analysis (Figure 28) indicates that a highly unsaturated residue is attached to the amide in the asparagine moiety, which may account for the absence of these singlet signals. Additionally, the downfield shift of the amide proton signal could be due to an anisotropic effect from a nearby double bond, potentially directly attached to the nitrogen. A similar downfield chemical shift for an amide proton (9.14 ppm) has been observed in the case of bacillaene (**18**), where a polyene moiety is directly attached to the nitrogen of the amide group (*N*-vinylamide moiety, Figure 41), suggesting that the anisotropic effect of the conjugated system influences the chemical shift of the amide proton in both compounds.[101]

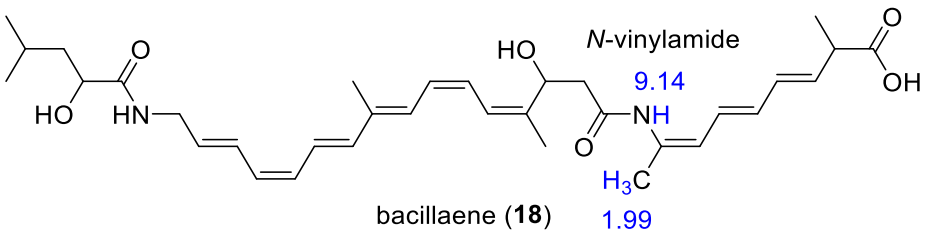

bacillaene (**18**)

Figure 41: Bacillaene (**18**) with assigned chemical shifts (blue) for selected protons in *N*-vinylamide moiety.

Furthermore, the α-H protons and aliphatic protons of the peptide moiety were assigned using 2D NMR spectra (Figures 97–102, experimental data 6.4.3.), which provided detailed correlation data, allowing for the assignment of these protons within the peptide moiety (Figure 42), despite partial overlap with the DMSO solvent signal in the aliphatic region. Additionally, the spectra revealed a methyl group attached to the polyene chain, exhibiting a chemical shift analogous to that observed in bacillaene (**18**, Figure 41), thereby further corroborating the proposed structure.[94]

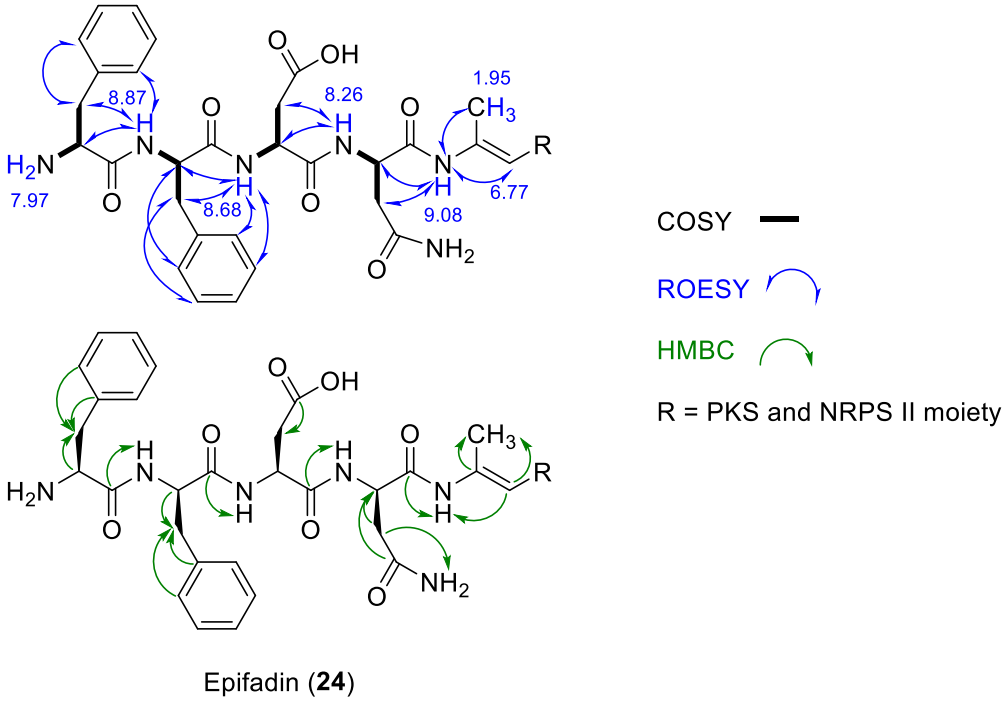

Epifadin (**24**)

Figure 42: Key correlations deduced from 2D NMR experiments. Chemical shifts of protons are given in blue numbers.

*NMR signal assignment for the polyene moiety in epifadin (**24**)*

With the connectivity between the peptide amide and the polyene moiety established, the remaining structure of the polyene moiety was elucidated using 2D NMR spectroscopy, particularly utilizing COSY correlations and spatial coupling interactions. The Nuclear Overhauser Effect (NOE) depends on the correlation time (influenced by molecular weight) and exhibits distinct behavior across molecular sizes. For small molecules, the NOE is positive; for medium-sized molecules, it approaches zero; and for large molecules, it becomes negative.[102] Given that epifadin (**24**) is a medium-sized molecule, the NOE is theoretically near zero, resulting in the absence of observable correlation peaks in the NOESY spectrum. Consequently, the ROESY experiment was chosen over the NOESY experiment, as the Rotating-Frame Overhauser Effect (ROE) in ROESY experiments is always positive and provides equivalent structural information, overcoming the limitations associated with the NOE for medium-sized molecules.

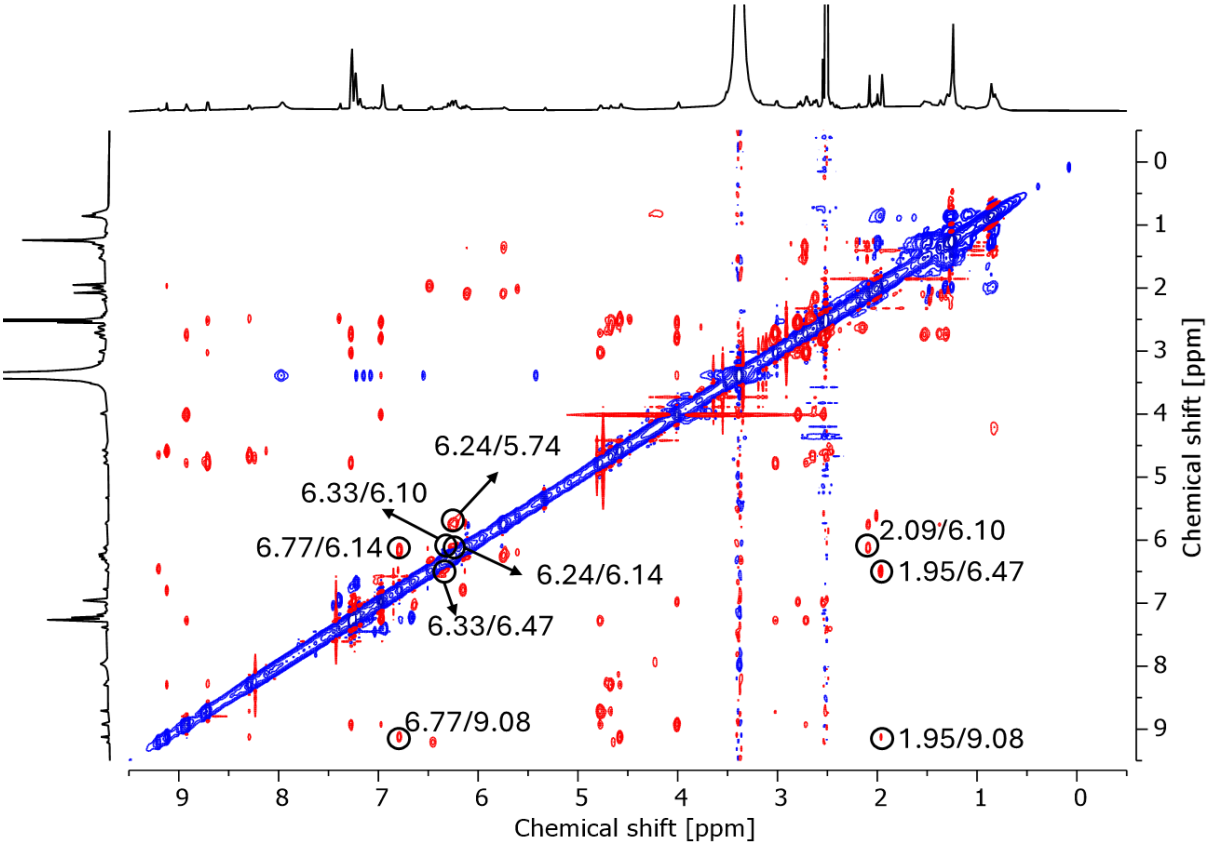

Figure 43: ^{1}H,^{1}H-ROESY spectrum of epifadin (**24**, DMSO-d_6, 700 MHz, 30°C). Key correlations for the polyene moiety in epifadin (**24**) are highlighted.

^{1}H,^{1}H-COSY (Figure 97, experimental data 6.4.3.) and ^{1}H,^{1}H-ROESY experiments (Figure 43, Figures 100 and 102 experimental data 6.4.3.) enabled the systematic assignment of proton signals, from the peptide moiety to the fully *trans*-configured

polyene moiety (Figure 44) through a sequential walkthrough of proton NMR signals. The COSY experiment provided key through-bond correlation data, while the ROESY experiment revealed important through-space interactions. This combination of techniques allowed for an unambiguous and comprehensive mapping of proton signals, offering critical insights into the full structural arrangement of epifadin (**24**).[94]

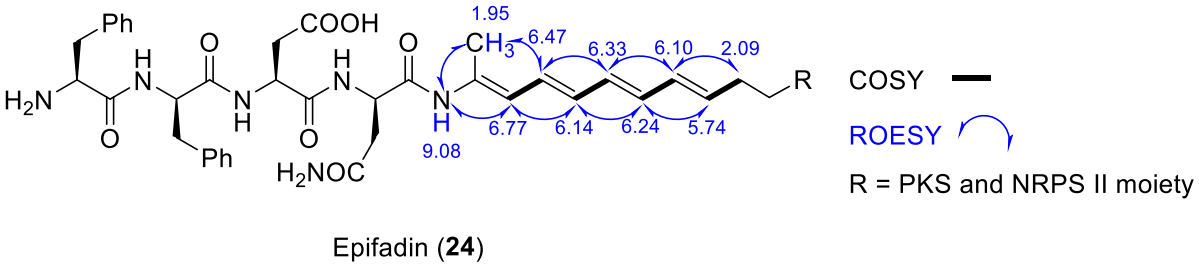

Epifadin (**24**)

Figure 44: Key correlations derived from ^{1}H,^{1}H-COSY and ^{1}H,^{1}H-ROESY experiments. Proton chemical shifts are indicated in blue.

The 2D NMR experiments reveal that the polyene moiety in epifadin (**24**) comprises four conjugated double bonds, consistent with the UV spectrum of epifadin (Figure 30). Additionally, a distinct cross-peak between 5.74 ppm and 2.09 ppm indicates that the carbon chain continues with sp^3-hybridized carbon atoms. If the chain extended with sp^2-hybridized carbons, the corresponding chemical shift (2.09 ppm) would appear significantly more downfield due to the anisotropic effects of the double bonds. However, due to overlap with impurities such as fatty acids, as indicated by the large signal around 1.26 ppm (attributable to CH_2 groups of fatty acids, Figure 39), the assignment in this region is not unambiguous. It is therefore assumed that the carbon chain remains saturated up to the polyenoyl-tetramic acid moiety.[94]

*NMR signal assignment of the polyenoyl-tetramic acid moiety in epifadin (**24**)*

In certain instances, polyenoyl-tetramic acids have been reported to lack detectable ^{13}C NMR signals for the carbon positions 4, 5 and 6, a phenomenon that poses significant challenge for the structural elucidation of the tetramic acid moiety.[103] This absence of signals can complicate the assignment of the carbon framework and hinder the detailed characterization of the compound. The most likely explanation for this observation is *keto-enol* tautomerism (Figure 12A), where the equilibrium between the *keto* and *enol* forms of the tetramic acid results in shifting of electron density away from certain carbon positions.

Due to the instability of epifadin (**24**) and the low yields obtained during purification, acquiring high-quality ^{13}C NMR spectra proved challenging. Consequently, while

$^{1}H,^{13}C$-HMBC and $^{1}H,^{13}C$-HSQC experiments were successfully performed to assign the structure of the tetramic acid moiety, the ^{13}C NMR data were of limited quality and did not provide conclusive support for the full carbon assignment. Nevertheless, the key correlations obtained from the $^{1}H,^{13}C$-HMBC and $^{1}H,^{13}C$-HSQC spectra (Figures 98 and 99, experimental data 6.4.3.) were crucial in assigning the structure of the tetramic acid moiety (Figure 45) and in corroborating the overall molecular structure of epifadin (**24**).[94]

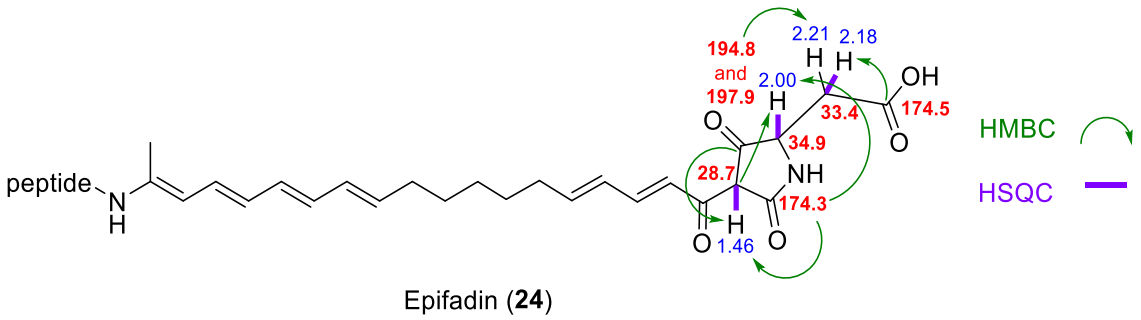

Epifadin (**24**)

Figure 45: Key correlations for tetramic acid moiety derived from $^{1}H,^{13}C$-HSQC and $^{1}H,^{13}C$-HMBC experiments. Proton chemical shifts are indicated in blue, while carbon chemical shifts are shown in red.

Based on the 2D NMR data, the *keto* form of epifadin (**24**) is presumed to be the dominant species. However, some unusual proton chemical shifts, notably at 1.46 ppm and 2.00 ppm, suggest the presence of alternative connectivity. The assignment of signals in the aliphatic region was challenging due to overlap with the DMSO solvent and impurities, such as fatty acids. Additionally, the presence of both an amino group and carboxylic acids in epifadin (**24**) raises the possibility of ionic interactions promoting a cyclic conformation (Figure 46).

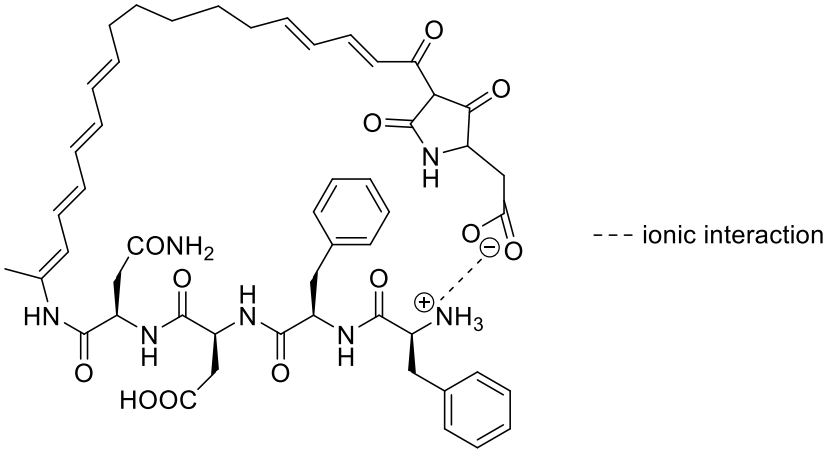

Epifadin (**24**)

Figure 46: Proposed cyclic conformation of epifadin (**24**) driven by ionic interactions.

This could bring the aromatic residues of the peptide moiety in close proximity to the tetramic acid moiety, potentially explaining the unusual chemical shifts at 1.46 ppm and 2.00 ppm due to anisotropic effects from the aromatic side chains.

Despite the challenges in acquiring ^{13}C NMR data, the 1D and 2D NMR experiments provided a comprehensive structural elucidation of epifadin (**24**). Carbon chemical shifts were determined through HSQC and HMBC spectra. The complete list of ^{1}H NMR and ^{13}C NMR signals is provided in Tables 3 and 4 (in experimental section 6.4.3).[94]

*Confirmation of N-vinylamide moiety in epifadin (**24**) through mass spectrometry*

The presence of an *N*-vinylamide (enamide) moiety in epifadin (**24**), as revealed by NMR analysis, is further supported by evidence from the tandem mass spectrum (Figure 26C) and the AntiSMASH prediction for the A_4-domain (Figure 15). AntiSMASH predicts the incorporation of a small lipophilic amino acid, such as glycine, alanine, or valine. Based on these predictions, the *N*-vinylamide moiety is presumed to originate from alanine.

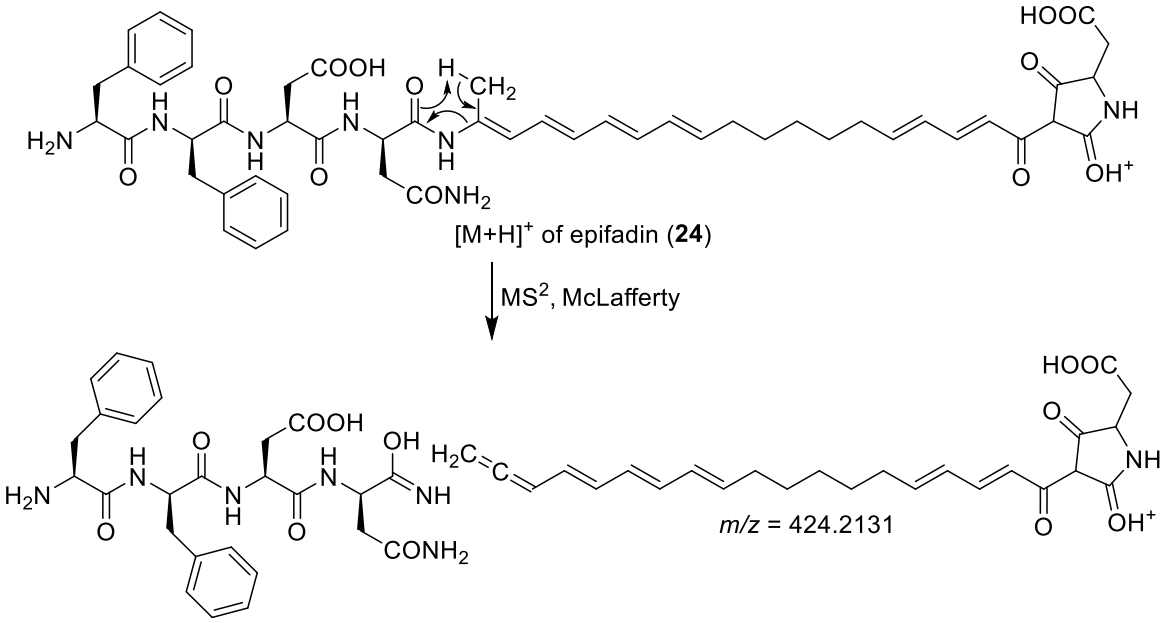

Figure 47: Proposed MCLAFFERTY-like rearrangement observed in HPLC-ESI-MS (positive mode, see experimental section 6.1.4.), resulting in the formation of an allene fragment with *m/z* = 424.2131.

However, in epifadin (**24**), the alanine residue is modified, lacking the carboxyl group and featuring a β,γ-double bond. This type of alanine modification has been previously described in the biosynthesis of bacillaene (**18**).[65, 74] This structural feature allows epifadin (**24**) to undergo a proposed MCLAFFERTY-like rearrangement (Figure 47), resulting in the formation of an allene. The *m/z*-value (424.2131) of the allene

corresponds to the third most abundant signal observed in the tandem mass spectrum (Figure 26C).[94]

*Investigation of the decomposition and reactivity of epifadin (**24**)*

N-vinlyamides (enamides) are known to hydrolyze under aqueous acidic conditions, yielding the corresponding amide (**25**) and carbonyl (**34**) compounds. This reaction likely explains the decomposition of epifadin (**24**) observed in the solvent used for HPLC purification (Figure 19).[104] The rate-determining step involves protonation of the adjacent carbon of **24**, followed by a nucleophilic attack of water (or methanol) on the resulting carbocation. This reaction results in cleavage of the molecule into the amide **25** and the carbonyl compound **34** (Figure 48). However, ketone **34** was not detected by HPLC-ESI-MS or NMR experiments, suggesting it may undergo further degradation under these conditions.

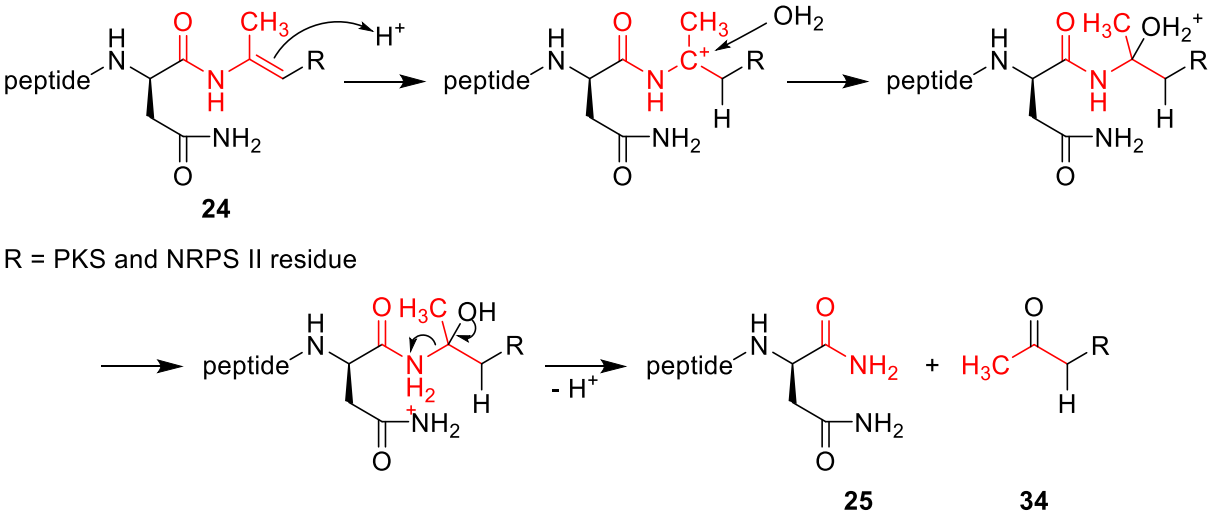

Figure 48: Proposed chemical decomposition of epifadin (**24**) under acidic aqueous conditions. *N*-vinylamide moiety is highlighted in red.

To stabilize epifadin (**24**), various derivatization experiments were conducted, including methylation and acetylation reactions using the precipitate and a purified epifadin (**24**) sample. The use of diazomethane and its less hazardous alternative, (diazomethyl)trimethylsilane resulted in the decomposition of epifadin (**24**). However, analysis via HPLC-ESI-MS indicated the formation of methylated peptide amide **35**, with no detection of polyene tetramic acid fragments or analogues thereof. Acetylation using acetic anhydride and pyridine also resulted in the decomposition of epifadin (**24**) and only acetylated peptide amide **36** was found via HPLC-MS (Figure 49).[94]

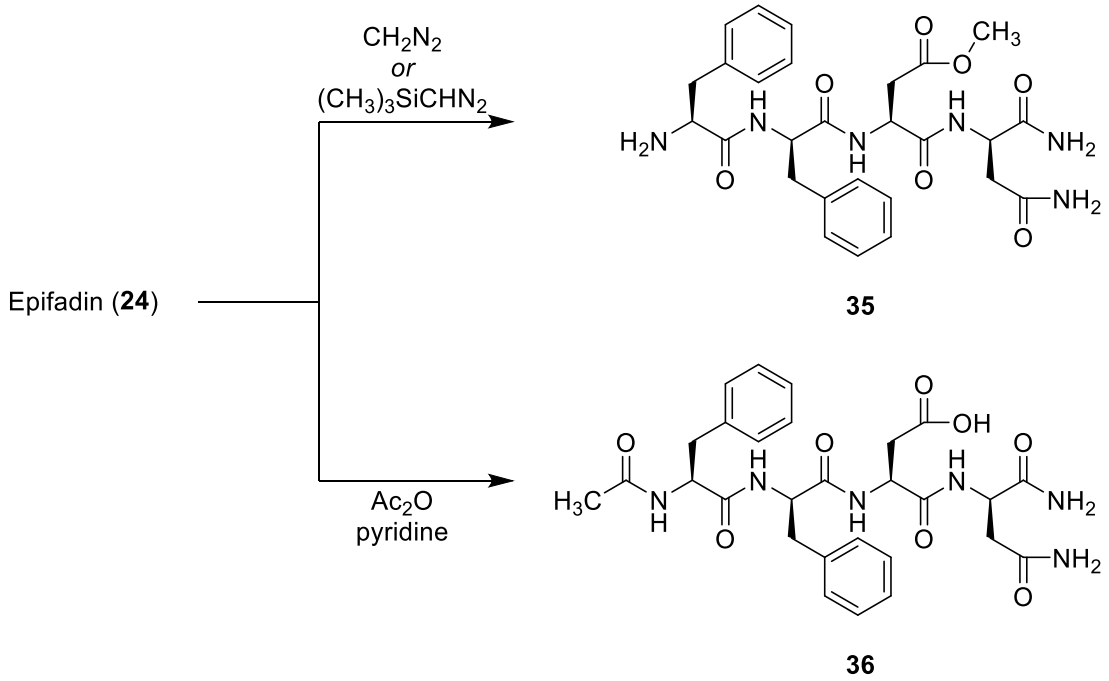

Figure 49: Derivatization approaches to stabilize epifadin (**24**). Methylated and acetylated peptide amides **35** and **36** were found via HPLC-ESI-MS (experimental section 6.1.4.).

Since both a tetramic acid moiety and a 2-pyridone ring could theoretically form through biosynthesis, their differentiation in epifadin (**24**) was pursued by investigating their reactivity in methylation reactions. Specifically, the tetramic acid-containing natural product reutericyclin (**7**) and the 2-pyridone-containing kirromycin (**31**) were subjected to methylation to explore potential differences in behavior. The objective was to confirm whether epifadin (**24**) harbors a tetramic acid moiety rather than a 2-pyridone ring. Methylation of reutericyclin (**7**) using an excess of (diazomethyl)trimethylsilane resulted in decomposition, with no methylated reutericyclin products detected in the reaction mixture by HPLC-ESI-MS analysis (experimental section 6.1.4.). In contrast, under identical conditions, kirromycin (**31**) yielded both mono- and di-methylated products, as determined by HPLC-ESI-MS analysis (experimental section 6.1.4.). These results indicate that the tetramic acid moiety is less reactive toward this methylation approach. Consequently, the comparable reactivity profiles of epifadin (**24**) and reutericyclin (**7**) strongly support the conclusion that epifadin (**24**) contains a tetramic acid moiety rather than a 2-pyridone ring.[94]

Since the derivatization reactions only led to decomposition of epifadin (**24**), different NMR solvents with additives were tested to stabilize epifadin (**24**) in solution. Switching from deuterated DMSO to deuterated acetonitrile or deuterated methanol resulted in a colorless solution and a brown insoluble residue. NMR experiments showed that the

colorless solution did not contain epifadin (**24**) but rather oleamide (**27**) (Figure 50), which was confirmed via HPLC-ESI-MS (Figure 22).

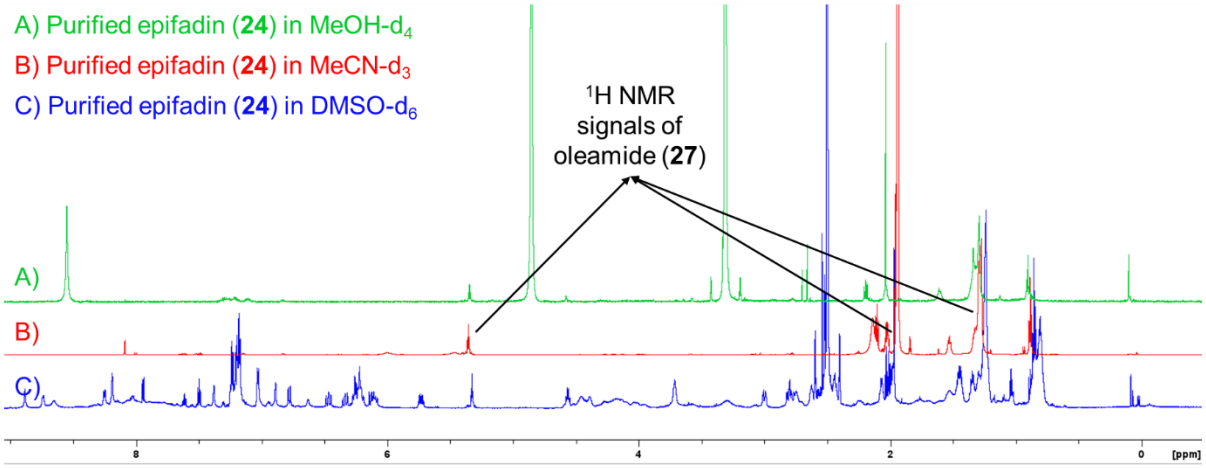

Figure 50: ^{1}H-NMR spectra of epifadin (**24**) in different deuterated solvents (700 MHz, 30°C).

Efforts to enhance the solubility of epifadin (**24**) in methanol or acetonitrile involved the use of formic acid or trifluoroacetic acid as additives. This resulted in quick dissolution of the brown residue and yielded NMR spectra, that could not be analyzed (Figure 51). Since tetramic acids are known to form metal complexes with bivalent cations, such as Zn^{2+} and Mg^{2+}[105], the brown residue was resolved in deuterated methanol with zinc(II) chloride as additive. However, this approach also resulted in highly unresolved spectra (Figure 51).[94]

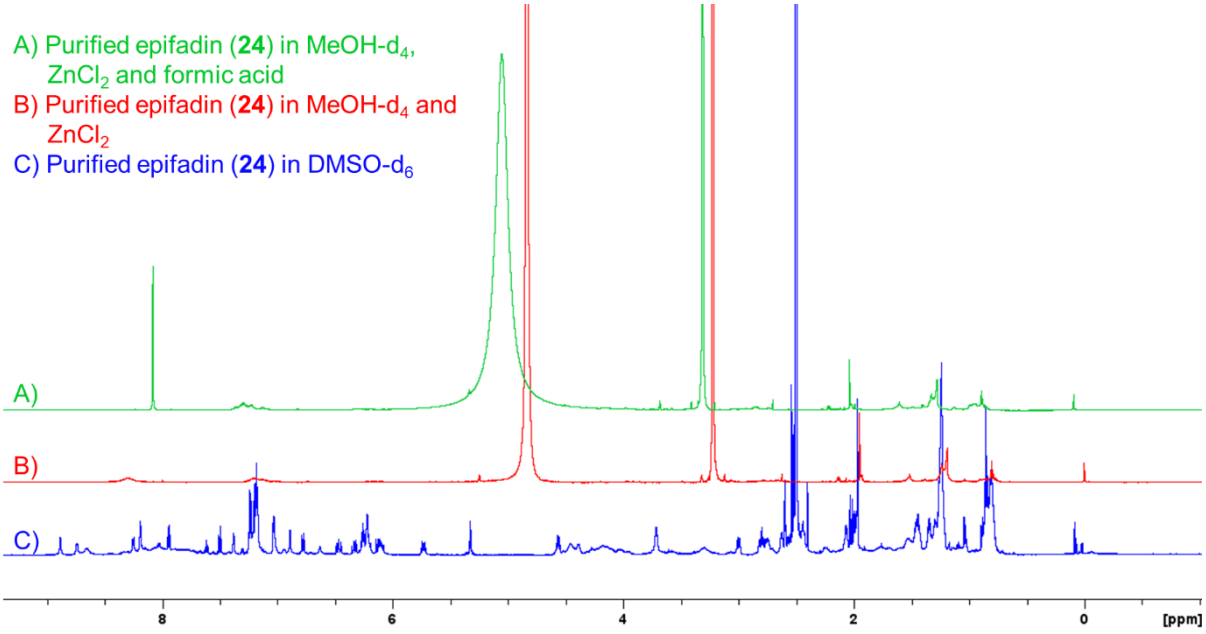

Figure 51: ^{1}H-NMR spectra of epifadin (**24**) in different deuterated solvents and additives (700 MHz, 30°C).

In conclusion, the proposed structure of epifadin (**24**) is in accordance with mass spectra, UV spectra, NMR spectra, chemical reactivity and bioinformatic data. The proposed biosynthesis of epifadin (**24**) is depicted in Figure 52.[94]

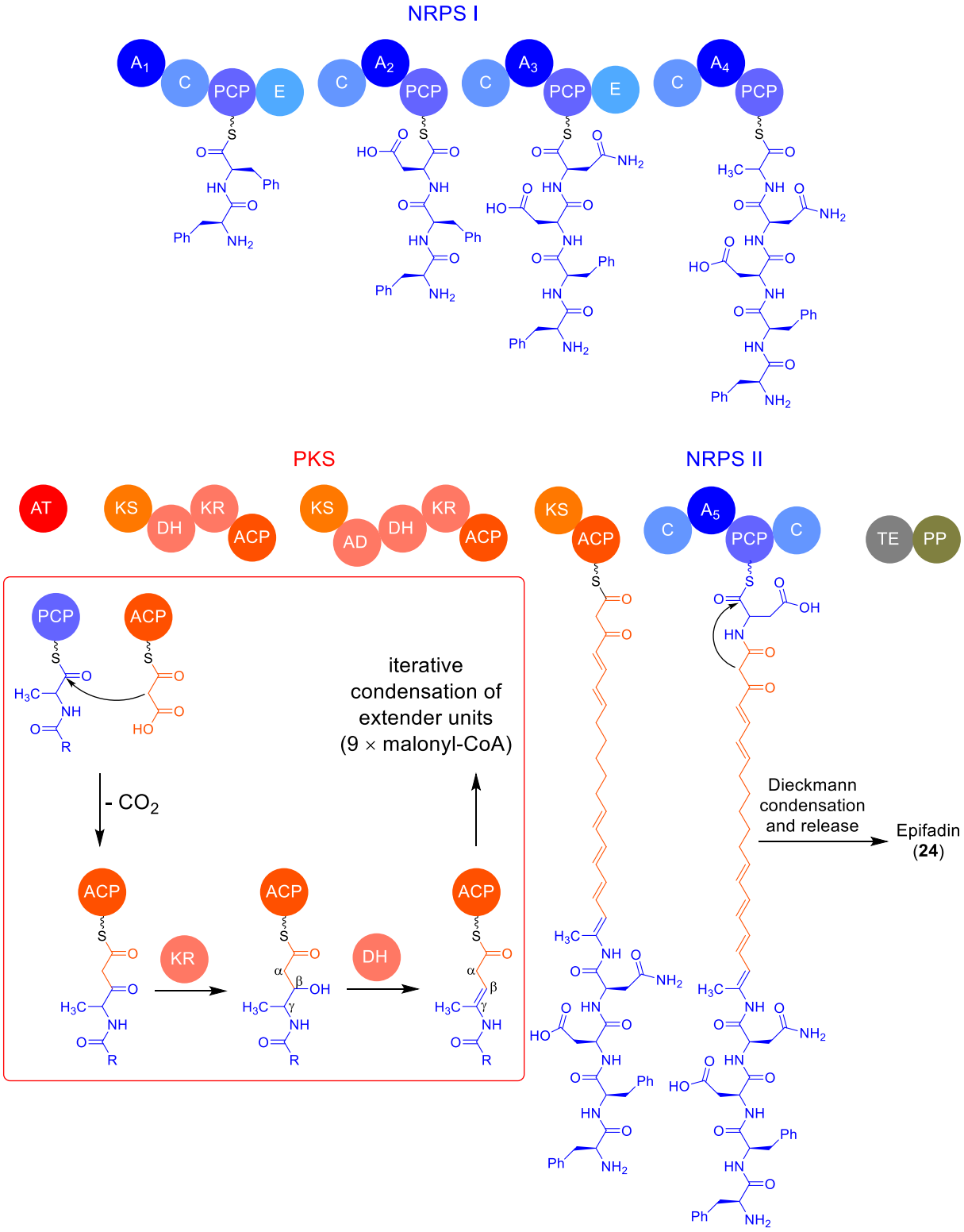

Figure 52: Proposed biosynthesis of epifadin (**24**). Blue structures derived from NRPS, orange structures derived from PKS, R = NRPS I residue.

3.1.3. Synthesis and stereo configuration of NRPS I peptide fragment **25**

N. SCHILLING demonstrated that the synthetic peptide amide **25** exhibited identical retention times to the natural peptide amide derived from decomposition of epifadin (**24**). This observation, combined with bioinformatic data, strongly suggests that the L-Phe-D-Phe-L-Asp-D-Asn configuration of synthetic amide **25** corresponds to that of the natural peptide amide.

To unambiguously confirm the absolute stereo configuration and to conduct a comprehensive chromatography study in collaboration with CORNELIUS KNAPPE (Research group LÄMMERHOFER), all 16 possible isomers of peptide amide **25** were synthesized using the Fmoc strategy in solid-phase peptide synthesis on a Rink Amide (RAM) resin (Figure 53).

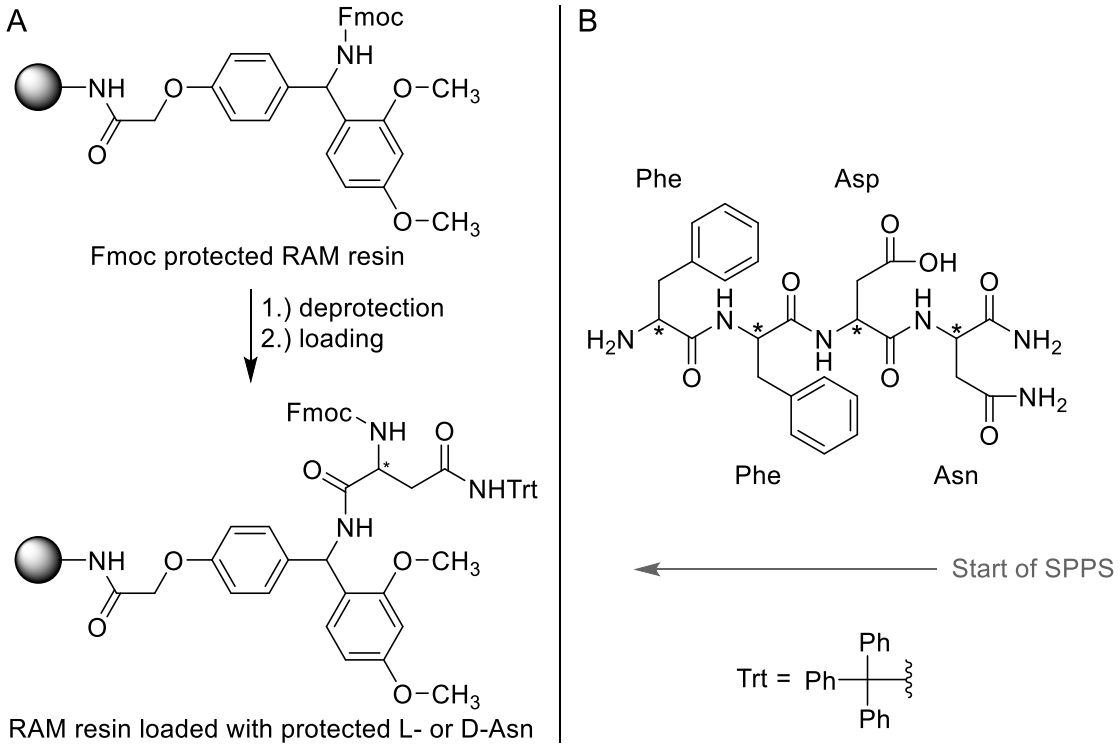

Figure 53: A) Fmoc protected RAM resin with Rink Amide linker and loaded RAM resin with protected starting amino acid. B) Structure of synthetic peptide amides **25** and **37**–**51**. The starting amino acid is L- or D-Asn, respectively. The direction of synthesis is depicted by a grey arrow. Stereocenters are marked with an asterisk.

The RAM resin facilitates the generation of peptide amides through acidic cleavage with TFA. The RAM resin was initially loaded with either L-Asn or D-Asn, followed by a stepwise elongation of the peptide chain. After completing the amino acid sequence, the peptides were cleaved from the solid support and purified via HPLC (see experimental section 6.4.2.1.), yielding the desired peptide amides **25** and **37**–**51** in moderate yields (10–20 mg scale; Figure 53, Table 2).

Table 2: Amino acid (AA) sequences and stereochemical configurations of peptide amides amides **25** and **37**–**51**. Comp. denotes compound.

Comp.	AA sequence and stereoconfiguration	Comp.	AA sequence and stereoconfiguration
25	L-Phe-D-Phe-L-Asp-D-Asn-NH_2	**44**	L-Phe-L-Phe-L-Asp-L-Asn-NH_2
37	D-Phe-D-Phe-D-Asp-D-Asn-NH_2	**45**	D-Phe-D-Phe-D-Asp-L-Asn-NH_2
38	L-Phe-L-Phe-L-Asp-D-Asn-NH_2	**46**	L-Phe-L-Phe-D-Asp-L-Asn-NH_2
39	D-Phe-D-Phe-L-Asp-D-Asn-NH_2	**47**	L-Phe-D-Phe-L-Asp-L-Asn-NH_2
40	D-Phe-L-Phe-D-Asp-D-Asn-NH_2	**48**	D-Phe-L-Phe-L-Asp-L-Asn-NH_2
41	L-Phe-D-Phe-D-Asp-D-Asn-NH_2	**49**	D-Phe-D-Phe-L-Asp-L-Asn-NH_2
42	L-Phe-L-Phe-D-Asp-D-Asn-NH_2	**50**	L-Phe-D-Phe-D-Asp-L-Asn-NH_2
43	D-Phe-L-Phe-L-Asp-D-Asn-NH_2	**51**	D-Phe-L-Phe-D-Asp-L-Asn-NH_2

With this strategy, the formation of aspartimide side products was observed. The formation of aspartimide during SPPS is well known phenomenon, induced by a repeated exposure to bases or strong acids. Subsequent reactions, such as hydrolysis or treatment with piperidine (for Fmoc deprotection) can lead to α- and β-peptides or α- and β-piperidides (Figure 54).[106-110]

Since a mixture of 2,3,4,6,7,8,9,10-octahydropyrimido[1,2-*a*]azepine (DBU) and morpholine in *N*,*N*-dimethylformamide is used for Fmoc deprotection, no piperidide side products were detected after cleavage from the solid support, as confirmed by HPLC-ESI-MS (experimental section 6.1.4.). However, aspartimide formation was observed for all peptide amides **25** and **37**–**51**. Except for the DDDD isomer **37**, where the aspartimide content was determined to be 30% via HPLC-UV (experimental section 6.1.4.), the aspartimide side products were removed by HPLC purification in other cases.

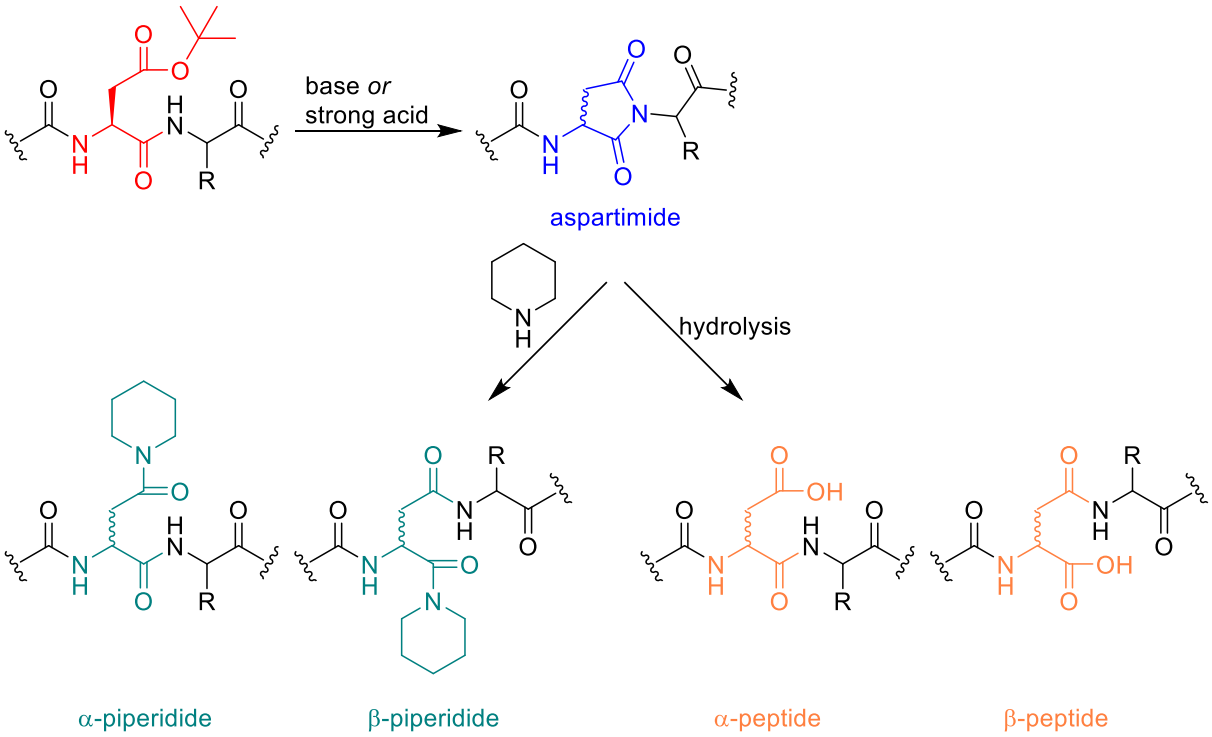

Figure 54: Formation of aspartimides and possible side products in SPPS. Protected L-Asp(O*t*Bu) in peptide chain is depicted in red, epimerized aspartimide moiety is depicted in blue, piperidides in green and peptides from hydrolysis of aspartimide in orange.

Various methods are known to mitigate the formation of aspartimide in SPPS. A straightforward approach involves using bulky esters of the aspartic acid side chain or protection of the amide backbone. Commercially available esters of aspartic acid and bulky alcohols (**52**–**54**), such as 3-methyl-3-pentanol, 3-ethyl-3-pentanol or 5-butyl-5-nonanol are effective but costly solutions.[111] In addition, more complex functional groups such as the cyanosulfurylide moiety (**55**) have also been reported to prevent the formation of aspartimide.[112]

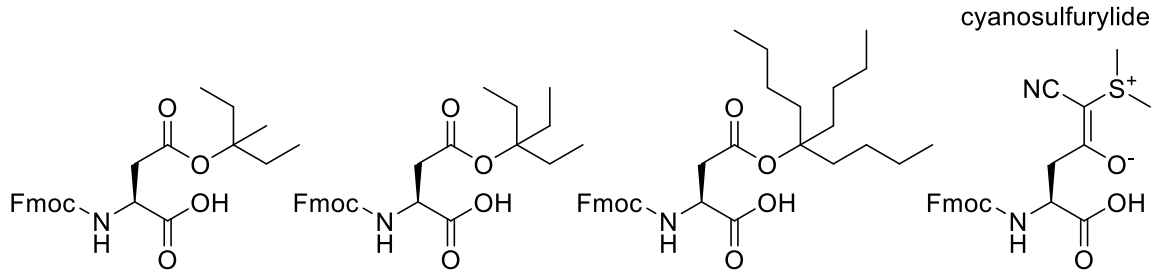

52 **53** **54** **55**

In this work, HPLC purification was sufficient to use the synthesized peptide amides **25** and **37**–**51** as standards in chiral HPLC (Figure 55). In addition, the natural peptide amide was isolated from a decomposed epifadin-sample using RP-HPLC to get an authentic sample.[94]

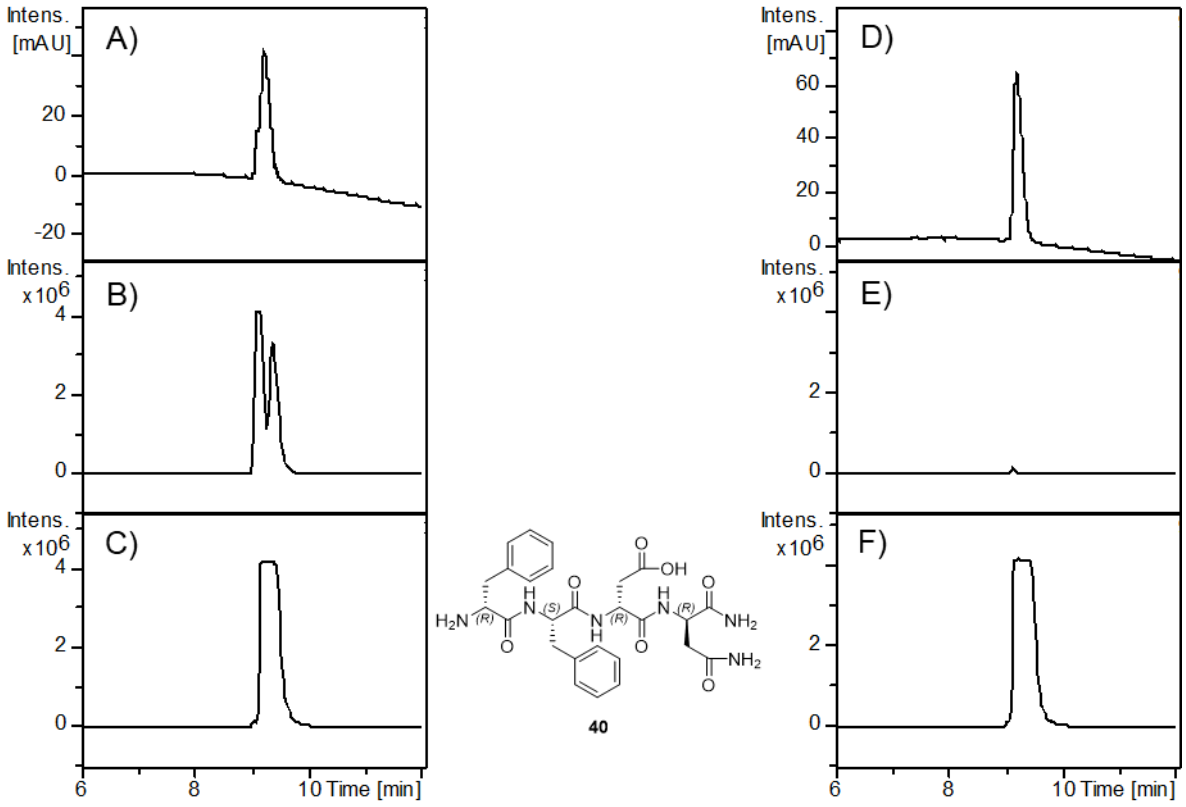

Figure 55: HPLC-ESI-MS analysis (experimental section 6.1.4.) of peptide amide **40** shown as representative example. Before purification: A) UV chromatogram at 220 nm, B) EIC of aspartimide side product ($C_{26}H_{30}N_6O_6$ $[M+H]^+$, *m/z* 523.2300±0.005 Da), C) EIC of peptide amide **40** ($C_{26}H_{32}N_6O_7$ $[M+H]^+$, *m/z* 541.2405±0.005 Da). After purification: D) UV chromatogram at 220 nm, E) EIC of aspartimide side product ($C_{26}H_{30}N_6O_6$ $[M+H]^+$, *m/z* 523.2300±0.005 Da), F) EIC of peptide amide **40** ($C_{26}H_{32}N_6O_7$ $[M+H]^+$, *m/z* 541.2405±0.005 Da).

Before purification, the signal of the aspartimide side product is observable in the extracted ion chromatogram ($C_{26}H_{30}N_6O_6$ $[M+H]^+$, *m/z* 523.2300±0.005 Da, Figure 55B). HPLC purification (experimental section 6.4.2.1.) was then performed, and the fractions containing peptide amide **40** were collected and lyophilized to yield pure peptide amide **40**. The absence of the side product signal in the chromatogram (Figure 55E) confirms the purity of the isolated peptide.

Chiral HPLC columns, such as Nucleodex beta-PM and ReproSil Chiral-NR, were tested under various conditions (Solvent composition, temperature, and flow rate) to separate the LDLD peptide amide **25** and its enantiomer **51**. However, these columns were not suitable for separating a mixture of **25** and **51**. The zwitterionic ion-exchanger columns Chiralpak ZWIX(+) and ZWIX(–), known for their successful separation of chiral zwitterionic small peptides and lipopeptides, were considered.[113, 114] The structure of the stationary phase of the Chiralpak ZWIX(+) column is derived from quinine and has an additional cyclohexane sulphonic acid moiety, which is responsible for the zwitterionic character of the column (Figure 56).[113, 114]

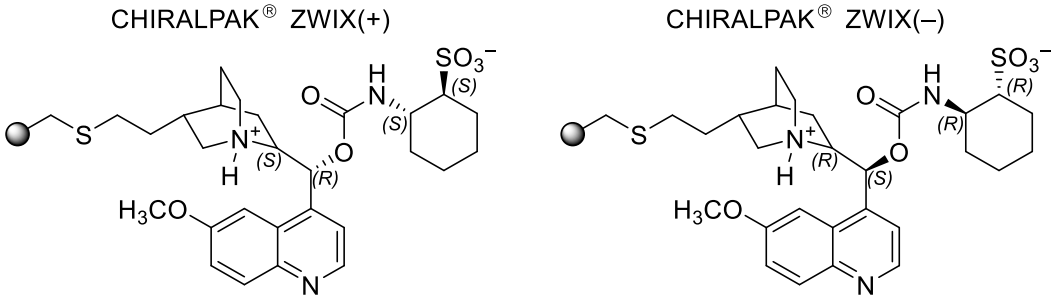

Figure 56: Structures of stationary phases of CHIRALPAK® ZWIX(+) and ZWIX(–).

To unambiguously assign the stereo configuration of the natural peptide amide via two-dimensional HPLC-MS, a collaboration with the research group LÄMMERHOFER was initiated. Initially, one-dimensional chiral HPLC-MS with a Chiralpak ZWIX(+) column (In collaboration with SIMON JAAG from research group LÄMMERHOFER, University of Tübingen) was conducted, analyzing peptide amides **25**, **51** and the isolated natural peptide amide. By comparing the retention times, the LDLD configuration (peptide amide **25**) was confirmed as the correct stereo configuration of the natural peptide amide (Figure 57).[94]

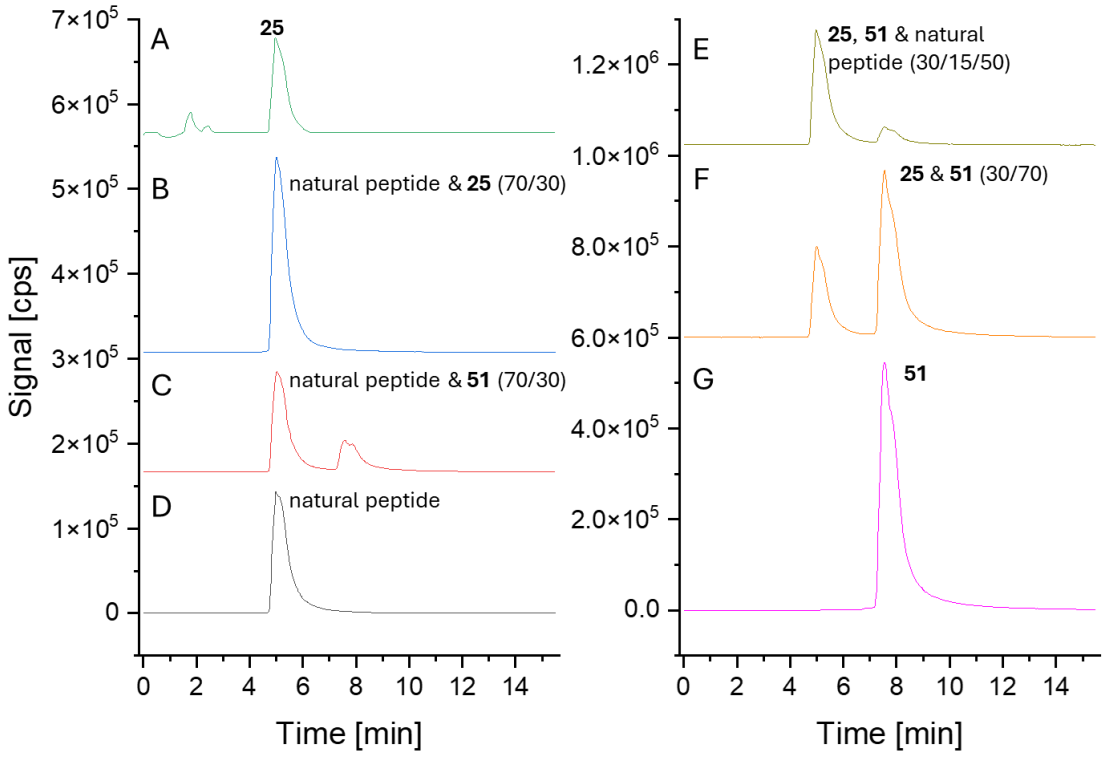

Figure 57: Extracted ion chromatograms (*m/z* = 541.2405±0.05 Da) of the peptide amides. All samples were prepared at a concentration of 0.1 mg·mL^{-1} in ACN/H_2O (v/v, 6/4).

All analytes were prepared at a concentration of 0.1 $mg \cdot mL^{-1}$, initially measured individually, and then analyzed in various binary and ternary mixtures. This approach facilitated the unambiguous assignment of the stereoconfiguration of the natural peptide amide (Figure 57). A more detailed and comprehensive analysis of the peptide amides would involve the use of two-dimensional HPLC techniques, which are increasingly gaining popularity in the field. The development of a method for determining the absolute stereoconfiguration using two-dimensional HPLC, including the analysis of all 16 isomers as well as the natural peptide amide, is an ongoing collaborative project with CORNELIUS KNAPPE from the LÄMMERHOFER research group.

3.1.4. Synthesis towards PKS-NRPS II fragment **64**

Due to its high instability, the total synthesis of epifadin (**24**) is not a practical goal for utilizing the pure compound as an antimicrobial agent. Instead, the focus is on producing core building blocks that can be used in the synthesis of derivatives with eventually higher stability and potentially higher bioactivity. Epifadin's (**24**) unique architecture suggests that both the overall size of the molecule and the individual structural elements, such as the peptide and the tetramic acid moieties, contribute significantly to its bioactivity.

The aim of this work is to synthesize a tetramic acid building block that could facilitate the coupling of various organic compounds via palladium-catalyzed cross-coupling reactions. For this purpose, BRÜCKNER's strategy has been already proven successful in the synthesis of various tetramic acids, such as the lipomycins **20** and **21**[115], militarinones **28** and **56**[103, 116] and pyranonigrins **57** and **58**.[117]

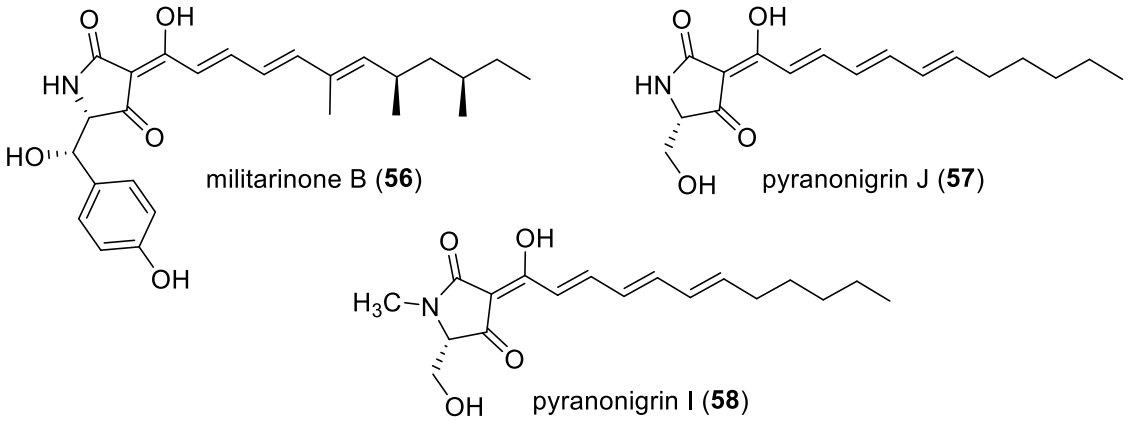

BRÜCKNER's strategy for synthesizing tetramic acids involves three key steps: aminolysis, the STILLE reaction and the LACEY-DIECKMANN cyclization. This strategy begins with the preparation of the bromoalkene building block **61**, which contains the corresponding amino acid with the sidechain R' and serves as the core intermediate (Figure 58). Designed for palladium-catalyzed cross-coupling reactions, this versatile intermediate enables structural modifications through the STILLE reaction. In the second step, the bromoalkene **61** undergoes a STILLE reaction, allowing the introduction of various organic moieties. The final step, the LACEY-DIECKMANN cyclization facilitates the formation of the tetramic acid core **59** by promoting intramolecular cyclization. This step is crucial for generating the characteristic five-membered ring structure of tetramic acids (Figure 58).

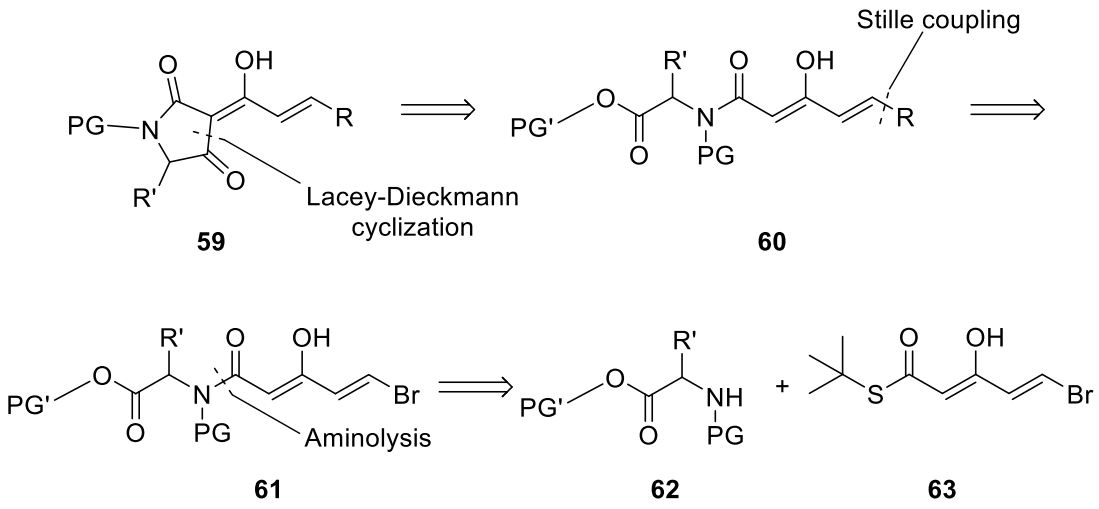

Figure 58: BRÜCKNER's strategy for the synthesis of tetramic acids **59**. PG = protecting group, R = alkenyl residue, R' = amino acid side chain.

In this work the aim is to synthesize the tetramic acid **64**, which would provide further mass spectrometric data to support the tetramic acid moiety in epifadin (**24**) and MCA17-1 (**30**) a potential liver fibrosis inhibitor, which would further emphasize the synthetic flexibility in alkenyl chain length.

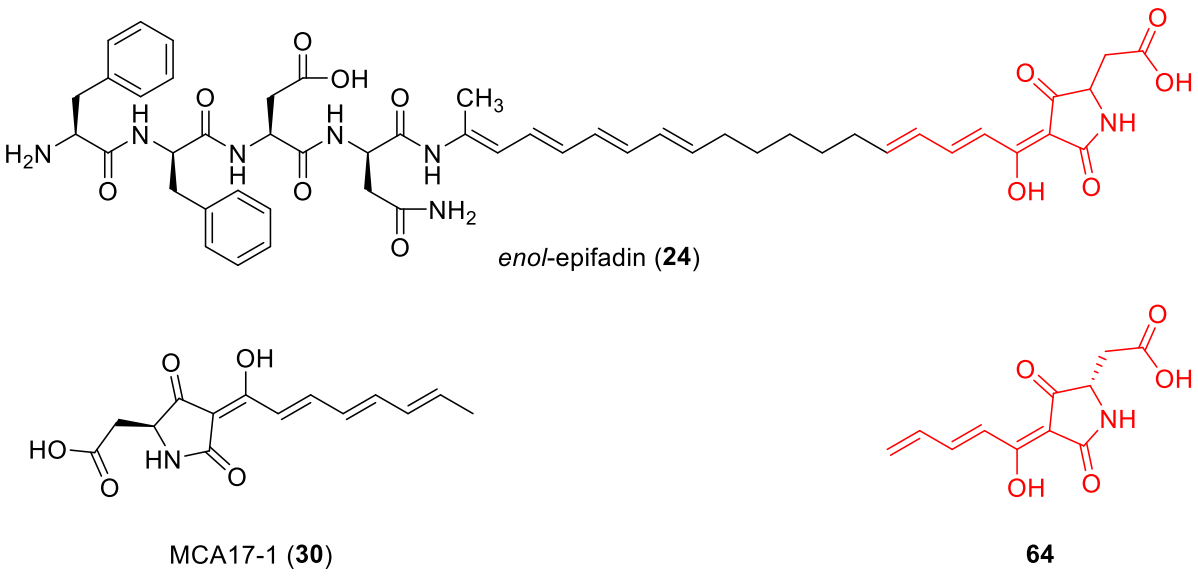

enol-epifadin (**24**)

MCA17-1 (**30**)

64

The retrosynthetic analyses for tetramic acids **30** and **64** are shown in Figure 59, outlining the strategic disconnections leading to their synthesis. Both analyses focus on identifying key intermediates and reaction pathways essential for constructing the characteristic tetramic acid core.

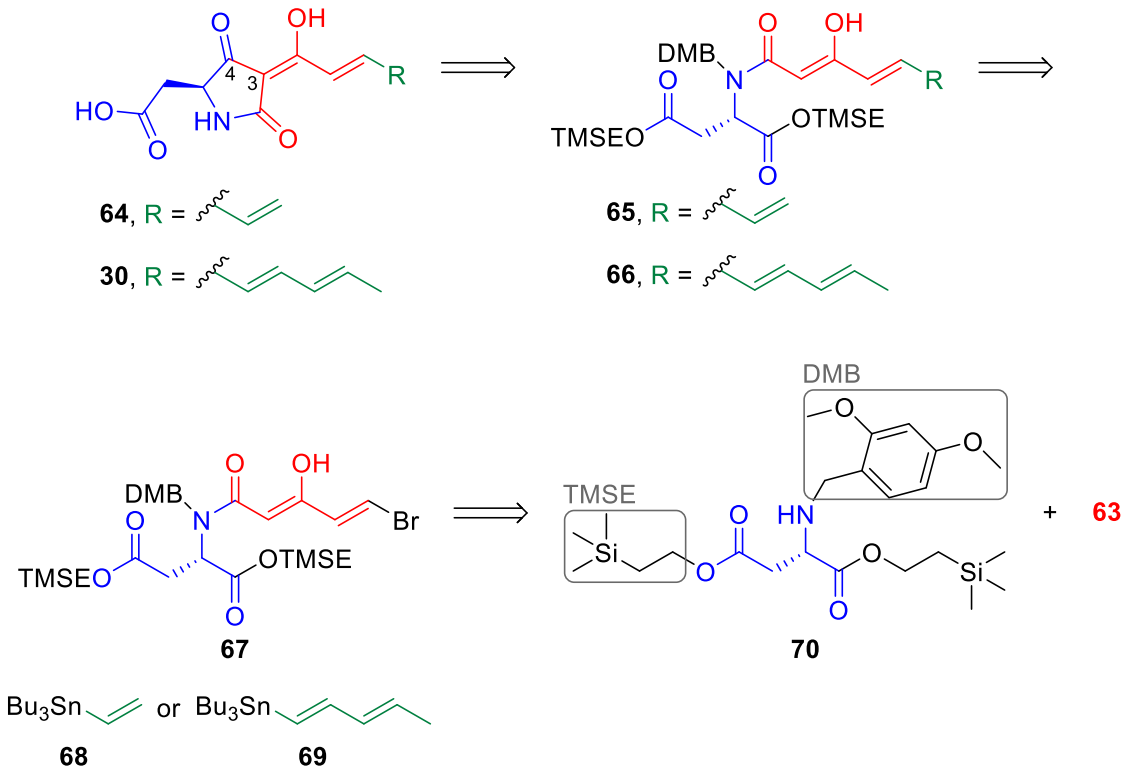

Figure 59: Retrosynthetic analyses of the tetramic acids **30** and **64**. Structural elements from L-aspartate are depicted in blue, structural elements from β-ketothioester **63** are depicted in red, and structural elements from stannanes **68** or **69** are depicted in green.

The C-3–C-4 bond of **30** and **64** should result from LACEY-DIECKMANN cyclizations. The substrates for this reaction are the β-ketoamides **65** and **66**, respectively (Figure 59). The *N*,*N*-disubstituted β-ketoamides **65** and **66** are 1-substituted *trans*,*trans*-butadien and 1,6-disubstituted *trans*,*trans*,*trans*-hexatrien, respectively, which can be synthesized via STILLE reactions using the appropriate tributylstannylated coupling partners **68** or **69** and the bromoalkene **67** (Figure 59). Bromoalkene **67** should result from the aminolysis of protected aspartate **70** and the β-ketothioester **63** (Figure 59). Protected aspartate **70** should result from a STEGLICH esterification of *N*-benzyloxycarbonyl-L-aspartic acid (**80**) with 2-(trimethylsilyl)ethanol and subsequent deprotection of benzyloxycarbonyl protecting group and reductive amination with 2,4-dimethoxybenzaldehyde (**83**). Tributyl(vinyl)tin (**68**) is commercially available and suitable for test reactions, whereas stannane **69** is not commercially available and thus also has to be produced synthetically.

Since the synthesis of aldehyde **71** is well known in the literature and has been described with good yields[118], it should be used as starting material for the synthesis of stannane **69** (Figure 60).

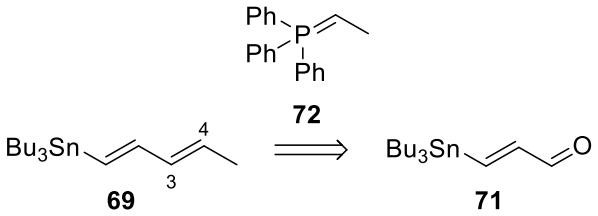

Figure 60: Retrosynthetic analysis of the stannane **69**.

The C-3–C-4 double bond of **69** should result from a WITTIG reaction between aldehyde **71** and ylene **72** (Figure 60). To achieve the *trans* configuration, a SCHLOSSER modification is applied, as the normal WITTIG reaction would produce a *cis* double bond (Figure 61).

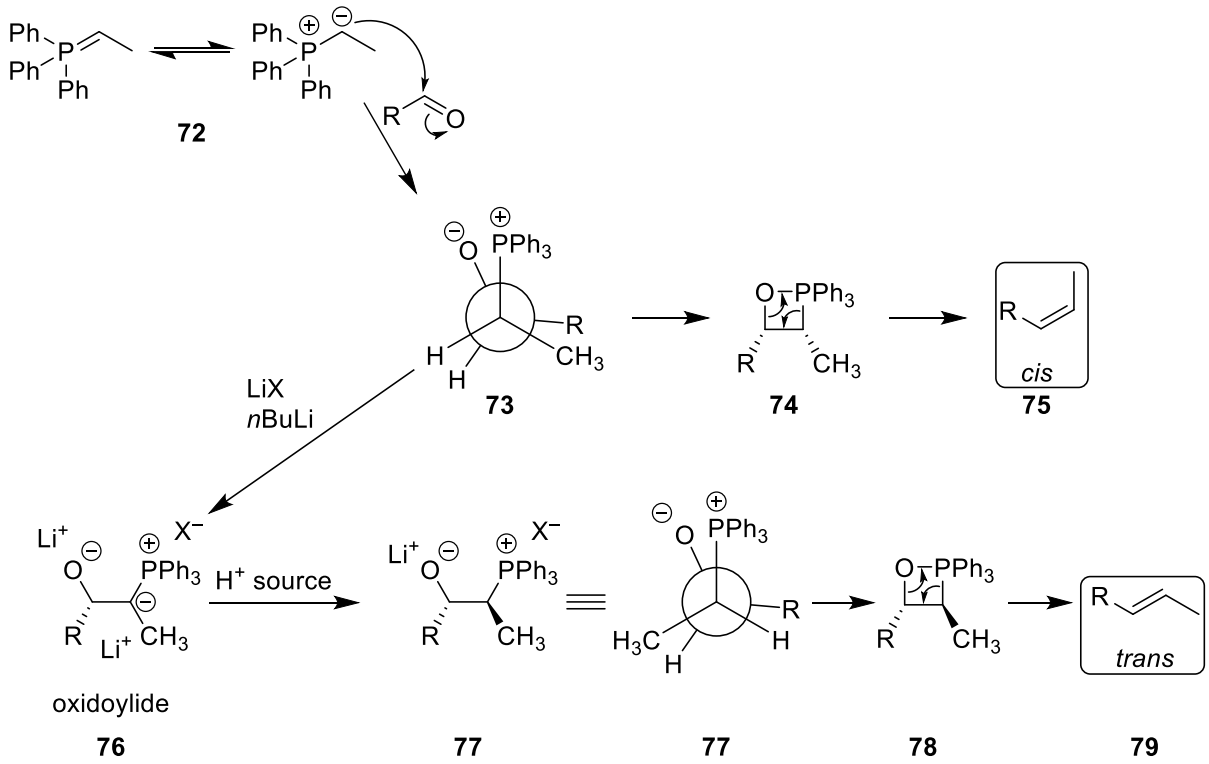

Figure 61: Mechanistic overview of the WITTIG reaction and SCHLOSSER modification.

In the WITTIG reaction, ylide **72** nucleophilically attacks the aldehyde, forming betaine **73**, which then undergoes cyclization to produce oxaphosphetane **74**, a four-membered cyclic intermediate. This intermediate decomposes to form the *cis*-alkene **75**, with the driving force being the formation of a stable phosphine oxide (Figure 61). In the SCHLOSSER modification, lithium salts are used to trap the betaine **73**, preventing the formation of oxaphosphetane **74**. The trapped betaine is

then deprotonated to yield oxidoylide **76**, which, upon reprotonation, forms betaine **77**. This intermediate is subsequently converted to oxaphosphetane **78**, leading to the formation of the *trans*-alkene **79** (Figure 61).

The first step towards the synthesis of tetramic acids **30** and **64** was a STEGLICH esterification of L-aspartic acid **80** and 2-(trimethylsilyl)ethanol, which resulted in diester **81** in 93% yield after purification on silica. For better solubility of **80** in dichloromethane, *N*,*N*-dimethylformamide was added to the mixture (Figure 62).

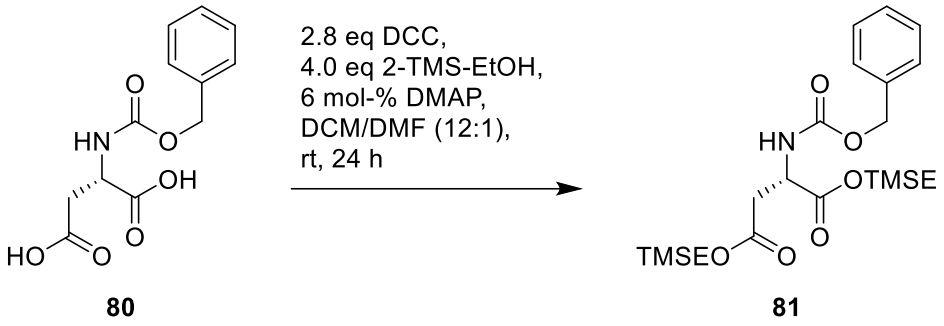

80 **81**

Figure 62: Synthesis of diester **81** using the STEGLICH approach.

Subsequent palladium-catalyzed hydrogenolysis of **81** in ethyl acetate yielded amine **82** quantitatively (Figure 63).

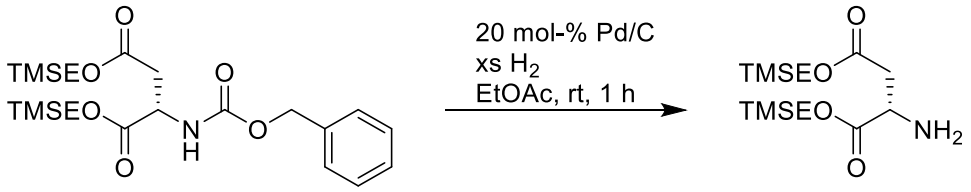

81 **82**

Figure 63: Deprotection of benzyloxycarbonyl protecting group of **81** using palladium-catalyzed hydrogenolysis. xs = excess.

The formation of **82** was confirmed by NMR spectroscopy and used without further purification.

Reductive amination reaction of amine **82** with 2,4-dimethoxybenzaldehyde (**83**) under catalysis of acetic acid gave *N*-protected aspartate **70** in 83% yield after purification on silica (Figure 64).

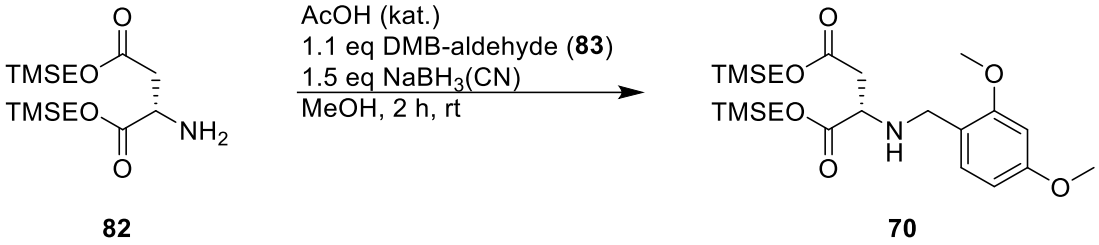

Figure 64: Reductive amination with aldehyde **83** and sodium cyanoborohydride as reducing agent.

As described in the literature, the reducing agent sodium cyanoborohydride was added 30 seconds after the addition of aldehyde **83** to avoid epimerization of the stereo center in **70**.[103]

For the aminolysis reaction β-ketothioester **63** was synthesized according to the literature using propiolic acid as starting material.[118]

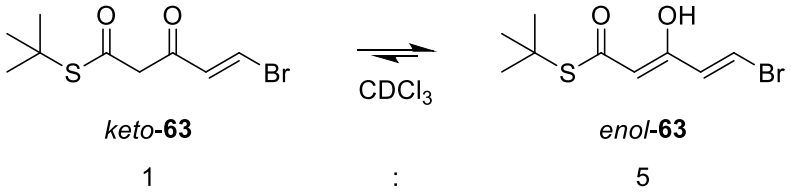

Figure 65: Ratio of *keto* and *enol*-forms of **63** observed via NMR spectroscopy in $CDCl_3$.

In deuterated chloroform *keto-enol* tautomerism of **63** is observed in NMR spectra, giving a ratio of 1:5 (*keto*:*enol*) (Figure 65). With β-ketothioester **63** in hand, aminolysis was carried out with amine **82** and disubstituted amine **70**, respectively (Figure 66).

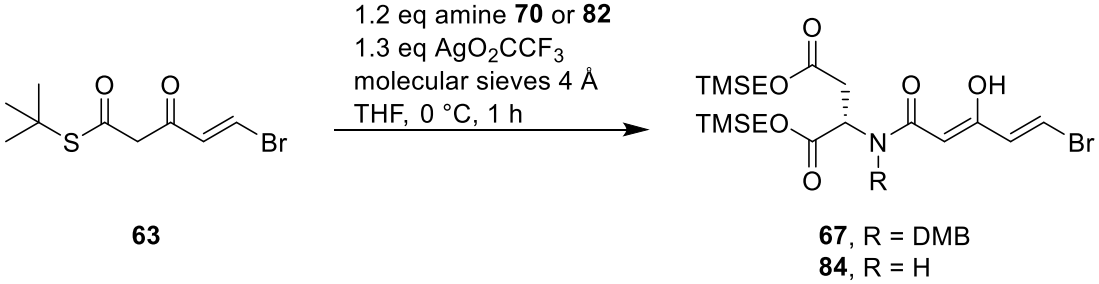

Figure 66: Aminolysis of β-ketothioester **63** with amine **82** or disubstituted amine **70**, respectively. For **67** and **84** only *enol*-forms are shown.

Under these conditions, the yield for the disubstituted amide **67** (97%) is significantly higher than the yield for the monosubstituted amide **67** (51%). This can be explained by the higher nucleophilicity of a disubstituted amine and thus a higher reactivity in a

nucleophilic attack at the carbonyl carbon of the thioester **63**.[119] The yields are consistent with similar reactions known in the literature.[103, 115-117] Moreover, more than two compounds are observed for amide **67**. Due to the disubstitution of the nitrogen in **67**, the rotation of the amide bond is slowed down, resulting in four observable compounds in the NMR spectra in deuterated chloroform (Figure 67), which is already known in the literature.[103, 116, 117]

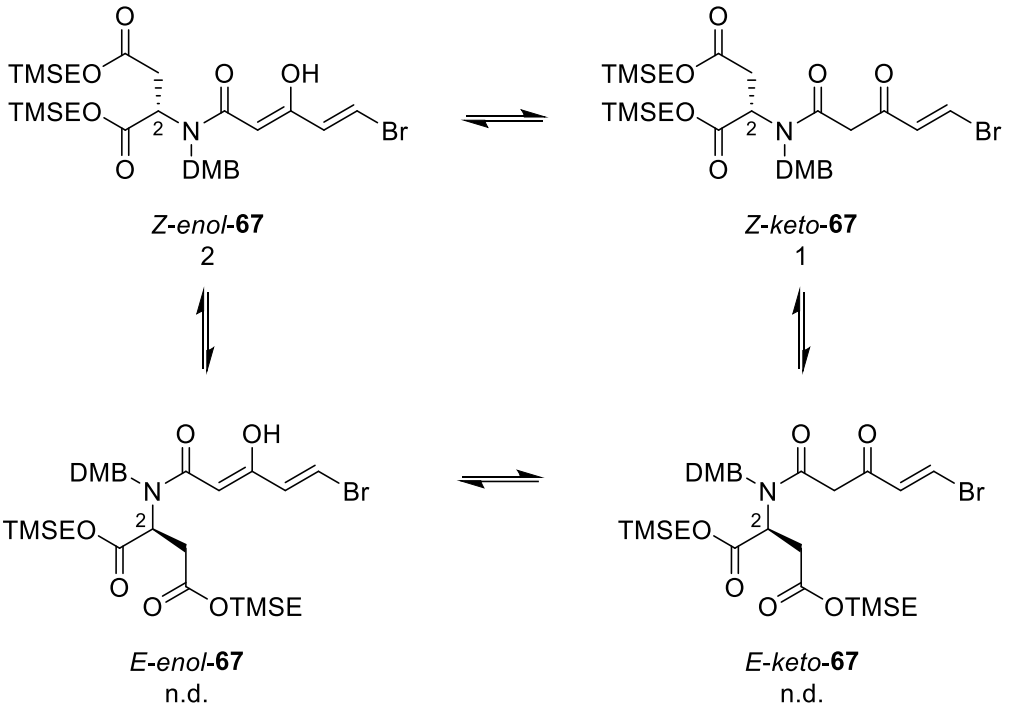

Figure 67: Four observable compounds for **67** in deuterated chloroform. The determinable ratios are given. n.d. = not determinable.

The ratio between *Z-keto*- and *Z-enol*-form can be determined via ^{1}H-NMR spectroscopy by integrating the ^{1}H-NMR signals of 2-H and calculating the ratio. The main components in this mixture are *Z-enol*-**67** and *Z-keto*-**67** (2:1). For *E-enol*-**67** and *E-keto*-**67** the contents are very small, so that the ratios cannot be unambiguously determined.

Analogous to amide **67**, *enol*- and *keto*-forms of amide **84** can be observed in the NMR spectra. The ratio for *enol*-**84** and *keto*-**84** is the same as for amide **67**.

The bromoalkenes **67** and **84** were then subjected to a STILLE reaction with tributyl(vinyl)tin (**68**) to yield amides **65** and **85** in 64% and 50% yield, respectively (Figure 68).

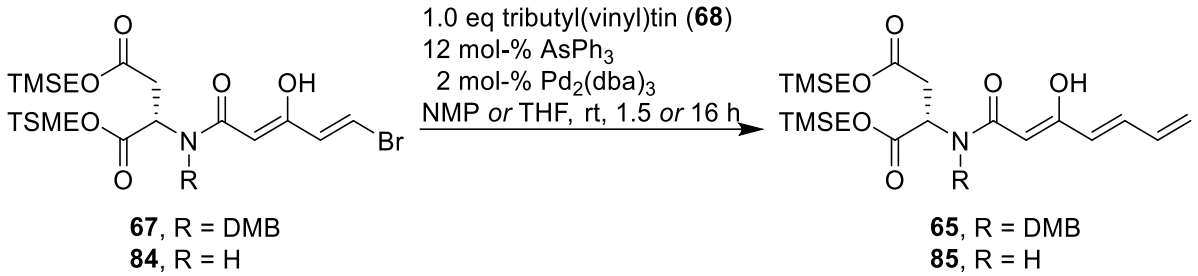

Figure 68: Stille reaction yielded amide **65** and amide **85**, respectively, in moderate yields. For the synthesis of **65** THF was used as a solvent and the reaction was stirred overnight. Only *enol*-forms are shown for **65** and **85**.

Compounds **65** and **85** decompose when stored in air at room temperature. For the synthesis of **65**, the solvent was changed from *N*-methyl-2-pyrrolidone (NMP) to THF. The removal of THF with a rotary evaporator proceeds much faster. This led to a faster work-up of the reaction and thus to a higher yield as less decomposition can occur. The yields are consistent with the literature.[103, 115-117]

With the tetramic acid precursors **65** and **85** at hand, LACEY-DIECKMANN cyclization reactions with tetra-*n*-butylammonium fluoride (TBAF) were carried out. For the disubstituted amide **65** this reaction proceeded smoothly and the desired protected tetramic acid **86** was isolated in 58% yield (Figure 69). The yield for tetramic acid **86** is in the range of typical yields for the LACEY-DIECKMANN cyclization reactions.[103, 115-117]

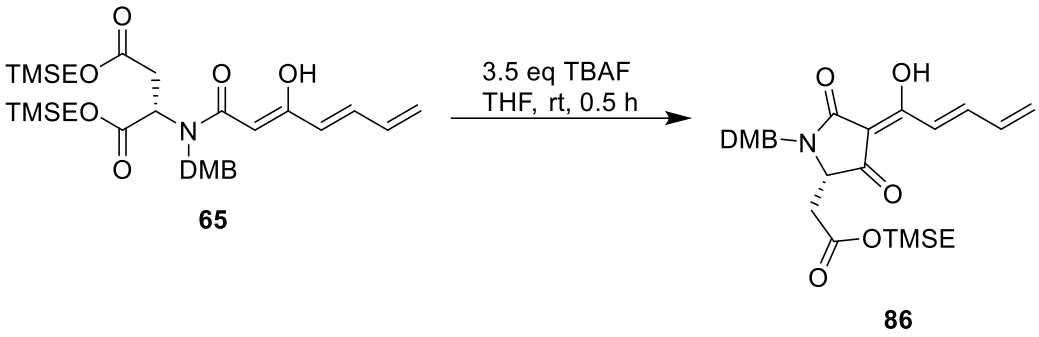

Figure 69: LACEY-DIECKMANN cyclization reaction yielded tetramic acid **86**.

In contrast, cyclization of **85** was not observed. Monosubstituted β-ketoamides do not cyclize well for geometrical reasons, which has already been described in literature.[120]

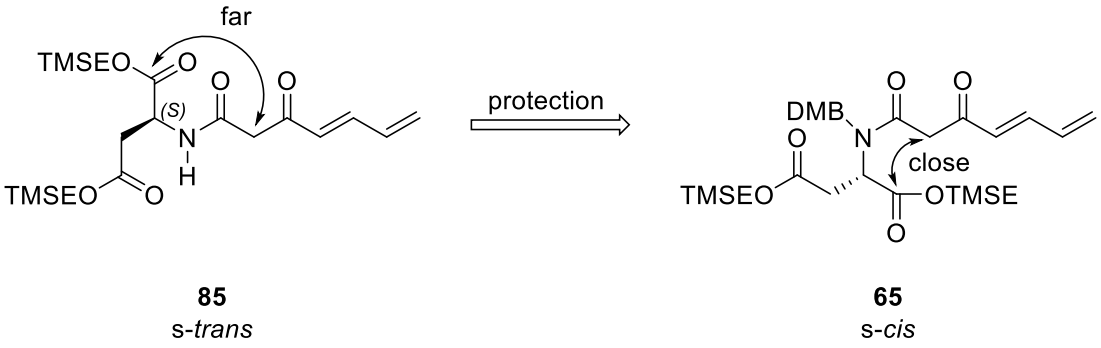

85
s-*trans*

65
s-*cis*

Figure 70: Conformational analysis of **65** and **85**.[120]

In an s-*trans* conformation, the distance between the two carbon atoms participating in the cyclization reaction is too large to allow successful cyclization. However, introducing a bulky protecting group such as DMB can enforce an s-*cis* conformation, bringing the reactive carbon atoms into optimal proximity to facilitate cyclization (Figure 70).[120] This approach was pursued because, if successful, the deprotection step of the DMB-protecting group is eliminated and thus compensates for the hypothetical poor yield.

Since the second TMSE-protecting group was not removed by treating tetramic acid **86** with TBAF at room temperature, **86** was treated a second time with TBAF at elevated temperatures (60°C) (Figure 71).

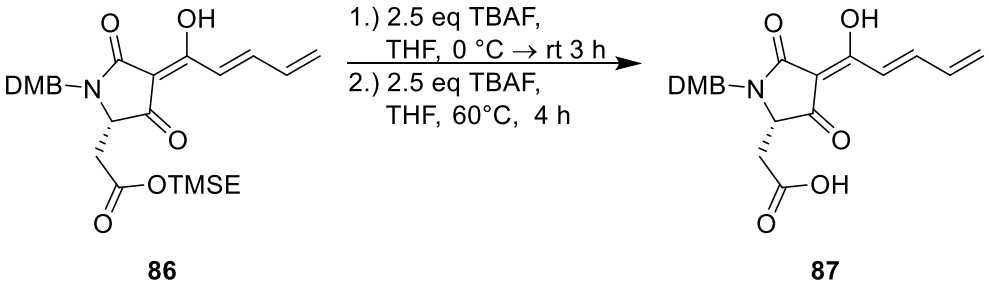

86

87

Figure 71: Deprotection of TMSE-group with TBAF at elevated temperatures (60°C).

At elevated temperatures (60°C), the desired DMB-protected tetramic acid **87** was formed but also the yield significantly dropped to 16%. Subsequent attempts to remove the DMB-protecting group using trifluoroacetic acid in dichloromethane did not result in isolation of the desired product. Only traces of the fully deprotected tetramic acid **64** were observed via LC-MS analysis (Figure 72).

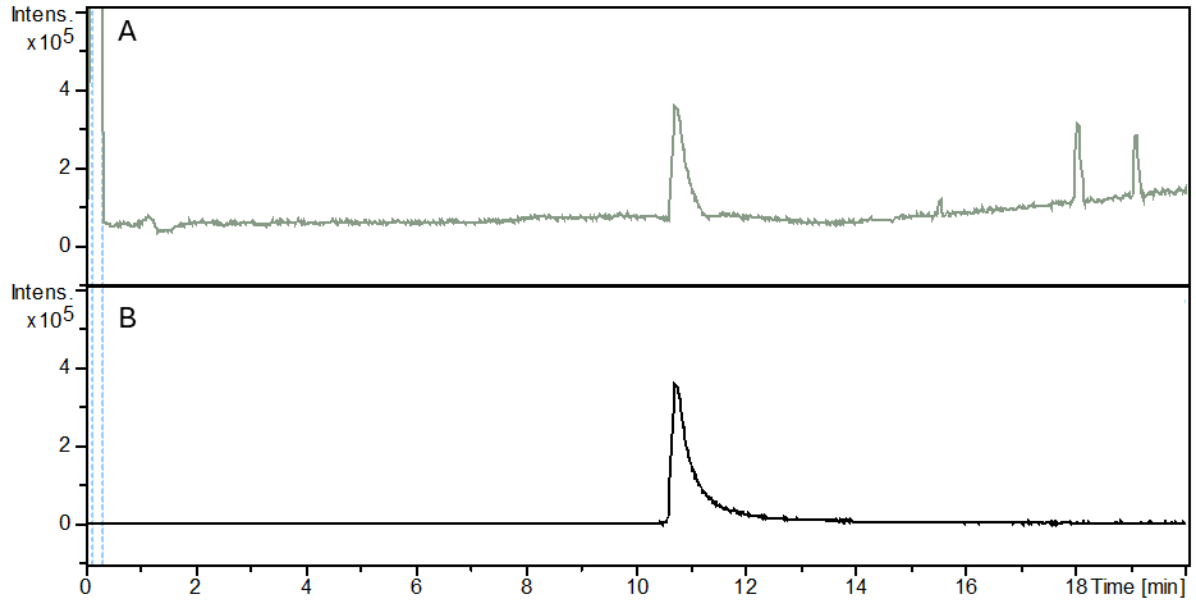

Figure 72: HPLC-ESI-MS analysis (experimental section 6.1.4.) of deprotection step of tetramic acid **86** with TFA in DCM. A) BPC (grey) of reaction mixture. B) EIC (black) of tetramic acid **64** ($C_{11}H_{12}NO_5^+$ $[M+H]^+$, *m/z* 238.0710±0.005).

Interestingly, tetramic acid **64** shows similar fragmentation patterns (Figure 73) as shown for the tetramic acid moiety in epifadin (**24**, Figures 33 and 36).

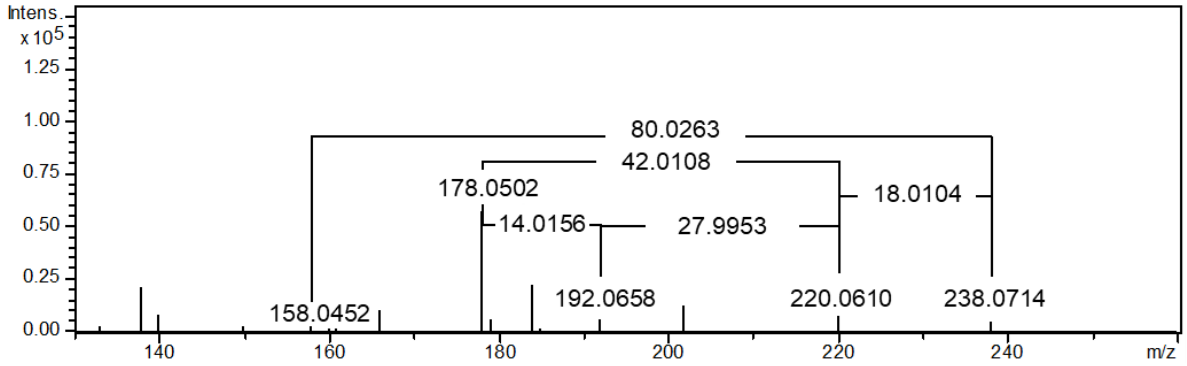

Figure 73: Tandem mass spectrum of **64** was acquired using HPLC-ESI-MS (positive mode, experimental section 6.1.4.). Selected m/z values were highlighted.

As in the fragmentation pathway of epifadin (**24**, Figures 33 and 36), the fragmentation of **64** reveals neutral losses of water (18.0104 Da) and carbon monoxide (27.9953 Da), which confirm the presence of a carboxyl group in **64**. A potential neutral loss of a carbene group (CH_2, 14.0156 Da) was observed, indicating cleavage of a CH_2 moiety. Alternatively, this fragmentation could correspond to the neutral loss of ketene (C_2H_2O, 42.0108 Da), resulting in a daughter ion with *m/z* = 178.0502. Additionally, a neutral loss of 80.0263 Da leads to the fragment **24-Frag 4** (Figure 74, *m/z* = 158.0454) which was also observed in the tandem MS of epifadin (**24**, Figure 36). These findings further support the tetramic acid moiety in epifadin (**24**).

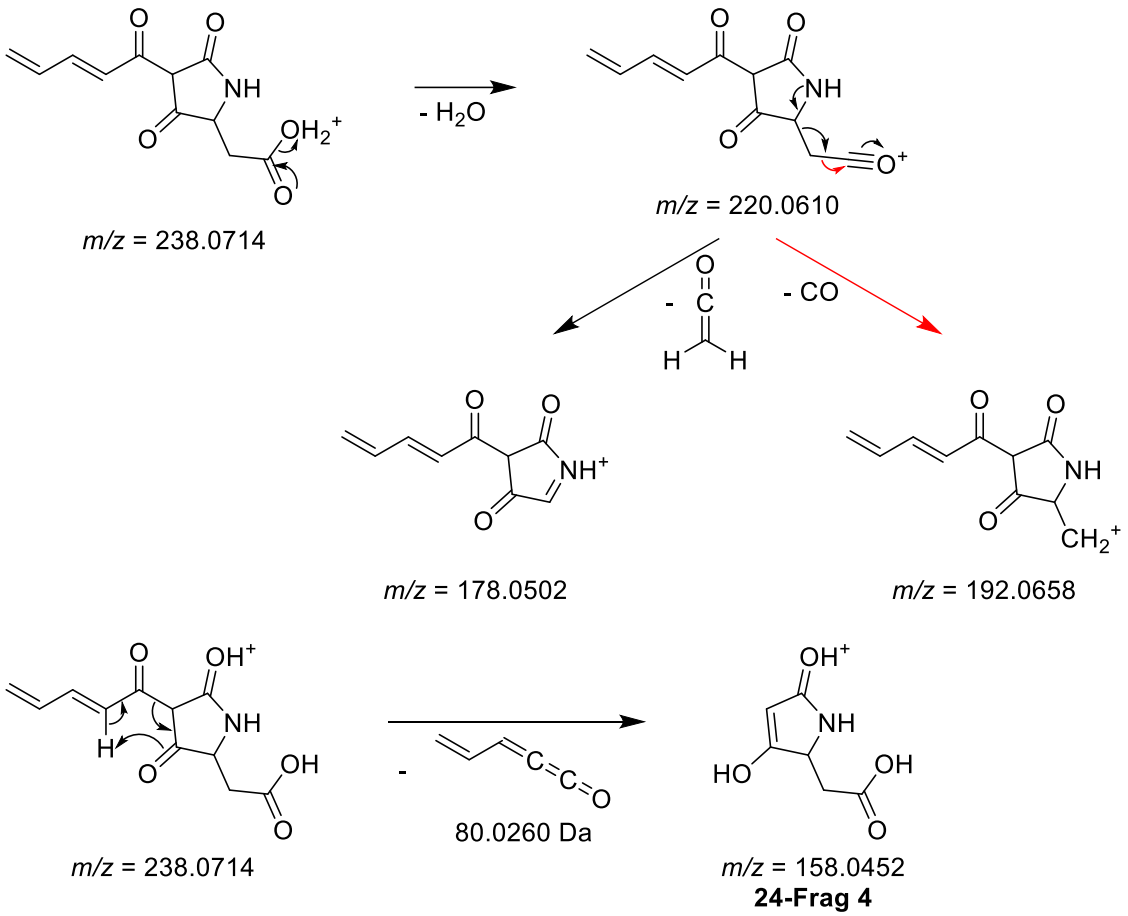

Figure 74: Fragmentation route for tetramic acid **64** from tandem MS experiments (experimental section 6.1.4.).

To synthesize tetramic acid **30**, the first step involves the preparation of the corresponding stannane **69**, which is required for the subsequent STILLE coupling reaction. Stannane **69** can be synthesized with *trans*,*trans*-configuration via a TAKAI-UTIMOTO olefination, in which chromium(II) chloride is often used in a multiple excess.[121, 122] However, chromium is considered a pollutant and is highly toxic, especially in its chromium(VI) oxidation state.[123] Therefore stannane **69** is synthesized using aldehyde **71** and WITTIG reagent **88**. The outcome of a reaction between a unstabilized ylene and an aldehyde, usually yields a *Z*-alkene, which should be the case for the reaction between aldehyde **71** and ylene **72**.[124] To prevent the forming of *Z*-alkene, the SCHLOSSER modification[125] is applied, which resulted in the desired *trans*,*trans*-configuration of stannane **69** in a 79% yield (Figure 75).

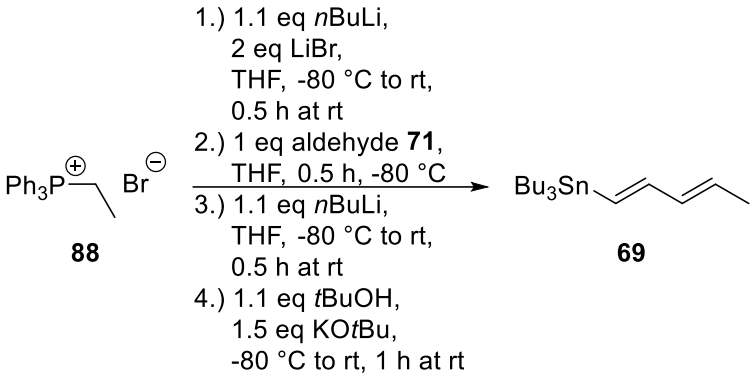

Figure 75: Synthesis of stannane **69** via a SCHLOSSER modification of a WITTIG reaction.

The fungal-derived tetramic acid natural product MCA17-1 (**30**), a potential liver fibrosis inhibitor, has been synthesized using a strategy analogous to that of tetramic acid **64**. First, a STILLE reaction between stannane **69** and bromoalkene **67** furnished the tetramic acid precursor **66** in 86% yield (Figure 76). Subsequent LACEY-DIECKMANN cyclization with tetra-*n*-butylammonium fluoride (TBAF) at elevated temperatures (45°C) afforded DMB-protected tetramic acid **89** in 49% yield (Figure 76). The final deprotection step was carried out with trifluoroacetic acid and thioanisole in dichloromethane, which gave MCA17-1 (**30**) in a 58% yield after HPLC (experimental section 6.5.1.) (Figure 76).

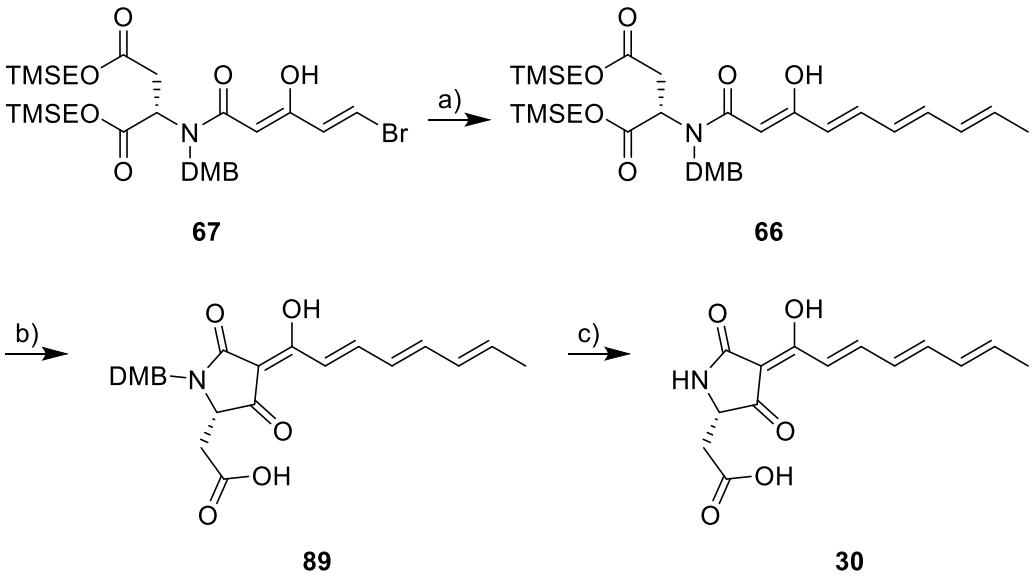

Figure 76: Synthesis route of MCA17-1 (**30**) starting from bromoalkene **67**. Reaction conditions: a) Bromoalkene **67**, stannane **69**, $AsPh_3$, $Pd_2(dba)_3$, THF, 16 h. b) Tetra-*n*-butylammonium fluoride, THF, room temperature 1.5 h then 45°C, 2 h. c) Thioanisole, trifluoroacetic acid/CH_2Cl_2 (1:4), 2.5 h.

A comparison of NMR data with literature confirmed the formation of MCA17-1 (**30**).[80, 126] However, this is not the first total synthesis of tetramic acid **30**. The first total synthesis was reported by GARY ROBERT WILLIAM PITT in his thesis in 2008 (Figure 77).

GARY ROBERT WILLIAM PITT introduced the polyene chain into the β-ketothioester **93** via a HORNER-WADSWORTH-EMMONS reaction. A subsequent aminolysis with protected aspartic acid **92** gave β-ketoamide **94**, which was cyclized using potassium *tert*-butoxide as a base to yield protected tetramic acid **95**. The acid-labile protecting groups were then removed by using trifluoroacetic acid, which gave the natural product **30** (Figure 77).

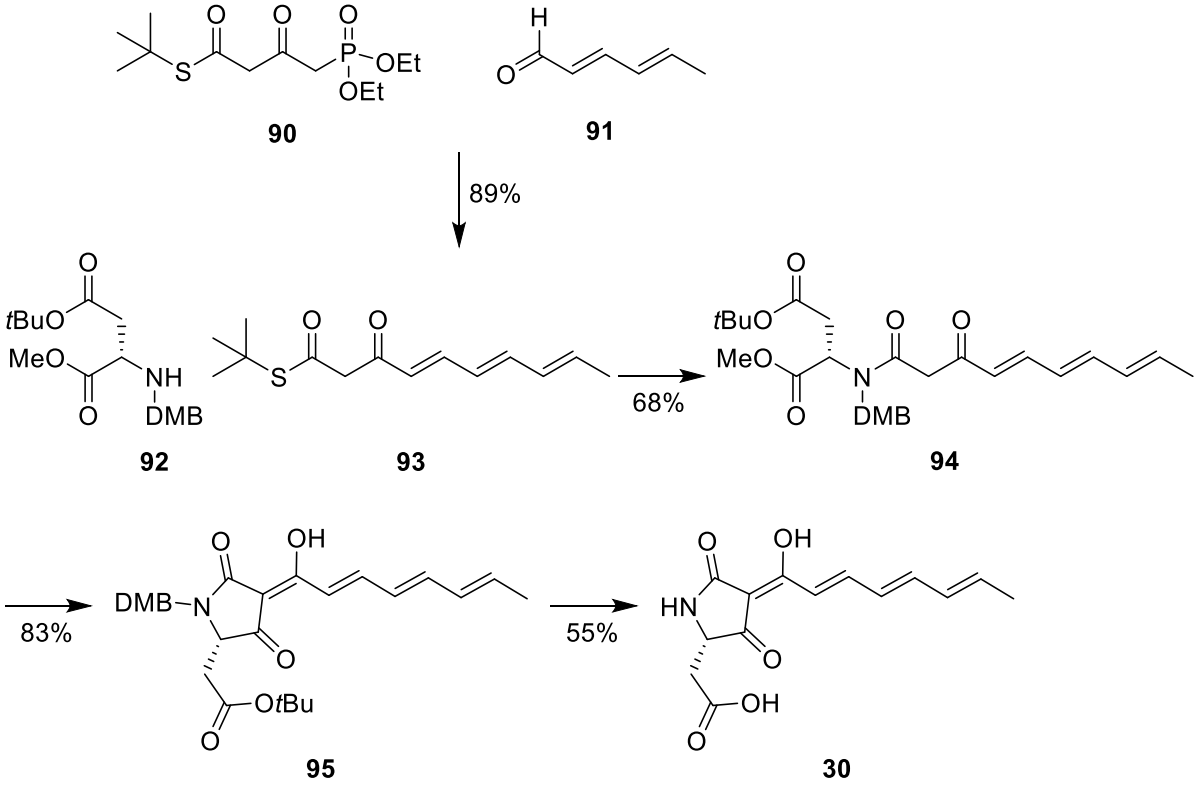

Figure 77: Synthesis route of GARY ROBERT WILLIAM PITT.[126]

In PITT's work, the polyene chain is introduced early in the total synthesis, making intermediates relatively sensitive to harsh reaction conditions, such as heat, strong acids, and strong bases. The use of only acid-labile protecting groups (DMB and *t*Bu) for the aspartic acid **92** allows for efficient removal of all protecting groups in a single deprotection step. The overall yield, from aminolysis of β-ketothioester **93** to tetramic acid **30** is 31%.

In contrast, in this work, the polyene chain is introduced prior to cyclization, which in turn ensures that only cyclization and subsequent deprotection steps need to be carried out with the sensitive polyene compounds. In addition, the bromoalkene building block **67** should be suitable for many palladium-catalyzed coupling reactions, which in turn should enable the introduction of various organic moieties. This approach thus lays the groundwork for future structure-activity relationship (SAR) studies. The

overall yield, from aminolysis of β-ketothioester **63** to tetramic acid **30**, is slightly lower at 24%. As seen with tetramic acid **64** (Figures 73 and 74) and epifadin (**24**, Figures 33 and 36), a similar fragmentation pattern is also observed for MCA17-1 (**30**) in tandem MS measurements (Figure 78 and 79).

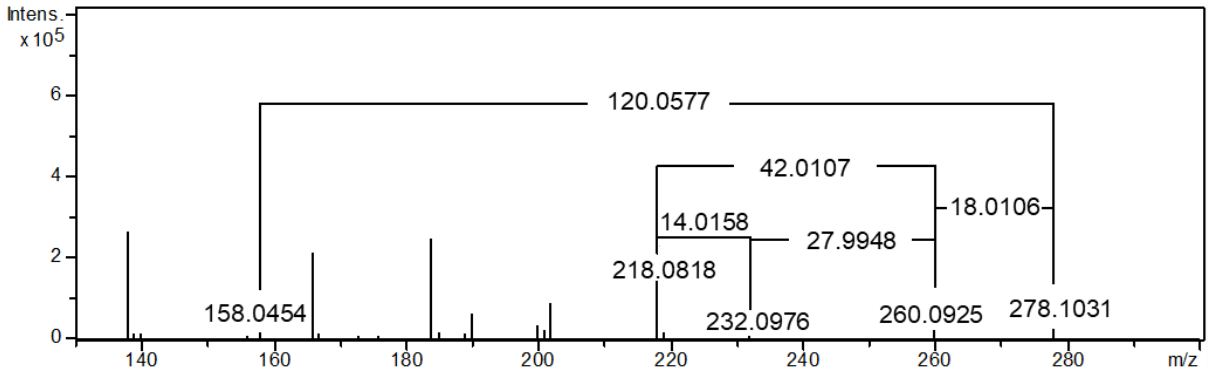

Figure 78: Tandem mass spectrum of **30** was acquired using HPLC-ESI-MS (positive mode, experimental section 6.1.4.). Selected m/z values were highlighted.

The fragmentation of **30** (Figures 78 and 79) reveals neutral losses of water (18.0106 Da) and carbon monoxide (27.9948 Da), which confirm the presence of a carboxyl group in **30** (Figure 79).

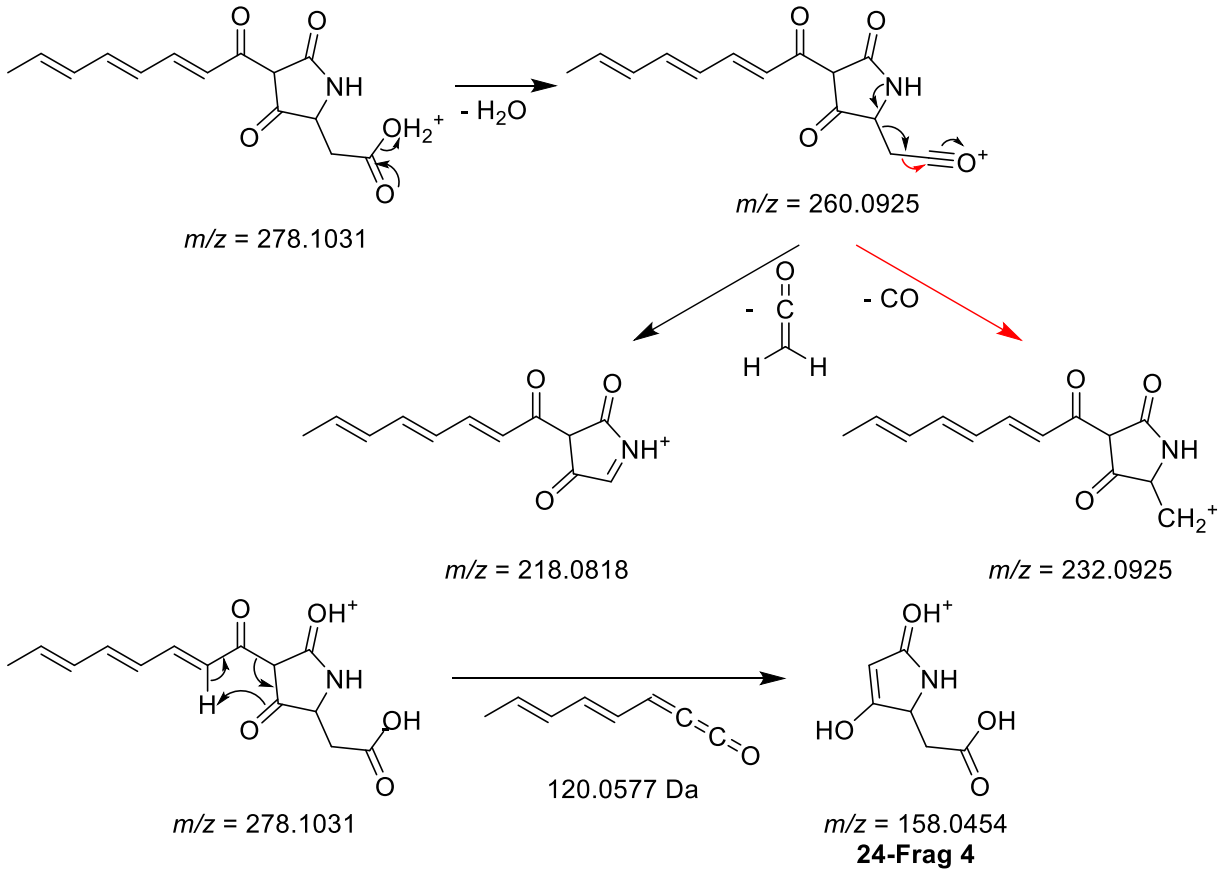

Figure 79: Fragmentation route for MCA17-1 (**30**) from tandem MS experiments.

A potential neutral loss of a carbene group (CH_2, 14.0158 Da) was observed, indicating cleavage of a CH_2 moiety. Alternatively, this fragmentation could correspond to the neutral loss of ketene (C_2H_2O, 42.0107 Da), resulting in a daughter ion with *m/z* = 218.0818. Additionally, a neutral loss of 120.0577 Da leads to the fragment **24-Frag 4** (*m/z* = 158.0454) which was also observed in the tandem MS of epifadin (**24**, Figure 36) and tetramic acid **64** (Figure 73). The presence of the same fragment (**24-Frag 4**, m/z = 158.0454) in tetramic acids **30** and **64**, as well as in epifadin (**24**) (Figures 36, 74 and 79), further supports the presence of a tetramic acid moiety in epifadin (**24**).

MCA17-1 (**30**) was tested against ESKAPE strains and in a cell viability assay by JAN STRAETNER (Research group HEIKE BRÖTZ-OESTERHELT, University of Tübingen). MCA17-1 (**30**) does not inhibit the growth of any ESKAPE pathogen tested and does not show any inhibition on MRC-5 cell culture line at 64 $\mu g \cdot mL^{-1}$ or lower (see experimental data Tables 5 and 9).
These results provide an important insight into the bioactivity of epifadin (**24**). Specifically, they suggest that the tetramic acid warhead, along with its polyene chain, is not solely responsible for the antimicrobial activity of epifadin (**24**). Rather, it is the unique architecture of epifadin (**24**), which includes the peptide moiety, polyene chain, tetramic acid moiety, and potentially the overall molecular size, that likely contributes to its bioactivity. Epifadin (**24**) was also tested in the same cell viability assay by JAN STRAETNER, and no inhibition was observed on MRC-5 cell culture line at 64 $\mu g \cdot mL^{-1}$ or lower (Table 9).

These findings suggest that epifadin (**24**) has potential as an antimicrobial agent, as it does not display cytotoxicity and exhibits a broad antimicrobial spectrum. The development of stable derivatives of epifadin (**24**) could significantly expand the antimicrobial arsenal and help combat the growing crisis of antimicrobial resistance.

3.2. Semi-synthesis of cystargolides **103** and **104** with optimized bioactivity

3.2.1. Caseinolytic protease P and its inhibitors

The caseinolytic protease P (ClpP) is a serine protease ubiquitously present in prokaryotic cells and mitochondria.[127] Recent studies have demonstrated, ClpP's significant role in protein homeostasis, as it is involved in the majority of cellular proteolysis and bacterial virulence, rendering this protease a promising target for antibacterial drugs.[128-131] Additionally, ClpP overexpression in various carcinomas highlights its potential as a target for anticancer drugs.[132, 133]

The ClpP core consists of two stacked heptameric rings, which together form a tetradecameric complex. The catalytic triads, located on the inside of this complex, are responsible for the degradation of proteins. Clp-ATPases facilitate the unfolding and translocation of protein substrates into the degradation chamber under ATP consumption (Figure 80).[127]

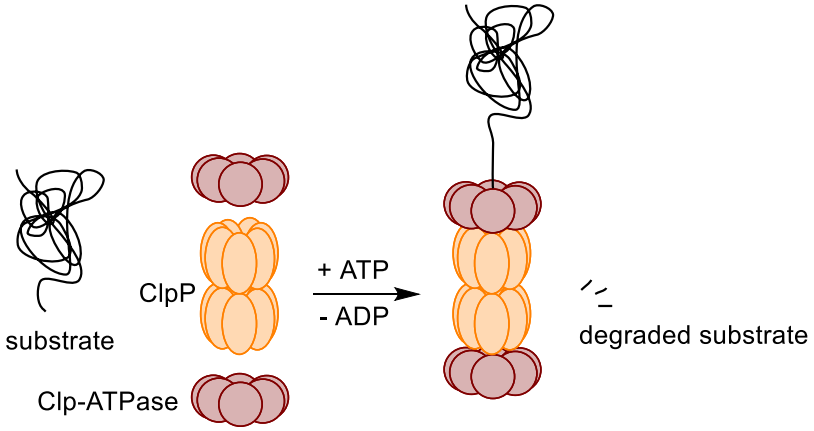

Figure 80: Model of Clp protease complex degrading protein substrate under ATP consumption. Hexameric Clp-ATPase is depicted in dark red, tetradecameric ClpP core is depicted in orange, protein substrate is depicted in black. This Figure is adapted from[127].

In recent years, various ClpP-targeting antibacterial compounds have been identified through screening methods or developed through lead optimization studies.[128, 134-136] These compounds can be divided into ClpP activating and ClpP inhibiting substances. Compounds from the acyldepsipeptide family (e.g., ADEP 1 (**96**)) have been shown to activate ClpP, leading to unregulated degradation of proteins, which results in bacterial self-digestion and eventual death of bacteria, including microbes in biofilm phase.[134, 137]

On the contrary, synthetic β-lactones such as D3 (**97**) and phenyl esters from chemical synthesis such as AV170 (**98**) have been found to irreversibly inhibit ClpP, leading to decreased expression of virulence factors such as α-hemolysin.[128, 135]

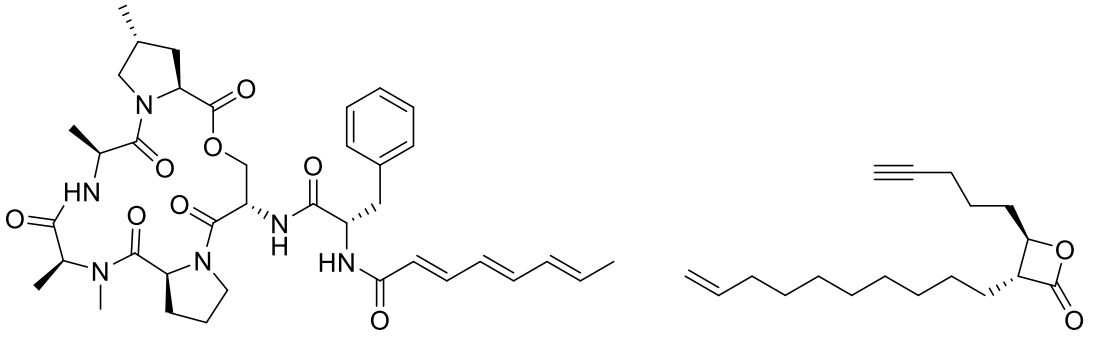

ADEP 1 (**96**)

D3 (**97**)

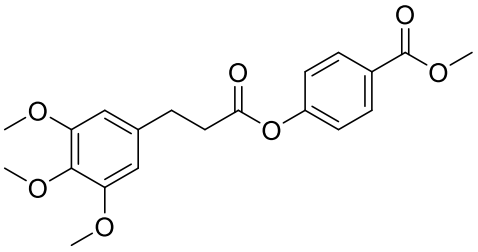

AV170 (**98**)

It was demonstrated that these compounds covalently bind to the active site of ClpP via a nucleophilic attack by the serine residue of the active site onto the carbonyl group of D3 (**97**) and AV170 (**98**), respectively (Figure 81).

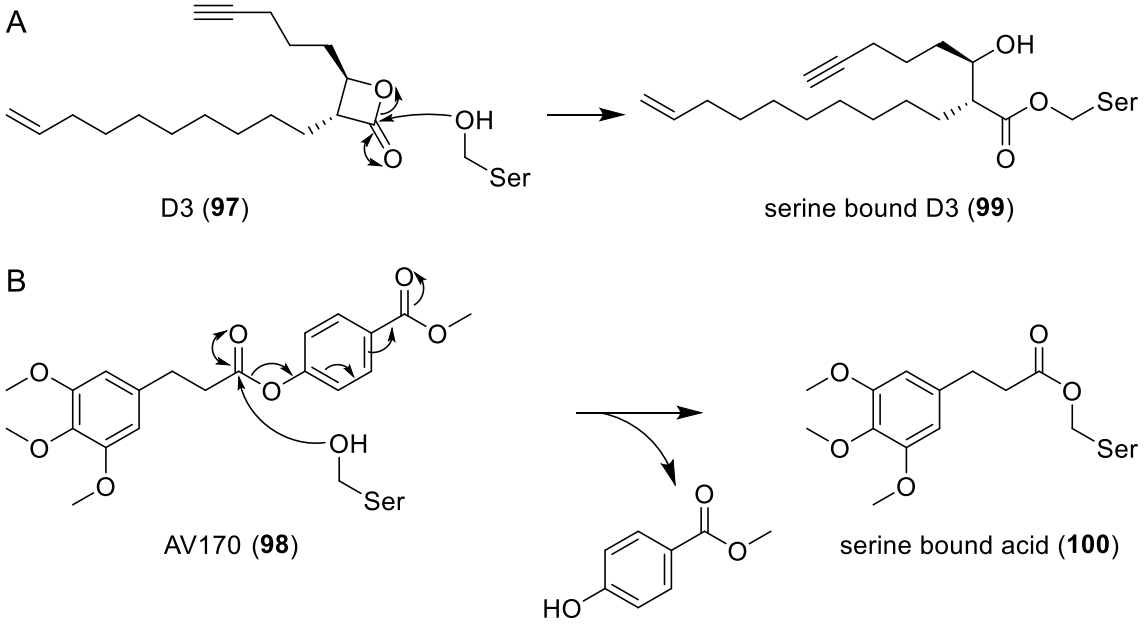

Figure 81: Proposed mode of action for the inhibition of ClpP. A) illustrated for D3 (**97**), B) illustrated for AV170 (**98**).

For β-lactone **97** the nucleophilic attack of a serine residue leads to a ring opening of the β-lactone, which results in the trapped acyl-enzyme intermediate **99**. However, the β-lactones are relatively labile electrophiles, which are quickly hydrolyzed in human plasma.[135] In contrast, phenyl esters, such as AV170 (**98**) exhibit significantly better

properties in terms of potency and plasma lifetime.[135] Structure-activity relationship studies revealed that changing electron-withdrawing groups on the phenol substituent to electron-donating groups such as methoxy and *N*,*N*-dimethylamine leads to a significantly reduced potency. Electron-withdrawing groups on the phenol substituent increase the reactivity of the ester making acylation of the enzyme a faster process (Figure 81). Only minor modifications to the carboxylic acid moiety, such as substituting the 1,2,3-trimethoxyphenyl moiety with an indole moiety, were tolerated without a significant loss of activity.[135]

Cystargolides A (**101**) and B (**102**) were isolated from *Kitasatospora cystarginea* and were initially reported as 20S proteasome inhibitors.[138] LEO KAYSSER's group (University of Leipzig Medical Center) in close cooperation with HEIKE BRÖTZ-OESTERHELT's research group (University of Tübingen) discovered that individual ClpP genes are located adjacent to the biosynthetic gene cluster of cystargolides A (**101**) and B (**102**). Given this co-occurrence and the presence of a β-lactone moiety in both compounds **101** and **102** (Figure 82A), they were tested for ClpP inhibition.

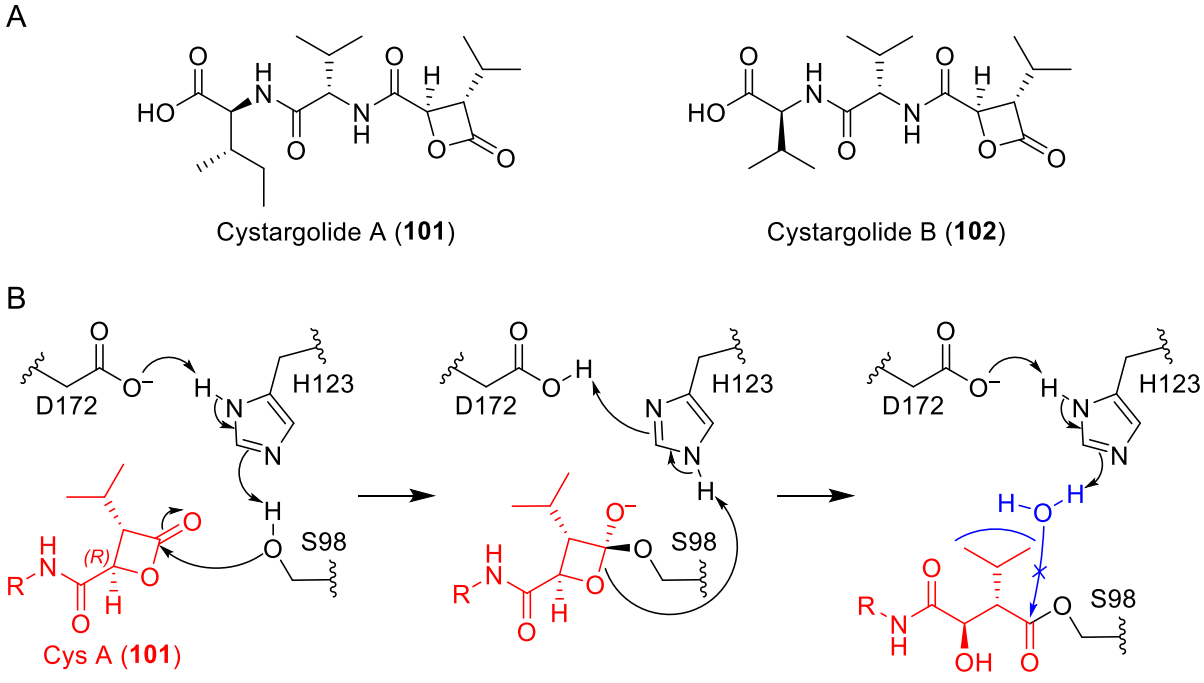

Figure 82: A) Chemical structures of cystargolides A (**101**) and B (**102**). B) Proposed mechanism for the inhibition of ClpP by cystargolide A (red, **83**), nucleophilic attack of water (blue) is blocked by cystargolide A (**83**) residues. Adapted from [139].

It was confirmed that cystargolides A (**101**) and B (**102**) inhibit ClpP. In a collaborative study between the University of Tübingen (BRÖTZ-OESTERHELT group) and the

Technical University of Munich (GROLL group), the co-crystal structure of the acyl-enzyme complex has been successfully solved.[139]

Cystargolide A (**101**) is nucleophilically attacked by Ser98, resulting in the ring opening of the β-lactone moiety via an oxy-anion formation. Hydrolytic release of cystargolide A (**101**) with water cannot occur due to the blocked BÜRGI DÜNITZ trajectory (Figure 82B).[139] Further research by HEIKE BRÖTZ-OESTERHELT's group has shown that α-hemolysin production of *S. aureus* NCTC 8325-4 was weakly inhibited in an agar-based assay by the purified cystargolides A (**101**) and B (**102**) compounds at 250 nmol (**101**: 92.6 µg, **102**: 89.1 µg). This led to the hypothesis that cell entry of cystargolides is low or impaired.[139]

In this work, semisynthetic derivatives are produced to enhance cell penetration and consequently improve ClpP inhibition. Given the properties of the cell membrane of Gram-positive bacteria, reducing the polarity of cystargolides A (**101**) and B (**102**), specifically by eliminating the negative charge of the carboxylic acid moiety is necessary in order to improve cell penetration or uptake (Figure 4).[48] The carboxylic acid moiety, being the furthest functional group from the β-lactone warhead, was identified as the optimal site for chemical modification. A straightforward amidation reaction would significantly reduce the polarity of the molecule, thus improving cell penetration (Figure 83). Among simple amines, ethylamine is chosen due to its lower polarity and handling benefits, with a boiling point of 16.6°C. However, special precautions need to be taken to protect the reactive β-lactone warhead, preventing its undesired interaction with nucleophiles during the reaction.

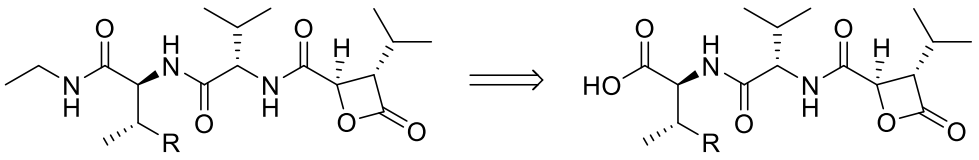

R = ethyl, NEt A (**103**)
R = methyl, NEt B (**104**)

R = ethyl, Cystargolide A (**101**)
R = methyl, Cystargolide B (**102**)

Figure 83: Retrosynthetic analysis for cystargolide amides A (**103**) and B (**104**).

3.2.2. Synthesis of amides **103** and **104** and their biological profiling

The *N*-ethylcystargolides A (**103**) and B (**104**) were successfully synthesized by an amidation reaction with ethylamine using purified cystargolides A (**101**) and B (**102**) as starting material, respectively (Figure 84).

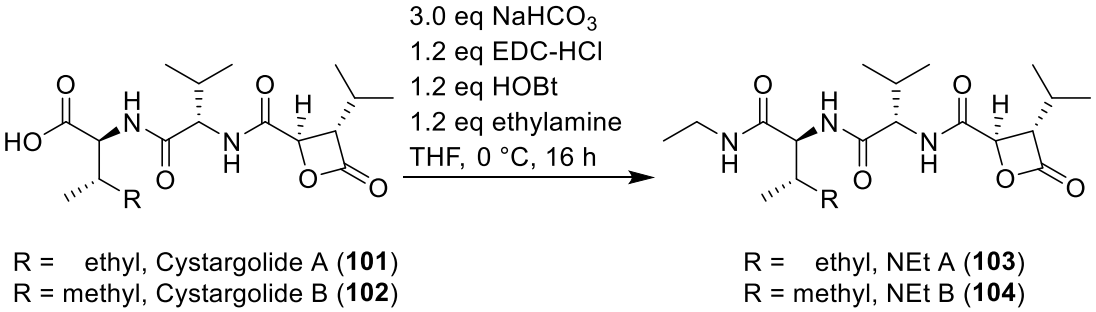

Figure 84: Amidation reaction of cystargolides **101** and **102** with ethylamine and EDC-HCl as coupling reagent.

The *N*-ethyl amides **103** and **104** were obtained in modest yields (3.5 mg (56%) for **103** and 1.6 mg (32%) for **104**) following HPLC purification (experimental section 6.5.1.), which was necessary for bioassay testing. The modest yields can be explained by the highly reactive β-lactone moiety, which can be opened by nucleophiles such as water and ethylamine, resulting in side-products **105**–**108**, as confirmed by LC-MS analysis (Figure 85).

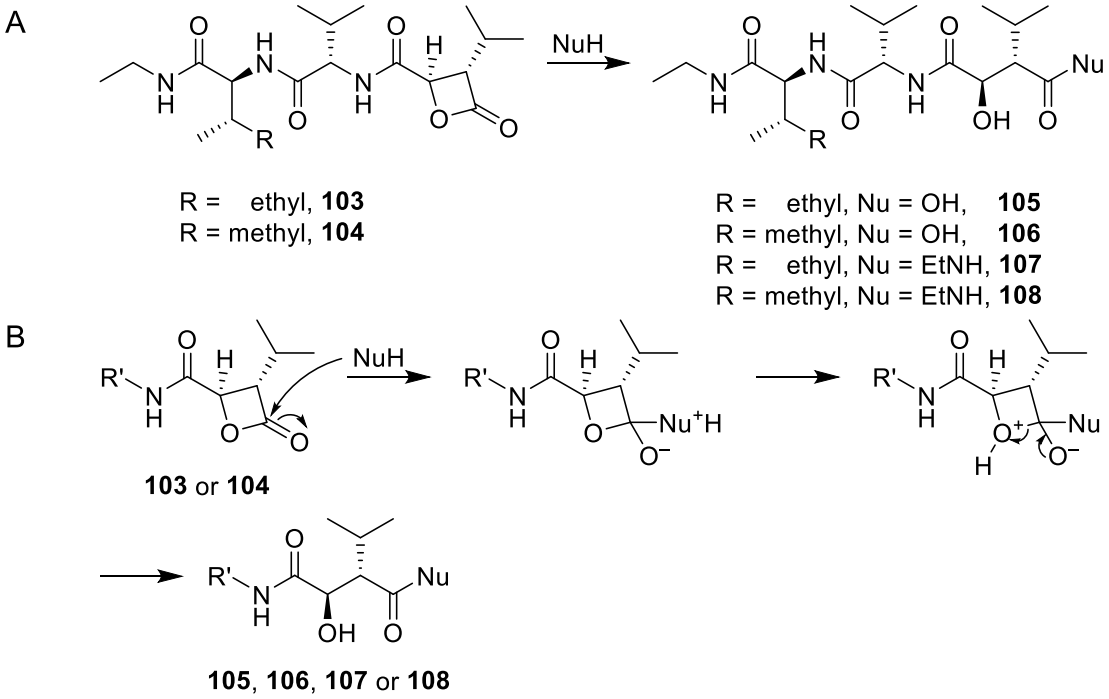

Figure 85: A) Side-product formation during synthesis and purification of **103** and **104**. B) Proposed mechanism of side-product formation. R' = NEt A (**103**) or NEt B (**104**) residues.

ASTRID ILLIGMANN, from the research group HEIKE BRÖTZ-OESTERHELT at the University of Tübingen, conducted assays to evaluate the biological activity of the obtained amides **103** and **104**, as well as the natural products **101** and **102**. In a hemolysis assay using *S. aureus* on blood agar, which measures the production of α-hemolysin, the *N*-ethylcystargolides **103** and **104** exhibited significantly stronger anti-hemolytic activity. For amide **103** nearly complete inhibition with 100 nmol added was observed, while amide **104** exhibited efficient inhibition with 250 nmol added. In contrast, the natural products **101** and **102** showed only moderate inhibition with 250 nmol added.[139] This suggests enhanced inhibitory potential of the tested compounds against ClpP. Additionally, all compounds were also subjected to a growth inhibition assay for *S. griseus* (tested by ASTRID ILLIGMANN). The *N*-ethylcystargolides **103** and **104** both showed dose-dependent inhibition of bacterial growth with inhibition observed at 31.25 nmol of **103** and 62.5 nmol of **104**. In contrast, the natural products **101** and **102**, exhibited no activity in this assay.[139] The enhanced efficacy of amides **103** and **104** in inhibiting ClpP and suppressing the growth of *S. griseus* is likely attributed to improved cell penetration or uptake. Notably, *N*-ethylcystargolide A (**103**) exhibited the most promising results in these tests.[139]

ClpP and Clp ATPases are critical targets in drug development, with Clp protease inhibition offering promising anti-virulence and anti-mycobacterial strategies. Additionally, ClpP activation has shown efficacy in inhibiting bacterial growth and tumor proliferation in preclinical and clinical studies.[140, 141] The potential to enhance bacterial cell penetration of cystargolides through modification underscores their suitability for further optimization.[139]

3.3. Total chemical synthesis of new lugdunins as tools in molecular studies

In the third part of this work, the focus is shifted from linear peptide structures to cyclic peptide structures. More specifically, selected lugdunin analogues are synthesized to investigate their ability to form peptide nanotubes in artificial membranes, as well as to evaluate their activity against Gram-negative bacteria in biological studies.

3.3.1. *N*-methyl analogues of lugdunin **110**–**115**

This part of the work aims to synthesize analogues of lugdunin to investigate its mode of action. *N*-methylated analogues will be synthesized to prevent β-sheet formation, thereby inhibiting channel formation, which can be measured using biophysical methods. These analogues will help determine whether lugdunin (**6**) functions as a carrier ionophore or a channel-forming ionophore.

Methods for the preparation of *N*-methylated peptides range from the use of *N*-methyl amino acids in peptide coupling chemistry[142-145] to selective *N*-methylation of peptides on solid support.[146-148] *N*-methylation is often used in pharmaceutical drug development to improve metabolic stability, membrane permeability and binding affinity of peptide pharmaceuticals.[149, 150] In this work, however, *N*-methylated lugdunin analogues are generated by selective *N*-methylation on solid support. These analogues are initially tested for their bioactivity against MRSA in whole-cell assays by B. KRISMER. Their ability to immerse in various artificial membranes and their ability to form peptide nanotubes, is then investigated through molecular dynamics simulations, UV, and IR spectroscopy (in collaboration with DOMINIK RUPPELT, Research group STEINEM, Georg-August-Universität Göttingen and MARIUS F.W. TROLLMANN, Research group BÖCKMANN, Friedrich-Alexander-Universität Erlangen-Nürnberg). This comprehensive analysis allows for a scientific determination of whether lugdunin (**6**) functions as proton shuttle carrier or as a channel-forming ionophore.

Since the 6-Trp-lugdunin analogue **109** has a lower MIC value than lugdunin (**6**)[40] and the tryptophan residue enables spectroscopy experiments in vesicles, it was chosen for the methylation at different positions of the peptide backbone. For amino acid positions 3, 4 ,5 and 6, selective *N*-methylation on solid support was performed using the standard Fmoc strategy and KESSLER's *N*-methylation protocol for *N*-methylated cyclic peptides (Figure 86).[148]

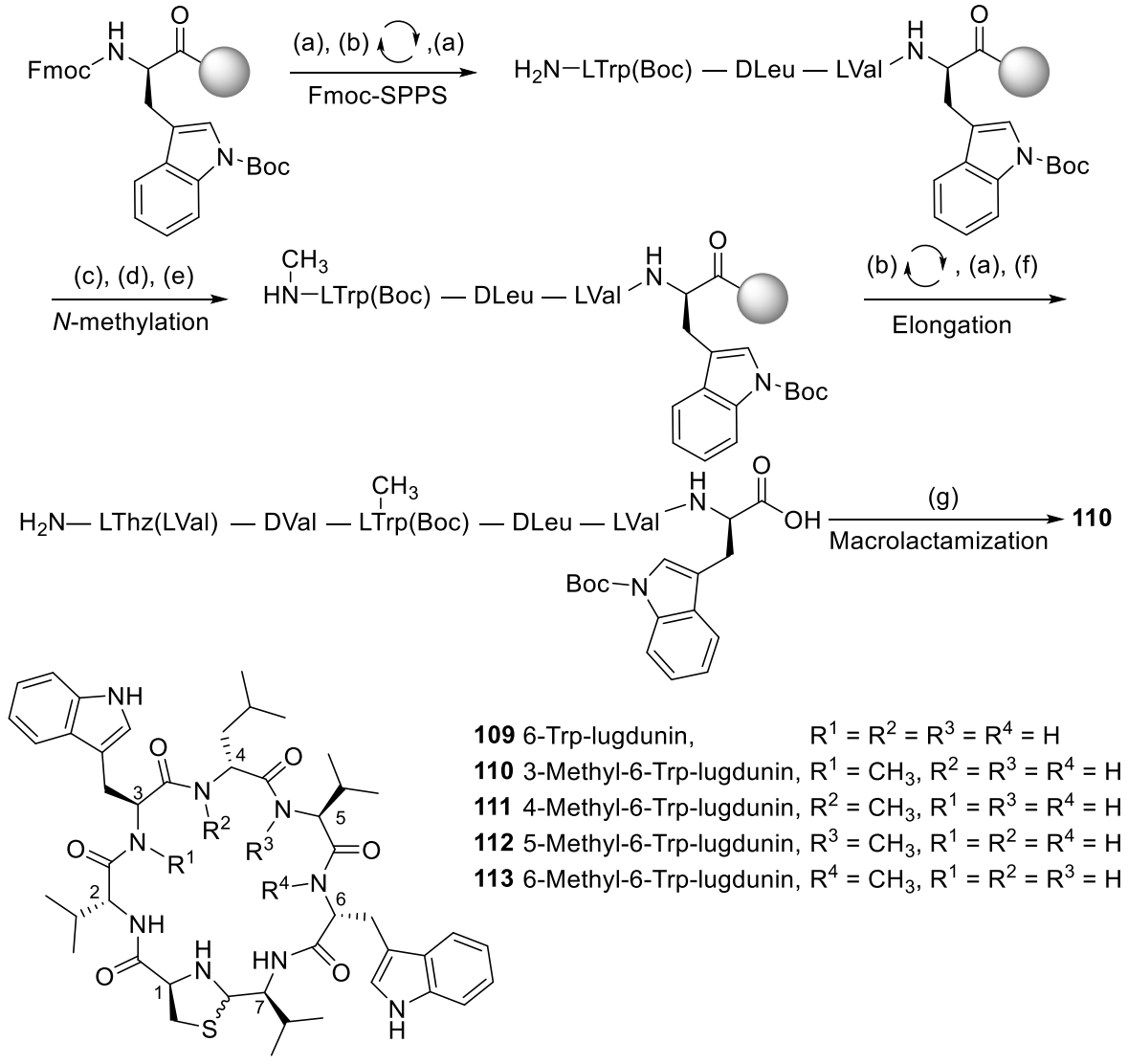

Figure 86: Synthesis of lugdunin analogue **110** and structures of lugdunin analogues **109**–**113**. (a) Fmoc deprotection with DBU and morpholine in DMF. (b) Elongation sequence with corresponding amino acids, HATU, HOBt and 4-methylmorpholine and deprotection steps in between. (c) Introduction of activating *o*NBS group with *o*NBSCl and collidine. (d) N-methylation with dimethyl sulfate and mTBD. (e) Removal of *o*NBS group with DBU and 2-mercaptoethanol. (f) Resin cleavage of linear peptide with TFA, TIPS and water. (g) Macrolactamization with HATU, HOAt and DIPEA.[151]

The coupling step after *N*-methylation was carried out twice, once for 3 h and once overnight to increase efficiency of coupling. Lugdunin analogues **111**–**113** were synthesized in moderate to good yields (12.0 mg–50.3 mg, 41%–88%) in the same manner as analogue **110**. After macrolactamization the reaction mixtures were worked up by extraction with a mixture of $CHCl_3$ and *n*BuOH (5:1), followed by washing the organic extracts with aqueous solutions of $KHSO_3$ (10%), saturated $NaHCO_3$, and brine. The organic solvent was then removed under vacuo, and the peptides were lyophilized before being purified by HPLC (experimental section 6.4.2.2.). Selective

N-methylation was confirmed via tandem MS by manual peptide sequencing as shown for lugdunin (**6**).[32]

For amino acid position 1, selective *N*-methylation was achieved by a biomimetic approach.[40] First, the corresponding *N*-methyl peptide aldehyde **114** is synthesized with an aldehyde generating resin using *N*-Fmoc-*N*-methyl-*S*-trityl-L-cysteine. Resin cleavage of aldehyde **114** under acidic conditions resulted in spontaneous cyclization to the corresponding 1-methyl-6-Trp-lugdunin (**115**) (Figure 61) in 64% (6.0mg) yield.

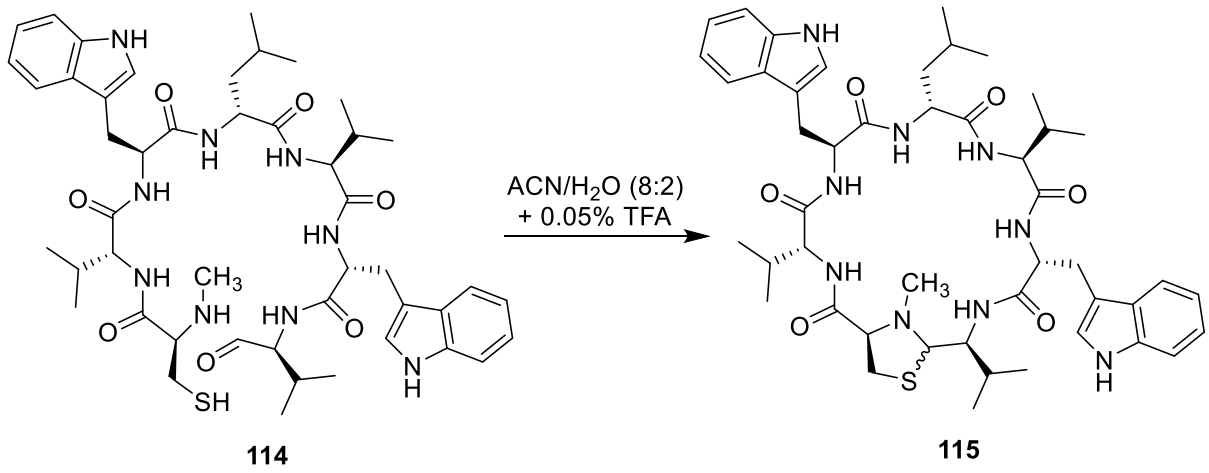

114 **115**

Figure 87: Spontaneous cyclization of aldehyde **114** under resin cleavage conditions.

After cleavage, peptide **115** was dissolved in a *t*BuOH/water (1:1) mixture, frozen, and lyophilized to yield a voluminous white powder. Analysis by HPLC-UV (experimental section 6.1.4.) confirmed a purity of 90%, determined by calculating the signal areas of the peptide **115** (5069) and impurities (595) (Figure 88). This degree of purity was considered adequate for bioactivity assays against MRSA.

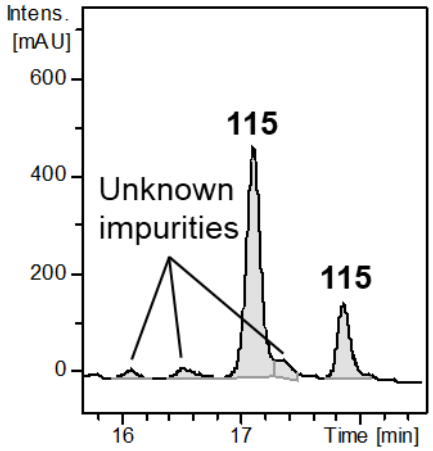

Figure 88: HPLC-UV analysis (experimental section 6.1.4.) of peptide **115** after lyophilization.

Compounds **110**–**113** and **115** were tested in a minimum inhibitory concentration assay against *S. aureus* USA300 LAC by B. KRISMER (Research group PESCHEL,

University of Tübingen). For all tested compounds no inhibition was observed even at 100 µg·mL^{-1} or lower (Table 6 experimental section 6.5.).

The research hypothesis suggests that lugdunin (**6**) forms peptide nanotubes, implying that methylation of the backbone prevents hydrogen bonding and thus formation of ion channels required for the translocation of protons across the membrane. On the other hand, methylation of the peptide backbone can also affect three-dimensionality of the molecule, which in turn can have a significant impact on bioactivity by modifying the peptides' overall conformation.[149]

In order to further analyze the mode of action of lugdunin (**6**), D. RUPPELT prepared various large unilamellar vesicles. The UV emission of the tryptophan residue was measured for different concentrations of the lipid 1-palmitoyl-2-oleoyl-*sn*-glycero-3-phosphocholine (POPC). The emission intensity of tryptophan was found to increase with higher concentrations of POPC and a blue-shift was observed, peaking at 18±2 nm for 2 mM of POPC.[151] Since the blue-shift and the intensity of emission depend on the insertion depth of the tryptophan residue into the membrane, quantification of the distribution of lugdunin (**6**) between the aqueous and the membrane phase was possible (partition coefficient $K_{\chi,exp} = (9 \pm 2) \cdot 10^5$).[151] The partition coefficient (K_χ) between an aqueous buffer and a lipid membrane is defined as:

$$K_\chi = \frac{\chi_{membrane}}{\chi_{aqueous\ solution}},$$

where $\chi_{membrane}$ and $\chi_{aqueous\ solution}$ refer to the mole fractions of the substance in the lipid membrane and aqueous phases, respectively.[151] The greater the partition coefficient, the more of the lugdunin (**6**) partitions into the membrane phase, indicating a preference for the lipid environment.[152-155] Moreover, water-accessibility of the tryptophan residue was measured and plotted in a STERN-VOLMER diagram, which showed that the tryptophan is most likely located within the membrane.[151, 156] Both experiments indicate that lugdunin (**6**) preferentially migrates into the membrane phase.[151]

Furthermore, molecular dynamics simulations were used to demonstrate that tryptophan is responsible for binding on the membrane surface, which is followed by the immersion of hydrophobic residues and the rest of the molecule.[151] Since lugdunin (**6**) shows inhibition for Gram-positive bacteria and to small extend for eukaryotic cells, the lipid composition was changed to mimic Gram-positive bacterial membranes and eukaryotic cell membranes. 1-Palmitoyl-2-oleoyl-*sn*-glycero-3-

phospho(1'-*rac*-glycerol) (POPG) and cardiolipin (CL) were used to mimic Gram-positive cell membranes and cholesterol was used to mimic eukaryotic cell membranes.[151, 157, 158] POPG and CL were found to have no significant effect on the partitioning of lugdunin (**6**) in lipid membranes, whereas the addition of cholesterol resulted in a lower affinity of lugdunin (**6**) for the lipid membrane, as observed in laboratory experiments.[151] Interestingly, *N*-methylation has no effect on partitioning of analogues **110**, **111** and **113** in lipid membranes in laboratory experiments. This suggests that *N*-methylation does not hinder membrane immersion but rather β-sheet formation, which likely accounts for the lack of bioactivity observed.[151]

Molecular dynamics simulations further supported the experimental data. The microsecond molecular dynamic simulations suggest that lugdunin (**6**) can form trimers, tetramers, and pentamers in lipid membranes, with the composition of the lipid membranes influencing the oligomerization state.[151] Specifically, in POPC with cholesterol, lugdunin (**6**) forms pentamers, whereas tetramers are most stable in POPC and 1,2-dioleoyl-*sn*-glycero-3-phosphocholine (DOPC), which simulate a Gram-positive membrane.[151] Additionally, the simulations indicate that the formed channels are filled with water molecules, facilitating proton translocation across the membrane.[151]

In order to determine the structure of lugdunin (**6**) and its derivatives in lipid membranes, D. RUPPELT measured polarized ATR-FTIR spectra of lugdunin analogues **109**–**111** and **113** in ordered 1,2-dimyristol-*sn*-glycero-3-phosphocholine (DMPC) bilayers.[151] IR bands in the amide I, amide II and amide A region provided information about the secondary structure of peptides.[159-161] For lugdunin (**6**) and the 6-Trp-lugdunin analogue **109** the IR spectra showed characteristic peaks for β-sheet formation that are very similar to known synthetic cyclopeptides and suggest the formation of peptide nanotubes in lipid membranes.[151, 162-164] Moreover, the tilt angle relative to the membrane of analogue **109** was found to be significantly lower than the angle for lugdunin (**6**), which would imply that analogue **109** forms better aligned peptide nanotubes.[151] A comparison of the structures of lugdunin (**6**) and analogue **109**, shows that **109** appears to be more symmetrical, which could also influence the tilt angle in the membrane due to the interaction between the membrane and the amino acid side chains (Figure 89).

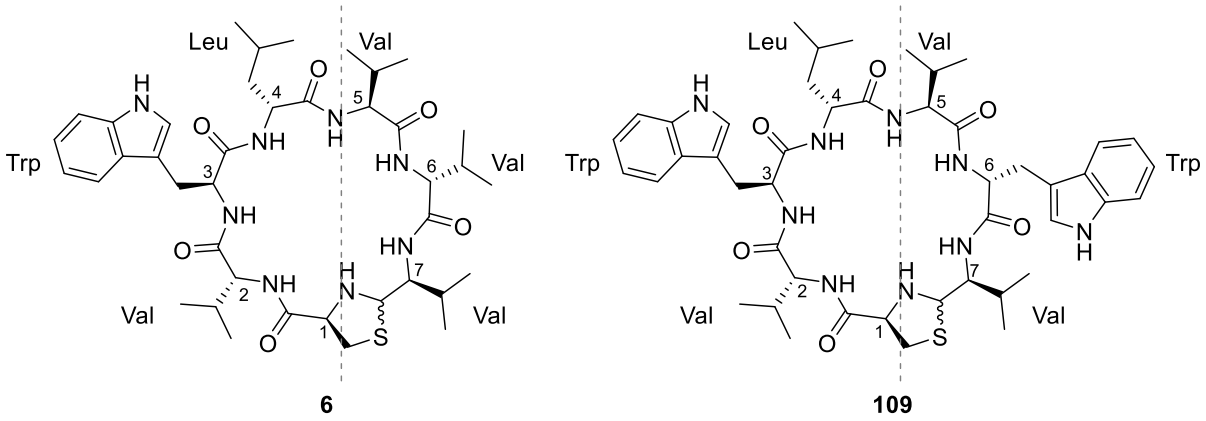

Figure 89: Geometric view of lugdunin (**6**) and its analogue **109**. Due to arrangement of the amino acid side chains, analogue **109** appears more symmetrical than lugdunin (**6**). Mirror planes are drawn in dark grey dashed lines.

By drawing a mirror plane from the peptide bond of D-leucine and L-valine through the thiazolidine moiety, the replacement of D-valine in position 6 by D-tryptophan results in almost identical side chains on the left and right sides of the mirror plane, stereochemistry excluded (Figure 89). Only the leucine side chain and the valine side chain do not match but are very similar and differ only by an additional CH_2 group in leucine.

Single-channel recordings on black lipid membranes in presence of monovalent ions revealed that lugdunin (**6**) does also translocate Na^+ and K^+ and creates a concentration imbalance of these crucial ions. In addition, the conductance state for K^+ is similar to that found for gramicidin S (**116**), indicating that the diameter of the lugdunin nanotube pore is approximately 4 Å.[165] This was also confirmed by in silico studies suggesting that the diameter is 3.66 Å.[151]

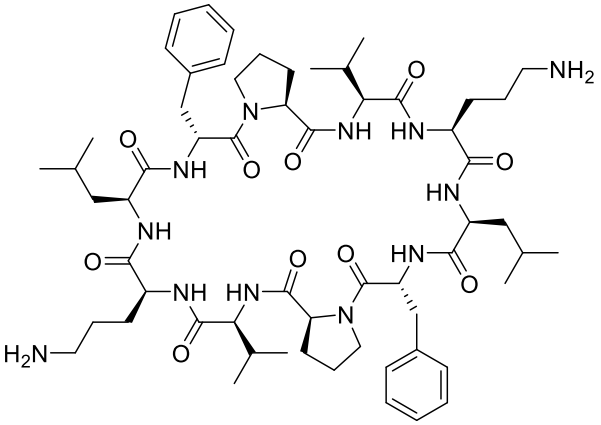

gramicidin S (**116**)

In contrast, *N*-methylated analogues **110**, **111** and **113** have a significantly lower proportion of β-sheets and a significantly higher proportion of disordered secondary structures.[151] This finding strongly suggests that *N*-methylation of the peptide backbone impairs hydrogen bonding and β-sheet formation. Without the formation of peptide nanotubes in the lipid membrane, translocation of protons cannot occur, so dissipation of membrane potential is not observed in Gram-positive bacteria.

Based on these results, the research hypothesis suggests that lugdunin (**6**) first immerses into the membrane, where peptide nanotubes are spontaneously formed through hydrogen bonding and β-sheet formation. The formed channels can then transport ions, such as protons, but also sodium and potassium cations (Figure 90). In contrast, *N*-methylated analogues **110**, **111** and **113** do partition into lipid membranes, but do not form ion channels, likely due to the disruption of β-sheet formation.[151]

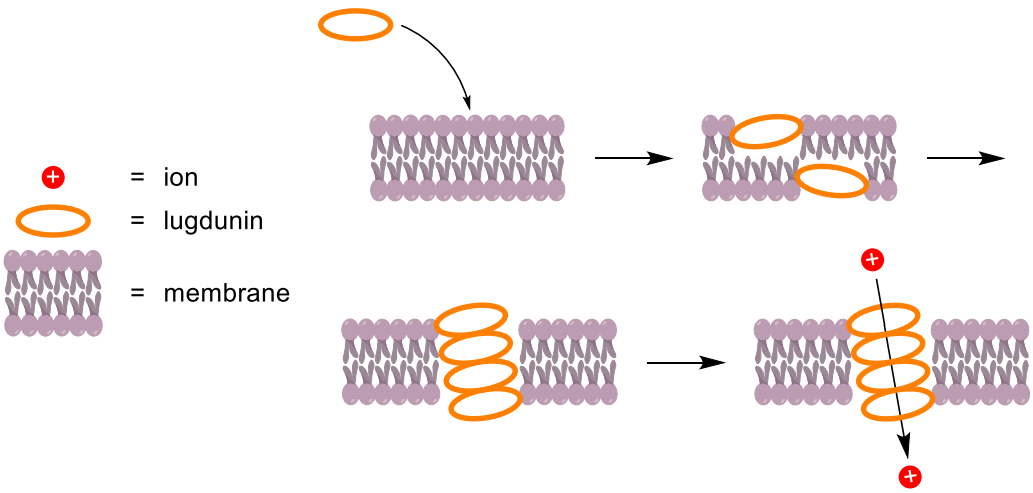

Figure 90: Proposed mode of action for lugdunin (**6**). First, lugdunin (**6**) penetrates the membrane and forms peptide nanotubes, which can then translocate protons and dissipate the membrane potential of susceptible bacteria. Adapted from[151].

3.3.2. Synthetic studies towards polar analogues of lugdunin

First, proof of principle is needed to show that lugdunin (**6**) can inhibit the growth of Gram-negative bacteria when the outer membrane is compromised. To this end, lugdunin (**6**) was tested against various *E. coli* strains in the presence and absence of polymyxin B nonapeptide (**117**), an additive that damages the outer membrane and allows diffusion of lugdunin (**6**) into the periplasm, where lugdunin (**6**) can find its target.[166] In addition, lugdunin (**6**) was also tested by A. BERSCHEID (Research group BRÖTZ-OESTERHELT, University of Tübingen) against efflux pump-deficient mutants of *E. coli* strains. The MIC assays showed that lugdunin (**6**) efficiently inhibited the growth of the tested *E. coli* strains only when the outer membrane was compromised by polymyxin B nonapeptide (**117**), with the efflux pump-deficient mutants being more susceptible to lugdunin (**6**) and polymyxin B nonapeptide (**117**).

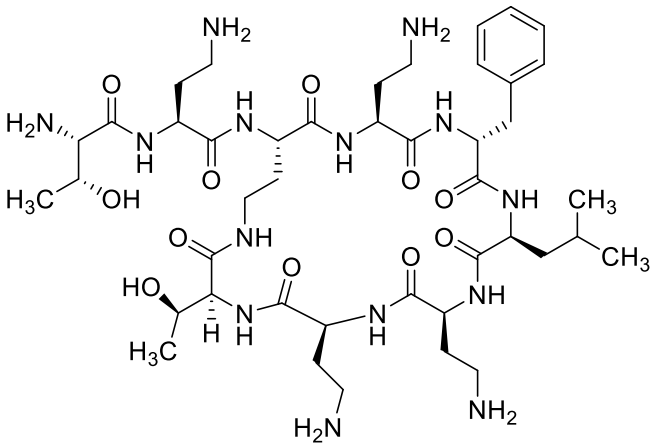

polymyxin B nonapeptide (**117**)

The MIC values ranged from 6.25 $\mu g \cdot mL^{-1}$ to 50 $\mu g \cdot mL^{-1}$ (Table 8, experimental section 6.5.). These results show that when lugdunin (**6**) passes through the outer membrane, it can exert its antimicrobial effect in Gram-negative bacteria. Derivatives, which do inhibit the growth of Gram-positive bacteria and can penetrate the outer membrane of Gram-negative bacteria should therefore also be active against Gram-negative bacteria. To achieve this, the eNTRy rules established by HERGENROTHER and colleagues provide valuable insights (Figure 7). These rules emphasize the importance of structural features like an ionizable nitrogen, reduced three-dimensionality, and rigidity for efficient penetration of the outer membrane in Gram-negative bacteria.[53-55] Applying these principles could guide modifications to enhance lugdunin's (**6**) uptake and activity against Gram-negative strains.

Consequently, primary amines are incorporated into the lugdunin molecule, which should increase the uptake in Gram-negative bacteria.[55]

Lugdunin analogues with polar amino acid side chains can be prepared using SPPS to produce the linear peptide, which then is subjected to macrolactamization reaction to yield the desired lugdunin analogue. However, when incorporating a primary amine into lugdunin (**6**) at amino acid position 2, 3 or 5, the formation of side products during macrolactamization needs to be considered. An unprotected primary amine of an amino acid side chain could lead to unintended intramolecular ring closures or even intermolecular condensation reactions resulting in incorrectly cyclized analogues, polymers or a mixture of both (Figure 91).

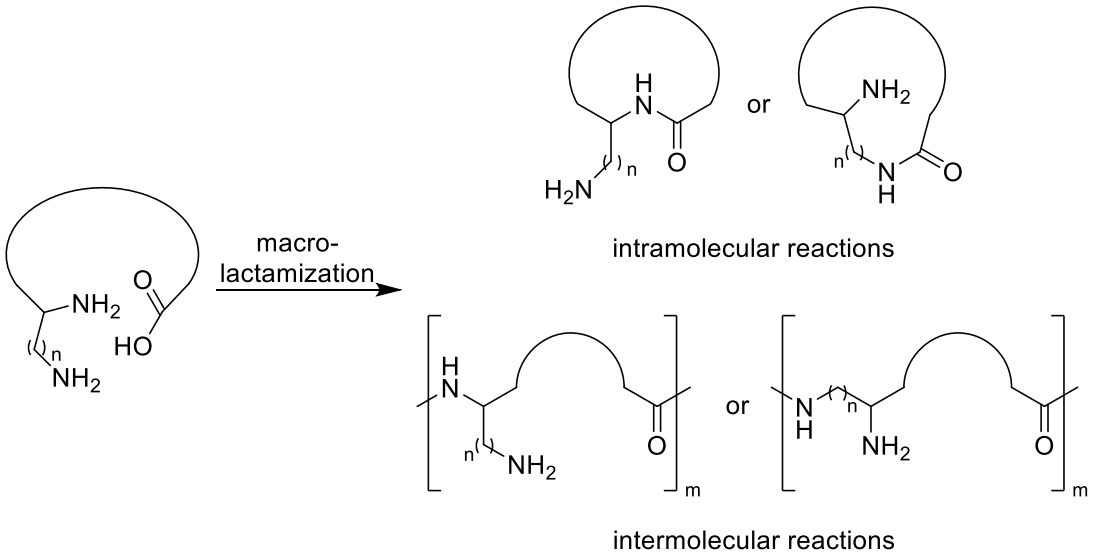

Figure 91: Schematic illustration of putative outcomes of the macrolactamization reaction of lugdunin analogues with unprotected primary amines in amino acid side chain.

The macrolactamization reaction is carried out in highly diluted solutions (2 mM of linear peptide), which favors an intramolecular reaction instead of an intermolecular reaction. To avoid undesired side products in the intramolecular reaction, amino protecting groups are removed after macrolactamization. These protecting groups should be stable under basic and acidic conditions, since coupling steps take place under basic conditions and the resin cleavage of the linear peptide under acidic conditions. In addition, the corresponding amino acids should be commercially available. These requirements for protecting groups are met by allyloxycarbonyl (Alloc), benzyloxycarbonyl (Cbz) or the 1-(4,4-dimethyl-2,6-dioxocyclohex-1-ylidene)ethyl (Dde) protecting groups. Alloc can be selectively deprotected using $Pd(PPh_3)_4$ and $PhSiH_3$, Cbz can be removed with a solution of thioanisole in TFA, and

Dde can be cleaved by treatment with 2% $N_2H_4 \cdot H_2O$ in THF (see experimental section 6.4.2.2.).[167-170]

Ornithine and the aromatic aniline-like amino acid 4-amino-L-phenylalanine were used with the appropriate protecting group to incorporate a primary amine into the lugdunin molecule. Therefore, protected 6-Trp-lugdunin-like derivatives **118**–**122** (Figure 92, experimental section 6.4.2.2.) were successfully synthesized in good yields (80%–98%, in 20–50 mg scale) using the Fmoc strategy for SPPS.

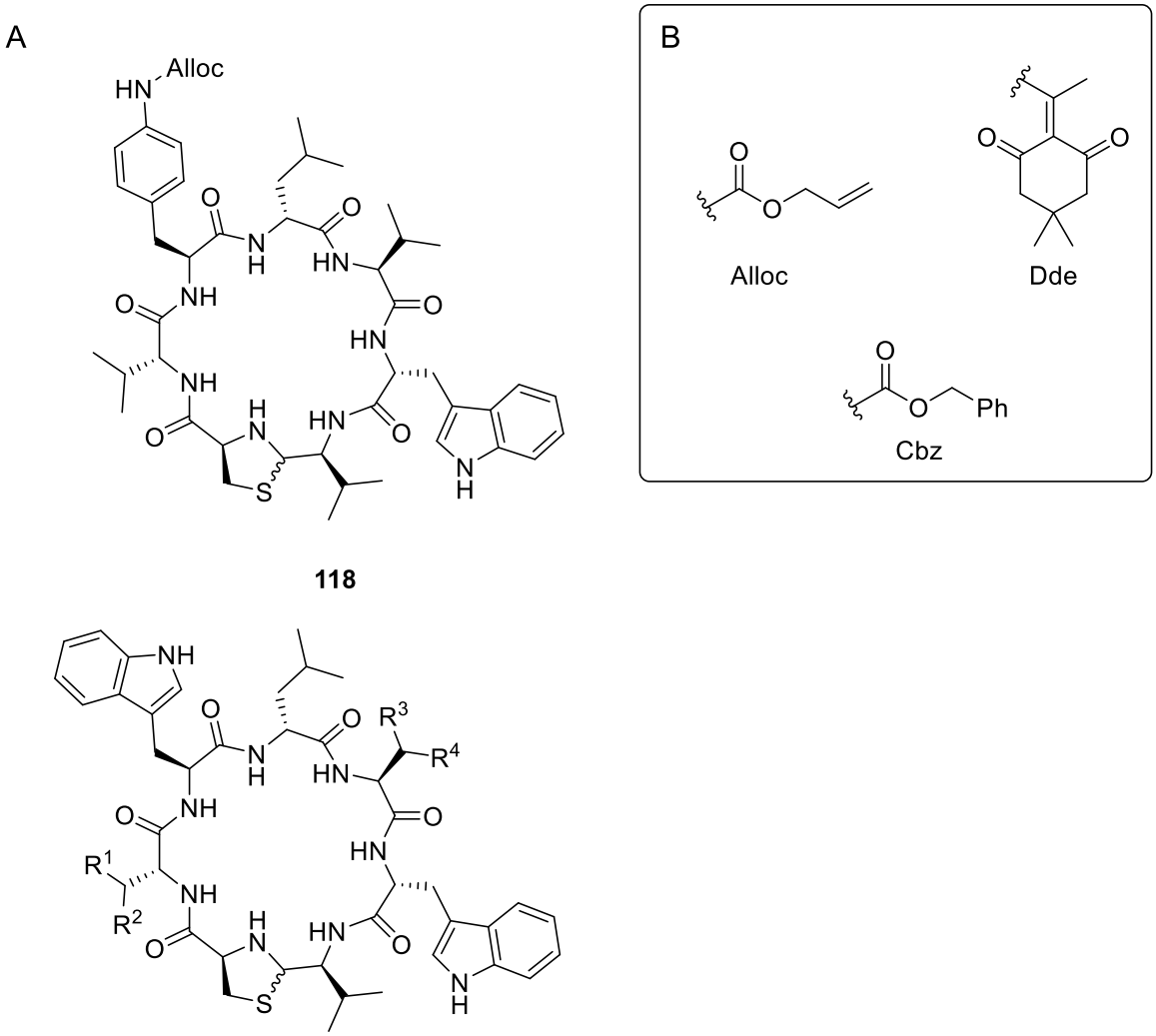

118

2-Orn(Cbz)-6-Trp-Lug (**119**), R^1 = H, R^3 = R^4 = CH_3, R^2 = $CH_2CH_2NH(Cbz)$
5-Orn(Cbz)-6-Trp-Lug (**120**), R^3 = H, R^1 = R^2 = CH_3, R^4 = $CH_2CH_2NH(Cbz)$
2,5-Di-Orn(Cbz)-6-Trp-Lug (**121**), R^1 = R^3 = H, R^2 = R^4 = $CH_2CH_2NH(Cbz)$
2,5-Di-Orn(Dde)-6-Trp-Lug (**122**), R^1 = R^3 = H, R^2 = R^4 = $CH_2CH_2NH(Dde)$

Figure 92: A) Synthesized protected 6-Trp-lugdunin derivatives **118**–**122**. B) Structures of Alloc, Dde and Cbz protecting groups for the amino residue.

The protected lugdunin-like derivatives **123**–**125** (Figure 93, experimental section 6.4.2.2.) were also successfully synthesized in good yields (78%–88%, in 20–50 mg scale) using the Fmoc strategy for SPPS.

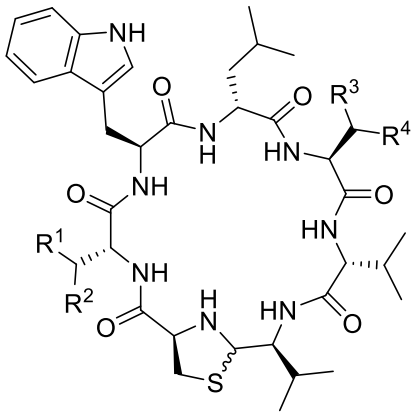

2-Orn(Cbz)-Lug (**123**),
R^1 = H, R^3 = R^4 = CH_3, R^2 = $CH_2CH_2NH(Cbz)$

5-Orn(Cbz)-Lug (**124**),
R^3 = H, R^1 = R^2 = CH_3, R^4 = $CH_2CH_2NH(Cbz)$

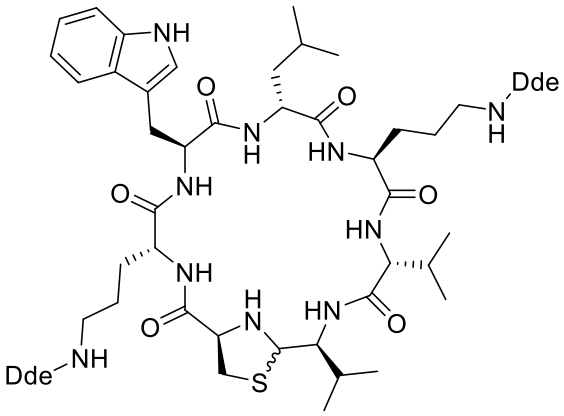

2,5-Di-Orn(Dde)-Lug (**125**)

Figure 93: Synthesized protected lugdunin derivatives **123**–**125**.

The synthesized compounds **118**–**125** were tested by B. KRISMER against MRSA. Only 2-Orn(Cbz)-Lug (**123**) showed an inhibitory effect at 6.25 µg·mL^{-1}, which shows that the 2-position in lugdunin (**6**) is more suitable for substitution than other positions in the molecule (experimental section 6.5., Table 6).

Palladium catalyzed deprotection of the Alloc protecting group in 3-(4-NH(Alloc)-Phe)-6-Trp-Lug (**118**) gave 3-(4-NH_2-Phe)-6-Trp-Lug (**126**) in only 9% yield after HPLC (experimental section 6.4.2.2.).

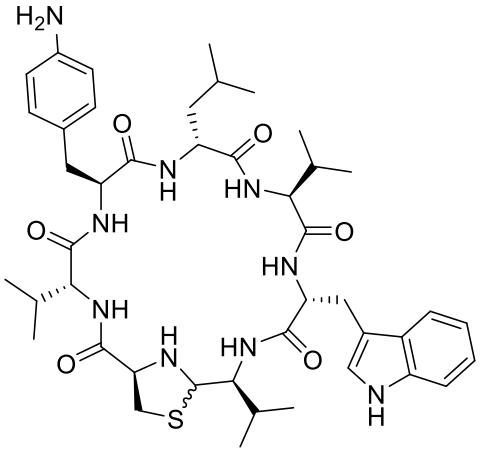

126

The poor yield can probably be explained by sulfur-poisoning of the palladium catalyst, which is likely caused by the sulfur containing thiazolidine moiety.[171, 172] However, the educt **118** could not be recovered.

The deprotection of Cbz protected derivatives **119**–**121**, **123** and **124** was achieved by using a mixture of trifluoroacetic acid and thioanisole (experimental section 6.4.2.2.). This method led to the corresponding products **127**, **128**, **130** and **131** in very good yields (90–95%, in 20–50 mg scale) for the mono-ornithine analogues **119**, **120**, **123** and **124**.

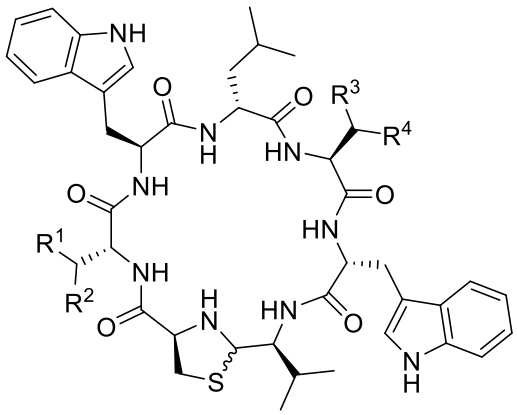

2-Orn-6-Trp-Lug (**127**),
R^1 = H, R^3 = R^4 = CH_3, R^2 = $CH_2CH_2NH_2$

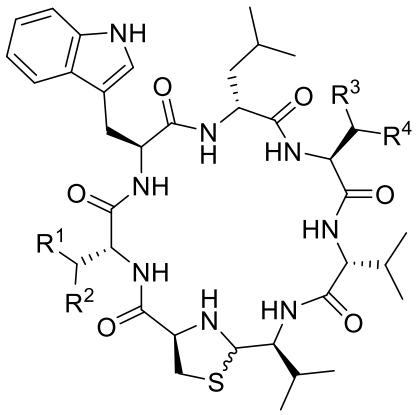

2-Orn-Lug (**130**),
R^1 = H, R^3 = R^4 = CH_3, R^2 = $CH_2CH_2NH_2$

5-Orn-6-Trp-Lug (**128**),
R^3 = H, R^1 = R^2 = CH_3, R^4 = $CH_2CH_2NH_2$

5-Orn-Lug (**131**),
R^3 = H, R^1 = R^2 = CH_3, R^4 = $CH_2CH_2NH_2$

Figure 94: Synthesized deprotected lugdunin analogues **127**, **128**, **130** and **131**.

For 2,5-Di-Orn(Cbz)-6-Trp-Lug (**121**), however, this deprotection strategy yielded a product mixture with 2,5-Di-Orn-6-Trp-Lug (**129**) as the main component. Using HPLC-ESI-MS (experimental section 6.1.4.) mono- and dibenzylated side products **132**–**134** (Figure 96) were identified in the mixture (Figure 95). These side products likely resulted from unintended alkylation in the reaction process. Given the presence of three amino groups in compounds **129** and **132**–**134**, and the acidic conditions (~pH 2) during HPLC-ESI-MS analysis (experimental section 6.1.4.), the most prominent signal observed for these compounds corresponds to the $[M+2H]^{2+}$ adduct. The extracted ion chromatograms (EIC) of the specified $[M+2H]^{2+}$ adducts are shown in Figure 95, facilitating a direct comparison of these compounds.

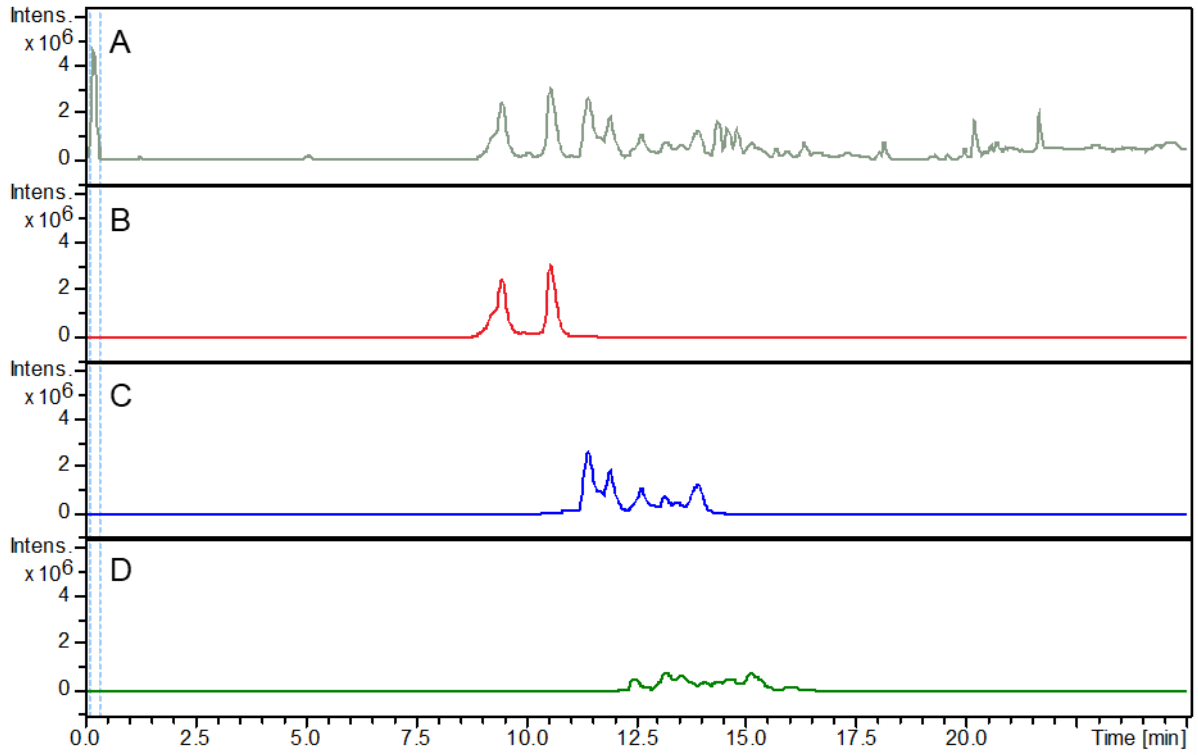

Figure 95: HPLC-MS analysis of deprotection of **121** after work-up (experimental section 6.4.2.2.). A) BPC (grey), B) EIC (red) of analogue **129** ($C_{46}H_{67}N_{11}O_6S^{2+}$ $[M+2H]^{2+}$, *m/z* 450.7493±0.05), C) EIC (blue) of mono benzylated side products **132** and **133** ($C_{53}H_{73}N_{11}O_6S^{2+}$ $[M+2H]^{2+}$, *m/z* 495.7728±0.05), D) EIC (green) of dibenzylated side product **134** ($C_{60}H_{79}N_{11}O_6S^{2+}$ $[M+2H]^{2+}$, *m/z* 540.7962±0.05).

The acidic deprotection of the Cbz groups in 2,5-Di-Orn(Cbz)-6-Trp-Lug (**121**) is initiated by protonation of the carbonyl oxygen of **121**, making the carbonyl carbon more electrophilic (Figure 96). This facilitates the nucleophilic attack of thioanisole on the benzyl carbon, leading to the formation of carbamic acid **135** and the benzylmethylphenyl sulfonium cation (**136**, Figure 96). Carbamic acid **135** subsequently undergoes decomposition, releasing carbon dioxide and yielding the desired product 2,5-Di-Orn-6-Trp-Lug (**129**). However, the cationic intermediate **136** remains in the reaction mixture and is highly reactive, making it prone to nucleophilic attack by a variety of nucleophiles, including the amino groups of 2,5-Di-Orn-6-Trp-Lug (**129**). This results in the formation of side products **132**–**135** as shown in Figure 96.[173]

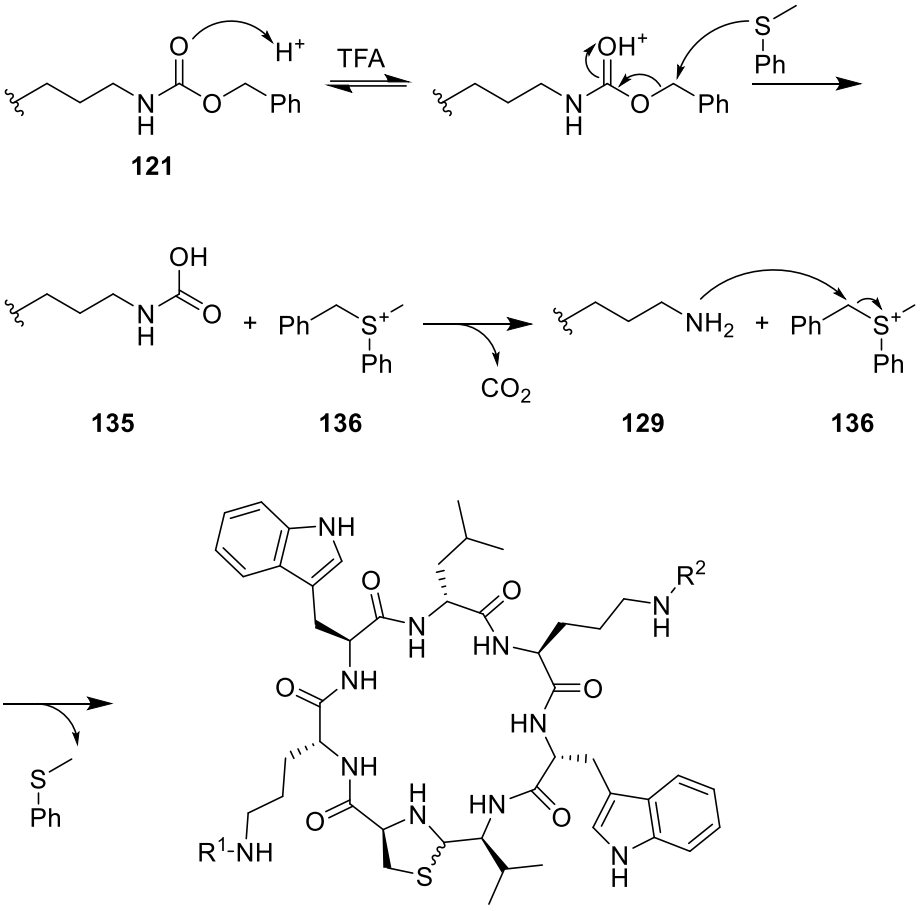

2,5-Di-Orn-6-Trp-Lug (**129**), $R^1 = R^2 = H$
2-Orn(Bn)-5-Orn-6-Trp-Lug (**132**), $R^2 = H$, $R^1 = Bn$
2-Orn-5-Orn(Bn)-6-Trp-Lug (**133**), $R^1 = H$, $R^2 = Bn$
2,5-Di-Orn(Bn)-6-Trp-Lug (**134**), $R^1 = R^2 = Bn$

Figure 96: Deprotection mechanism of Cbz using trifluoroacetic acid and thioanisole.

However, trifluoroacetic acid is both an acid and a solvent in this reaction, so that the amines should be predominantly protonated, which significantly should reduce their nucleophilicity. After HPLC purification, 2,5-Di-Orn-6-Trp-Lug (**129**) was isolated in 20% (4.5 mg) yield.

Hydrazinolysis of Dde-protected derivatives 2,5-Di-Orn(Dde)-6-Trp-Lug (**122**) and 2,5-Di-Orn(Dde)-Lug (**125**) with a solution of hydrazine monohydrate in tetrahydrofuran gave the corresponding products 2,5-Di-Orn-6-Trp-Lug (**129**) and 2,5-Di-Orn-Lug (**137**) in moderate yields (49%, 7.5 mg and 55%, 8.3 mg respectively) after HPLC purification (experimental data 6.4.2.2.). In this case, no formation of side products was observed.

The synthesized compounds **126**–**131**, **137**, and the obtained crude mixture of 2,5-Di-Orn-6-Trp-Lug (**129**) and **132**–**134** were tested against MRSA. Inhibition of growth was observed for 2-Orn-6-Trp-Lug (**127**, 100 µg · mL^{-1}, experimental

section 6.5., Table 6) and **126**–**131** (50 µg·mL^{-1}, experimental section 6.5., Table 6). The MIC values observed are comparable with the MIC value of lugdunin (**6**) for *E. coli* with polymyxin B nonapeptide (**117**) as additive (50 µg·mL^{-1}). Interestingly, the MIC value observed for the crude mixture of **132**–**134** and 2,5-Di-Orn-6-Trp-Lug (**129**) was at 12.5 µg·mL^{-1}. After isolation of 2,5-Di-Orn-6-Trp-Lug (**129**) from the crude mixture by HPLC (experimental section 6.4.2.2.), the MIC assay against MRSA was repeated with purified 2,5-Di-Orn-6-Trp-Lug (**129**), resulting in an observed MIC value of 50 µg·mL^{-1}. The additional benzyl groups in compounds **132**–**134** can either increase the bioactivity due to interactions with the bacterial membrane or transporter systems[174, 175], or the interaction between the compounds contained in the mixture could have a synergistic effect leading to increased bioactivity.[176, 177]

2-Orn-6-Trp-Lug (**127**), 5-Orn-6-Trp-Lug (**128**), 2,5-Di-Orn-6-Trp-Lug (**129**), 2-Orn-Lug (**130**), 5-Orn-Lug (**131**) and 2,5-Di-Orn-Lug (**137**) were then tested against *E. coli*, and 2-Orn-6-Trp-Lug (**127**) and 2,5-Di-Orn-Lug (**137**) were found to have an MIC value of 50 µg·mL^{-1}, respectively. No inhibition was observed for the other compounds (experimental section 6.5., Table 7).

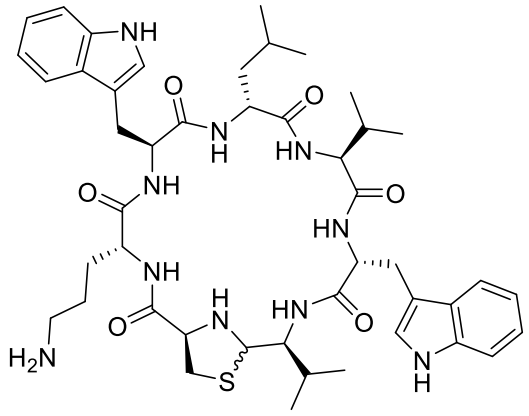

2-Orn-6-Trp-Lug (**127**)

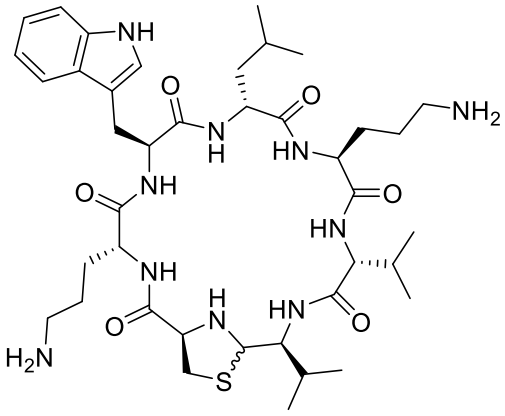

2,5-Di-Orn-Lug (**137**)

These results indicate that penetration of the outer membrane in Gram-negative bacteria was achieved by the introduction of ornithine in the lugdunin molecule. However, the MIC values are not in the low micromolar range as with other potent antimicrobial agents, such as quinolone or β-lactam antibiotics.[178, 179] On the one hand, the efflux pumps are efficient at actively transporting antimicrobial agents out of the cell, leading to less accumulation and thus to a lower activity of antimicrobial compounds.[180]

On the other hand, the interaction of ornithine analogues with the membrane of bacterial cells could be impaired by introducing a polar side chain, as the bacterial membrane is lipophilic and thus immersion in this membrane is hindered by polar moieties (see chapter 3.3.1).

4. Summary of results

The global spread of antimicrobial resistance is increasing at an alarming rate. This threat requires not only ways to prevent infections, but also the development of novel drugs and new mechanisms to fight infections.

1. Epifadin (**24**)

In this thesis, a novel natural product class of peptide-polyene-tetramic acid was isolated from *Staphylococcus epidermidis* IVK83 in collaboration with the KRISMER/PESCHEL group. Comprehensive analytical, biological and chemical methods were used to elucidate the structure of epifadin (**24**). It is a highly instable NRPS-PKS-NRPS hybrid compound that requires mild handling conditions, including a pH of 5.5, protection from light, an inert argon atmosphere, and DMSO as solvent for dissolution. The unprecedented and unique structure consists of a tetrapeptide moiety, a polyene chain and an aspartate-tetramic acid moiety.

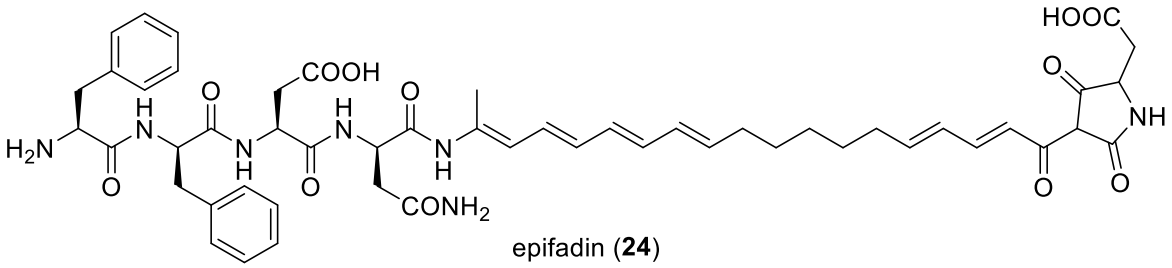

epifadin (**24**)

Epifadin (**24**) effectively inhibits growth of Gram-positive bacteria, including resistant *Staphylococcus aureus* strains that pose a global threat, Gram-negative bacteria and yeasts. In addition, epifadin (**24**) does not exhibit cytotoxicity in the cell viability assays conducted on MRC5 cells. Its wide target spectrum and short-lifespan under *in vivo*-like conditions could limit the collateral damage of bacteria, which would be beneficial for the human microbiota. These results were successfully published in *Nature Microbiology* 2024.

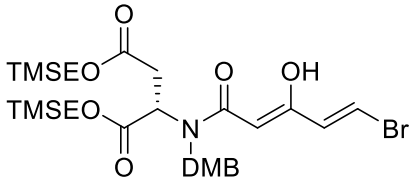

67

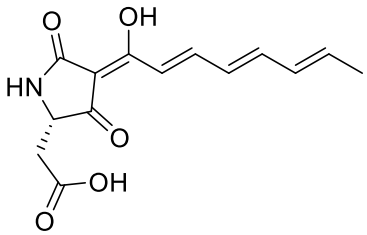

30

Furthermore, synthetic studies were carried out to study the building blocks for a potentially stable epifadin derivative. Therefore, the flexible building block **67** was

synthesized which was used to produce the potential liver fibrosis inhibitor MCA17-1 (**30**).

2. Cystargolides

In addition, semi-syntheses of *N*-ethylcystargolides **103** and **104** were carried out, which led to optimized bioactivity compared to the natural carboxylic acids **101** and **102**. In collaboration with BRÖTZ-OESTERHELT group hemolysis assays and growth inhibition assays were carried out and suggest that bioactivity was increased through improved cell penetration and inhibition of ClpP. These findings were successfully published in *Angewandte Chemie* 2024.

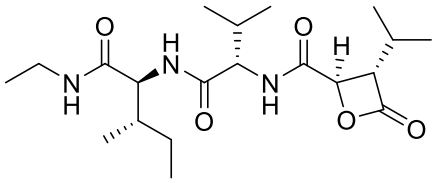

103

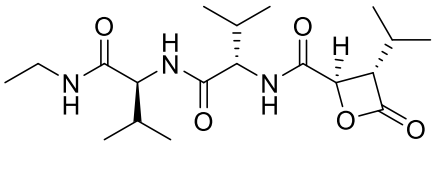

104

3. Lugdunins

3.1. *N*-Methyl lugdunins

In the next part of this thesis lugdunin analogues (e.g. **110**) were synthesized using solid support and subsequently analyzed using analytical, biological, biophysical, chemical and computational methods. These derivatives were used to investigate the mechanism of action of lugdunin (**6**). *N*-methylation of various positions in the peptide backbone showed that hydrogen bonds are crucial for the bioactivity of lugdunin (**6**). Moreover, it was shown that lugdunin (**6**) first interacts with the bacterial membrane, then immerses into the membrane and forms peptide nanotube structures that translocate protons and monovalent ions. These results were successfully published in *Nature Communications* 2024.

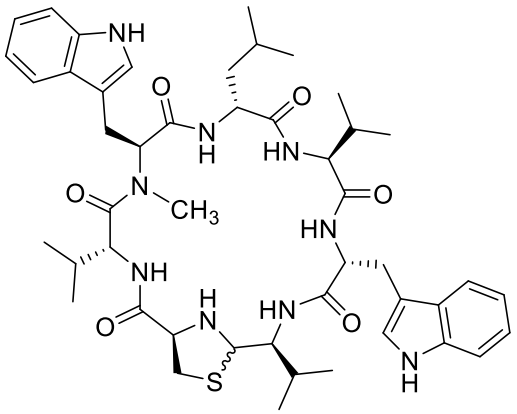

110

3.2. Lugdunins against Gram-negative bacteria

In the last part of this thesis, lugdunin (**6**), a Gram-positive-only antimicrobial peptide, was converted into an antimicrobial agent that can inhibit the growth of Gram-negative bacteria. The HERGENROTHER strategy of an introduction of primary amines into the lugdunin structure (see **127** and **137**) enabled penetration into the outer membrane of Gram-negative bacteria, allowing lugdunin (**6**) to exert its antimicrobial effect, presumably acting as a protonophore, in the inner membrane of Gram-negative bacteria.

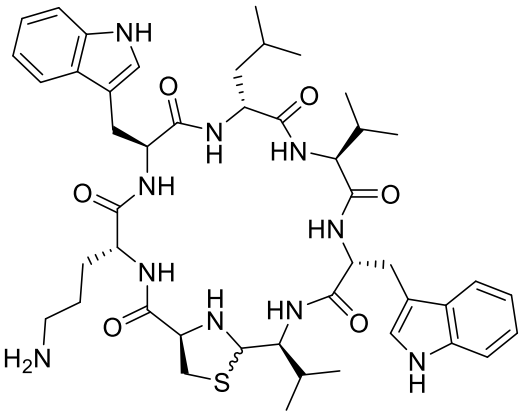

2-Orn-6-Trp-Lug (**127**)

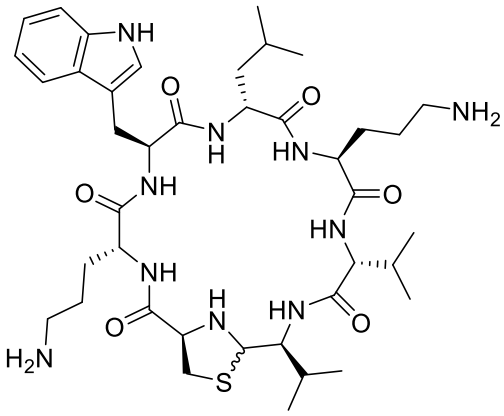

2,5-Di-Orn-Lug (**137**)

4.1. Zusammenfassung

Die weltweite Ausbreitung der antimikrobiellen Resistenz steigt mit einer alarmierenden Rate an. Diese Bedrohung erfordert nicht nur Maßnahmen zur Prävention von Infektionen, sondern auch die Entwicklung neuartiger Medikamente und Mechanismen zur Bekämpfung von Infektionen.

1. Epifadin (**24**)

Im Rahmen dieser Dissertation wurde eine neuartige Naturstoffklasse mit Peptid-Polyen-Tetramsäure-Struktur aus dem *Staphylococcus epidermidis* IVK83-Stamm in Zusammenarbeit mit der KRISMER/PESCHEL-Gruppe isoliert. Um die Struktur von Epifadin (**24**) aufzuklären, wurden umfassende analytische, biologische und chemische Methoden angewandt. Es handelt sich um eine höchst instabile NRPS-PKS-NRPS-Hybridverbindung, die unter sehr milden Bedingungen gehandhabt werden muss. Die schließt einen pH-Wert von 5.5, Schutz vor Licht, eine inerte Argonatmosphäre und DMSO als Lösungsmittel ein. Die neuartige und einzigartige Struktur besteht aus einem Tetrapeptid, einer Polyenkette und einer Aspartat-Tetramsäure.

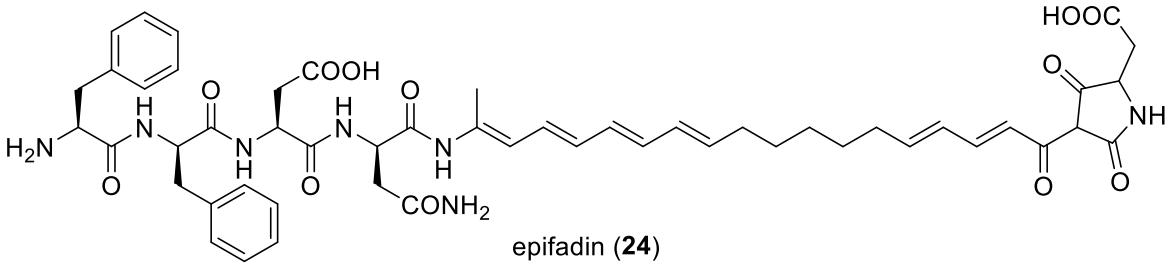

epifadin (**24**)

Epifadin (**24**) hemmt wirksam das Wachstum Gram-positiver Bakterien, einschließlich resistenter *Staphylococcus aureus*-Stämme, welche eine globale Bedrohung darstellen, sowie Gram-negativer Bakterien und Hefen. Darüber hinaus zeigte Epifadin (**24**) in Zellviabilitätsassays mit MRC5-Zellen keine Zytotoxizität. Das breite Wirkspektrum und die kurze Lebensdauer unter *in vivo*-ähnlichen Bedingungen könnten den Kollateralschaden für Bakterien begrenzen, was für die menschliche Mikrobiota von Vorteil wäre. Diese Ergebnisse wurden erfolgreich in *Nature Microbiology* 2024 veröffentlicht.

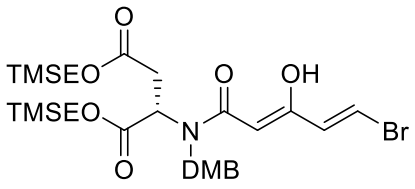

67

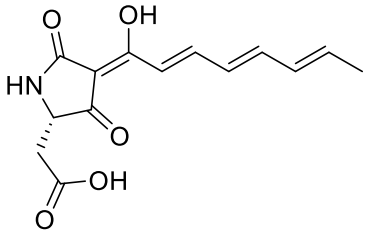

30

Des Weiteren wurden synthetische Studien durchgeführt, um Bausteine für potenziell stabile Epifadin-Derivate zu untersuchen. Dabei wurde der synthetisch flexible Baustein **67** synthetisiert, der zur Herstellung des potenziellen Leberfibrose-Inhibitors MCA17 1 (**30**) verwendet wurde.

2. Cystargolide

Darüber hinaus wurden Semisynthesen der *N*-Ethylcystargoliden **103** und **104** durchgeführt, welche im Vergleich zu den natürlichen Carbonsäuren **101** und **102** eine optimierte Bioaktivität aufwiesen. In Zusammenarbeit mit der BRÖTZ-OESTERHELT-Gruppe wurden Hämolyse- und Wachstumshemmungsassays durchgeführt, welche darauf hindeuten, dass die Bioaktivität durch eine verbesserte Zellpenetration und Hemmung von ClpP gesteigert wurde. Diese Ergebnisse wurden erfolgreich in *Angewandte Chemie* 2024 veröffentlicht.

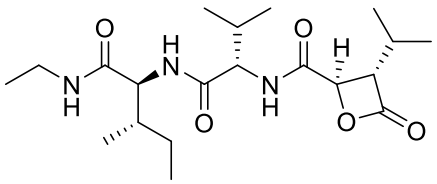

103

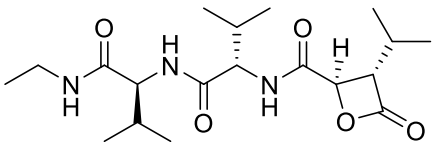

104

3. Lugdunine

3.1. *N*-Methyl-Lugdunine

In einem weiteren Teil dieser Arbeit wurden Lugdunin-Derivate (z.B. **110**) unter Verwendung von Festphasenpeptidsynthese hergestellt und anschließend mittels analytischer, biologischer, biophysikalischer, chemischer und computergestützter Methoden untersucht. Diese Derivate wurden verwendet, um den Wirkmechanismus von Lugdunin (**6**) zu erforschen. Die *N*-Methylierung verschiedener Positionen im Peptidrückgrat zeigte, dass Wasserstoffbrückenbindungen entscheidend für die Bioaktivität von Lugdunin (**6**) sind. Es wurde zudem nachgewiesen, dass Lugdunin (**6**) zunächst mit der bakteriellen Membran interagiert, dann in die Membran eintaucht und

Peptidnanotubes bildet, welche Protonen und einwertige Ionen transportieren. Diese Ergebnisse wurden erfolgreich in *Nature Communications* veröffentlicht.

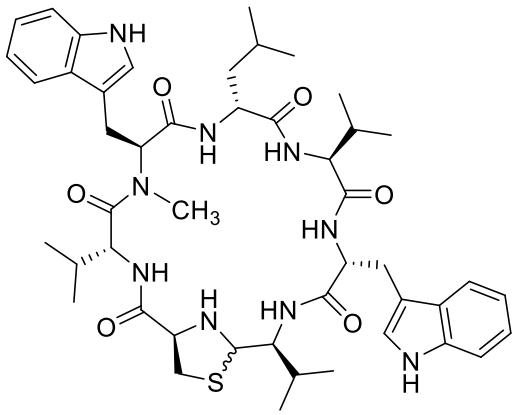

110

3.2. Lugdunine gegen Gram-negative Bakterien

Im letzten Teil dieser Arbeit wurde Lugdunin (**6**), ein antimikrobielles Peptid welches ausschließlich gegen Gram-positive Bakterien wirkt, in eine antimikrobielle Verbindung überführt, welche auch das Wachstum Gram-negativer Bakterien hemmen kann. Die HERGENROTHER-Strategie der Einführung primärer Amine in die Lugdunin-Struktur (siehe **127** und **137**) ermöglichte das Eindringen in die äußere Membran Gram-negativer Bakterien, wodurch Lugdunin (**6**) seine antimikrobielle Wirkung, vermutlich als Protonophor, in der inneren Membran Gram-negativer Bakterien entfalten konnte.

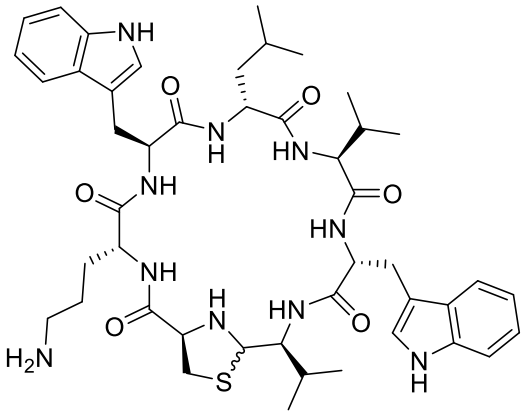

2-Orn-6-Trp-Lug (**127**)

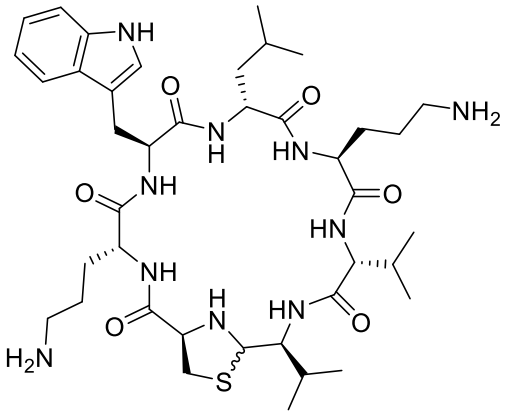

2,5-Di-Orn-Lug (**137**)

5. Outlook

- The high instability of epifadin (**24**) complicates or even impedes its use as an antimicrobial compound. However, stabilizing chemical adjuvants might be attractive for daily-use applications and could help to prevent *Staphylococcus aureus* colonization in and on humans, which should be further investigated. In order to study the unprecedented and unique structure of epifadin (**24**), synthetic work should focus on producing a stable epifadin-like molecule with the same unique structural features of epifadin (**24**). Specifically, we here suggest that the molecule should match molecular size of epifadin (**24**). Once a synthetic route is developed, structure-activity relationships could provide further information about epifadin's mechanism of action and thus a stable and possibly more effective antimicrobial compound could subsequently be produced.

- *N*-Ethylcystargolides **103** and **104** showed promising inhibitory properties against ClpP, which is also overexpressed in various carcinomas. The cystargolides **101**–**104** could therefore be investigated as potential anticancer drugs.

- The elucidation of lugdunin's mode of action provided information on which amino acids interact with the bacterial membrane and how exactly the peptide nanotubes are formed. Furthermore, the tilt angle of 6-Trp-lugdunin (**109**) is significantly lower compared to lugdunin (**6**), and interestingly, 6-Trp-lugdunin (**109**) also exhibits higher bioactivity. This suggests that the tilt angle may as well have an influence on the proton translocation properties, which should be further investigated by producing more symmetrical bioactive lugdunin derivatives.

- Converting lugdunin (**6**) into a broad-spectrum antimicrobial compound focused on Gram-negative bacteria in this thesis. Bioactivity against Gram-negative bacteria was also achieved, albeit still too low (50 $\mu g \cdot mL^{-1}$). However, modifications on the amine of the ornithine residue, such as selective benzylation or alkylation could lead to improved accumulation in Gram-negative bacteria and thus to higher bioactivity. Furthermore, the removal of lugdunin (**6**)

from the cellular interior by efflux pumps should be addressed. The primary amines in position 2 or 5 can now be used to couple a linker to lugdunin analogues that can carry an efflux pump inhibitor, such as reserpine, eugenol or polyamines.[181, 182] Enzymatic cleavage of the efflux pump inhibitor in the periplasmic space could inhibit the pumping out of antimicrobial agents.

B. EXPERIMENTAL PART

6. Materials and Methods

6.1. Instrumental analytics

6.1.1. HPLC instruments

(Semi)-preparative HPLC

Thermo Scientific Ultimate 3000 with HPG 3200 BX pump, Knauer online degasser and DAD-3000RS detector with a semipreparative detection cell, operated by Chromeleon® version 6.80. A manual Rheodyne valve with a 1000 µL loop for sample injection was used.

*Method A: SCHILLING's method for purification of epifadin (**24**).*

Precipitate (Experimental section 6.4.1.) was extracted with DMSO, freeze-dried and extracted again with MeCN/water/TFA (50/50/0.05) prior to injecting into HPLC.

Solvent 1: Water with 0.05% TFA, solvent 2: MeCN/water (8/2) with 0.05% TFA; gradient: 50% of solvent 2 to 100% of solvent 2 in 30 min; column: Kromasil 100 C18, 7 µm, 250 × 20 mm, Dr. Maisch GmbH; flow rate: 12 $mL \cdot min^{-1}$.

*Method B: Stability of epifadin (**24**) in MeCN/H_2O/TFA in dark and light-exposed.*

Two samples were prepared by extracting the dried DMSO extract ⑤ with acetonitrile/water/TFA, (50/50/0.05) and exposing one to ambient light, while the other sample is stored in the dark at room temperature. Chromatograms at 383 nm were then recorded four times every 90 minutes.

Solvent 1: Water with 0.05% TFA, solvent 2: MeCN with 0.05% TFA; gradient: 40% of solvent 2 to 80% of solvent 2 in 30 minutes; column: Kromasil 100 C18, 5 µm, 250 × 8 mm, Dr. Maisch GmbH; flow rate: 2 $mL \cdot min^{-1}$.

*Method C: Purification of epifadin (**24**).*

Solvent 1: Water with 0.1% FA, solvent 2: MeCN with 0.1% FA; gradient: 40% of solvent 2 for 20 min then 50% of solvent 2 for 20 min; column: Kromasil 100 C18, 7 µm, 250 × 20 mm, Dr. Maisch GmbH; flow rate: 12 $mL \cdot min^{-1}$. Fractions were collected in a round-bottom flask with Argon atmosphere at –80°C in the dark.

Analytical HPLC

1260 Infinity (Agilent) system: Pump: 1260 binary pump, detector: 1260 DAD WR, autosampler: 1260 Infinity standard autosampler with a 100 µL sample loop, fraction collector: 1260 A-FC, column oven: 1290 MCT, software: Open LAB CDC, Chem Station Edition (Agilent Technologies).

*Method D: Optimizing DMSO content in extraction of epifadin (**24**) from precipitate*

For each sample, 10 mg of the precipitate was first treated with the corresponding amount (0–40 µL) of DMSO and then 160 µL of acetonitrile-water-TFA (80/20/0.05) were added. The samples were vortexed, centrifuged, and 10 µL of the supernatant was injected into an analytical HPLC system.

Solvent 1: Water with 0.05% TFA, solvent 2: MeCN with 0.05% TFA, gradient: 40% of solvent 2 to 80% of solvent 2 in 30 minutes, column: Kromasil 100 C18, 5 µm, 250 × 4 mm, Dr. Maisch GmbH; flow rate: 0.5 $mL \cdot min^{-1}$.

*Method E: Testing stability of epifadin (**24**) in different organic solvents*

For each sample, 20 mg of the precipitate was extracted with 1 mL of the corresponding solvent (DMSO, DMSO + 0.03% TFA, MeOH, MeOH + 0.03% TFA, nitrobenzene), then vortexed and centrifuged. 20 µL of the supernatant was injected into HPLC.

Solvent 1: Water with 0.05% TFA, solvent 2: MeCN with 0.05% TFA, gradient: 40% of solvent 2 to 80% of solvent 2 in 30 minutes, column: Kromasil 100 C18, 5 µm, 250 × 4 mm, Dr. Maisch GmbH; flow rate: 0.5 $mL \cdot min^{-1}$.

6.1.2. Flash chromatography

Purification of crude products after synthesis was performed on a Varian IntelliFlash 971-FP with its own software version 3.1.524. For this purpose, prepacked Chromabond® Flash RS SiOH (4 g–80 g of silica gel,15–40 µm or 40–63 µm) cartridges from Macherey-Nagel GmbH & Co. KG were used. All solvents used were analytical or HPLC grade. Prior to injecting the samples, column equilibration and system flushing were done manually. For injection, liquid samples were directly injected onto the column and solid samples were dissolved in an appropriate solvent, mixed with small amounts of silica gel, and then evaporated to dryness. The residue was transferred

into an empty cartridge replacing the proprietary DASi module and automatically injected onto the column.

6.1.3. Nuclear magnetic resonance (NMR) spectroscopy

NMR spectra were recorded on Bruker Avance III HDX 700, Bruker Avance III HDX 600 or Bruker Avance III HD 400 instruments at 298 K, if not stated otherwise. Chemical shifts are given as δ-values (ppm) relative to the solvent as internal standard.[183] Coupling constants (*J*) are given in Hertz (Hz). Abbreviations for multiplicity description are as follows: s: singlet, s (br): broad singlet, d: duplet, dd: duplet of duplet, ddd: duplet of duplet of duplet, dtd: duplet of triplet of duplet, dtt: duplet of triplet of triplet, dp: duplet of quintet, t: triplet, td: triplet of duplet, m: multiplet.

6.1.4. HPLC-ESI-MS

High resolution mass spectrometry data were acquired on a Bruker MaXis 4G ESI-qTOF instrument coupled to a Dionex Ultimate 3000 HPLC system (Thermo Fisher Scientific). Each analysis was calibrated using sodium formiate as internal calibrant. The nebulizer pressure of the ESI source was set to 2.0 bar and dry gas was set to 8.0 $L \cdot min^{-1}$ at an operating temperature of 200°C. For MS/MS spectra acquisition, auto MS/MS mode with collision energy stepping was used. The mass spectrometer was operated in positive and negative ion mode. Mass spectra were recorded from 50 to 1250 Da. The capillary voltage was set to 3000 V and the end plate voltage was set to –500 V.

The routine gradient was 10% B to 100% B (A: water with 0.1% formic acid, B: methanol with 0.06% formic acid) in 20 min with a flow rate of 0.3 $mL \cdot min^{-1}$ on a Nucleoshell® EC RP-C18 (150 x 2 mm, 2.7 µm) from Macherey-Nagel GmbH & Co. KG at 40°C.

6.2. Thin layer chromatography

TLC silica gel 60 F254 (normal phase, 0.2 mm layer thickness) chromatography plates were purchased from Merck KGaA.

For staining, a freshly prepared solution of anisaldehyde was used: Stock solution (500 mL) contained the following: 50 mL acetic acid, 25 mL sulfuric acid and 425 mL methanol. 1 mL 4-methoxybenzaldehyde (from Sigma-Aldrich) was added to 50 mL of stock solution for staining.

6.3. Other devices

Balance: Sartorius CP26P, Sartorius Entris, Sartorius BP2215.

Centrifuge: Eppendorf Centrifuge 5424

Lyophilizer: Christ Beta 2-8 LD Plus with Vacuubrand Chemistry Hybrid Pump RC6

6.4. Purification and experimental data for epifadin (**24**)

6.4.1. Cultivation of *S. epidermidis* IVK83 and generation of precipitate

All steps were performed under reduced light exposure. An overnight culture of *S. epidermidis* IVK83 in TSB was used to inoculate fresh TSB at a dilution of 1:1000, which was then incubated for 4 hours at 37°C with constant shaking at 160 rpm to achieve exponential growth. Subsequently, fresh TSB (5 L) containing 5 $g \cdot L^{-1}$ glucose was inoculated with an OD_{600} of 0.00125 of IVK83 and incubated for 44 hours at 30°C with continuous shaking at 160 rpm. After incubation, the cultures were centrifuged, and the supernatant was adjusted to pH 2 using 37% HCl (Thermo Fisher Scientific) and incubated for 2 hours at 4°C. The acidified supernatants were then centrifuged at 8000 g for 15 minutes at 4°C, and the clear supernatant was discarded. The resulting precipitate was resuspended in small volumes of deionized water and frozen at −80°C. Finally, the precipitate was lyophilized at −20°C and 1 mbar until all water was removed, yielding 1.2 g of the precipitate.[94]

6.4.2. Extraction and purification via HPLC

All steps were performed under reduced light exposure. A total of 1.2 g of the precipitate was washed with acetonitrile (3 × 30 mL), centrifuged and the supernatant was discarded. The residue was then aliquoted into 2.0 mL Eppendorf tubes (200 mg per tube) and immediately stored at −80°C. For HPLC purification, 2 mL of DMSO is added to one Eppendorf tube with precipitate and the tube is then closed and vortexed. After centrifugation, the supernatant is injected into the HPLC system. Purification method C from experimental section 6.1.1. is employed, and the epifadin-containing fractions were collected into a 500 mL round-bottom flask equipped with a septum and an argon ballon. Throughout the process the flask is immersed in an isopropyl alcohol-liquid nitrogen cooling bath (−80°C). Following freeze-drying a total of 3.5 mg of purified epifadin (**24**) is obtained.

6.4.3. Structure of epifadin (**24**) and NMR data

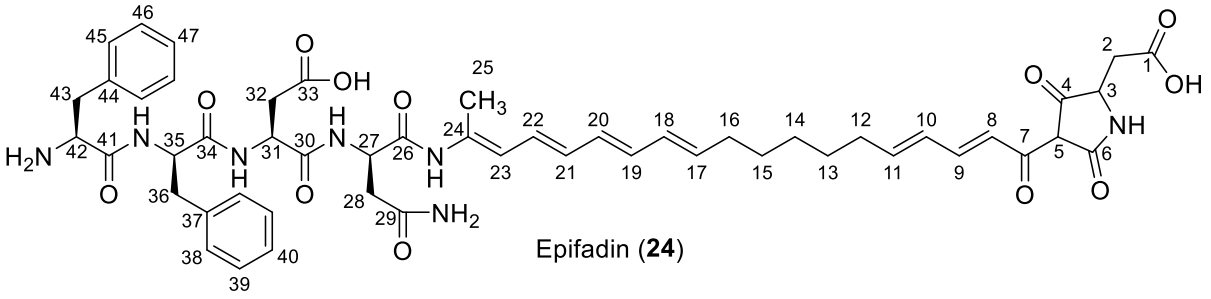

Epifadin (**24**)

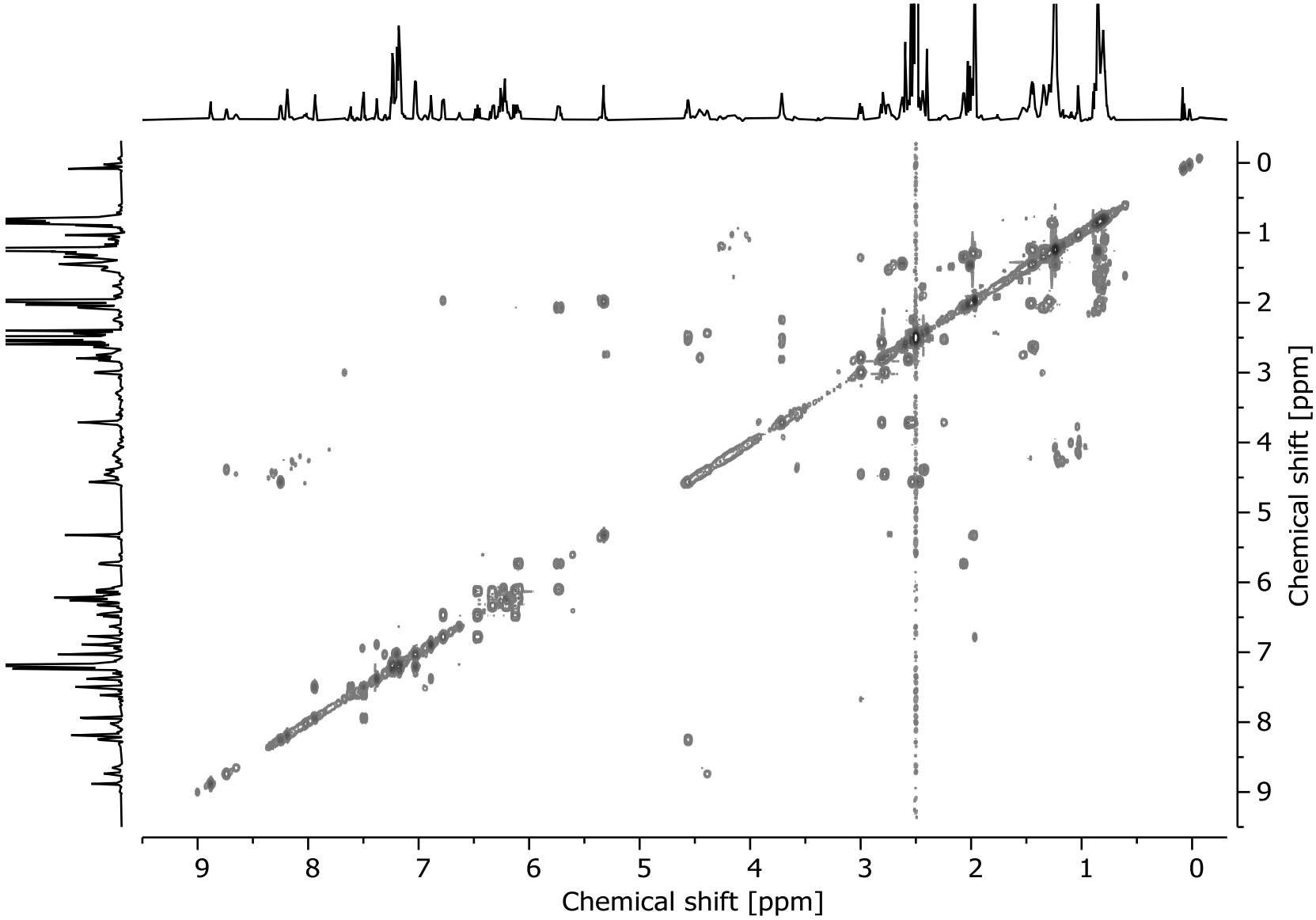

Figure 97: $^{1}H,^{1}H$-COSY spectrum of epifadin (**24**) in DMSO-d_6 (700 MHz, 303 K).

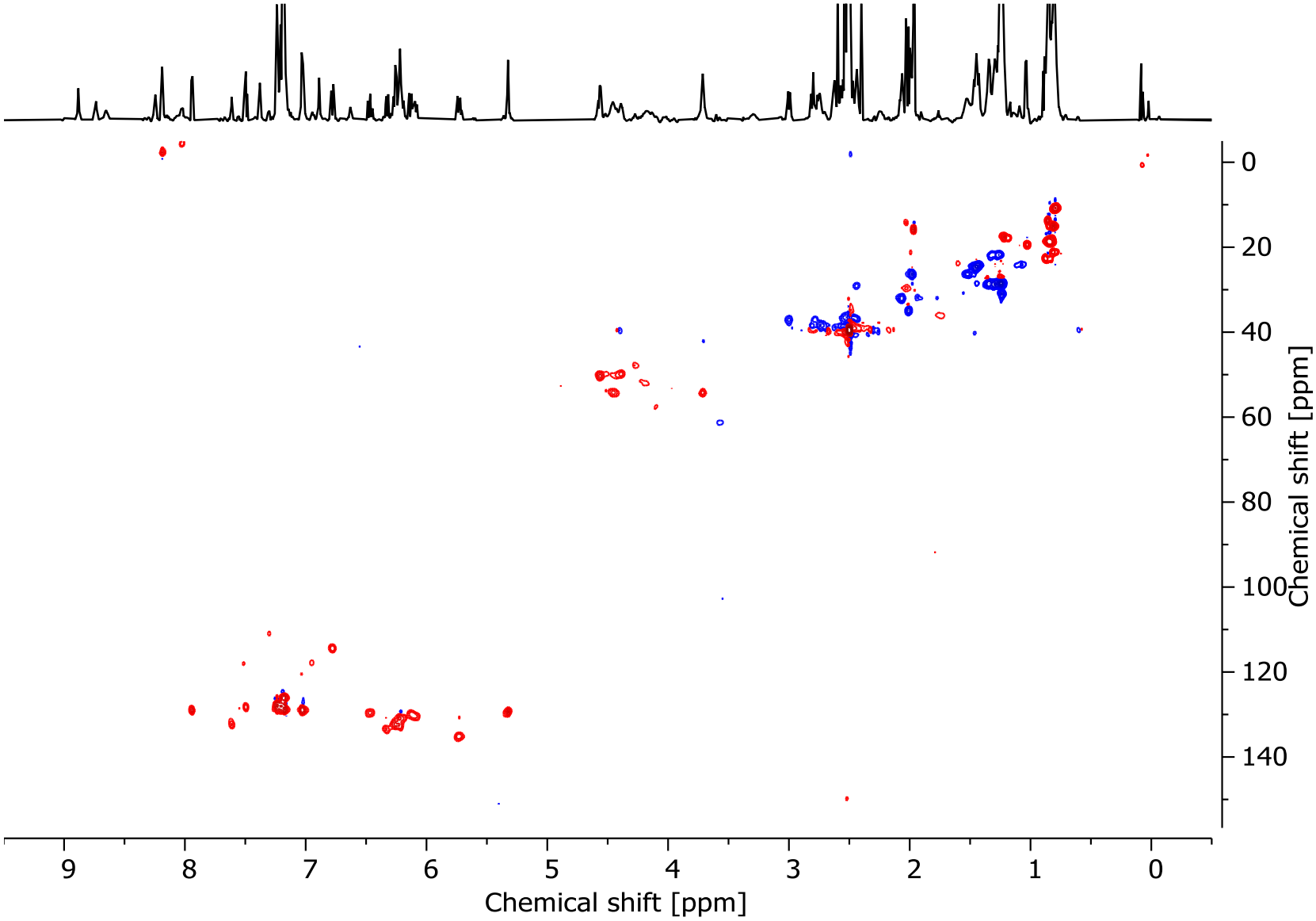

Figure 98: $^{1}H,^{13}C$-HSQC spectrum of epifadin (**24**) in DMSO-d_6 (700 MHz, 303 K).

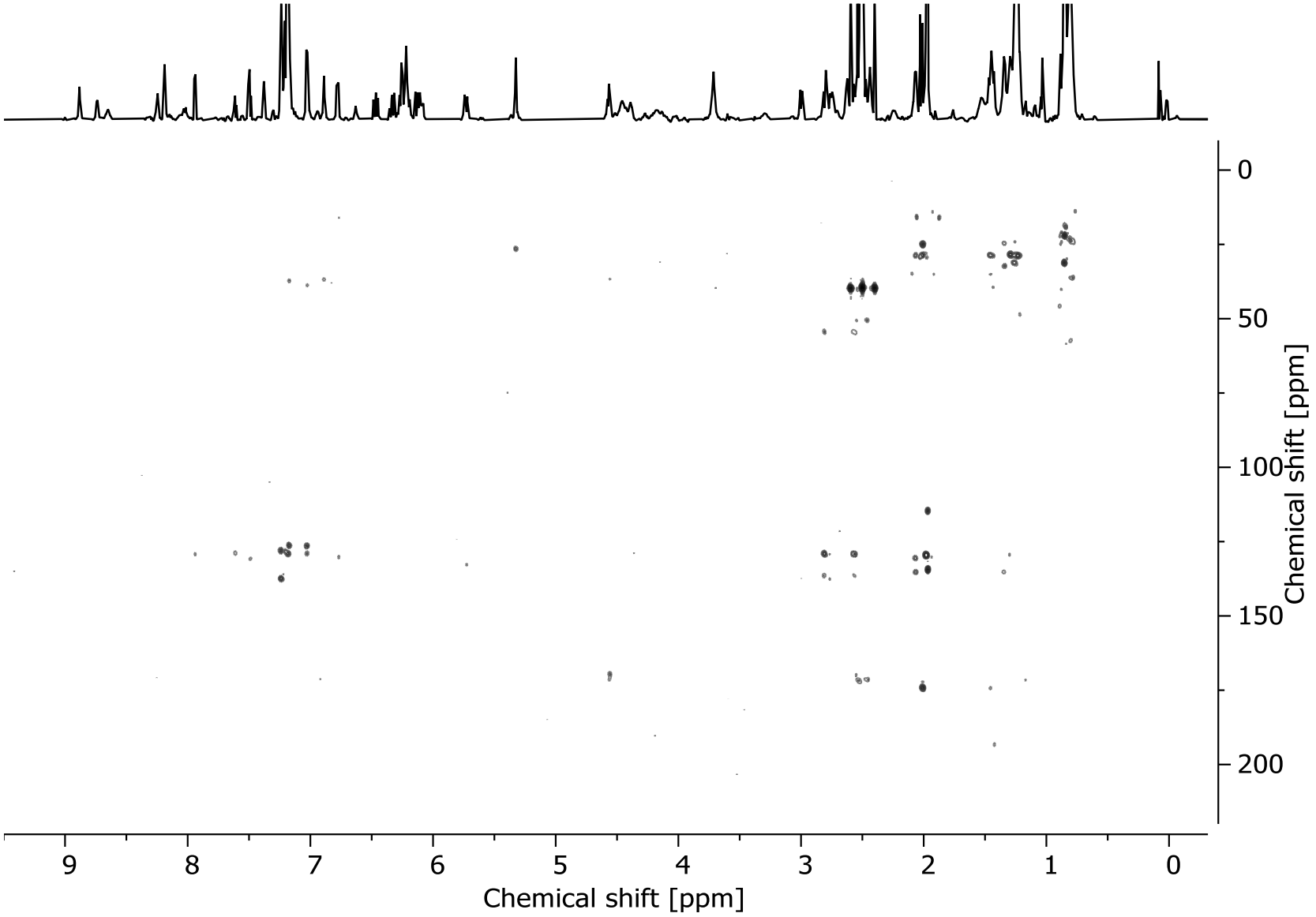

Figure 99: $^{1}H,^{13}C$-HMBC spectrum of epifadin (**24**) in DMSO-d_6 (700 MHz, 303 K).

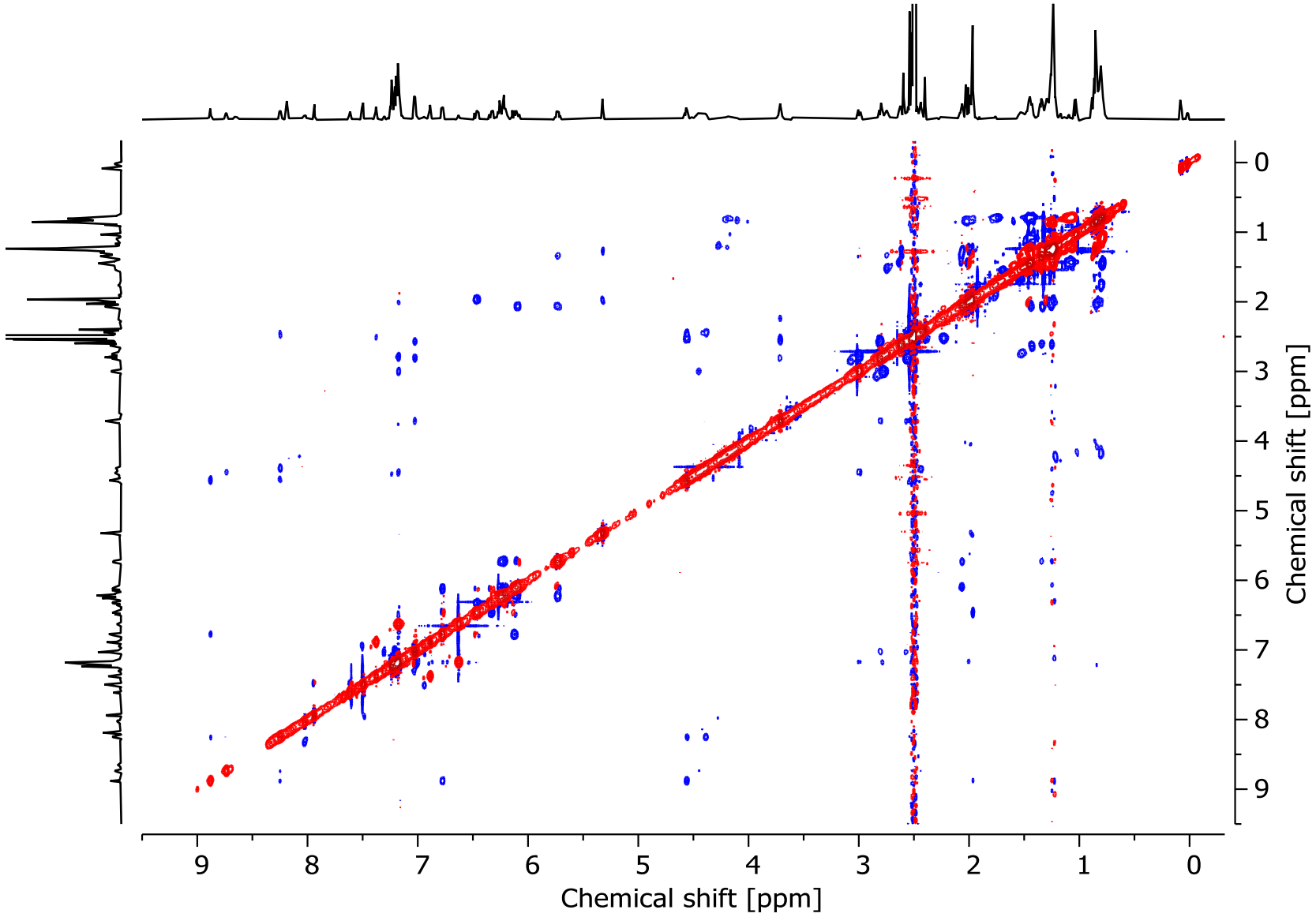

Figure 100: ^{1}H,^{1}H-ROESY spectrum of epifadin (**24**) in DMSO-d_6 (700 MHz, 303 K).

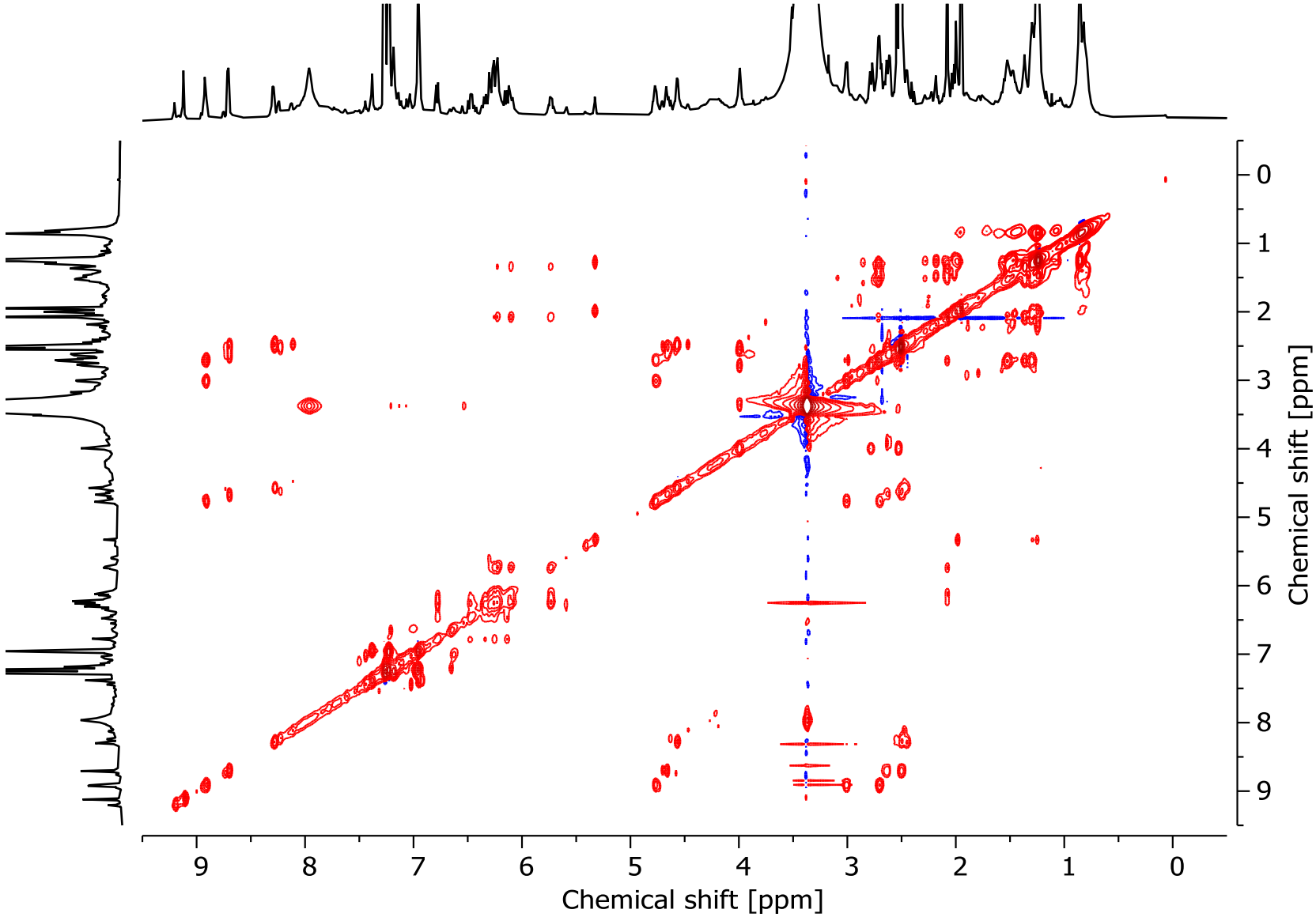

Figure 101: ^{1}H,^{1}H-TOCSY spectrum of epifadin (**24**) in DMSO-d_6 (700 MHz, 303 K). Batch from N. SCHILLING's purification protocol.

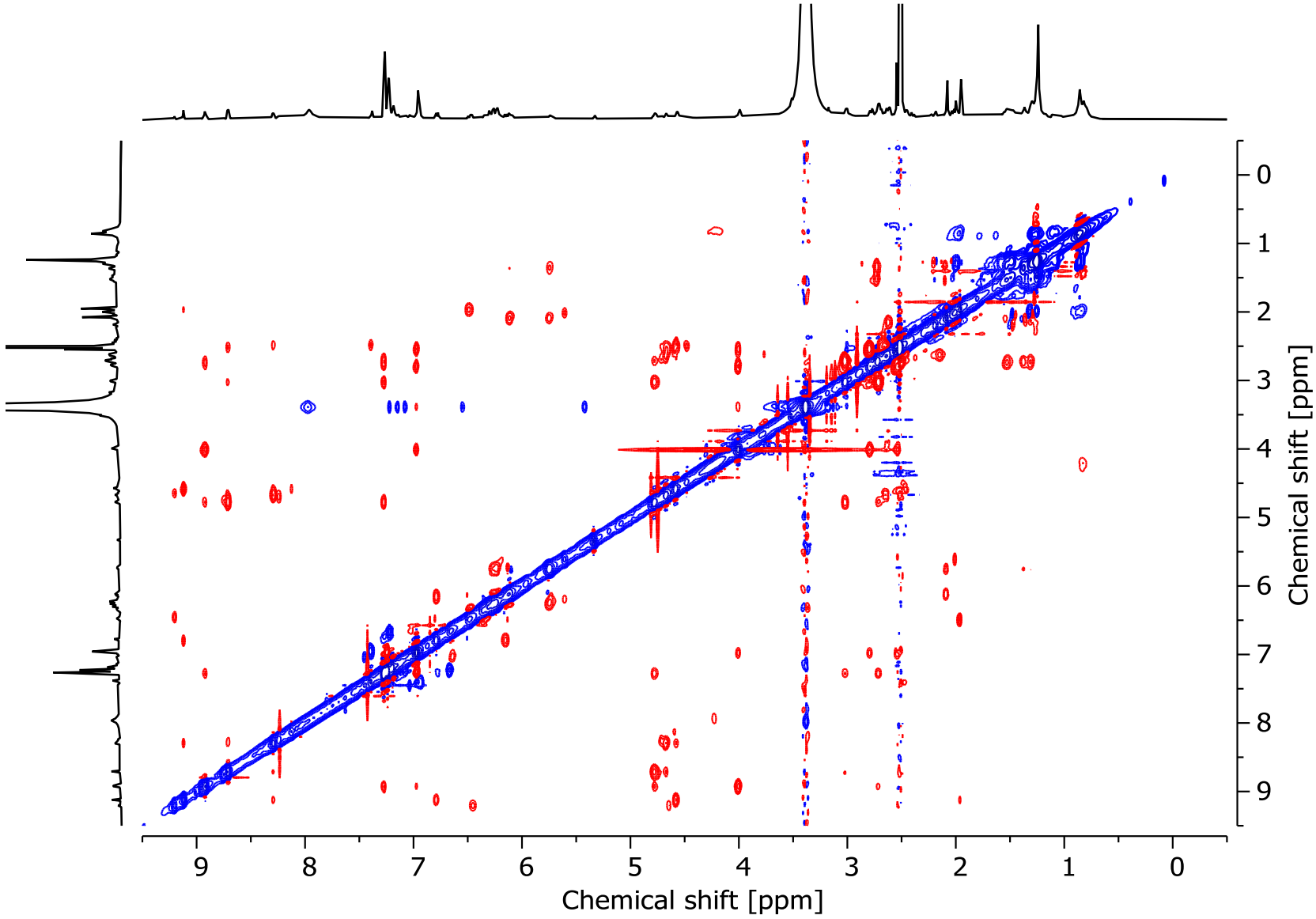

Figure 102: $^{1}H,^{1}H$-ROESY spectrum of epifadin (**24**) in DMSO-d_6 (700 MHz, 303 K). Batch from N. SCHILLING's purification protocol.

Table 3: Signals of ^{1}H NMR (700 MHz) of epifadin (**24**) in DMSO-d_6 at 303 K. n.a. = not assigned, n.d. = not detected.

Signal [ppm]	Atom number	Moiety
7.23	46 and 47	Phe 1
6.97	45	
2.53 and 2.77	43	
3.97	42	
7.97	42-NH_2	
8.87	41-NH	Phe 2
7.18	40	
7.27	38 and 39	
3.01 and 2.71	36	
4.78	35	
8.68	34-NH	Asp
n.d.	33-OH	
2.51 and 2.64	32	
4.67	31	
8.26	30-NH	Asn
7.38 and 6.95	29-NH_2	
2.48	28	
4.57	27	
9.08	26-NH	Enamide
1.95	25	Polyene
6.77	23	
6.47	22	
6.14	21	
6.33	20	
6.24	19	
6.10	18	
5.74	17	
2.09	16	Saturated tail
1.36	15	
1.31	14	
n.a.	13	
n.a.	12	
n.d.	11	3-Polyenoyltetramic acid moiety
n.d.	10	
n.d.	9	
n.d.	8	
1.46	5	
2.00	3	
2.18 and 2.21	2	

Table 4: ^{13}C NMR (175 MHz) signals of epifadin (**24**) in DMSO-d_6 at 303 K. All signals were assigned through 2D NMR spectra. n.a. = not assigned, n.d. = not detected.

Signal [ppm]	Atom number	Moiety
126.75	47	Phe 1
128.09	46	
129.14	45	
134.44	44	
36.63	43	
52.99	42	
167.82	41	
126.15	40	Phe 2
127.75	39	
129.01	38	
137.26	37	
38.06	36	
53.46	35	
170.50	34	
171.29	33	Asp
36.54	32	
49.11	31	
170.17	30	
171.22	29	Asn
36.68	28	
50.38	27	
169.9	26	
15.76	25	Polyene
134.26	24	
114.11	23	
129.64	22	
129.74	21	
133.44	20	
132.29	19	
130.46	18	
134.98	17	
31.97	16	Saturated tail
28.39	15	
25.55	14	
n.a.	13	
n.a.	12	
n.d.	11	Polyenoyltetramic acid moiety
n.d.	10	
n.d.	9	
n.d.	8	
n.d.	7	
174.3	6	
28.70	5	
34.9	3	
33.4	2	
174.5	1	

6.5. Chemical synthesis

Unless otherwise stated all chemicals were obtained from commercial sources and used without further purification. *S*-*tert*-butyl (*E*)-5-bromo-3-oxopent-4-enethioate (**63**) and *trans*-3-(tributylstannyl)-2-propen-1-al (**71**) were synthesized according to literature procedures.[115, 118] HPLC or higher-grade solvents were used. Dry solvents were obtained from a Solvent Purification System from MBRAUN and degassed by the freeze-pump-thaw method if required.

6.5.1. Synthesis procedures

Methylation of epifadin (**24**) using diazomethane

All procedures were performed under reduced light exposure to minimize photodegradation. A total of 10.0 mg of precipitate ③ was extracted using 2 mL of an acetonitrile-water mixture (8:2, adjusted to pH 2 with H_2SO_4). The suspension was cooled to 0°C, and diazomethane in diethyl ether (approximately 1 mL, 0.24 mol·L^{-1}) was added dropwise until the suspension no longer decolorized and remained yellow, with no further gas evolution observed. The mixture was stirred at room temperature for 30 minutes and then treated with acetic acid until the yellow color dissipated. The solvent was removed under vacuum, and the residue was dissolved in 1 mL of methanol. The resulting solution was vortexed, centrifuged and analyzed by HPLC-ESI-MS (see experimental section 6.1.4).

Methylation of epifadin (**24**) using (diazomethyl)trimethylsilane

All procedures were performed under reduced light exposure to minimize photodegradation. A total of 10.0 mg of precipitate ③ or a purified epifadin (**24**) sample (0.5 mg) was suspended in a toluene:methanol mixture (8:2, 1.0 mL) and treated with a solution of (diazomethyl)trimethylsilane in diethyl ether (200 µL, 2.0 mol·L^{-1}, 200 µL, 400 µmol). The resulting yellow solution was stirred at room temperature for 24 hours. The mixture was then treated with acetic acid until the yellow color disappeared. The solvent was removed under vacuum, and the residue was dissolved in 1 mL of methanol. The solution was vortexed, centrifuged, and analyzed by HPLC-ESI-MS (see experimental section 6.1.4).

Acetylation of epifadin (**24**) with acetic anhydride and pyridine

All procedures were performed under reduced light exposure to minimize photodegradation. A total of 10.0 mg of precipitate ③ or a purified epifadin (**24**) sample (0.5 mg) was suspended in an acetic anhydride:pyridine mixture (2:1, 800 µL). The resulting yellow solution was stirred at room temperature for 24 hours. Subsequently, water (500 µL) and acetic acid (500 µL) were added. The mixture was lyophilized, and the residue was dissolved in 1 mL of methanol. The solution was vortexed, centrifuged, and analyzed by HPLC-ESI-MS (see experimental section 6.1.4).

Methylation of reutericyclin (**7**) using (diazomethyl)trimethylsilane

All procedures were performed under reduced light exposure. Reutericyclin (**7**, 1.5 mg, 4.3 µmol, 1.0 eq) was suspended in a toluene:methanol mixture (8:2, 3.0 mL) and treated with a solution of (diazomethyl)trimethylsilane (2.0 $mol \cdot L^{-1}$, 43 µL, 86 µmol, 20.0 eq). The resulting yellow solution was stirred at room temperature for 24 hours. Subsequently, glacial acetic acid (approximately 100 µL) was added dropwise until no further gas evolution was observed. The solvent was removed under vacuum, yielding a yellow residue (27.6 mg). The residue was dissolved in 1 mL of methanol. The solution was vortexed, centrifuged, and analyzed by HPLC-ESI-MS (see experimental section 6.1.4).

Methylation of kirromycin (**31**) using (diazomethyl)trimethylsilane

All procedures were performed under reduced light exposure. Kirromycin (**31**, 5.0 mg, 6.3 µmol, 1.0 eq) was suspended in a toluene:methanol mixture (8:2, 3.0 mL) and treated with a solution of (diazomethyl)trimethylsilane (2.0 $mol \cdot L^{-1}$, 12.5 µL, 25 µmol, 4.0 eq). The resulting yellow solution was stirred at room temperature for 24 hours. Subsequently, glacial acetic acid (approximately 25 µL) was added dropwise until no further gas evolution was observed. The solvent was removed under vacuum, yielding a yellow residue (6.9 mg). The residue was dissolved in 1 mL of methanol. The solution was vortexed, centrifuged, and analyzed by HPLC-ESI-MS (see experimental section 6.1.4).

Bis[2-(trimethylsilyl)ethyl] (2*S*)-2-[*N*-(benzyloxycarbonyl)amino]butane-1,4-dioate (**81**)

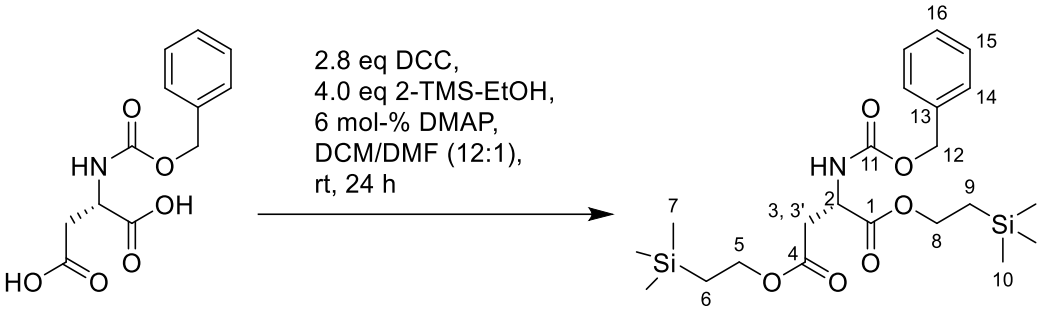

80 **81**

At 0°C a suspension of *N*,*N*′-dicyclohexylcarbodiimide (2.31 g, 11.2 mmol, 2.8 eq) in dichloromethane (4 mL) was added dropwise to a suspension of *N*-benzyloxycarbonyl-*L*-aspartic acid (**80**, 1.07 g, 4.00 mmol, 1.0 eq), 2-(trimethylsilyl)ethanol (2.28 mL, 16.0 mmol, 4.0 eq) and 4-(dimethylamino)pyridine (0.03 g, 0.24 mmol, 6 mol-%) in dichloromethane (4 mL) and *N*,*N*-dimethylformamide (0.6 mL). A colorless precipitate is formed. After complete addition, the suspension was stirred overnight at rt. The suspension was cooled to 0°C and added to a saturated aqueous ammonium chloride solution (30 mL) and filtered off over celite®. The organic phase was separated from the aqueous phase and the aqueous phase was then extracted with dichloromethane (3 × 40 mL). The joint organic phases were washed with brine (1 × 100 mL), dried over sodium sulfate and the solvent was removed under vacuo. Purification of the colorless oily residue by column chromatography (NP-silica, cyclohexane:ethyl acetate 8:2) afforded the title compound as a colorless oil (1.74 g, 3.72 mmol, 93%).

Rf (cyclohexane:ethyl acetate 2:1): 0.70.

^{1}H NMR (600 MHz, $CDCl_3$) δ = 0.03 (s, 9H, 7-H or 10-H), 0.04 (s, 9H, 7-H or 10-H), 0.94–1.03 (m, 4H, 6-H and 9-H), 2.81 (dd, $J_{3,2}$ = 4.5 Hz, $J_{3,3'}$ = 17.0 Hz, 1H, 3-H), 3.00 (dd, $J_{3',2}$ = 4.4 Hz, $J_{3',3}$ = 17.0 Hz, 1H, 3‘-H), 4.14–4.19 (m, 2H, 5-H or 8-H), 4.21–4.27 (m, 2H, 5-H or 8-H), 4.59 (ddd, $J_{2,3'}$ = 4.4 Hz, $J_{2,3}$ = 4.5 Hz, $J_{2,NH}$ = 8.5 Hz, 1H, 2-H), 5.12 (s, 2H, 12-H), 5.76 (d, $J_{NH,2}$ = 8.5 Hz, 1H, NH), 7.30–7.37 (m, 5H, 14-H,15-H, 16-H) ppm.

^{13}C NMR (150 MHz, $CDCl_3$) δ = –1.4 (C-7 and C-10), 17.4 (C-6 or C-9), 17.5 (C-6 or C-9), 36.9 (C-3), 50.7 (C-2), 63.5 (C-5/C-8), 64.5 (C-5/C-8), 67.2 (C-11), 128.2 (C-16),

128.3 (C-14 or C-15), 128.7 (C-14 or C-15), 136.4 (C-13), 156.1 (C-11), 171.0 (C-1 or C-4), 171.1 (C-1 or C-4) ppm.

HRMS (ESI-qTOF, positive ion mode): *m/z* calcd. for $C_{22}H_{37}NO_6Si_2$: 467.2159 [M]; calcd. for $[M+H]^+$: 468.2232, found: 468.2232; calcd. for $[M+Na]^+$: 490.2057, found: 490.2052.

Bis[2-(trimethylsilyl)ethyl] *L*-aspartate (**82**)

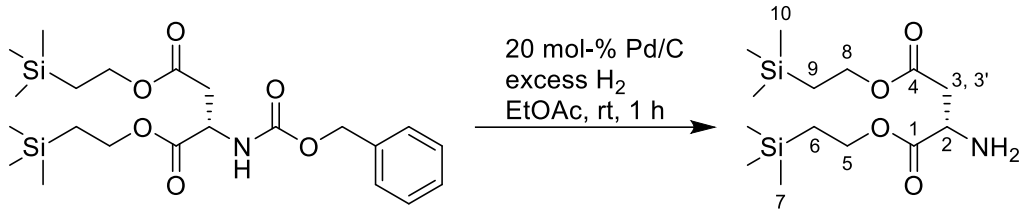

81 **82**

81 (0.50 g, 1.00 mmol, 1.0 eq) was dissolved in ethyl acetate (17 mL) and the solution and the flask were flushed with Argon. Pd/C (10 wt.-% Pd on carbon, 0.20 g, 0.19 mmol, 20 mol-%) was added to the solution and hydrogen gas (excess) was passed into the solution through a septum using a balloon with a canula. The reaction was monitored using thin layer chromatography. After 1 h the black suspension was filtered off over celite® and the solvent was removed under vacuo. The product was obtained as a colorless oil (0.33 g, 0.99 mmol, 99%) and used without further purification.

Rf (cyclohexane:ethyl acetate 2:1): 0.32.

^{1}H NMR (400 MHz, $CDCl_3$) δ = 0.03 (s, 9H, 7-H or 10-H), 0.04 (s, 9H, 7-H or 10-H), 0.95–1.05 (m, 4H, 6-H and 9-H), 2.71 (s (br), 2H, NH_2), 2.77 (dd, $J_{3,2}$ = 6.9 Hz, $J_{3,3'}$ = 16.8 Hz, 1H, 3-H), 2.90 (dd, $J_{3',2}$ = 4.5 Hz, $J_{3',3}$ = 16.8 Hz, 1H, 3'-H), 3.90 (dd, $J_{2,3'}$ = 4.5 Hz, $J_{2,3}$ = 6.8 Hz, 1H, 2-H), 4.16–4.27 (m, 4H, 5-H and 8-H) ppm.

^{13}C NMR (100 MHz, $CDCl_3$): δ = -1.4 (C-7 and C-10), 17.5 (C-6 and C-9), 38.0 (C-3), 51.1 (C-2), 63.5 and 64.3 (C-5 and C-8), 171.4 (C-1 and C-4) ppm.

HRMS (ESI-qTOF, positive ion mode): *m/z* calcd. for $C_{14}H_{32}NO_4Si_2$: 333.1792 [M]; calcd. for $[M+H]^+$: 334.1870, found: 334.1862; calcd. for $[M+Na]^+$: 356.1689, found: 356.1683.

Bis(2-(trimethylsilyl)ethyl)-*N*-(2,4-dimethoxybenzyl)-*L*-aspartate (**70**)

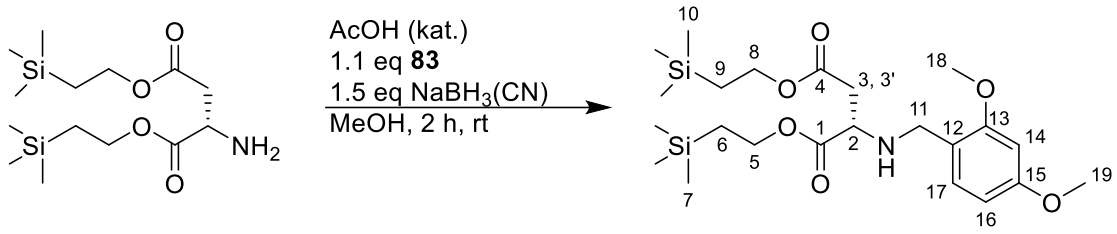

82 **70**

82 (5.50 g, 16.4 mmol, 1.0 eq) was dissolved in Methanol (200 mL) and six drops of acetic acid were added. 2,4-dimethoxybenzaldehyde (**83**, 3.02 g, 18.2 mmol, 1.1 eq) was added to the solution and within 30 seconds sodium cyanoborohydride (1.56 g, 24.8 mmol, 1.5 eq) was added in one portion. The solution was stirred 2 h at rt. The solvent was removed under vacuo and the residue dissolved in diethyl ether (200 mL). The organic phase was washed with water (1 × 100 mL). The organic phase was dried over sodium sulfate and the solvent was removed under vacuo. Purification of the crude product using column chromatography (NP-silica, cyclohexane:ethyl acetate 9:1, changing to 3:1 after 100 mL) afforded the product as a colorless oil (6.55 g, 13.6 mmol, 83%).

Rf (cyclohexane:ethyl acetate 2:1): 0.62.

^{1}H NMR (700 MHz, $CDCl_3$) δ = 0.02 and 0.03 (s, 18H, 7-H and 10-H), 0.95–0.99 (m, 4H, 6-H and 9-H), 2.68 (dd, $J_{3,2}$ = 6.6 Hz, $J_{3,3'}$ = 15.9 Hz, 1H, 3-H), 2.76 (dd, $J_{3',2}$ = 6.1 Hz, $J_{3',3}$ = 15.9 Hz, 1H, 3‘-H), 3.65 (t, $J_{2,3 \text{ and } 3'}$ = 6.4 Hz, 1H, 2-H), 3.78 (d, $J_{11,NH}$ = 12.4 Hz, 2H, 11-H), 3.78 (s, 3H, 18-H), 3.80 (s, 3H, 19-H), 4.14–4.17 (m, 4H, 5-H and 8-H), 6.41–6.42 (m, 2H, 14-H and 17-H), 7.15 (d, $J_{16,17}$ = 8.0 Hz, 16-H) ppm.

^{13}C NMR (175 MHz, $CDCl_3$): δ = -1.4 (C-7 and C-10), 17.4 and 17.5 (C-6 and C-9), 37.9 (C-3), 47.0 (C-11), 55.4 and 55.5 (C-18 and C-19), 57.1 (C-2), 63.1 (C-5 or C-8), 63.6 (C-5 or C-8), 98.6 (C-16), 103.9 (C-14), 119.6 (C-12), 130.7 (C-17), 158.8 (C-13), 160.5 (C-15), 171.2 and 173.4 (C-1 and C-4) ppm.

HRMS (ESI-qTOF, positive ion mode): *m/z* calcd. for $C_{23}H_{41}NO_6Si_2$: 483.2472 [M]; calcd. for $[M+H]^+$: 484.2551, found: 484.2549; calcd. for $[M+Na]^+$: 506.2365, found: 506.2358.

Bis[2-(trimethylsilyl)ethyl] ((2*Z*,4*E*)-5-bromo-3-hydroxypenta-2,4-dienoyl)-*L*-aspartate (*enol*-**84**) in equilibrium with bis[2-(trimethylsilyl)ethyl] (*E*)-(5-bromo-3-oxopent-4-enoyl)-*L*-aspartate (*keto*-**84**)

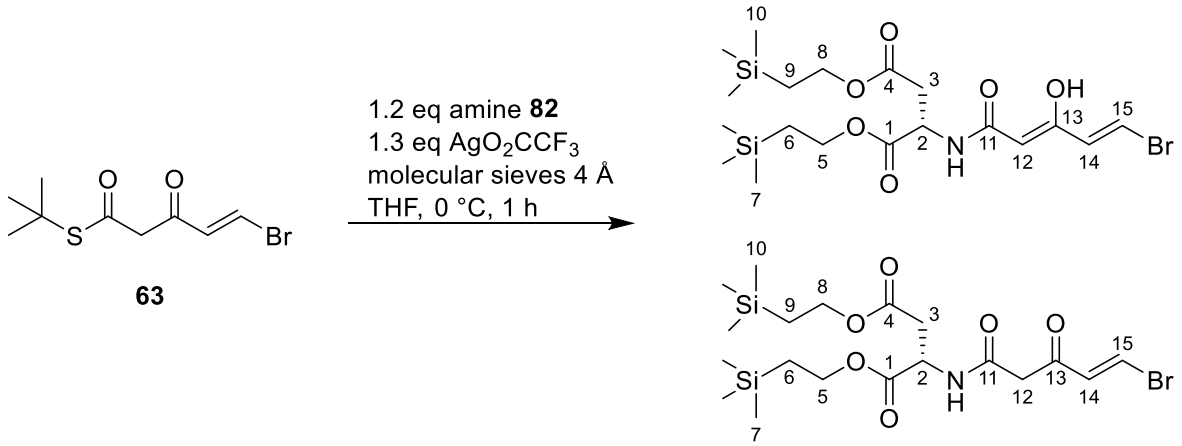

Powdered molecular sieves (4 Å, 1.00 g) was added to a solution of β-ketothioester **63** (1.20 g, 4.52 mmol, 1.0 eq) and amine **82** (1.91 g, 5.73 mmol, 1.3 eq) in anhydrous THF (40 mL). The suspension was stirred for 30 min at rt. Then at 0°C silver triflate (1.40 g, 6.34 mmol, 1.4 eq) was added to the suspension and the mixture was stirred for 1 h at 0°C. The reaction mixture was filtered through celite® and the solvent was removed under vacuo. The resulting brown oil was then resuspended in diethyl ether (30 mL) and filtered again through celite®. The solvent was removed under vacuo and the crude product was obtained as a brown viscous oil. Purification of the crude product using column chromatography (NP-silica, cyclohexane:ethyl acetate 20:1) afforded the product as a slightly brown oil (1.17 g, 2.30 mmol, 51%).

The product consists of two compounds which results from the keto-enol tautomerism. The ratio between *keto*- and *enol*-form can be determined via ^{1}H NMR spectroscopy by integrating the 2-H-signals and calculating the ratio. The ratio is determined to be 1(*keto*):2(*enol*).

Rf (cyclohexane:ethyl acetate 4:1): 0.40.

^{1}H NMR (700 MHz, $CDCl_3$) *enol*-**84**: δ = 0.03 and 0.04 (s, 18H, 7-H and 10-H), 0.96–1.02 (m, 4H, 6-H and 9-H), 2.84 (dd, $J_{3,2}$ = 4.5 Hz, $J_{3,3'}$ = 17.2 Hz, 1H, 3-H), 3.03 (dd, $J_{3',2}$ = 4.3 Hz, $J_{3',3}$ = 17.2 Hz, 1H, 3'-H), 4.15–4.21 (m, 4H, 5-H and 8-H), 4.83 (ddd, $J_{2,3'}$ = 4.3 Hz, $J_{2,3}$ = 4.5 Hz, $J_{2,NH}$ = 7.9 Hz, 1H, 2-H), 4.93 (s, 1H, 12-H), 6.36 (d, $J_{NH,2}$ = 7.9 Hz, 1H, NH), 6.42 (d, $J_{14,15}$ = 13.6 Hz, 1H, 14-H), 7.18 (d, $J_{15,14}$ = 13.6 Hz, 1H, 15-H), 13.10 (s (br), 1H, 13-OH) ppm.
Keto-**84**: δ = 0.04 (overlayed s, 18H, 7-H and 10-H), 0.96–1.02 (m, 4H, 6-H and 9-H), 2.81 (dd, $J_{3,2}$ = 4.6 Hz, $J_{3,3'}$ = 17.1 Hz, 1H, 3-H), 3.00 (dd, $J_{3',2}$ = 4.4 Hz, $J_{3',3}$ = 17.1 Hz, 1H, 3'-H), 3.53 (s, 2H, 12-H), 4.15–4.21 (m, 2H, 5-H or 8-H), 4.22–4.28 (m, 2H, 5-H or 8-H), 4.81 (ddd, $J_{2,3'}$ = 4.4 Hz, $J_{2,3}$ = 4.6 Hz, $J_{2,NH}$ = 8.0 Hz, 1H, 2-H), 6.89 (d, $J_{14,15}$ = 14.0 Hz, 1H, 14-H), 7.52 (d, $J_{NH,2}$ = 8.0 Hz, 1H, NH), 7.71 (d, $J_{15,14}$ = 14.0 Hz, 1H, 15-H) ppm.

^{13}C NMR (175 MHz, $CDCl_3$) *enol*-**84**: δ = –1.4 (C-7 and C-10), 17.5 (C-6 and C-9), 36.6 (C-3), 49.0 (C-2), 63.6–64.7 (3 s, C-5 and C-8), 93.2 (C-12), 116.9 (C-15), 131.9 (C-14), 165.7 (C-13), 170.7 (C-1), 171.0 (C-11), 171.1 (C-4).
Keto-**84**: –1.4 (C-7 and C-10), 17.5 (C-6 and C-9), 36.4 (C-3), 47.9 (C-12), 48.4 (C-2), 63.6–64.7 (3 s, C-5 and C-8), 129.2 (C-15), 136.0 (C-14), 165.0 (C-1), 170.5 (C-11), 171.3 (C-4), 191.4 (C-13) ppm.

HRMS (ESI-qTOF, positive ion mode): *m/z* calcd. for $C_{19}H_{34}BrNO_6Si_2$: 507.1108 [M]; calcd. for $[M+H]^+$: 508.1181, found: 508.1176; calcd. for $[M+Na]^+$: 530.1000, found: 530.0996.

Bis[2-(trimethylsilyl)ethyl] (*Z*)-*N*-((2*Z*,4*E*)-5-bromo-3-hydroxypenta-2,4-dienoyl)-*N*-(2,4-dimethoxybenzyl) *L*-aspartate (*Z-enol*-**67**) in equilibrium with bis[2-(trimethylsilyl)ethyl] (*Z*)-*N*-[(4*E*)-5-bromo-3-oxopent-4-enoyl)-*N*-(2,4-dimethoxybenzyl) *L*-aspartate (*Z-keto*-**67**)

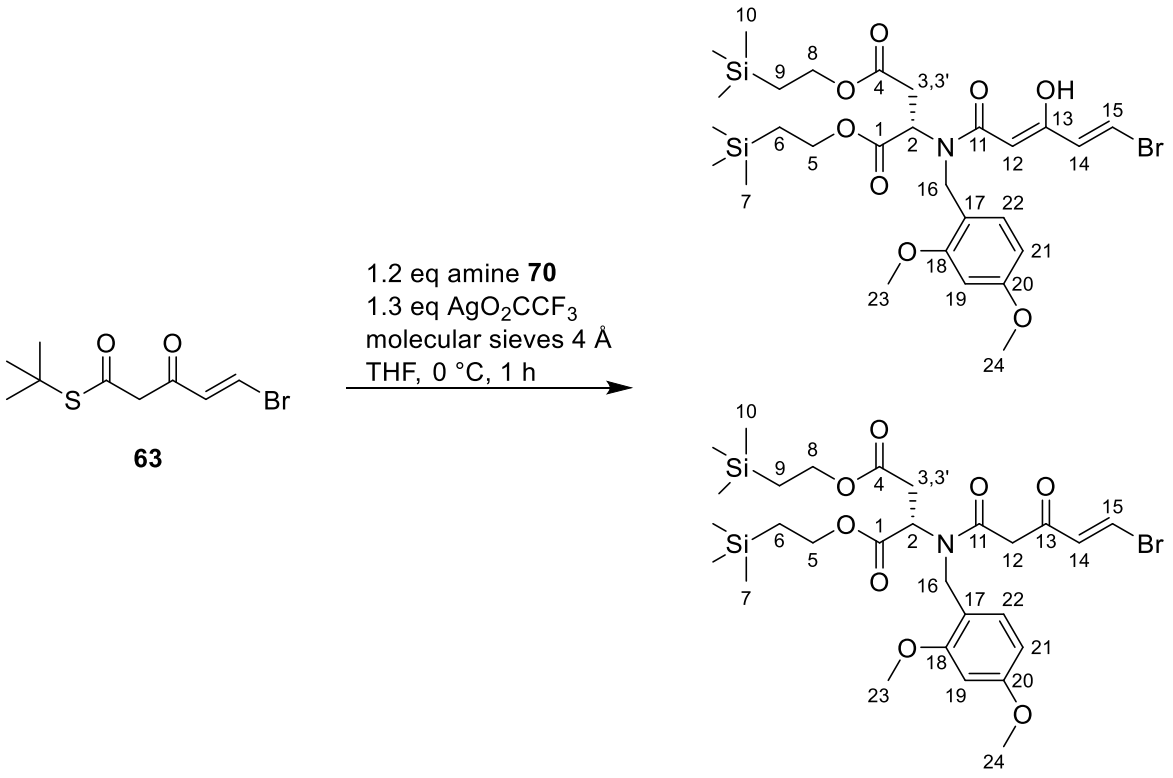

Powdered molecular sieves (4 Å, 200 mg) was added to a solution of β-ketothioester **63** (110 mg, 0.42 mmol, 1.5 eq) and amine **70** (134 mg, 0.28 mmol, 1.0 eq) in anhydrous THF (10 mL). The suspension was stirred for 30 min at rt. Silver triflate (91.8 mg, 0.42 mmol, 1.5 eq) was added to the suspension and the mixture was stirred for 16 h at rt. The reaction mixture was filtered through celite® and the solvent was removed under vacuo. The resulting brown oil was then resuspended in diethyl ether (20 mL) and filtered again through celite®. The solvent was removed under vacuo and the crude product was obtained as a brown viscous oil. Purification of the crude product using column chromatography (NP-silica, cyclohexane:ethyl acetate 9:1) afforded the product as a red brown solid (171 mg, 0.27 mmol, 97%).

The product consists of at least two compounds which results from the keto-enol tautomerism and the rotation of the amide bond. The main compound is the *Z-enol*-form. The ratio between *Z-keto*- and *Z-enol*-form can be determined via ^{1}H-NMR spectroscopy by integrating the 2-H-signals and calculating the ratio. The ratio

is determined to be 1(*Z-keto*):2(*Z-enol*). Due to overlapping only the signals of the *Z-enol*-form can be unambiguously assigned.

Rf (cyclohexane:ethyl acetate 4:1): 0.55.

^{1}H NMR (700 MHz, $CDCl_3$) *Z-enol*-**67**: δ = 0.00 (s, 9H, 7-H or 10-H), 0.01 (s, 9H, 7-H or 10-H), 0.82–1.04 (m, 4H, 9-H and 6-H), 2.52 (dd, $J_{3,2}$ = 5.9 Hz, $J_{3,3'}$ = 16.8 Hz, 1H, 3-H), 3.25 (dd, $J_{3',2}$ = 7.5 Hz, $J_{3',3}$ = 16.8 Hz, 1H, 3'-H), 3.79 (s, 3H, 23-H), 3.80 (s, 3H, 24-H), 4.04–4.19 (m, 4H, 8-H and 5-H), 4.49 (s, 2H, 16-H), 4.66 (dd as t, $J_{2,3}$ = 5.9 Hz, $J_{2,3'}$ = 7.5 Hz, 1H, 2-H), 5.20 (s, 1H, 12-H), 6.41 (d, $J_{14,15}$ = 11.4 Hz, 1H, 14-H), 6.41–6.46 (m, 2H, 19-H and 22-H), 7.15–7.18 (m, 2H, 15-H and 21-H), 13.88 (s, 1H, 13-OH) ppm.

^{13}C NMR (175 MHz, $CDCl_3$) *Z-enol*-**67**: δ = –1.5 and –1.4 (C-7 and C-10), 17.3 (C-6 and C-9), 35.0 (C-3), 47.7 (C-16), 55.3 (C-24), 55.4 (C-23), 63.1 (C-5 or C-8), 64.0 (C-5 or C-8), 90.6 (C-12), 98.5 (C-19), 103.9 (C-21), 116.4 (C-15), 116.7 (C-17), 129.3 (C-22), 132.6 (C-14), 158.0 (C-18), 160.8 (C-20), 166.9 (C-13), 170.2 (C-4), 171.4 (C-1), 172.5 (C-11) ppm.

HRMS (ESI-qTOF, positive ion mode): *m/z* calcd. for $C_{28}H_{45}BrNO_8Si_2$: 657.1789 [M]; calcd. for $[M+H]^+$: 658.1867, found: 658.1856; calcd. for $[M+Na]^+$: 680.1687, found: 680.1672.

Bis[2-(trimethylsilyl)ethyl] ((2*Z*,4*E*)-3-hydroxyhepta-2,4,6-trienoyl)-*L*-aspartate (*enol*-**85**) in equilibrium with bis[2-(trimethylsilyl)ethyl] (*E*)-(3-oxopent-4,6-dienoyl)-*L*-aspartate (*keto*-**85**)

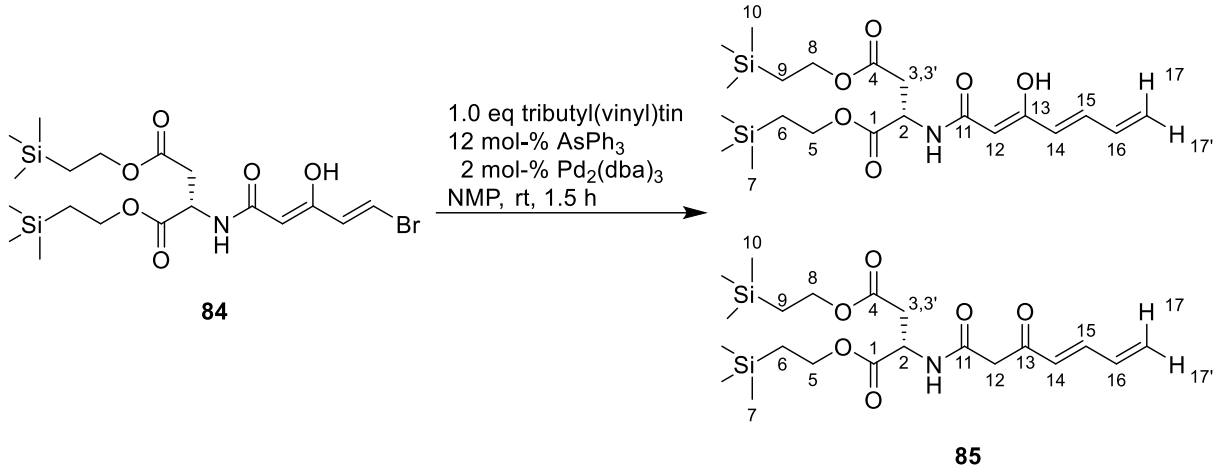

At room temperature $Pd_2(dba)_3$ (11.0 mg, 0.01 mmol, 3 mol-%) was added to a solution of tributyl(vinyl)tin (**68**, 127 µL, 126.7 mg, 0.40 mmol, 1.0 eq), β-ketoamide **84** (264.2 mg, 0.52 mmol, 1.3 eq) and triphenylarsane (20.8 mg, 0.07 mol, 17 mol-%) in 1-methylpyrrolidin-2-one (10 mL). The mixture is stirred for 4 h and glacial acetic acid (2 mL) was added. Then the orange solution was stirred for 15 min. 2-Methoxy-2-methylpropane (50 mL) and a brine (30 mL) were added to the solution. The organic phase was separated from the aqueous phase, washed with brine (3 × 25 mL), and dried over sodium sulfate. The solvent was removed under vacuo and the oily residue was purified using column chromatography (NP-silica, toluene:ethyl acetate 9:1). The product was obtained as a slightly brown oil (90.0 mg, 0.20 mmol, 50%).

The product consists of two compounds which results from the keto-enol tautomerism. The ratio between *keto*- and *enol*-form can be determined via ^{1}H-NMR spectroscopy by integrating the 2-H-signals and calculating the ratio. The ratio is determined to be 1.4(*keto*):1(*enol*).

Rf (toluene:ethyl acetate 9:1): 0.40.

^{1}H NMR (700 MHz, $CDCl_3$) *enol*-**85**: δ = 0.00 (s, 18H, 7-H and 10-H), 0.92–1.02 (m, 4H, 6-H and 9-H), 2.83 (dd, $J_{3,2}$ = 4.6 Hz, $J_{3,3'}$ = 17.3 Hz, 1H, 3-H), 3.00 (dd, $J_{3',2}$ = 4.5 Hz, $J_{3',3}$ = 17.3 Hz, 1H, 3'-H), 4.10–4.28 (m, 4H, 5-H and 8-H), 4.79–4.87 (m, 1H, 2-H), 4.97 (s, 1H, 12-H), 5.31 (d, $J_{17',16}$ = 10.1 Hz, 1H, 17'-H), 5.45 (d,

$J_{17,16}$ = 16.9 Hz, 1H, 17-H), 5.85 (d, $J_{14,15}$ = 15.2 Hz, 1H, 14-H), 6.37 (d, $J_{NH,2}$ = 15.6 Hz, 1H, NH), 6.39 (m, 1H, 16-H), 6.98 (dd, $J_{15,16}$ = 11.0 Hz, $J_{15,14}$ = 15.2 Hz, 1H, 15-H), 13.10 (s, 1H, 13-OH) ppm.
Keto-**85**: δ = 0.00 (s, 18H, 7-H and 10-H), 0.92–1.02 (m, 4H, 6-H and 9-H), 2.79 (dd, $J_{3,2}$ = 4.7 Hz, $J_{3,3'}$ = 17.0 Hz, 1H, 3-H), 2.97 (dd, $J_{3',2}$ = 4.5 Hz, $J_{3',3}$ = 17.0 Hz, 1H, 3'-H), 3.57 (s, 2H, 12-H), 4.10–4.28 (m, 4H, 5-H and 8-H), 4.79–4.87 (m, 1H, 2-H), 5.59 (d, $J_{17',16}$ = 10.0 Hz, 1H, 17'-H), 5.70 (d, $J_{17,16}$ = 16.9 Hz, 1H, 17-H), 6.22 (d, $J_{14,15}$ = 15.6 Hz, 1H, 14-H), 6.45 (ddd, $J_{16,17'}$ = 10.0 Hz, $J_{16,15}$ = 10.9 Hz, $J_{16,17}$ = 16.9 Hz, 1H, 16-H), 7.21 (dd, $J_{15,16}$ = 10.9 Hz, $J_{15,14}$ = 15.6 Hz, 1H, 15-H), 7.78 (d, $J_{NH,2}$ = 8.1 Hz, 1H, NH) ppm.

^{13}C NMR (175 MHz, $CDCl_3$) *enol*-**85**: δ = 0.0 (C-7 and C-10), 17.4 (C-6 and C-9), 36.6 (C-3), 48.3 (C-2), 64.5 (C-5 and C-8), 93.2 (C-12), 122.4 (C-17), 126.6 (C-14), 135.7 (C-16), 136.4 (C-15), 167.7 (C-11), 170.9 (C-1), 171.2 (C-4), 171.3 (C-13) ppm.
Keto-**85**: 0.0 (C-7 and C-10), 17.4 (C-6 and C-9), 36.4 (C-3), 47.1 (C-12), 48.9 (C-2), 63.5 (C-5 and C-8), 128.1 (C-17), 129.7 (C-14), 135.0 (C-16), 145.0 (C-15), 165.8 (C-11), 170.6 (C-1), 170.9 (C-4), 194.7 (C-13) ppm.

HRMS (ESI-qTOF, positive ion mode): *m/z* calcd. for $C_{21}H_{37}NO_6Si_2$: 455.2159 [M]; calcd. for $[M+H]^+$: 456.2232, found: 456.2221; calcd. for $[M+Na]^+$: 478.2052, found: 478.2041.

Bis[2-(trimethylsilyl)ethyl] *N*-(2,4-dimethoxybenzyl)-*N*-((2*Z*,4*E*)-3-hydroxyhepta-2,4,6-trienoyl)-*L*-aspartate (**65**)

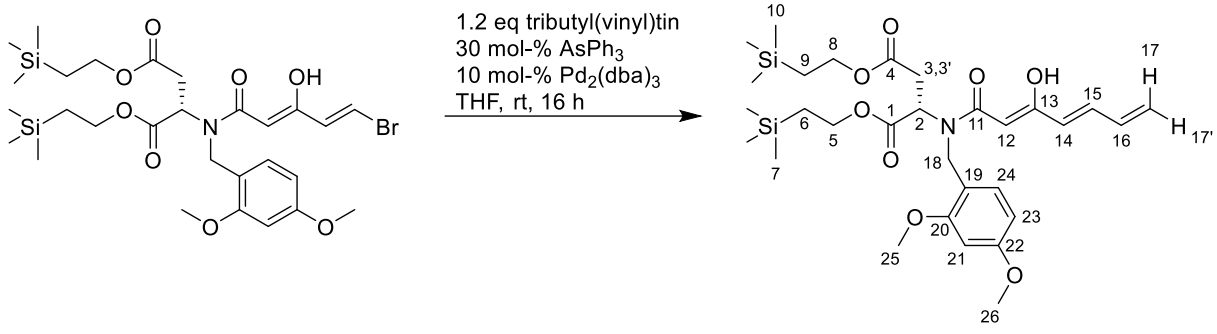

67 **65**

At room temperature $Pd_2(dba)_3$ (4.0 mg, 4 µmol, 10 mol-%) was added to a solution of tributyl(vinyl)tin (**68**, 14.6 µL, 15.9 mg, 50 µmol, 1.2 eq), alkenyl bromide **67** (28.0 mg, 43 µmol, 1.0 eq) and triphenylarsane (4.0 mg, 13 µmol, 30 mol%) in absolute

tetrahydrofuran (2 mL). The mixture was stirred for 16 h. Then water (10 mL) and diethyl ether (10 mL) were added, and the organic phase was separated. The aqueous phase was then extracted with diethyl ether (3 × 15 mL). The combined organic phases were washed with brine (3 × 20 mL) and dried over sodium sulfate. The solvent was removed under vacuo and the crude product was obtained as a brown oil. Purification of the brown oily residue by column chromatography (NP-silica, cyclohexane:ethyl acetate 10:1) afforded the title compound as a slightly yellow oil (16.6 mg, 27 µmol, 64%).

This compound consists of at least two compounds due to keto-enol tautomerism and amide bond rotation. However, only the signals for the *enol*-form can be assigned unambiguously.

Rf (cyclohexane:ethyl acetate 4:1): 0.43.

^{1}H NMR (700 MHz, $CDCl_3$) *Z-enol*-**65**: δ = 0.01 (s, 9H, 7-H or 10-H), 0.02 (s, 9H, 7-H or 10-H), 0.87–0.98 (m, 4H, 9-H and 6-H), 2.53 (dd, $J_{3,2}$ = 5.8 Hz, $J_{3,3'}$ = 16.8 Hz, 1H, 3-H), 3.26 (dd, $J_{3',2}$ = 7.6 Hz, $J_{3',3}$ = 16.8 Hz, 1H, 3'-H), 3.79 (s, 3H, 25-H), 3.80 (s, 3H, 26-H), 4.08–4.19 (m, 4H, 8-H and 5-H), 4.51 (s, 2H, 18-H), 4.67 (dd as t, $J_{2,3}$ = 5.8 Hz, $J_{2,3'}$ = 7.6 Hz, 1H, 2-H), 5.24 (s, 1H, 12-H), 5.32 (d, $J_{17',16}$ = 10.2 Hz, 1H, 17'-H), 5.46 (d, $J_{17,16}$ = 16.9 Hz, 1H, 17-H), 5.87 (d, $J_{14,15}$ = 15.2 Hz, 1H, 14-H), 6.38 (ddd, $J_{16,17'}$ = 10.2 Hz, $J_{16,15}$ = 11.0 Hz, $J_{16,17}$ = 16.9 Hz, 1H, 16-H), 6.41–6.45 (m, 2H, 21-H and 23-H), 7.21 (d, $J_{24,23}$ = 8.2 Hz, 1H, 24-H), 13.87 (s, 1H, 13-OH) ppm.

^{13}C NMR (175 MHz, $CDCl_3$) *Z-enol*-**65**: δ = –1.4 (C-7 and C-10), 17.3 (C-6 and C-9), 35.2 (C-3), 47.7 (C-18), 55.4 (C-26), 55.5 (C-25), 63.2 and 64.0 (C-5 and C-8), 90.8 (C-12), 98.5 (C-21), 103.9 (C-23), 116.8 (C-19), 122.5 (C-17), 127.4 (C-14), 129.3 (C-24), 135.8 (C-16), 136.4 (C-15), 158.1 (C-20), 160.7 (C-22), 169.1 (C-13), 170.5 (C-4), 171.5 (C-1), 172.7 (C-11) ppm.

HRMS (ESI-qTOF, positive ion mode): *m/z* calcd. for $C_{30}H_{47}NO_8Si_2$: 605.2840 [M]; calcd. for $[M+H]^+$: 606.2913, found: 606.2907; calcd. for $[M+Na]^+$: 628.2732, found: 628.2724.

2-(Trimethylsilyl)ethyl 2-((*S*,*Z*)-1-(2,4-dimethoxybenzyl)-4-((*E*)-1-hydroxypenta-2,4-dien-1-ylidene)-3,5-dioxopyrrolidin-2-yl)acetate (**86**)

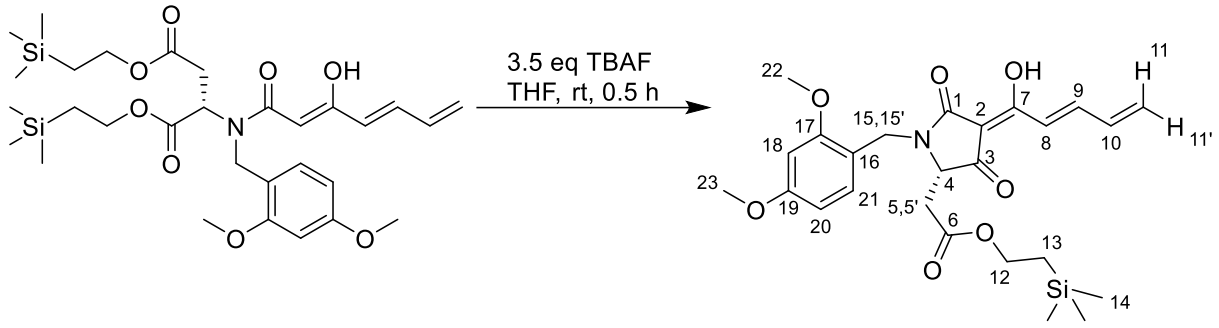

65 **86**

At room temperature a freshly prepared tetra-*n*-butylammonium fluoride trihydrate solution in tetrahydrofuran (1M, 57.8 µL, 57.8 µmol, 3.5 eq) was added to a solution of **65** (10.0 mg, 16.5 µmol, 1.0 eq) in tetrahydrofuran (1 mL) and the mixture was stirred for 30 min at rt. The solvent was removed under vacuo and the residue was dissolved in 500 µL methanol and purified by RP-HPLC (column: Kromasil C18, 100A, 250×8 mm, 5 µm, A: H_2O with 0.1% formic acid, B: acetonitrile with 0.1% formic acid, 50% B → 100% B in 30 min, then 100% B 10 min, product retention time at 31.2 min). The product was obtained as a yellow oil (4.7 mg, 9.6 µmol, 58%).

Rf (cyclohexane:ethyl acetate 3:2): 0.49.

^{1}H NMR (700 MHz, $CDCl_3$): δ = 0.00 (s, 9H, 14-H), 0.88 (t, $J_{13,12}$ = 8.8 Hz, 2H, 13-H), 2.82 (dd, $J_{5,4}$ = 5.7 Hz, $J_{5,5'}$ = 16.4 Hz, 1H, 5-H), 2.92 (dd, $J_{5',4}$ = 3.8 Hz, $J_{5',5}$ = 16.4 Hz, 1H, 5'-H), 3.79 (s, 3H, 22-H), 3.80 (s, 3H, 23-H), 3.86 (dd, $J_{4,5'}$ = 3.8 Hz, $J_{4,5}$ = 5.7 Hz), 4.00–4.12 (m, 2H, 12-H), 4.24 (d, $J_{15,15'}$ = 14.9 Hz, 1H, 15-H), 4.91 (d, $J_{15',15}$ = 14.9 Hz, 1H, 15'-H), 5.58 (d, $J_{11',10}$ = 10.2 Hz, 1H, 11'-H), 5.69 (d, $J_{11,10}$ = 16.9 Hz, 1H, 11-H), 6.41–6.47 (m, 2H, 20-H and 21-H), 6.58 (dt, $J_{10,11' \text{ and } 9}$ = 10.5 Hz, $J_{10,11}$ = 16.9 Hz, 1H, 10-H), 7.20 (d, $J_{8,9}$ = 8.8 Hz, 1H, 8-H), 7.22 (s (br), 1H, 18-H), 7.41 (dd, $J_{9,8}$ = 11.0 Hz, $J_{9,10}$ = 15.4 Hz, 1H, 9-H) ppm.

^{13}C NMR (175 MHz, $CDCl_3$): δ = –1.4 (C-14), 17.3 (C-13), 34.1 (C-5), 38.1 (C-15), 55.5 (C-22 and C-23), 61.4 (C-4), 63.4 (C-12), 98.6 (C-20), 101.3 (C-2), 104.7 (C-21), 116.3 (C-16), 122.7 (C-8), 127.2 (C-11), 131.5 (C-18), 135.9 (C-10), 144.0 (C-9), 158.5 (C-17), 161.0 (C-19), 169.6 (C-6), 172.8 (C-7), 173.7 (C-1), 193.7 (C-3) ppm.

HRMS (ESI-qTOF, positive ion mode): *m/z* calcd. for $C_{25}H_{33}NO_7Si$: 487.2026 [M]; calcd. for $[M+H]^+$: 488.2099, found: 488.2095; calcd. for $[M+Na]^+$: 510.1919, found: 510.1910.

2-((*S*,*Z*)-1-(2,4-Dimethoxybenzyl)-4-((*E*)-1-hydroxypenta-2,4-dien-1-ylidene)-3,5-dioxopyrrolidin-2-yl)acetic acid (**87**)

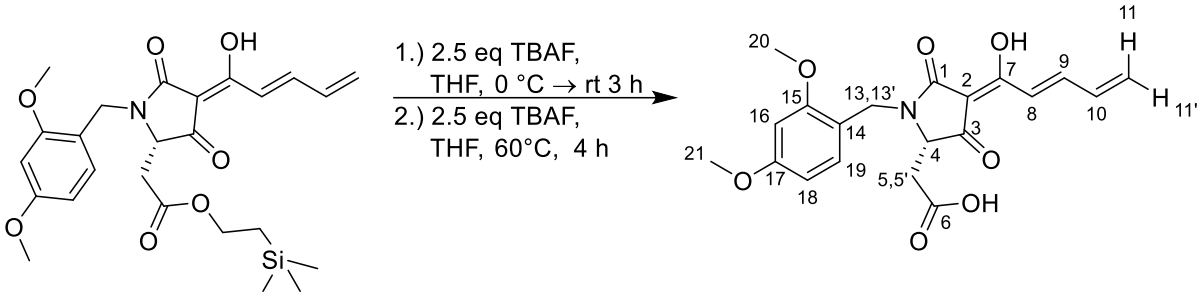

86 **87**

At 0°C a freshly prepared tetra-*n*-butylammonium fluoride trihydrate solution in tetrahydrofuran (1M, 106 µL, 106 µmol, 2.5 eq) was added to a solution of **86** (20.7 mg, 42.5 µmol, 1.0 eq) in tetrahydrofuran (2 mL) and the mixture was warmed up to rt and stirred for 3 h. An additional 2.5 eq of tetra-*n*-butylammonium fluoride trihydrate solution in tetrahydrofuran (1M, 106 µL, 106 µmol, 2.5 eq) were added to the mixture at rt. Then the mixture was heated to 60°C for 4 h. The solvent was removed under vacuo and the residue was dissolved in 1 mL methanol, and after centrifugation purified by RP-HPLC (column: Kromasil C18, 100A, 250×20 mm, 7 µm, A: H_2O with 0.1% formic acid, B: acetonitrile with 0.1% formic acid, 30% B → 100% B in 30 min, then 100% B 10 min, product retention time at 19.6 min). After lyophilization the product was obtained as a brown solid (2.7 mg, 7.0 µmol, 16%).

^{1}H NMR (600 MHz, DMSO-d_6): δ = 2.69 (d, $J_{5,4}$ = 15.7 Hz, 1H, 5-H), 2.79 (d, $J_{5',4}$ = 14.9 Hz, 1H, 5'-H), 3.74 (s, 3H, 22-H), 3.78 (s, 3H, 23-H), 3.84–3.94 (m, 1H, 4-H), 4.20 (d, $J_{13,13'}$ = 15.0 Hz, 1H, 13-H), 4.72 (d, $J_{13',13}$ = 15.0 Hz, 1H, 13'-H), 5.65 (s (br), 1H, 11'-H), 5.85 (d, $J_{11,10}$ = 14.4 Hz, 1H, 11-H), 6.48 (d, $J_{19,18}$ = 8.3 Hz, 1H, 19-H), 6.56 (d, $J_{18,19}$ = 2.0 Hz, 18-H), 6.60–6.76 (m, 1H, 10-H), 7.03–7.21 (m, 2H, 16-H and 8-H), 7.39 (s (br), 1H, 9-H), 12.39 (s (br), 1H, 7-OH) ppm.

^{13}C NMR (150 MHz, DMSO-d_6): δ = 33.1 (C-5), 37.8 (C-13), 55.2 and 55.5 (C-20 and C-21), 61.1 (C-4), 98.3 (C-18), 104.8 (C-19), 115.6 (C-14), 129.8 (C-16), 130.2 (C-8),

135.6 (C-10), 158.0 (C-15), 160.2 (C-17), 170.7 (C-6) ppm. C-1, C-2, C-3, C-7, C-9 and C-11 were not detected.

HRMS (ESI-qTOF, positive ion mode): *m/z* calcd. for $C_{20}H_{21}NO_7$: 387.1318 [M]; calcd. for $[M+H]^+$: 388.1391, found: 388.1387; calcd. for $[M+Na]^+$: 410.1210, found: 410.1205. Negative ion mode: calcd. for $[M-H]^-$: 386.1245, found: 386.1245

Tributyl((1*E*,3*E*)-penta-1,3-dien-1-yl)stannane (**69**)

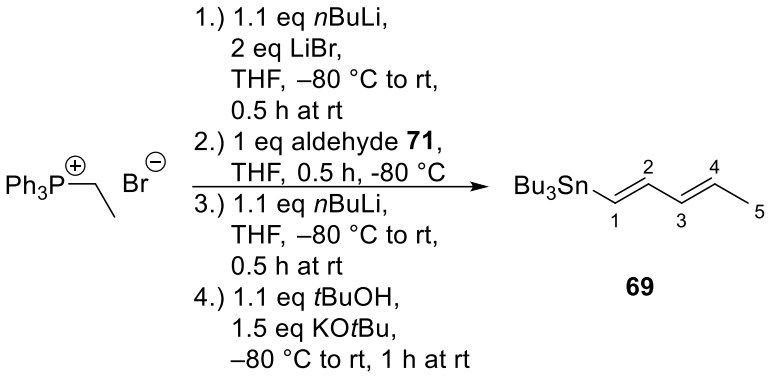

69

At –80°C a solution of *n*-butyllithium in hexanes (2.5M, 128 µL, 0.32 mmol, 1.1 eq) was added to a suspension of ethyltriphenylphosphonium bromide (143 mg, 0.39 mmol, 1.3 eq) and anhydrous LiBr (55.4 mg, 0.64 mmol, 2.2 eq) in THF (4 mL). The mixture was allowed to warm up to room temperature, stirred for 0.5 h and turned dark orange in color. The reaction mixture was cooled down to –80°C to be treated with a solution of *trans*-3-(tributylstannyl)-2-propen-1-al (**71**, 100 mg, 0.29 mmol, 1.0 eq) in THF (1 mL) and a few minutes later, complete decolorization occurred. After stirring for 0.5 h at –80°C, a solution of *n*-butyllithium in hexanes (2.5M, 128 µL, 0.32 mmol, 1.1 eq) was added to the mixture and the mixture was allowed to warm up to room temperature, stirred for 0.5 h and turned dark brown in color. The reaction mixture was cooled down to –80°C to be treated with *tert*-butyl alcohol (93.5 µL, 0.99 mmol, 3.4 eq) and potassium *tert*-butoxide (48.8 mg, 0.44 mmol, 1.5 eq) in this order. After stirring for 1 h at room temperature pentane (5 mL) and water (10 mL) were added to the reaction mixture and allowed to warm up to room temperature. The aqueous phase was extracted with pentane (3 × 10 mL) and the combined organic phases were dried over sodium sulfate. The solvent was removed under vacuo and the crude product purified by column chromatography (silica, cyclohexane). The product was obtained as a slightly yellow oil (82.0 mg, 0.23 mmol, 79%).

Rf (cyclohexane): 0.82.

^{1}H NMR (300 MHz, $CDCl_3$): δ = 0.91 (t, *J* = 7.2 Hz, 18H, $SnCH_2CH_2CH_2\underline{CH_3}$ and $Sn\underline{CH_2}$), 1.20–1.39 (m, 6H, $SnCH_2CH_2\underline{CH_2}CH_3$), 1.42–1.63 (m, 6H, $SnCH_2\underline{CH_2}CH_2CH_3$), 1.76 (dd, $J_{5,4}$ = 6.7 Hz, $J_{5,3}$ = 1.3 Hz, 3H, 5-H), 5.56–5.76 (m, 1H, 4-H), 5.87–6.20 (m, 2H, 1-H and 3-H), 6.48 (dd, *J* = 18.8, 9.8 Hz, 1H, 2-H) ppm.

^{13}C NMR (75 MHz, $CDCl_3$): δ = 9.6 ($SnCH_2CH_2CH_2\underline{CH_3}$), 13.8 ($Sn\underline{CH_2}$), 18.1 (C-5), 27.4 ($SnCH_2CH_2\underline{CH_2}CH_3$), 29.3 ($SnCH_2\underline{CH_2}CH_2CH_3$), 128.7 (C-4), 130.6 (C-1 or C-3), 135.2 (C-3 or C-1), 147.2 (C-2) ppm.

Bis[2-(trimethylsilyl)ethyl] *N*-(2,4-dimethoxybenzyl)-*N*-((2*Z*,4*E*,6*E*,8*E*)-3-hydroxydeca-2,4,6,8-tetraenoyl)-*L*-aspartate (**66**)

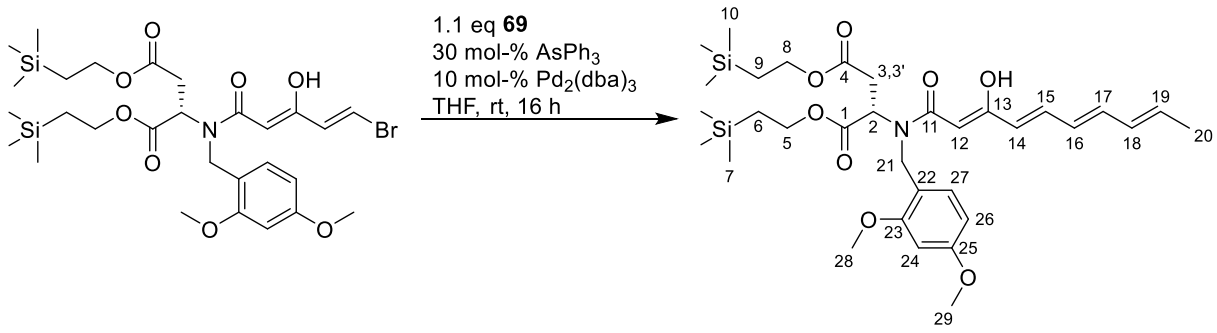

67 **66**

At room temperature $Pd_2(dba)_3$ (19.3 mg, 0.02 mmol, 10 mol-%) was added to a solution of stannane **69** (82.7 mg, 0.23 mmol, 1.1 eq), alkenyl bromide **67** (138 mg, 0.21 mmol, 1.0 eq) and triphenylarsane (19.3 mg, 0.06 mmol, 30 mol-%) in absolute tetrahydrofuran (20 mL). The mixture was stirred for 16 h. Then water (10 mL) and diethyl ether (10 mL) were added, and the organic phase was separated. The aqueous phase was then extracted with diethyl ether (3 × 15 mL). The combined organic phases were washed with brine (3 × 20 mL) and dried over sodium sulfate. The solvent was removed under vacuo and the crude product was obtained as a brown oil. Purification of the brown oily residue by column chromatography (silica, cyclohexane:ethyl acetate stepwise gradient from 100:0 to 95:5) afforded the title compound as an orange oil (113 mg, 0.17 mmol, 83%).

This compound consists of at least two compounds due to keto-enol tautomerism and amide bond rotation. However, only the signals for the *enol*-form can be assigned unambiguously.

Rf (cyclohexane:ethyl acetate 4:1): 0.40.

^{1}H NMR (700 MHz, $CDCl_3$) *Z-enol*-**66**: δ = 0.01 (s, 9H, 7-H or 10-H), 0.02 (s, 9H, 7-H or 10-H), 0.87–0.98 (m, 4H, 9-H and 6-H), 1.80 (d, $J_{20,19}$ = 6.8 Hz, 3H, 20-H) 2.53 (dd, $J_{3,2}$ = 5.7 Hz, $J_{3,3'}$ = 16.8 Hz, 1H, 3-H), 3.22–3.32 (m, 1H, 3'-H), 3.78–3.81 (m, 6H, 28-H and 29-H), 4.05–4.20 (m, 4H, 8-H and 5-H), 4.46–4.54 (m, 2H, 21-H), 4.66 (dd as t, $J_{2,3and3'}$ = 6.1 Hz, 1H, 2-H), 5.19 (s, 1H, 12-H), 5.81 (d, $J_{14,15}$ = 15.2 Hz, 1H, 14-H), 5.85 (dq, $J_{19,20}$ = 7.5 Hz, $J_{19,18}$ = 14.6 Hz, 1H, 19-H), 6.08–6.18 (m, 2H, 16-H and 18-H), 6.41 (dd, $J_{17,18}$ = 10.3 Hz, $J_{17,16}$ = 14.2 Hz, 1H, 17-H), 6.41–6.46 (m, 2H, 26-H and 27-H), 7.04 (dd, $J_{15,16}$ = 11.3 Hz, $J_{15,14}$ = 15.0 Hz, 1H, 15-H), 7.21 (d, $J_{24,26}$ = 8.2 Hz, 1H, 24-H), 13.91 (s (br), 1H, 13-OH) ppm.

^{13}C NMR (175 MHz, $CDCl_3$) *Z-enol*-**66**: δ = –1.4 (C-7 and C-10), 17.4 (C-6 and C-9), 18.7 (C-20), 35.2 (C-3), 47.6 (C-21), 55.4 (C-28), 55.5 (C-29), 57.0 (C-2), 63.1 and 64.0 (C-5 and C-8), 90.1 (C-12), 98.5 (C-27), 103.9 (C-26), 116.9 (C-22), 125.7 (C-14), 128.9 (C-16 or C-18), 129.3 (C-24), 131.7 (C-16 or C-18), 133.4 (C-19), 136.5 (C-15), 138.3 (C-17), 158.1 (C-23), 160.7 (C-25), 169.6 (C-13), 170.6 (C-4), 171.6 (C-1), 172.9 (C-11) ppm.

<u>2-(Trimethylsilyl)ethyl 2-((*S*,*Z*)-1-(2,4-dimethoxybenzyl)-4-((2*E*,4*E*,6*E*)-1-hydroxyocta-2,4,6-trien-1-ylidene)-3,5-dioxopyrrolidin-2-yl)acetate (**89**)</u>

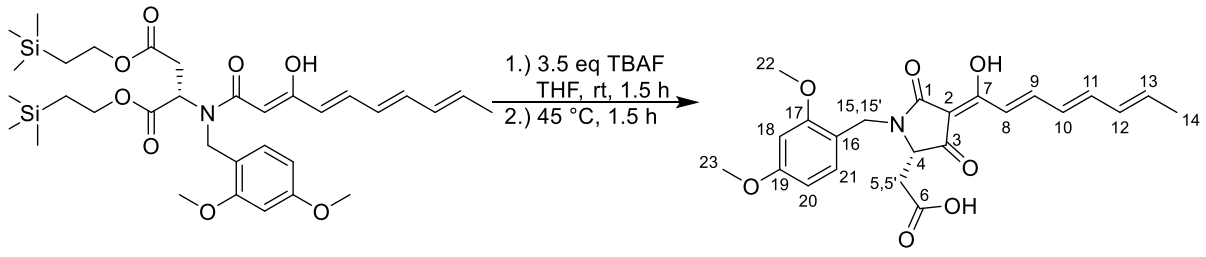

66 **89**

At rt a freshly prepared tetra-*n*-butylammonium fluoride trihydrate solution in tetrahydrofuran (1M, 540 µL, 0.54 mmol, 3.5 eq) was added dropwise to a solution of **66** (100 mg, 0.15 mmol, 1.0 eq) in tetrahydrofuran (15 mL) and the mixture was stirred for 1.5 h min at rt. Then the mixture was stirred for 1.5 h at 45°C. The mixture was allowed to cool down to room temperature and the solvent was removed under vacuo. The residue was dissolved in 2 mL methanol and purified by RP-HPLC (column:

Kromasil C18, 100A, 250×8 mm, 5 µm, A: H_2O with 0.1% formic acid, B: acetonitrile with 0.1% formic acid, 30% B → 100% B in 20 min, then 100% B 15 min, product retention time at 31.2 min). After lyophilization the product was obtained as a yellow solid (32.0 mg, 0.07 mmol, 49%).

Rf (acetonitrile:water 7:3 with formic acid, RP-TLC): 0.40.

^{1}H NMR (700 MHz, DMSO-d_6): δ = 1.83 (d, $J_{14,13}$ = 6.1 Hz, 3H, 14-H), 2.69 (dd, $J_{5,4}$ = 5.5 Hz, $J_{5,5'}$ = 16.9 Hz, 1H, 5-H), 2.80 (dd, $J_{5',4}$ = 3.2 Hz, $J_{5',5}$ = 16.8 Hz, 1H, 5'-H), 3.74 (s, 3H, 23-H), 3.77 (s, 3H, 23-H), 3.86 (s (br), 1H, 4-H), 4.21 (d, $J_{15,15'}$ = 15.1 Hz, 1H, 15-H), 4.73 (d, $J_{15',15}$ = 15.1 Hz, 1H, 15'-H), 6.09 (dq, $J_{13,14}$ = 7.4 Hz, $J_{13,15}$ = 14.3 Hz, 1H, 13-H), 6.30 (dd, $J_{12,11}$ = 13.5 Hz, $J_{12,13}$ = 11.3 Hz, 1H, 12-H), 6.41–6.52 (m, 2H, 10-H and 21-H), 6.56 (d, $J_{20,21}$ = 2.2 Hz, 1H, 20-H), 6.85 (dd, $J_{11,12}$ = 11.1 Hz, $J_{11,10}$ = 14.7 Hz, 1H, 11-H), 7.03 (d, $J_{8,9}$ = 15.1 Hz, 1H, 8-H), 7.13 (d, $J_{18,20}$ = 7.8 Hz, 1H, 18-H), 7.47 (dd, $J_{9,10}$ = 11.7 Hz, $J_{9,8}$ = 15.0 Hz, 1H, 9-H), 12.36 (s (br), 1H, 7-OH or 6-OH) ppm.

^{13}C NMR (175 MHz, $CDCl_3$): δ = 18.5 (C-14), 33.0 (C-5), 37.8 (C-15), 55.2 and 55.5 (C-22 and C-23), 61.1 (C-4), 98.4 (C-20), 100.2 (C-2), 104.9 (C-21), 115.8 (C-16), 119.6 (C-8), 128.7 (C-10), 130.3 (C-18), 131.7 (C-12), 137.1 (C-13), 144.3 (C-9), 158.0 (C-17), 160.3 (C-19), 170.7 (C-6), 170.9 (C-7), 173.2 (C-1), 193.0 (C-3) ppm.

HRMS (ESI-qTOF, positive ion mode): *m/z* calcd. for $C_{23}H_{25}NO_7$: 427.1631 [M]; calcd. for $[M+H]^+$: 428.1704, found: 428.1702; calcd. for $[M+Na]^+$: 450.1523, found: 450.1523. Negative ion mode: calcd. for $[M-H]^-$: 426.1558, found: 426.1539.

2-((*S*,*Z*)-4-((2*E*,4*E*,6*E*)-1-hydroxyocta-2,4,6-trien-1-ylidene)-3,5-dioxopyrrolidin-2-yl)acetic acid (**30**)

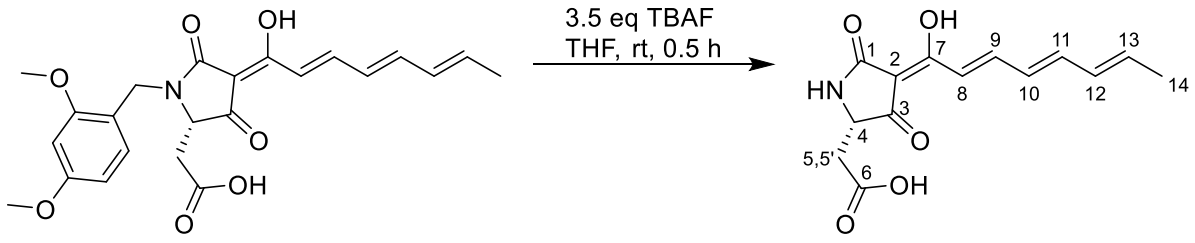

89 **30**

At room temperature thioanisole (180 µL, 1.54 mmol, 30 eq) and trifluoroacetic acid (1.2 mL) were added to a solution of **89** (22.0 mg, 51.5 µmol, 1.0 eq) in dichloromethane (2.8 mL) and the mixture was stirred for 2 h at rt. Dichloromethane (5 mL) and water (5 mL) were added to the mixture and the organic phase was separated. The aqueous phase was then extracted with dichloromethane (3 × 5 mL). The combined organic phases were washed with brine (3 × 20 mL) and dried over sodium sulfate. The solvent was removed under vacuo and the residue was dissolved in 2 mL methanol and purified by RP-HPLC (column: Kromasil C18, 100A, 250×8 mm, 5 µm, A: H_2O with 0.1% formic acid, B: acetonitrile with 0.1% formic acid, 40% B isocratic, product retention time at 20.7 min). After lyophilization the product was obtained as a yellow solid (8.3 mg, 29.9 µmol, 58%).

^{1}H NMR (700 MHz, DMSO-d_6): δ = 1.83 (d, $J_{14,13}$ = 6.6 Hz, 3H, 14-H), 2.58 (dd, $J_{5,4}$ = 6.4 Hz, $J_{5,5'}$ = 16.7 Hz, 1H, 5-H), 2.64 (dd, $J_{5',4}$ = 4.5 Hz, $J_{5',5}$ = 16.8 Hz, 1H, 5'-H), 4.07 (s (br), 1H, 4-H), 6.08 (dq, $J_{13,14}$ = 7.3 Hz, $J_{13,15}$ = 14.0 Hz, 1H, 13-H), 6.30 (ddd, $J_{12,14}$ = 1.2 Hz, $J_{12,11}$ = 10.8 Hz, $J_{12,13}$ = 15.0 Hz, 1H, 12-H), 6.47 (dd, $J_{9,8}$ = 11.5 Hz, $J_{9,10}$ = 14.8 Hz 1H, 9-H), 6.84 (dd, $J_{11,12}$ = 10.7 Hz, $J_{11,10}$ = 14.7 Hz, 1H, 11-H), 7.03 (d, $J_{8,9}$ = 15.3 Hz, 1H, 8-H), 7.46 (dd, $J_{9,10}$ = 11.3 Hz, $J_{9,8}$ = 15.3 Hz, 1H, 9-H), 8.81 (s (br), 1H, NH), 12.42 (s (br), 1H, 7-OH or 6-OH) ppm.
^{13}C NMR (175 MHz, DMSO-d_6): δ = 18.6 (C-14), 35.9 (C-5), 58.1 (C-4), 100.2 (C-2), 119.9 (C-8), 128.8 (C-10), 131.8 (C-12), 137.0 (C-13), 143.8 (C-11), 144.2 (C-9), 171.3 (C-6), 172.3 (C-7), 175.3 (C-1), 194.4 (C-3) ppm.

HRMS (ESI-qTOF, positive ion mode): *m/z* calcd. for $C_{23}H_{25}NO_7$: 277.0950 [M]; calcd. for $[M+H]^+$: 278.1023, found: 278.1028; calcd. for $[M+Na]^+$: 300.0842, found: 300.0849. Negative ion mode: calcd. for $[M-H]^-$: 276.0877, found: 276.0877.

N-Ethylcystargolide A (**103**)[139]

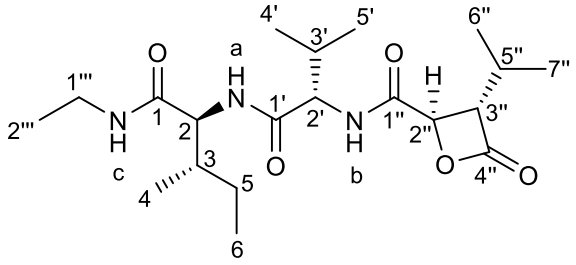

103

1 mL of dry tetrahydrofuran (THF) was added to sodium bicarbonate (4.1 mg, 48.6 µmol, 3.0 eq) under an argon atmosphere and the resulting suspension was stirred for 5 minutes at RT. Cystargolide A (**101**, 6.0 mg, 16.2 µmol, 1.0 eq) was added in one portion and the mixture was cooled to 0°C. 1-Ethyl-3-(3-dimethylaminopropyl)carbodiimide hydrochloride (3.6 mg, 19.0 µmol, 1.2 eq) and 1-hydroxybenzotriazole monohydrate (2.9 mg, 19.0 µmol, 1.2 eq) were added in portions over 10 minutes. Ethylamine in tetrahydrofuran (2.0 M, 9.5 µL, 19.0 µmol, 1.2 eq) was then added at 0°C and the mixture was stirred overnight at 0°C. The sodium bicarbonate was filtered off and washed three times with cold tetrahydrofuran. The combined filtrates were concentrated to approximately 1 mL at 18°C under vacuum and purified by semi-preparative HPLC (column: Kromasil 100 C18, 250 x 8 mm, 5 µm, Dr. Maisch, gradient: acetonitrile-water with 0.1% formic acid, 20% to 80% acetonitrile in 30 minutes at 2.5 mL·min^{-1}). For this purpose, 200 µl of the concentrated solution was diluted with 400 µl of water in a Hamilton syringe before injection into the HPLC system. Monitored at 210 nm, *N*-ethylcystargolide A (**103**) eluted at 19 to 21 minutes (yield: 3.5 mg, 9.1 µmol, 56%).

^{1}H NMR (600 MHz, DMSO-d$_6$, 303 K): δ = 0.85–0.78 (H-4, H-6, H-4’ and H-5’,m, 12H), 1.02–0.95 (H-6’’, H-7’’ and H-2’’’, m, 9H), 1.10–1.04 (m, 1H), 1.50–1.38 (H-5, m, 1H), 1.75–1.64 (H-3, m, 1H), 2.05–1.96 (H-3’, m, 1H), 2.12 (H-5’’, oct, *J* = 6.9, 1H), 3.15–2.93 (H-1’’’, m, 2H), 3.53 (H-3’’, dd, *J* = 8.3, 4.5 Hz, 1H), 4.08 (H-2, t, *J* = 8.3 Hz, 1H), 4.30–4.24 (H-2’, m, 1H), 5.01 (H-2’’, d, *J* = 4.0 Hz, 1H), 8.09–7.91 (H-a and H-c, m, 2H), 8.55–8.48 (H-b, m, 1H) ppm.

^{13}C NMR (150.3 MHz, DMSO-d$_6$, 303 K): δ = 10.8 (C-6), 14.6 (C-2‘‘‘), 15.3 (C-4), 17.9 (C-5‘), 19.1 (C-4‘), 19.2 (C-6‘‘), 19.4 (C-7‘‘), 24.4 (C-5), 26.6 (C-5‘‘), 30.5 (C-3‘),

33.2 (C-1‘‘‘), 36.4 (C-3), 56.9 (C-2), 57.7 (C-2‘), 62.7 (C-3‘‘), 70.2 (C-2‘‘), 167.3 (C-1‘‘), 170.0 (C-4‘‘), 170.1 (C-1‘), 170.3 (C-1) ppm.

HRMS (ESI-qTOF, positive ion mode): *m/z* calcd. for $C_{20}H_{35}N_3O_5$: 397.2577 [M]; calcd. for $[M+H]^+$: 398.2649, found: 398.2658; calcd. for $[M+Na]^+$: 420.2469, found: 420.2479.

N-Ethylcystargolide B (**104**)[139]

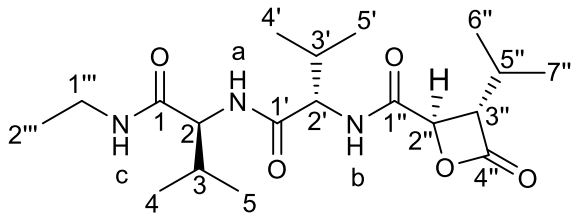

104

1 mL of dry THF was added to sodium bicarbonate (3.2 mg, 37.9 µmol, 3.0 eq) under an argon atmosphere and the resulting suspension was stirred for 5 minutes at room temperature. Cystargolide B (**102**, 4.5 mg, 12.6 µmol, 1.0 eq) was added in one portion, and the mixture was cooled to 0°C. EDC-HCl (2.9 mg, 15.0 µmol, 1.2 eq) and HOBt (2.3 mg, 15.0 µmol, 1.2 eq) were added in portions over 10 minutes. Ethylamine in tetrahydrofuran (2.0 M, 7.5 µL, 15.0 µmol, 1.2 eq) was then added and the mixture was stirred overnight at 0°C. The sodium bicarbonate was filtered off and washed three times with cold tetrahydrofuran. The combined filtrates were concentrated to approximately 1 mL at 18°C on vacuum and purified by semi-preparative HPLC (column: Kromasil 100 C18, 250 x 8 mm, 5 µm, Dr. Maisch, gradient: acetonitrile-water with 0.1% formic acid, 20 to 80% acetonitrile in 30 minutes at 2.5 $mL \cdot min^{-1}$). For this purpose, 200 µl of the concentrated solution was diluted with 400 µl of water in a Hamilton syringe before injection into the HPLC system. Monitored at 210 nm, *N*-ethylcystargolide B (**104**) eluted at 17 to 20 minutes (yield: 1.6 mg, 4.0 µmol, 32%). **^{1}H NMR** (600 MHz, DMSO-d_6, 303 K): δ = 0.85–0.80 (H-4, H-5, H-4’ and H-5’, m, 12H), 1.02–0.96 (H-6’’, H-7’’ and H-2’’’, m, 9H), 1.91 (H-3, oct, *J* = 6.8 Hz, 1H), 2.01 (H-3’, oct, *J* = 7.0 Hz, 1H), 2.16–2.09 (H-5’’, m, 1H), 3.14–3.00 (H-1’’’, m, 2H), 3.54 (H-3’’, dd, *J* = 8.3, 4.2 Hz, 1H), 4.05 (H-2’, dd, *J* = 8.6, 7.5 Hz, 1H), 4.29 (H-2, dd, *J* = 8.9, 7.0 Hz, 1H), 5.00 (H-2’’, d, *J* = 4.1 Hz, 1H), 7.95–7.86 (H-a and H-c, m, 2H), 8.51 (H-b, d, *J* = 8.9 Hz, 1H) ppm.

^{13}C NMR (150.3 MHz, DMSO-d_6, 303 K): δ = 14.6 (C-2‘‘‘), 18.0 (C-5‘), 18.4 (C-4), 19.1 (C-4‘), 19.1 (C-5), 19.2 (C-6‘‘), 19.4 (C-7‘‘), 30.4 (C-3), 30.5 (C-3‘), 33.2 (C-1‘‘‘), 57.7 (C-2), 57.9 (C-2‘), 62.7 (C-3‘‘), 70.2 (C-2‘‘), 167.4 (C-1‘‘), 170.1 (C-4‘‘), 170.2 (C-1‘), 170.2 (C-1) ppm.

HRMS (ESI-qTOF, positive ion mode): *m/z* calcd. for $C_{19}H_{33}N_3O_5$: 383.2420 [M]; calcd. for $[M+H]^+$: 384.2493, found: 384.2499; calcd. for $[M+Na]^+$: 406.2312, found: 406.2322.

6.5.2. Synthesis of peptides on solid support

6.5.2.1. Peptide amides **25**, **37**–**51**

General Procedure for peptide amides **37**–**51** and **25**:[94]

Loading of rink amide resin:

Fmoc protected TentaGel S RAM resin (150 mg, maximum loading: 0.23 mmol·g^{-1}, Rapp Polymere, Tübingen, Germany) was subjected to Fmoc removal conditions (2% DBU and 10% morpholine in 2 mL DMF, 2 × 10 min) and washed with DMF (3 × 2 mL), DCM (3 × 2 mL) and DMF (3 × 2 mL). The resin was loaded using 5 eq protected starting amino acid (Fmoc-D-Asn(Trt)-OH or Fmoc-L-Asn(Trt)-OH), 5 eq HATU, 5 eq HOAt and 6 eq NMM in 2 mL DMF. The loading reaction was run over night at rt. The resin was washed with DMF (3 × 2 mL), DCM (3 × 2 mL) and DMF (3 × 2 mL) and then capped using a mixture of DMF/Ac_2O/pyridine (7/2/1, v/v/v) for 30 min at rt. After washing with DMF (3 × 2 mL), DCM (3 × 2 mL) and DMF (3 × 2 mL) the resin was ready for the SPPS procedure.

Solid phase peptide synthesis:

Fmoc-D-Asn(Trt) TG S RAM or Fmoc-L-Asn(Trt) TG S RAM resin (loading: 0.23 mmol·g^{-1}, 150 mg, 34.5 µmol scale, TG S RAM, Rapp Polymere) was swollen in 2 mL DMF for 30 min. The Fmoc group was removed by treatment with a solution of 2% DBU/10% morpholine (v/v) in DMF (2 mL) for 3 min and additional 12 min. The resin-bound residue was submitted to iterative peptide assembly (Fmoc-SPPS) using 2% DBU/10% morpholine (v/v) in DMF (2 mL, 3 + 12 min) for Fmoc-deprotection and Fmoc-D- or Fmoc-L-AA-OH (Fmoc-L-Asp(O*t*Bu)-OH, Fmoc-D-Asp(O*t*Bu)-OH, Fmoc-D-Phe-OH and Fmoc-L-Phe-OH) (6 eq), HATU (6 eq), HOBt (6 eq) and NMM (8 eq) in DMF (2 mL) for 45 min to couple each amino acid. After full assembly of linear peptide amide with desired stereo configuration on the solid support, the resin was washed

with DMF (3 × 2 mL), DCM (3 × 2 mL), toluene (3 × 2 mL), isopropyl alcohol (3 × 2 mL), diethyl ether (3 × 2 mL) and dried under reduced pressure for 3 h. The peptide was cleaved by treatment with TFA/TIPS/H_2O (95:5:5 v/v/v, 2 mL) for 3 × 1 h and one washing step with TFA (2 mL) for 10 min. The solvent was removed under reduced pressure, the residue was washed with diethyl ether (3 × 2 mL) and centrifuged. The precipitate was lyophilized using *tert*-butanol/water (1:1 v/v, 10 mL) to afford the desired crude peptide amide. Crude peptide amides were dissolved in a mixture of acetonitrile/water/formic acid (50/50/0.1 v/v/v, 500 µL) and injected to a semi preparative HPLC system equipped with a RP column (Kromasil 100 C18, 5 µm, 250 × 8 mm, Dr. Maisch GmbH). HPLC was performed using a gradient ranging from 10% B (A: water with 0.1% formic acid, B: acetonitrile with 0.1% formic acid) to 100% B within 30 min. The flow rate was set to 2 mL·min^{-1}. The peptide containing fractions were frozen and lyophilized to yield the peptide amides (yields after purification: 29%–82%).

*Separation of enantiomers **25** and **51***: Column: Daicel CHIRALPAK ZWIX(+), 3 x 150 mm, 3 µm; mobile phase: 49% ACN, 49% MeOH, 25mM NH_3, 50mM formic acid; flow rate: 0.5 mL·min^{-1}, isocratic conditions for 16 minutes.

Experimental data for each peptide amide:

L-Phe-D-Phe-L-Asp-D-Asn-NH_2 (**25**)

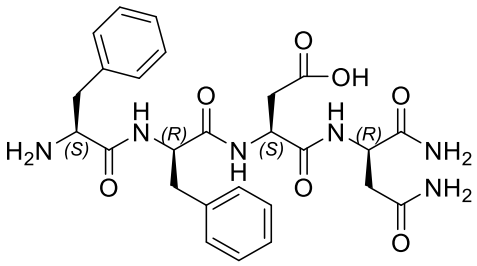

25

Yield: 76%, 14.2 mg

^{1}H NMR (700 MHz, DMSO-d_6, 303 K) δ = 8.71 (s (br), 1H), 8.60 (d, *J* = 7.1 Hz, 1H), 8.02 (d, *J* = 8.1 Hz, 1H), 7.31 (s, 1H), 7.28–7.14 (m, 9H), 7.09 (s, 1H), 7.02 (s, 1H), 7.01 (d, *J* = 7.8 Hz, 1H), 6.86 (s, 1H), 4.57–4.49 (m, 1H), 4.44 (td, *J* = 6.4 Hz, 8.1 Hz, 1H), 4.40–4.34 (m, 1H), 3.70–3.58 (m, 1H), 3.08 (dd, *J* = 3.7 Hz, 13.9 Hz, 1H), 2.82–2.72 (m, 2H), 2.58–2.46 (m, 5H, overlayed by solvent signal) ppm.

^{13}C NMR (175 MHz, DMSO-d_6, 303 K) δ = 173.0, 172.7, 172.2, 171.9, 171.3, 170.5, 137.7, 137.0, 129.2, 129.2, 128.1, 128.1, 126.4, 126.3, 54.8, 54.1, 50.4, 49.8, 39.0 (overlayed by solvent signal), 37.3, 37.0, 36.6 ppm.

HRMS (ESI-qTOF, positive ion mode): *m/z* calcd. for $C_{26}H_{32}N_6O_7$: 540.2332 [M]; calcd. for $[M+H]^+$: 541.2405, found: 541.2401; calcd. for $[M+Na]^+$: 563.2225, found: 563.2225.

D-Phe-D-Phe-D-Asp-D-Asn-NH_2 (**37**)

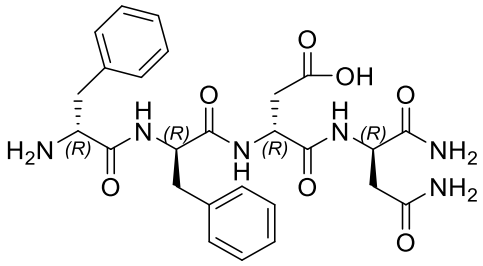

37

Yield: 51%, 9.5 mg

^{1}H NMR (700 MHz, DMSO-d_6, 303 K) δ = 8.57 (d, *J* = 6.9 Hz, 1H), 8.44 (s (br), 1H), 8.08 (d, *J* = 7.9 Hz, 1H), 7.40–7.05 (m, 16H), 7.01 (s, 1H), 6.86 (s, 1H), 4.60–4.53 (m, 1H), 4.50 (td, *J* = 6.2 Hz, 6.6 Hz, 1H), 4.44 (td, J = 6.2 Hz, 7.3 Hz, 1H), 3.72–3.59 (m, 1H, overlayed by water signal), 3.08 (dd, *J* = 3.5 Hz, 13.9 Hz, 1H), 3.00–2.90 (m, 1H), 2.82 (dd, *J* = 4.2 Hz, 9.6 Hz, 1H), 2.72 (dd, *J* = 5.6 Hz, 16.5 Hz, 1H), 2.69–2.62 (m, 1H), 2.53 (dd, *J* = 5.4 Hz, 15.5 Hz, 1H, overlayed by solvent signal), 2.42–2.26 (m, 1H) ppm.

^{13}C NMR (175 MHz, DMSO-d_6, 303 K) δ = 172.7, 172.1, 171.8, 171.1, 170.0, 169.7, 137.6, 129.4, 129.3, 128.3, 128.1, 126.6, 126.3, 54.6, 53.7, 49.6, 39.4 (overlayed by solvent signal) 37.4, 36.5, 36.1 ppm.

HRMS (ESI-qTOF, positive ion mode): *m/z* calcd. for $C_{26}H_{32}N_6O_7$: 540.2332 [M]; calcd. for $[M+H]^+$: 541.2405, found: 541.2422; calcd. for $[M+Na]^+$: 563.2225, found: 563.2237.

L-Phe-L-Phe-L-Asp-D-Asn-NH_2 (**38**)

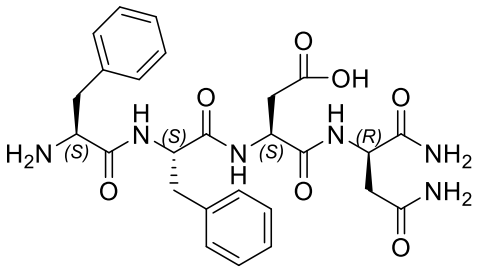

38

Yield: 47%, 8.8 mg

^{1}H NMR (700 MHz, DMSO-d_6, 303 K) δ = 8.61 (d, *J* = 7.5 Hz, 1H), 7.97 (d, *J* = 8.4 Hz, 1H), 7.49 (s (br), 1H), 7.35 (s, 1H), 7.29–7.12 (m, 16H), 7.10 (d, *J* = 7.3 Hz, 1H), 6.99 (s, 1H), 6.82 (s, 1H), 4.47–4.39 (m, 2H), 4.28 (td, *J* = 5.8 Hz, 6.6 Hz, 1H), 3.42–3.37 (m, 1H, overlayed by water signal), 3.08 (dd, *J* = 4.0 Hz, 14.0 Hz, 1H), 2.87 (dd, *J* = 9.6 Hz, 13.9 Hz, 1H), 2.82 (dd, *J* = 4.7 Hz, 14.7 Hz, 1H), 2.52–2.45 (m, 4H, overlayed by solvent signal) ppm.

^{13}C NMR (175 MHz, DMSO-d_6, 303 K) δ = 173.2, 172.3, 171.8, 171.0, 170.8, 138.4, 137.8, 129.2, 129.2, 128.1, 128.0, 126.2, 126.1, 56.3, 54.1, 50.4, 49.8, 40.2, 40.0, 36.8, 35.1 ppm.

HRMS (ESI-qTOF, positive ion mode): *m/z* calcd. for $C_{26}H_{32}N_6O_7$: 540.2332 [M]; calcd. for $[M+H]^+$: 541.2405, found: 541.2415; calcd. for $[M+Na]^+$: 563.2225, found: 563.2231.

D-Phe-D-Phe-L-Asp-D-Asn-NH_2 (**39**)

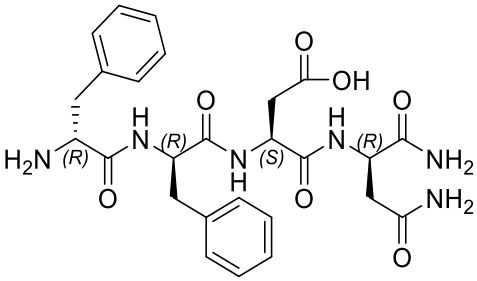

39

Yield: 29%, 5.4 mg

^{1}H NMR (700 MHz, DMSO-d_6, 303 K) δ = 8.51 (d, *J* = 5.4 Hz, 1H), 8.62 (d, *J* = 7.6 Hz, 1H), 8.10 (d, *J* = 8.3 Hz, 1H), 7.35–7.18 (m, 10H), 7.14 (s, 1H), 7.04 (s, 1H), 6.87 (s, 1H), 4.58 (td, *J* = 5.7 Hz, 7.0 Hz, 1H), 4.53 (td, *J* = 5.4 Hz, 7.6 Hz, 1H), 4.48 (td, J = 5.6 Hz, 7.7 Hz, 1H), 3.89 (dd, *J* = 4.0 Hz, 8.2 Hz, 1H), 3.09 (dd, *J* = 4.1 Hz, 14.2 Hz, 1H), 3.04 (dd, *J* = 5.0 Hz, 13.9 Hz, 1H), 2.87 (dd, *J* = 8.8 Hz, 13.9 Hz, 1H), 2.80 (dd, *J* = 8.9 Hz, 14.1 Hz, 1H), 2.64 (dd, *J* = 5.3 Hz, 16.6 Hz, 1H), 2.53 (dd, *J* = 5.4 Hz, 15.5 Hz, 1H, overlayed by solvent signal), 2.46 (dd, J = 7.7 Hz, 16.0 Hz, 2H) ppm.

^{13}C NMR (175 MHz, DMSO-d_6, 303 K) δ = 172.8, 171.8, 171.8, 170.8, 170.0, 169.5, 137.3, 135.6, 129.5, 129.2, 128.5, 128.1, 126.9, 126.4, 54.3, 53.8, 49.7, 49.7, 37.6, 37.5, 36.8, 36.1 ppm.

HRMS (ESI-qTOF, positive ion mode): *m/z* calcd. for $C_{26}H_{32}N_6O_7$: 540.2332 [M]; calcd. for $[M+H]^+$: 541.2405, found: 541.2415; calcd. for $[M+Na]^+$: 563.2225, found: 563.2231.

D-Phe-L-Phe-D-Asp-D-Asn-NH_2 (**40**)

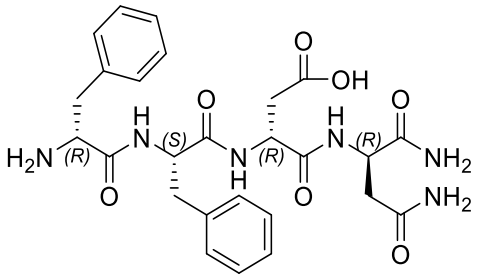

40

Yield: 31%, 5.8 mg

^{1}H NMR (700 MHz, DMSO-d_6, 303 K) δ = 8.72 (d, *J* = 6.8 Hz, 1H), 8.66 (s (br), 1H), 8.11 (d, *J* = 8.1 Hz, 1H), 7.34 (s, 1H), 7.27–7.15 (m, 9H), 7.11 (s, 1H), 7.08 (s, 1H), 7.02 (d, *J* = 7.3 Hz, 1H), 6.86 (s, 1H), 4.53–4.45 (m, 1H), 4.44–4.37 (m, 2H), 3.79–3.69 (m, 1H), 2.99 (dd, *J* = 4.3 Hz, 14.0 Hz, 1H), 2.81 (dd, *J* = 5.5 Hz, 13.8 Hz, 1H), 2.77 (dd, *J* = 10.1 Hz, 14.0 Hz, 1H), 2.61–2.52 (m, 2H), 2.39 (dd, *J* = 8.2 Hz, 15.8 Hz, 1H) ppm.

^{13}C NMR (175 MHz, DMSO-d_6, 303 K) δ = 172.9, 172.4, 171.8, 171.3, 170.9, 170.3, 137.5, 136.4, 129.2, 129.1, 128.2, 128.1, 126.6, 126.3, 54.4, 54.4, 49.7, 38.5, 37.5, 37.1, 36.5 ppm.

HRMS (ESI-qTOF, positive ion mode): *m/z* calcd. for $C_{26}H_{32}N_6O_7$: 540.2332 [M]; calcd. for $[M+H]^+$: 541.2405, found: 541.2412; calcd. for $[M+Na]^+$: 563.2225, found: 563.2231.

L-Phe-D-Phe-D-Asp-D-Asn-NH_2 (**41**)

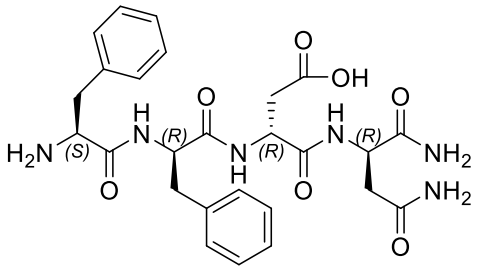

41

Yield: 43%, 8.0 mg

^{1}H NMR (700 MHz, DMSO-d_6, 303 K) δ = 8.66 (s (br), 1H), 8.53 (d, *J* = 7.0 Hz, 1H), 8.03 (d, *J* = 8.2 Hz, 1H), 7.35 (s, 1H), 7.26–7.14 (m, 10H), 7.06 (s, 1H), 7.02 (d, *J* = 6.8 Hz, 2H), 6.85 (s, 1H), 4.55–4.50 (m, 1H), 4.46–4.42 (m, 1H), 4.40 (dd, *J* = 6.6 Hz, 13.1 Hz, 1H), 3.62 (dd, *J* = 5.4 Hz, 7.8 Hz, 1H), 3.06 (dd, *J* = 4.3 Hz, 14.0 Hz, 1H), 2.78 (dd, *J* = 5.4 Hz, 13.8 Hz, 1H), 2.74 (dd, *J* = 10.0 Hz, 14.0 Hz, 1H) 2.61 (dd, *J* = 5.9 Hz, 16.0 Hz, 1H), 2.49–2.45 (m, 1H, overlayed by solvent signal) ppm.

^{13}C NMR (175 MHz, DMSO-d_6, 303 K) δ = 172.9, 172.6, 172.0, 171.2, 170.4, 137.7, 137.0, 129.2, 129.2, 128.1, 128.0, 126.3, 126.2, 54.8, 53.9, 50.6, 49.8, 39.6 (overlayed by solvent signal), 37.3, 37.0, 36.6 ppm.

HRMS (ESI-qTOF, positive ion mode): *m/z* calcd. for $C_{26}H_{32}N_6O_7$: 540.2332 [M]; calcd. for $[M+H]^+$: 541.2405, found: 541.2420; calcd. for $[M+Na]^+$: 563.2225, found: 563.2234.

L-Phe-L-Phe-D-Asp-D-Asn-NH_2 (**42**)

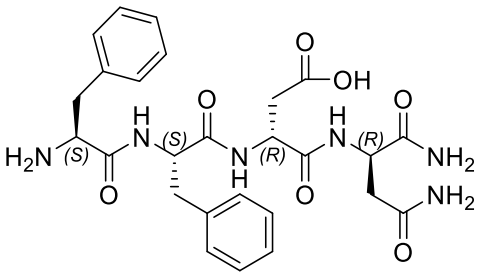

42

Yield: 45%, 8.4 mg

^{1}H NMR (700 MHz, DMSO-d_6, 303 K) δ = 8.59 (d, *J* = 7.4 Hz, 1H), 8.32 (s (br), 1H), 8.06 (d, *J* = 8.1 Hz, 1H), 7.31 (s, 1H), 7.29–7.13 (m, 10H), 7.09 (s, 1H), 7.01 (s, 1H), 6.83 (s, 1H), 4.55–4.50 (m, 1H), 4.48 (td, *J* = 5.9 Hz, 6.7 Hz, 1H), 4.44 (td, *J* = 5.6 Hz, 7.7 Hz, 1H), 3.50 (dd, *J* = 4.3 Hz, 8.6 Hz, 1H), 2.99 (dd, *J* = 5.0 Hz, 13.8 Hz, 1H), 2.90 (dd, *J* = 4.3 Hz, 13.7 Hz, 1H), 2.84 (dd, *J* = 8.7 Hz, 13.8 Hz, 1H), 2.64 (dd, *J* = 5.7 Hz, 16.5 Hz, 1H), 2.58–2.51 (m, 2H, overlayed by solvent signal), 2.49–2.40 (m, 2H, overlayed by solvent signal) ppm.

^{13}C NMR (175 MHz, DMSO-d_6, 303 K) δ = 173.2, 172.9, 172.1, 171.7, 171.1, 170.2, 137.9, 137.3, 129.3, 129.3, 128.2, 128.0, 126.3, 55.5, 53.8, 50.0, 49.8, 39.7 (overlayed by solvent signal), 37.4, 36.7, 36.3 ppm.

HRMS (ESI-qTOF, positive ion mode): *m/z* calcd. for $C_{26}H_{32}N_6O_7$: 540.2332 [M]; calcd. for $[M+H]^+$: 541.2405, found: 541.2410; calcd. for $[M+Na]^+$: 563.2225, found: 563.2236.

D-Phe-L-Phe-L-Asp-D-Asn-NH_2 (**43**)

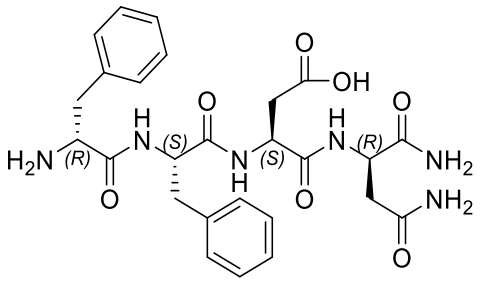

43

Yield: 54%, 10.1 mg

^{1}H NMR (700 MHz, DMSO-d_6, 303 K) δ = 8.66 (s (br), 1H), 8.59 (d, *J* = 7.4 Hz, 1H), 8.00 (d, *J* = 8.3 Hz, 1H), 7.30 (s, 1H), 7.27–7.15 (m, 9H), 7.08 (s, 1H), 7.03 (s, 1H), 7.02 (d, *J* = 6.8 Hz, 1H), 6.86 (s, 1H), 4.54–4.48 (m, 1H), 4.43 (td, *J* = 6.3 Hz, 8.2 Hz, 1H), 4.36 (td, *J* = 6.2 Hz, 7.0 Hz, 1H), 3.60 (dd, *J* = 5.2 Hz, 8.1 Hz, 1H), 3.07 (dd, *J* = 4.1 Hz, 14.1 Hz, 1H), 2.80–2.73 (m, 2H), 2.56–2.47 (m, 4H, overlayed by solvent signal) ppm.

^{13}C NMR (175 MHz, DMSO-d_6, 303 K) δ = 173.0, 172.6, 172.5, 171.9, 171.2, 170.5, 137.7, 137.2, 129.2, 129.1, 128.1, 128.1, 126.3, 126.3, 54.9, 54.1, 50.4, 49.8, 39.8 (overlayed by solvent signal), 37.3, 36.9, 36.6 ppm.

HRMS (ESI-qTOF, positive ion mode): *m/z* calcd. for $C_{26}H_{32}N_6O_7$: 540.2332 [M]; calcd. for $[M+H]^+$: 541.2405, found: 541.2413; calcd. for $[M+Na]^+$: 563.2225, found: 563.2230.

L-Phe-L-Phe-L-Asp-L-Asn-NH_2 (**44**)

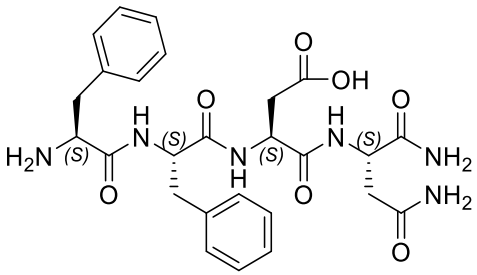

44

Yield: 29%, 5.4 mg

^{1}H NMR (700 MHz, DMSO-d_6, 303 K) δ = 8.53 (d, *J* = 7.1 Hz, 1H), 8.23 (s (br), 1H), 8.07 (d, *J* = 8.1 Hz, 1H), 7.32 (s, 1H), 7.29–7.12 (m, 11H), 7.09 (s, 1H), 7.05 (s, 1H), 6.85 (s, 1H), 4.55–4.48 (m, 1H), 4.48–4.39 (m, 2H), 3.44 (m, 1H, overlayed by water signal), 3.06 (dd, *J* = 4.3 Hz, 13.9 Hz, 1H), 2.88–2.78 (m, 2H), 2.67 (dd, *J* = 5.8 Hz, 16.3 Hz, 1H), 2.53–2.45 (m, 4H, overlayed by solvent signal) ppm.

^{13}C NMR (175 MHz, DMSO-d_6, 303 K) δ = 172.8, 172.1, 171.8, 171.2, 170.1, 137.6, 129.3, 129.3, 128.2, 128.0, 126.2, 126.2, 55.5, 53.4, 50.1, 49.7, 39.8 (overlayed by solvent signal), 37.4, 36.5, 35.1 ppm.

HRMS (ESI-qTOF, positive ion mode): *m/z* calcd. for $C_{26}H_{32}N_6O_7$: 540.2332 [M]; calcd. for $[M+H]^+$: 541.2405, found: 541.2404; calcd. for $[M+Na]^+$: 563.2225, found: 563.2219.

D-Phe-D-Phe-D-Asp-L-Asn-NH_2 (**45**)

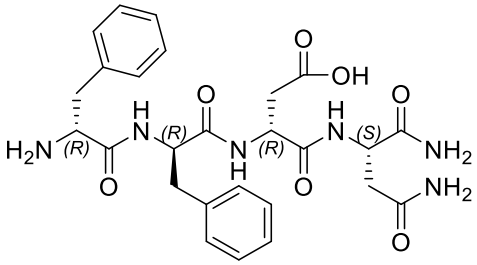

45

Yield: 47%, 8.8 mg

^{1}H NMR (700 MHz, DMSO-d_6, 303 K) δ = 8.80 (d, *J* = 7.6 Hz, 1H), 8.60 (d, *J* = 7.0 Hz, 1H), 8.02 (d, *J* = 8.3 Hz, 1H), 7.35 (s, 1H), 7.30–7.08 (m, 45H, aspartic imide sideproduct), 7.04 (s, 1H), 6.83 (s, 1H), 6.77 (d, *J* = 9.7 Hz, 1H), 4.60–4.48 (m, 1H), 4.50 (m, 2H), 4.32 (td, *J* = 6.2 Hz, 6.6 Hz, 1H), 3.44–3.38 (m, 1H, overlayed by water signal), 3.11–3.02 (m, 2H), 3.01–2.91 (m, 2H), 2.90–2.79 (m, 2H), 2.55–2.47 (m, 2H, overlayed by solvent signal) ppm.

^{13}C NMR (175 MHz, DMSO-d_6, 303 K) δ = 173.0, 172.6, 172.5, 171.9, 171.2, 170.5, 137.7, 137.2, 129.2, 129.1, 128.1, 128.1, 126.3, 126.3, 54.9, 54.1, 50.4, 49.8, 39.8 (overlayed by solvent signal), 37.3, 36.9, 36.6 ppm.

HRMS (ESI-qTOF, positive ion mode): *m/z* calcd. for $C_{26}H_{32}N_6O_7$: 540.2332 [M]; calcd. for $[M+H]^+$: 541.2405, found: 541.2410; calcd. for $[M+Na]^+$: 563.2225, found: 563.2224.

L-Phe-L-Phe-D-Asp-L-Asn-NH_2 (**46**)

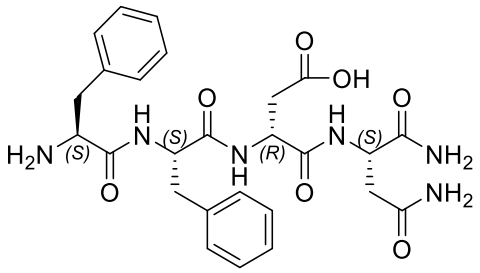

46

Yield: 33%, 6.2 mg

^{1}H NMR (700 MHz, DMSO-d_6, 303 K) δ = 8.54 (d, *J* = 7.6 Hz, 1H), 8.39 (s (br), 1H), 8.07 (d, *J* = 8.2 Hz, 1H), 7.32–7.14 (m, 11H), 7.13 (s, 1H), 7.09 (s, 1H), 6.85 (s, 1H), 4.52–4.39 (m, 3H), 3.51 (dd, *J* = 4.5 Hz, 8.6 Hz, 1H), 3.02 (dd, *J* = 5.0 Hz, 13.8 Hz, 1H), 2.90 (dd, J = 4.3 Hz, 13.7 Hz, 1H), 2.86 (dd, J = 8.7 Hz, 13.8 Hz, 1H), 2.59–2.44 (m, 4H, overlayed by solvent signal) ppm.

^{13}C NMR (175 MHz, DMSO-d_6, 303 K) δ = 173.2, 173.0, 172.3, 171.8, 170.9, 170.3, 137.9, 137.4, 129.3, 129.3, 128.2, 128.0, 126.3, 55.5, 54.1, 49.9, 49.8, 39.6 (overlayed by solvent signal), 37.3, 36.8, 36.7 ppm.

HRMS (ESI-qTOF, positive ion mode): *m/z* calcd. for $C_{26}H_{32}N_6O_7$: 540.2332 [M]; calcd. for $[M+H]^+$: 541.2405, found: 541.2400; calcd. for $[M+Na]^+$: 563.2225, found: 563.2212.

L-Phe-D-Phe-L-Asp-L-Asn-NH_2 (**47**)

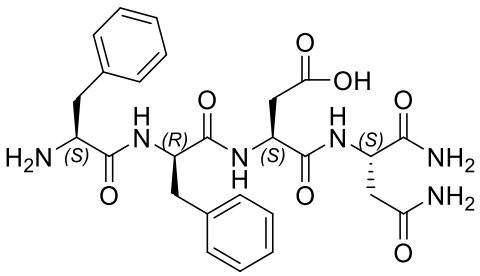

47

Yield: 43%, 8.0 mg

^{1}H NMR (700 MHz, DMSO-d_6, 303 K) δ = 8.73 (d, *J* = 6.4 Hz, 1H) 8.59 (s (br), 1H), 8.12 (d, *J* = 8.2 Hz, 1H), 7.35 (s, 1H), 7.27–7.12 (m, 9H), 7.09–7.02 (m, 3H), 6.86 (s,

1H), 4.42 (td, *J* = 6.2 Hz, 7.9 Hz, 2H), 4.34 (dd, *J* = 6.6 Hz, 13.7 Hz, 1H), 3.63 (dd, *J* = 6.0 Hz, 7.5 Hz, 1H), 3.00 (dd, *J* = 4.4 Hz, 14.1 Hz, 1H), 2.82 (d, *J* = 13.8 Hz, 1H), 2.81 (dd, *J* = 4.4 Hz, 13.7 Hz, 1H), 2.55 (dd, *J* = 8.0 Hz, 13.7 Hz, 1H), 2.56–2.47 (m, 1H, overlayed by solvent signal), 2.37 (dd, *J* = 7.9 Hz, 15.5 Hz, 1H) ppm.

^{13}C NMR (175 MHz, DMSO-d_6, 303 K) δ = 173.0, 172.6, 172.3, 171.9, 171.5, 170.5, 137.6, 137.2, 129.2, 129.0, 128.1, 128.1, 126.3, 126.3, 54.9, 54.6, 50.5, 49.7, 39.8 (overlayed by solvent signal), 37.6, 37.2, 36.5 ppm.

HRMS (ESI-qTOF, positive ion mode): *m/z* calcd. for $C_{26}H_{32}N_6O_7$: 540.2332 [M]; calcd. for $[M+H]^+$: 541.2405, found: 541.2404; calcd. for $[M+Na]^+$: 563.2225, found: 563.2219.

D-Phe-L-Phe-L-Asp-L-Asn-NH_2 (**48**)

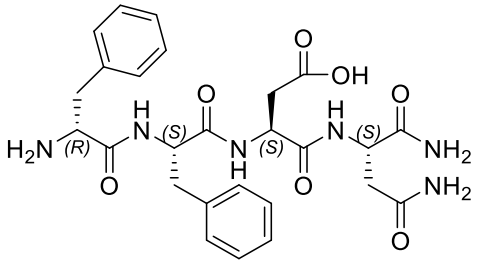

48

Yield: 42%, 7.8 mg

^{1}H NMR (700 MHz, DMSO-d_6, 303 K) δ = 8.62 (s (br), 1H), 8.51 (d, *J* = 7.1 Hz, 1H), 8.03 (d, *J* = 8.1 Hz, 1H), 7.35 (s, 1H), 7.27–7.14 (m, 10H), 7.06 (s, 1H), 7.03 (s, 1H), 7.02 (d, *J* = 6.9 Hz, 1H), 6.85 (s, 1H), 4.56–4.49 (m, 1H), 4.44 (td, *J* = 5.6 Hz, 7.5 Hz, 1H), 4.40 (dd, *J* = 6.6 Hz, 13.1 Hz, 1H), 3.61 (dd, *J* = 5.3 Hz, 8.0 Hz, 1H), 3.05 (dd, *J* = 4.3 Hz, 14.0 Hz, 1H), 2.77 (dd, *J* = 5.3 Hz, 13.8 Hz, 1H), 2.74 (dd, *J* = 10.0 Hz, 14.1 Hz, 1H), 2.61 (dd, *J* = 5.9 Hz, 15.9 Hz, 1H), 2.55–2.45 (m, 4H, overlayed by solvent signal) ppm.

^{13}C NMR (175 MHz, DMSO-d_6, 303 K) δ = 172.9, 172.5, 172.1, 172.0, 171.2, 170.3, 137.7, 137.1, 129.2, 129.2, 128.1, 128.0, 126.3, 126.2, 54.8, 53.8, 50.5, 49.7, 39.2 (overlayed by solvent signal), 37.2, 37.0, 36.6 ppm.

HRMS (ESI-qTOF, positive ion mode): *m/z* calcd. for $C_{26}H_{32}N_6O_7$: 540.2332 [M]; calcd. for $[M+H]^+$: 541.2405, found: 541.2399; calcd. for $[M+Na]^+$: 563.2225, found: 563.2212.

D-Phe-D-Phe-L-Asp-L-Asn-NH_2 (**49**)

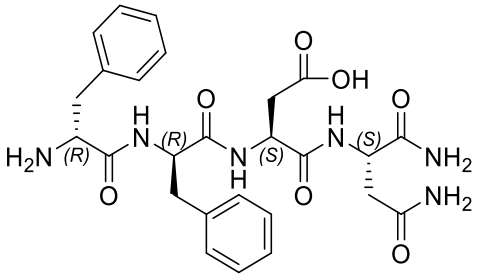

49

Yield: 29%, 5.4 mg

^{1}H NMR (700 MHz, DMSO-d_6, 303 K) δ = 8.61 (d, *J* = 7.4 Hz, 1H), 8.28 (s (br), 1H), 8.08 (d, *J* = 8.1 Hz, 1H), 7.32 (s, 1H), 7.29–7.12 (m, 10H), 7.08 (s, 2H), 6.83 (s, 1H), 4.55–4.48 (m, 1H), 4.48–4.40 (m, 2H), 3.43 (dd, *J* = 4.5 Hz, 8.8 Hz, 1H), 3.00 (dd, *J* = 5.0 Hz, 13.8 Hz, 1H), 2.88 (dd, *J* = 4.3 Hz, 13.8 Hz, 1H), 2.85 (dd, *J* = 8.4 Hz, 13.6 Hz, 1H), 2.61 (dd, *J* = 5.8 Hz, 16.4 Hz, 1H), 2.57–2.45 (m, 3H, overlayed by solvent signal), 2.42 (dd, *J* = 7.4 Hz, 16.3 Hz, 1H) ppm.

^{13}C NMR (175 MHz, DMSO-d_6, 303 K) δ = 173.8, 173.0, 172.2, 171.7, 171.1, 170.4, 138.3, 137.4, 129.3, 129.3, 128.1, 128.0, 126.2, 126.2, 55.8, 53.7, 50.1, 49.9, 40.0, 37.4, 36.7, 36.7 ppm.

HRMS (ESI-qTOF, positive ion mode): *m/z* calcd. for $C_{26}H_{32}N_6O_7$: 540.2332 [M]; calcd. for $[M+H]^+$: 541.2405, found: 541.2408; calcd. for $[M+Na]^+$: 563.2225, found: 563.2227.

L-Phe-D-Phe-D-Asp-L-Asn-NH_2 (**50**)

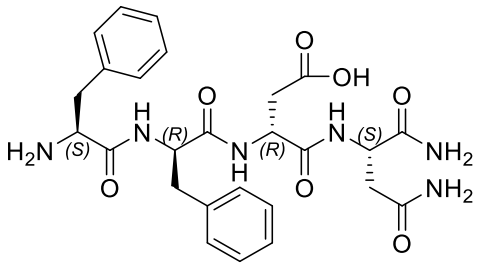

50

Yield: 52%, 9.7 mg

^{1}H NMR (700 MHz, DMSO-d_6, 303 K) δ = 8.71 (s (br), 1H), 8.60 (d, *J* = 7.1 Hz, 1H), 8.02 (d, *J* = 8.1 Hz, 1H), 7.31 (s, 1H), 7.28–7.14 (m, 9H), 7.09 (s, 1H), 7.02 (s, 1H), 7.01 (d, *J* = 7.8 Hz, 1H), 6.86 (s, 1H), 4.57–4.49 (m, 1H), 4.44 (td, *J* = 6.4 Hz, 8.1 Hz, 1H), 4.40–4.34 (m, 1H), 3.70–3.58 (m, 1H), 3.08 (dd, *J* = 3.7 Hz, 13.9 Hz, 1H), 2.82–2.72 (m, 2H), 2.58–2.46 (m, 5H, overlayed by solvent signal) ppm.

^{13}C NMR (175 MHz, DMSO-d_6, 303 K) δ = 173.0, 172.7, 172.2, 171.9, 171.3, 170.5, 137.7, 137.0, 129.2, 129.2, 128.1, 128.1, 126.4, 126.3, 54.8, 54.1, 50.4, 49.8, 39.0 (overlayed by solvent signal), 37.3, 37.0, 36.6 ppm.

HRMS (ESI-qTOF, positive ion mode): *m/z* calcd. for $C_{26}H_{32}N_6O_7$: 540.2332 [M]; calcd. for $[M+H]^+$: 541.2405, found: 541.2398; calcd. for $[M+Na]^+$: 563.2225, found: 563.2212.

D-Phe-L-Phe-D-Asp-L-Asn-NH_2 (**51**)

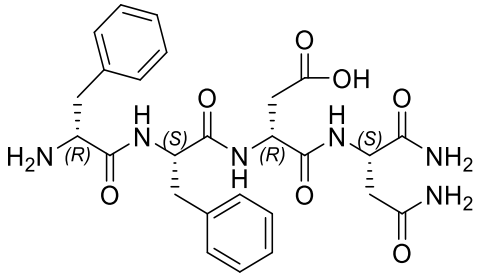

51

Yield: 82%, 15.3 mg

^{1}H NMR (700 MHz, DMSO-d_6, 303 K) δ = 8.53 (d, *J* = 7.1 Hz, 1H), 8.23 (s (br), 1H), 8.07 (d, *J* = 8.1 Hz, 1H), 7.32 (s, 1H), 7.29–7.12 (m, 11H), 7.09 (s, 1H), 7.05 (s, 1H),

6.85 (s, 1H), 4.55–4.48 (m, 1H), 4.48–4.39 (m, 2H), 3.44 (m, 1H, overlayed by water signal), 3.06 (dd, *J* = 4.3 Hz, 13.9 Hz, 1H), 2.88–2.78 (m, 2H), 2.67 (dd, *J* = 5.8 Hz, 16.3 Hz, 1H), 2.53–2.45 (m, 4H, overlayed by solvent signal) ppm.

^{13}C NMR (175 MHz, DMSO-d_6, 303 K) δ = 172.8, 172.1, 171.8, 171.2, 170.1, 137.6, 129.3, 129.3, 128.2, 128.0, 126.2, 126.2, 55.5, 53.4, 50.1, 49.7, 39.8 (overlayed by solvent signal), 37.4, 36.5, 35.1 ppm.

HRMS (ESI-qTOF, positive ion mode): *m/z* calcd. for $C_{26}H_{32}N_6O_7$: 540.2332 [M]; calcd. for $[M+H]^+$: 541.2405, found: 541.2393; calcd. for $[M+Na]^+$: 563.2225, found: 563.2201.

6.5.2.2. Cyclic fibupeptides **109**–**113** and **118**–**125**

General procedure for cyclic fibupeptides **110**–**113** and **118**–**125**:[40, 46, 148]

Solid-phase peptide synthesis: For the synthesis of linear peptides a preloaded Fmoc-D-Trp(Boc) (for **110**–**113** and **118**), Fmoc-D-Val (for **115** and **125**) or Fmoc-D-Leu (for **119**–**122** and **124**) TentaGel S AC resin (loading: 0.23 mmol·g^{-1}, 150 mg, 34.5 µmol, Rapp Polymere Tübingen) was used and swollen for 20 min in DMF (2 mL). Stepwise SPPS was performed in a 5 mL polypropylene syringe equipped with a 25 µm polyethylene frit purchased from Multisyntech GmbH (Witten, Germany) applying Fmoc strategy.

Fmoc removal: The Fmoc protecting group was removed by treating the resin with the following washing solutions: DBU (2%) and morpholine (10%) in DMF (2 mL) (1 × 12 min), DBU (2%) and morpholine (10%) in DMF (2 mL) (1 × 3 min), DMF (2 mL, 1 × 5 min), DCM (2 mL, 1 × 5 min) and DMF (2 mL, 1 × 5 min). The resin was then ready for the next coupling reaction.

Coupling reaction: Coupling reactions were performed in DMF (2 mL) using 6 eq of the corresponding Fmoc-protected amino acids (Fmoc-L-Val-OH, Fmoc-D-Leu-OH, Fmoc-L-Trp(Boc)-OH, Fmoc-D-Val-OH, Fmoc-L-Thz(L-Val)-OH, Fmoc-D-Orn(Cbz)-OH, Fmoc-D-Orn(Dde)-OH, Fmoc-L-Orn(Dde)-OH, Boc-L-Orn(Cbz)-OH, Fmoc-D-Cys(Acm)-OH, Fmoc-L-Phe(4-NH-Alloc)-OH) 6 eq of HATU, 6 eq of HOBt and 8 eq of NMM. Coupling reactions were run for 45 min each while shaking at room temperature (Thermomixer 5437, Eppendorf). The reaction mixture was drained, and the resin was

washed with the following washing solutions: DMF (2 mL, 1 × 5 min), DCM (2 mL, 1 × 5 min) and DMF (2 mL, 1 × 5 min). The resin was subjected to Fmoc removal.

On resin N-methylation: a.) Introduction of 2-nitrobenzenesulfonyl activating group (oNBS). The resin bound peptide with a free amine was washed with DCM (2 mL, 3 × 5 min) and treated with a mixture of oNBSCl (4 eq) and 2,4,6-trimethylpyridine (5 eq) in DCM (2 mL) for 1.5 h while shaking at room temperature. The reaction mixture was drained, and the resin was washed with the following washing solutions: DCM (2mL, 3 × 5 min) and DMF (2 mL, 3 × 5 min). *b.) N-methylation:* Selective *N*-methylation was achieved treating the *N*-oNBS protected on resin bound peptide with a mixture of dimethyl sulfate (3 eq) and mTBD (3 eq) in DMF (2 mL) for 30 min while shaking at room temperature. The reaction mixture was drained, and the resin was washed with DMF (2 mL, 3 × 5 min). *c.) oNBS removal:* Removal of oNBS moiety was achieved by treating the resin with a mixture of DBU (5 equiv.) and 2-mercaptoethanol (10 equiv.) in DMF (2 mL) for 30 min while shaking at room temperature. The reaction mixture was drained, and the resin was washed with DMF (2 mL, 3 × 5 min). The resin was then ready for the next coupling reaction, which was performed two times (1 × 3 h, 1 × overnight) for more efficient coupling.

Resin cleavage of linear peptide: Once the desired peptide was generated, the final Fmoc protecting group was removed following Fmoc removal procedure with the following additional washings: DMF (2 mL, 3 × 5 min), DCM (2 mL, 3 × 5 min), toluene (2 mL, 3 × 5 min), isopropyl alcohol (2 mL, 3 × 5 min), and diethyl ether (2 mL, 3 × 5 min). The resin was dried in vacuo for 2 h and cleaved from the linear peptide using a mixture of TFA, TIPS and H_2O (95/5/5, v/v/v, 2 mL, 3 × 1 h). The filtrate was concentrated in vacuo and the resulting residue was dissolved in a mixture of *tert*-butyl alcohol and water (1/1, v/v), frozen and lyophilized.

Macrolactamization: The linear fibupeptides were applied to macrolactamization under high dilution conditions (2 mM) in DMF using HATU (4 eq), HOAt (6 eq), DIPEA (8 eq) as coupling reagents for 24 h. The yellow solution was then diluted with 20 mL H_2O and extracted one time with a *n*-butanol/$CHCl_3$ (1/5, v/v) solution and two times with $CHCl_3$. The joint organic phases were washed three times with an aqueous 10% $KHSO_4$ solution, three times with a saturated aqueous $NaHCO_3$ solution, a saturated

aqueous NaCl solution, and an aqueous 15% acetonitrile solution. The solvent was removed under vacuo and the residue was taken up in a mixture of *tert*-butyl alcohol and water (1/1, v/v), frozen and lyophilized.to obtain the product as a white voluminous powder, which was then applied to HPLC (column: Kromasil C18, 100A, 250×8 mm, 5 µm, A: H_2O with 0.1% formic acid, B: acetonitrile with 0.1% formic acid, gradient 10% B to 100% B within 30 min) to get pure cyclic fibupeptides (yield: 32% to 98%).

Procedure for the synthesis of **115***:*
The peptide aldehyde was prepared by manual SPPS using a commercially available preloaded H-Val-H NovaSyn® TG resin (loading: 0.21 mmol·g^{-1}, 50 mg, 10.5 µmol, Novabiochem, Switzerland). Peptide synthesis was performed following Fmoc strategy using 4 eq of protected amino acids (Fmoc-D-Trp(Boc)-OH; Fmoc-L-Val-OH, Fmoc-D-Leu-OH, Fmoc-L-Trp(Boc)-OH, Fmoc-D-Val-OH, Fmoc-L-Me-Cys(Trt)-OH), 4 eq of HATU, 4 eq of HOBt and 8 eq of NMM in acetonitrile (1 mL). Due to low solubility in acetonitrile Fmoc-Me-Cys(Trt)-OH was coupled in a mixture of DMF/acetonitrile (1 mL, 1/1, v/v). Coupling reactions were carried out in a polypropylene syringe (2 mL) equipped with a 25 µm polyethylene frit (Multisyntech GmbH; Witten, Germany) for 1 h at rt. The resin was washed with acetonitrile (5 × 1 mL) and subjected to Fmoc removal as described in the procedure for cyclic fibupeptides, then washed with acetonitrile (5 × 1 mL) and the resin was ready for the next coupling reaction. The steps were repeated until the desired amino acid sequence was fully assembled on the resin and the resin was washed with the following solutions: DMF (3 × 1 mL), acetonitrile (3 × 1 mL), isopropyl alcohol (3 × 1 mL) and diethyl ether (3 × 1 mL). The resin was dried in vacuo for 2 h and trifluoroacetic acid (1 mL, 20 min) was used for global deprotection of protected sidechain residues. Then the resin was washed with DCM (5 × 1 mL) and cleaved using acetonitrile/H_2O/TFA (3 × 1 mL, 8/2/0.05, v/v/v, 30 min). The linear peptide aldehyde spontaneously cyclized after cleavage and the product was obtained as a colourless powder (6.0 mg, 6.8 µmol, 64%) after lyophilization.

Deprotection of Alloc: The Alloc protected 4-amino phenlyalanine residue of the cyclic fibupeptide **118** was deprotected by adding $Pd(PPh_3)_4$ (0.8 mg, 10 mol-%) and $PhSiH_3$ (7.7 mg, 71 µmol, 10 eq) to a solution of fibupeptide **118** (6.6 mg, 7.1 µmol, 1.0 eq) in THF (2 mL). The yellow mixture was stirred for 30 min at rt. The solvent was removed in vacuo and the yellow residue was dissolved in a mixture of *tert*-butyl alcohol and

water (1/1, v/v), frozen and lyophilized. The crude voluminous red brownish powder was then taken up in methanol (1 mL), centrifuged and applied to HPLC (column: Kromasil C18, 100A, 250×8 mm, 5 µm, A: H_2O with 0.1% formic acid, B: acetonitrile with 0.1% formic acid, gradient 10% B to 100% B within 30 min) to get pure fibupeptide **126** as a white powder (0.5 mg, 0.6 µmol, 9%).

Deprotection of Cbz: The Cbz protected ornithine residues of the cyclic fibupeptides were deprotected using a solution of thioanisole (50 eq per Cbz protecting group) and TFA (250 µL per Cbz protecting group). The mixture was stirred overnight at rt. The solvent was removed under reduced pressure and the resulting residue was dissolved in a mixture of *tert*-butyl alcohol and water (1/1, v/v), frozen and lyophilized. (yields: 20% to 95%)

Deprotection of Dde: The Dde protected ornithine residues of the cyclic fibupeptides were deprotected using a solution of 2% $N_2H_4 \cdot H_2O$ in THF. The mixture was stirred overnight at rt. The solvent was removed under reduced pressure and the resulting residue was dissolved in a mixture of *tert*-butyl alcohol and water (1/1, v/v), frozen and lyophilized.

Here experimental data for each cyclic fibupeptide is given. NMR data is given as a List of ^{1}H and ^{13}C NMR signals. Since all fibupeptides show more than one set of NMR signals, the proton integrals may deviate from the actual proton number. This is a typical phenomenon of lugdunin-like compounds. For lugdunin (**6**) full assignment of NMR signals is given in its original publication.[32]

3-Methyl-6-Trp-lugdunin (**109**)

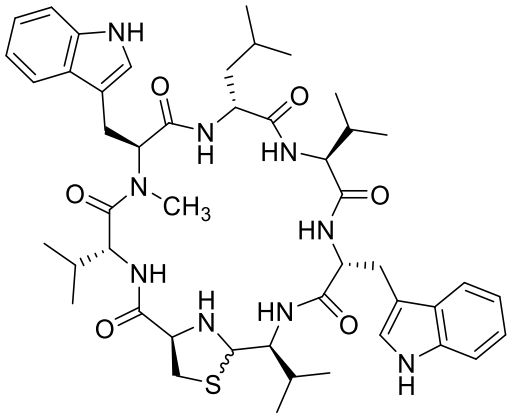

109

Yield: 86%, 26.2 mg

^{1}H NMR (700 MHz, DMSO-d_6, 303 K) δ = 10.84 (d, *J* = 2.4 Hz, 1H), 10.73 (dd, *J* = 8.1, 2.4 Hz, 1H), 7.90 (dd, *J* = 14.7, 8.5 Hz, 1H), 7.78–7.65 (m, 3H), 7.51 (dd, *J* = 22.1, 7.9 Hz, 1H), 7.31 (d, *J* = 8.2 Hz, 1H), 7.26 (d, *J* = 8.1 Hz, 1H), 7.21–7.13 (m, 1H), 7.13–7.09 (m, 1H), 7.08–6.88 (m, 6H), 5.10 (dh, *J* = 15.3, 7.6 Hz, 1H), 4.98 (ddd, *J* = 19.5, 9.2, 6.7 Hz, 1H), 4.89 (td, *J* = 9.0, 5.7 Hz, 1H), 4.77–4.63 (m, 2H), 4.30 (dd, *J* = 9.5, 8.0 Hz, 1H), 4.20 (dd, *J* = 9.3, 6.6 Hz, 1H), 3.98 (dtd, *J* = 16.8, 7.4, 3.6 Hz, 2H), 3.75–3.68 (m, 1H), 3.51 (s, 1H), 3.09–3.01 (m, 3H), 2.95–2.84 (m, 6H), 2.77–2.66 (m, 1H), 2.64–2.56 (m, 2H), 2.05–1.95 (m, 2H), 1.90 (dtt, *J* = 9.8, 6.9, 2.8 Hz, 2H), 1.77–1.63 (m, 3H), 1.35 (s, 4H), 1.31–1.19 (m, 14H), 0.92–0.49 (m, 29H), 0.42 (d, *J* = 6.8 Hz, 3H) ppm.

^{13}C NMR (175 MHz, DMSO-d_6, 303 K) δ = 172.44, 171.52, 170.62, 170.03, 169.90, 169.84, 139.04, 136.11, 136.05, 136.02, 129.60, 127.25, 126.88, 124.17, 124.06, 123.79, 123.66, 120.82, 120.64, 118.71, 118.36, 118.30, 117.87, 117.80, 111.31, 111.25, 110.94, 109.91, 108.88, 72.09, 69.75, 63.73, 63.54, 57.18, 56.74, 56.38, 52.81, 52.45, 49.17, 40.02, 39.88, 39.76, 39.64, 39.52, 39.40, 39.28, 39.16, 38.03, 37.94, 35.54, 35.08, 34.39, 31.49, 31.23, 31.10, 30.51, 30.45, 30.36, 30.09, 29.53, 29.49, 29.08, 29.05, 29.00, 28.96, 28.93, 28.88, 28.83, 28.77, 28.68, 28.64, 28.62, 28.52, 28.06, 27.88, 26.56, 26.53, 25.26, 25.06, 24.05, 22.88, 22.49, 22.04, 21.79, 21.38, 20.46, 19.61, 19.41, 19.27, 19.06, 18.95, 18.84, 18.38, 18.20, 17.63, 17.49, 15.05, 13.90 ppm.

HRMS (ESI-qTOF, positive ion mode): *m/z* calcd. for $C_{47}H_{65}N_9O_6S$: 883.4779 [M]; calcd. for $[M+H]^+$: 884.4851, found: 884.4852; calcd. for $[M+Na]^+$: 906.4671, found: 906.4672.

4-Methyl-6-Trp-lugdunin (**110**)

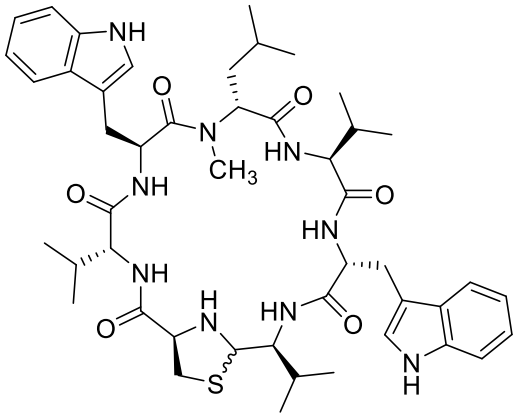

110

Yield: 88%, 26.8 mg

^{1}H NMR (700 MHz, DMSO-d_6, 303 K) δ = 10.76 (ddd, *J* = 21.8, 8.2, 2.5 Hz, 2H), 8.70 (d, *J* = 4.3 Hz, 1H), 8.40 (dd, *J* = 16.4, 8.0 Hz, 1H), 7.74–7.64 (m, 1H), 7.60 (d, *J* = 7.9 Hz, 1H), 7.51 (d, *J* = 7.9 Hz, 1H), 7.34–7.25 (m, 3H), 7.19 (t, *J* = 11.0 Hz, 1H), 7.15–7.09 (m, 2H), 7.08–6.99 (m, 2H), 6.99–6.88 (m, 3H), 5.58 (dd, *J* = 11.8, 4.7 Hz, 1H), 4.73–4.65 (m, 1H), 4.51–4.28 (m, 3H), 4.15 (t, *J* = 9.5 Hz, 1H), 4.00–3.88 (m, 2H), 3.66 (dtd, *J* = 13.3, 10.6, 10.0, 6.3 Hz, 1H), 3.51 (s, 2H), 3.38 (d, *J* = 4.9 Hz, 2H), 3.18–3.01 (m, 5H), 2.99 (s, 2H), 2.92 (ddd, *J* = 14.2, 11.7, 7.8 Hz, 1H), 2.58–2.52 (m, 2H), 2.04–1.95 (m, 1H), 1.80–1.67 (m, 1H), 1.53 (dtd, *J* = 17.4, 7.9, 7.0, 4.8 Hz, 2H), 1.48–1.32 (m, 8H), 1.32–1.21 (m, 10H), 0.94–0.60 (m, 20H), 0.57 (d, *J* = 6.6 Hz, 1H), 0.52 (dd, *J* = 15.3, 6.7 Hz, 3H), 0.14 (d, *J* = 6.7 Hz, 1H), 0.09 (d, *J* = 6.8 Hz, 2H) ppm.

^{13}C NMR (175 MHz, DMSO-d_6, 303 K) δ = 173.03, 171.65, 171.36, 171.24, 170.83, 168.61, 139.05, 136.18, 136.16, 135.98, 129.60, 127.15, 127.04, 124.06, 123.95, 123.36, 120.73, 120.70, 120.65, 118.46, 118.17, 118.08, 118.03, 117.97, 111.09, 111.03, 109.81, 109.56, 109.53, 71.76, 69.75, 65.37, 63.73, 57.61, 56.46, 55.77, 54.70, 54.25, 52.93, 41.07, 40.02, 39.88, 39.76, 39.64, 39.52, 39.40, 39.28, 39.16, 37.65, 35.54, 34.39, 32.40, 31.24, 31.15, 30.98, 30.96, 30.49, 30.36, 29.81, 29.78, 29.71, 29.05, 28.97, 28.94, 28.89, 28.83, 28.77, 28.69, 28.64, 28.52, 28.06, 25.98,

25.27, 24.19, 24.16, 22.94, 22.71, 22.12, 22.08, 22.04, 21.76, 20.34, 19.56, 19.16, 19.05, 19.00, 18.88, 18.52, 17.99, 17.78, 17.60, 16.92, 15.07, 13.90 ppm.

HRMS (ESI-qTOF, positive ion mode): *m/z* calcd. for $C_{47}H_{65}N_9O_6S$: 883.4779 [M]; calcd. for $[M+H]^+$: 884.4851, found: 884.4841; calcd. for $[M+Na]^+$: 906.4671, found: 906.4658.

5-Methyl-6-Trp-lugdunin (**111**)

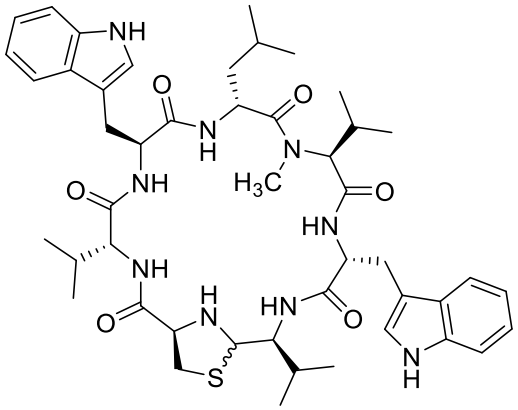

111

Yield: 70%, 21.4 mg

^{1}H NMR (700 MHz, DMSO-d_6, 303 K) δ = 10.83–10.78 (m, 4H), 7.68–7.59 (m, 1H), 7.61 (s, 2H), 7.57–7.45 (m, 2H), 7.36–7.25 (m, 3H), 7.16–7.10 (m, 1H), 7.08–7.01 (m, 3H), 7.03–6.96 (m, 1H), 6.98–6.90 (m, 3H), 6.91 (s, 1H), 4.86 (s, 2H), 4.82–4.67 (m, 2H), 4.50–4.41 (m, 1H), 3.65–3.58 (m, 1H), 3.51 (s, 26H), 3.51–3.46 (m, 7H), 3.48–3.38 (m, 1H), 3.09 (s, 1H), 3.03 (ddd, *J* = 14.2, 11.7, 5.8 Hz, 1H), 2.99–2.86 (m, 2H), 2.77–2.67 (m, 1H), 2.69 (s, 2H), 2.67–2.60 (m, 1H), 2.09–1.95 (m, 2H), 1.80–1.72 (m, 1H), 1.53–1.41 (m, 1H), 1.35 (s, 1H), 1.31–1.17 (m, 8H), 1.11 (s, 1H), 1.06–0.97 (m, 2H), 0.96 (dd, *J* = 7.4, 2.3 Hz, 4H), 0.87–0.81 (m, 2H), 0.81–0.71 (m, 4H), 0.66 (d, *J* = 2.9 Hz, 2H), 0.66–0.60 (m, 2H), 0.62–0.55 (m, 2H), 0.51 (dd, *J* = 23.9, 6.8 Hz, 2H), 0.36 (t, *J* = 6.9 Hz, 3H) ppm.

^{13}C NMR (175 MHz, DMSO-d_6, 303 K) δ = 174.3, 172.9, 171.9, 171.0, 170.7, 170.5, 170.3, 170.1, 169.7, 169.3, 169.0, 168.6, 167.8, 166.8, 165.0, 164.0, 158.0, 157.1, 152.0, 147.2, 139.1, 136.2, 136.1, 136.0, 135.3, 134.9, 134.5, 133.7, 132.6, 132.0, 130.3, 129.9, 129.6, 129.5, 127.3, 127.2, 125.4, 125.2, 124.4, 124.2, 124.1, 123.8,

123.7, 123.6, 123.4, 121.0, 120.7, 120.6, 118.5, 118.4, 118.3, 118.2, 118.1, 118.0, 111.3, 111.1, 109.7, 109.5, 109.4, 109.2, 108.3, 107.6, 105.1, 98.9, 72.3, 72.1, 71.6, 69.8, 69.5, 68.8, 67.2, 66.9, 65.2, 64.8, 63.8, 61.8, 60.3, 60.2, 60.1, 57.4, 57.0, 55.2, 54.9, 54.6, 53.5, 52.9, 52.4, 48.8, 47.4, 42.7, 41.2, 40.0, 39.9, 39.8, 39.6, 39.5, 39.4, 39.3, 39.2, 38.2, 37.6, 36.3, 35.5, 35.1, 34.7, 34.4, 33.6, 32.9, 32.4, 31.3, 31.2, 30.9, 30.4, 30.2, 30.1, 29.8, 29.5, 29.4, 29.1, 29.0, 28.9, 28.8, 28.7, 28.6, 28.5, 28.3, 28.1, 28.0, 27.1, 26.7, 26.6, 26.5, 25.8, 25.3, 25.1, 24.1, 23.5, 23.3, 23.0, 22.6, 22.3, 22.0, 21.8, 21.1, 20.8, 20.0, 19.7, 19.6, 19.5, 19.4, 19.0, 18.9, 18.8, 18.7, 18.6, 18.5, 18.2, 18.1, 17.8, 17.7, 17.5, 17.4, 17.3, 17.2, 17.0, 15.2, 14.7, 13.9, 13.8, 13.1, 12.9, 12.5, 12.1 ppm.

HRMS (ESI-qTOF, positive ion mode): *m/z* calcd. for $C_{47}H_{65}N_9O_6S$: 883.4779 [M]; calcd. for $[M+H]^+$: 884.4851, found: 884.4847; calcd. for $[M+Na]^+$: 906.4671, found: 906.4666.

6-Methyl-6-Trp-lugdunin (**112**)

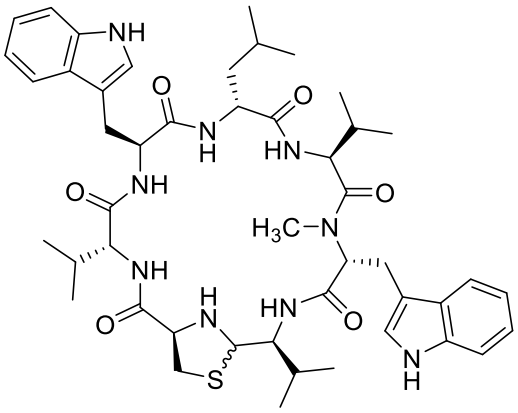

112

Yield: 41%, 12.5 mg

^{1}H NMR (700 MHz, DMSO-d_6, 303 K) δ = 10.85–10.72 (m, 2H), 8.22 (dd, *J* = 26.5, 9.0 Hz, 1H), 7.79–7.70 (m, 1H), 7.68–7.56 (m, 1H), 7.56–7.45 (m, 1H), 7.33–7.25 (m, 2H), 7.16–7.08 (m, 2H), 7.07–6.88 (m, 5H), 4.77–4.69 (m, 1H), 4.54–4.39 (m, 2H), 4.07–3.93 (m, 1H), 3.75–3.66 (m, 1H), 3.51 (s, 4H), 3.36–3.24 (m, 16H), 3.23–3.02 (m, 7H), 2.97 (ddd, *J* = 13.7, 8.9, 6.1 Hz, 2H), 2.90–2.82 (m, 1H), 2.81–2.70 (m, 1H), 2.59–2.51 (m, 1H), 2.48 (s, 1H), 1.73 (dp, *J* = 8.8, 6.6 Hz, 1H), 1.55–1.48 (m, 1H), 1.38–1.17

(m, 12H), 1.17–1.09 (m, 1H), 0.98–0.41 (m, 26H), 0.35 (d, *J* = 6.8 Hz, 2H), 0.30 (d, *J* = 6.7 Hz, 1H) ppm.

^{13}C NMR (175 MHz, DMSO-d_6, 303 K) δ = 171.98, 171.48, 171.45, 171.40, 171.11, 171.06, 170.81, 170.72, 170.57, 170.15, 169.99, 169.70, 139.06, 136.19, 136.09, 136.00, 127.18, 127.00, 126.94, 124.13, 124.07, 123.53, 123.43, 123.09, 120.87, 120.75, 120.72, 120.58, 118.85, 118.62, 118.55, 118.12, 118.08, 118.05, 117.91, 111.18, 111.01, 110.97, 110.19, 109.80, 109.73, 109.55, 72.33, 71.91, 69.76, 65.08, 63.80, 63.74, 60.20, 57.16, 56.80, 56.48, 55.60, 54.31, 53.69, 53.15, 52.74, 52.55, 52.20, 50.46, 41.60, 41.30, 40.02, 39.88, 39.76, 39.64, 39.52, 39.40, 39.28, 39.16, 37.97, 37.59, 35.55, 34.40, 32.59, 31.25, 31.21, 30.65, 30.37, 30.07, 29.72, 28.97, 28.94, 28.89, 28.83, 28.77, 28.69, 28.65, 28.52, 28.06, 27.97, 26.82, 26.70, 25.27, 24.94, 24.08, 24.04, 22.79, 22.38, 22.05, 21.98, 21.83, 20.76, 19.60, 19.57, 19.28, 18.88, 18.79, 18.73, 18.57, 18.05, 16.70, 15.27, 13.91 ppm.

HRMS (ESI-qTOF, positive ion mode): *m/z* calcd. for $C_{47}H_{65}N_9O_6S$: 883.4779 [M]; calcd. for $[M+H]^+$: 884.4851, found: 884.4849; calcd. for $[M+Na]^+$: 906.4671, found: 906.4665.

1-Methyl-6-Trp-lugdunin (**115**)

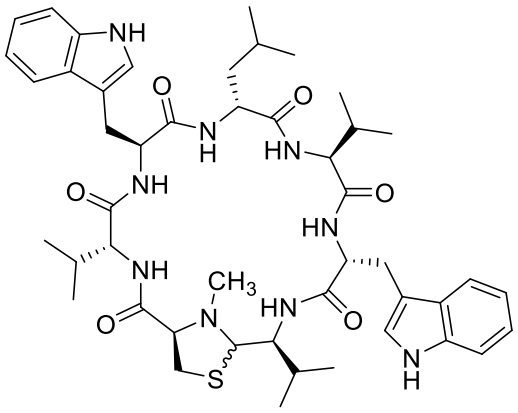

115

Yield: 64%, 6.0 mg

^{1}H NMR (700 MHz, DMSO-d_6, 303 K) δ = 10.87 (d, *J* = 2.4 Hz, 1H), 10.80 (d, *J* = 2.4 Hz, 1H), 10.76 (s, 1H), 10.71 (dd, *J* = 7.4, 2.4 Hz, 2H), 8.37 (d, *J* = 8.0 Hz, 1H), 8.31–8.19 (m, 3H), 8.10 (d, *J* = 8.3 Hz, 1H), 7.95 (d, *J* = 9.6 Hz, 1H), 7.90 (dd, *J* = 9.3,

6.2 Hz, 2H), 7.79 (d, *J* = 8.6 Hz, 1H), 7.74 (d, *J* = 9.6 Hz, 1H), 7.63–7.53 (m, 3H), 7.46 (dd, *J* = 20.9, 8.7 Hz, 2H), 7.35–7.25 (m, 5H), 7.14 (t, *J* = 2.7 Hz, 1H), 7.12–6.88 (m, 14H), 4.92 (td, *J* = 8.7, 5.6 Hz, 1H), 4.67 (td, *J* = 8.4, 5.8 Hz, 1H), 4.60 (q, *J* = 7.2 Hz, 1H), 4.53 (dd, *J* = 9.7, 4.9 Hz, 1H), 4.49 (d, *J* = 10.9 Hz, 1H), 4.42 (q, *J* = 6.5 Hz, 1H), 4.37 (dd, *J* = 9.6, 5.5 Hz, 1H), 4.31–4.21 (m, 2H), 4.17 (d, *J* = 2.2 Hz, 1H), 4.12 (t, *J* = 6.7 Hz, 1H), 4.03 (dt, *J* = 8.7, 6.3 Hz, 1H), 4.00–3.95 (m, 2H), 3.91–3.82 (m, 1H), 3.79 (td, *J* = 10.4, 2.8 Hz, 1H), 3.51 (s, 14H), 3.49 (s, 1H), 3.40 (td, *J* = 9.5, 5.8 Hz, 2H), 3.30–3.26 (m, 1H), 3.15–3.08 (m, 3H), 3.07–2.89 (m, 3H), 2.87–2.71 (m, 3H), 2.68 (dd, *J* = 14.6, 8.3 Hz, 1H), 2.56–2.51 (m, 1H), 2.41 (s, 3H), 2.13–2.06 (m, 4H), 1.99 (dt, *J* = 22.4, 7.0 Hz, 1H), 1.86–1.77 (m, 2H), 1.76 (dt, *J* = 13.6, 6.8 Hz, 1H), 1.66 (s, 1H), 1.51 (ddd, *J* = 13.9, 8.6, 5.8 Hz, 2H), 1.41 (dt, *J* = 13.1, 5.4 Hz, 2H), 1.35 (s, 5H), 1.33 (d, *J* = 14.7 Hz, 0H), 1.32–1.27 (m, 1H), 1.29–1.22 (m, 14H), 1.21–1.12 (m, 2H), 0.97 (dd, *J* = 7.4, 2.4 Hz, 1H), 0.93 (dd, *J* = 6.6, 3.9 Hz, 1H), 0.90–0.85 (m, 4H), 0.87–0.81 (m, 6H), 0.83–0.76 (m, 14H), 0.78–0.71 (m, 6H), 0.72 (d, *J* = 5.0 Hz, 3H), 0.70–0.53 (m, 14H), 0.52–0.42 (m, 1H), 0.30 (d, *J* = 6.8 Hz, 2H) ppm.

^{13}C NMR (175 MHz, DMSO-d_6, 303 K) δ = 172.4, 171.9, 171.8, 171.6, 171.5, 171.2, 171.1, 170.5, 170.4, 169.5, 152.0, 139.0, 136.1, 136.0, 131.3, 129.6, 127.3, 127.2, 127.1, 124.1, 124.0, 123.4, 123.3, 120.8, 120.7, 118.5, 118.3, 118.2, 118.0, 111.2, 111.1, 111.0, 110.3, 109.8, 109.1, 108.5, 78.8, 73.7, 73.3, 72.3, 70.3, 69.7, 63.7, 60.2, 59.5, 57.8, 56.3, 55.6, 54.4, 54.0, 53.8, 53.6, 53.5, 51.3, 51.0, 43.7, 40.0, 39.9, 39.8, 39.6, 39.5, 39.4, 39.3, 39.2, 37.3, 35.5, 35.1, 34.4, 33.4, 32.2, 31.3, 31.2, 30.8, 30.4, 30.3, 30.1, 30.0, 29.8, 29.0, 28.9, 28.8, 28.7, 28.6, 28.5, 28.2, 28.1, 27.8, 27.6, 27.0, 26.9, 26.6, 25.3, 25.1, 24.3, 24.0, 23.9, 23.0, 22.7, 22.3, 22.2, 22.0, 21.5, 21.2, 20.2, 19.8, 19.7, 19.6, 19.5, 19.3, 19.0, 18.2, 18.0, 17.9, 17.2, 17.1, 14.9, 13.9 ppm.

HRMS (ESI-qTOF, positive ion mode): *m/z* calcd. for $C_{47}H_{65}N_9O_6S$: 883.4779 [M]; calcd. for $[M+H]^+$: 884.4851, found: 884.4857; calcd. for $[M+Na]^+$: 906.4671, found: 906.4674.

3-(4-NH(Alloc)-Phe)-6-Trp-lugdunin (**118**)

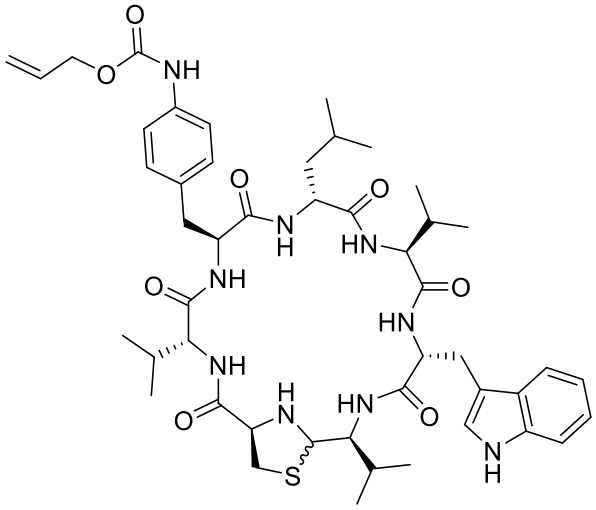

118

Yield: 80%, 25.7 mg

^{1}H NMR (700 MHz, DMSO-d_6, 303 K) δ = 10.76 (dd, *J* = 16.7, 2.4 Hz, 2H), 9.60 (s, 2H), 8.45 (dd, *J* = 12.5, 7.2 Hz, 2H), 8.23 (d, *J* = 7.7 Hz, 1H), 8.17 (d, *J* = 8.7 Hz, 1H), 7.80 (d, *J* = 9.3 Hz, 1H), 7.70–7.64 (m, 3H), 7.33–7.25 (m, 9H), 7.19–7.12 (m, 3H), 7.13 (s, 1H), 7.11 (dd, *J* = 22.4, 8.6 Hz, 3H), 7.06–6.91 (m, 5H), 6.01–5.92 (m, 2H), 5.37–5.30 (m, 4H), 5.22 (dq, *J* = 10.5, 1.4 Hz, 3H), 4.74–4.67 (m, 1H), 4.65–4.50 (m, 9H), 4.28 (t, *J* = 8.1 Hz, 1H), 4.20–4.13 (m, 2H), 4.05 (td, *J* = 9.3, 2.4 Hz, 1H), 3.67 (tdd, *J* = 15.7, 6.7, 3.8 Hz, 3H), 3.51 (s, 29H), 3.31 (s, 2H), 3.14–2.96 (m, 4H), 2.95–2.82 (m, 3H), 2.80–2.70 (m, 2H), 2.70–2.64 (m, 1H), 2.64–2.51 (m, 2H), 2.10–1.98 (m, 2H), 2.00–1.95 (m, 1H), 1.76–1.65 (m, 2H), 1.49–1.41 (m, 2H), 1.34 (d, *J* = 10.4 Hz, 3H), 1.28–1.21 (m, 3H), 1.23 (s, 17H), 1.20–1.13 (m, 1H), 1.11 (s, 1H), 1.09–0.99 (m, 2H), 0.96 (dd, *J* = 7.4, 2.4 Hz, 1H), 0.92–0.70 (m, 22H), 0.70–0.44 (m, 26H) ppm.

^{13}C NMR (175 MHz, DMSO-d_6, 303 K) δ = 174.3, 172.1, 171.6, 171.5, 171.4, 171.2, 170.7, 170.5, 170.4, 170.1, 169.9, 169.8, 169.7, 153.1, 139.1, 137.3, 136.1, 136.0, 133.4, 131.9, 129.7, 129.5, 129.3, 127.3, 127.2, 124.2, 123.8, 120.7, 118.8, 118.1, 118.0, 117.7, 117.5, 117.4, 111.0, 109.8, 109.7, 101.6, 76.8, 75.8, 75.6, 72.4, 72.1, 69.8, 68.8, 65.2, 64.5, 63.8, 63.7, 60.3, 60.2, 57.4, 57.2, 57.1, 56.5, 54.5, 54.1, 53.7, 53.6, 52.7, 52.0, 50.5, 41.4, 41.1, 40.0, 39.9, 39.8, 39.6, 39.5, 39.4, 39.3, 39.2, 38.3, 37.5, 36.0, 35.1, 34.4, 32.6, 31.6, 31.3, 31.1, 30.8, 30.4, 29.9, 29.7, 29.4, 29.1, 29.0, 28.8, 28.7, 28.6, 27.2, 26.6, 26.6, 25.1, 24.0, 23.9, 23.5, 23.1, 23.0, 22.6, 22.4, 22.1,

22.0, 21.9, 21.7, 20.4, 20.1, 20.1, 19.6, 19.5, 19.3, 19.1, 19.0, 18.9, 18.8, 18.6, 18.3, 18.1, 17.9, 17.8, 17.6, 17.2, 17.2, 15.2, 15.0, 13.9, 12.9 ppm.

HRMS (ESI-qTOF, positive ion mode): *m/z* calcd. for $C_{48}H_{67}N_9O_8S$: 929.4833 [M]; calcd. for $[M+H]^+$: 930.4906, found: 930.4917; calcd. for $[M+Na]^+$: 952.4726, found: 952.4719.

2-Orn(Cbz)-6-Trp-Lug (**119**)

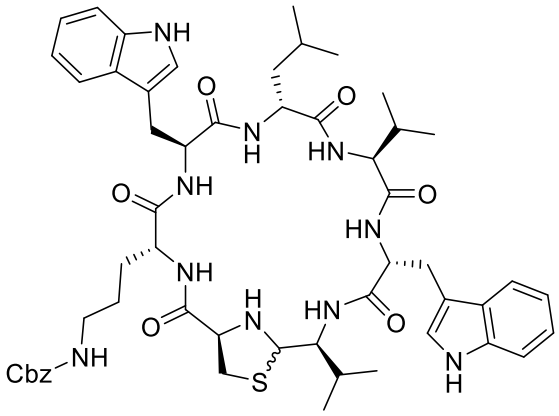

119

Yield: 98%, 34.4 mg

^{1}H NMR (700 MHz, DMSO-d_6, 303 K) δ = 10.77–10.71 (m, 2H), 8.48–8.45 (m, 1H), 8.19–8.13 (m, 1H), 7.86 (d, *J* = 9.2 Hz, 1H), 7.70–7.64 (m, 2H), 7.60 (dd, *J* = 25.7, 8.7 Hz, 1H), 7.52 (d, *J* = 7.8 Hz, 1H), 7.38–7.25 (m, 8H), 7.23 (d, *J* = 2.4 Hz, 1H), 7.19–7.08 (m, 2H), 7.03 (tdd, *J* = 11.7, 5.6, 3.1 Hz, 3H), 6.99–6.91 (m, 3H), 5.00 (d, *J* = 10.4 Hz, 3H), 4.72 (dd, *J* = 13.0, 2.4 Hz, 1H), 4.69–4.54 (m, 2H), 4.41 (ddt, *J* = 18.0, 14.8, 5.3 Hz, 1H), 4.22–4.15 (m, 1H), 4.05 (td, *J* = 9.3, 2.2 Hz, 1H), 4.00–3.91 (m, 1H), 3.75–3.66 (m, 1H), 3.61 (ddd, *J* = 16.0, 8.0, 4.4 Hz, 1H), 3.51 (s, 11H), 3.51–3.40 (m, 2H), 3.29 (s, 1H), 3.06 (dddd, *J* = 39.2, 25.1, 12.0, 6.0 Hz, 2H), 2.98–2.85 (m, 2H), 2.88 (s, 4H), 2.82 (ddd, *J* = 28.9, 14.1, 8.0 Hz, 1H), 2.69 (s, 1H), 2.47 (t, *J* = 13.0 Hz, 1H), 1.72 (ddq, *J* = 13.5, 10.5, 6.6 Hz, 1H), 1.46 (qt, *J* = 9.5, 4.6 Hz, 1H), 1.37–1.24 (m, 2H), 1.25 (s, 5H), 1.24 (s, 2H), 1.11 (s, 1H), 1.06 – 0.94 (m, 3H), 0.85 (dd, *J* = 10.1, 6.8 Hz, 3H), 0.80–0.69 (m, 5H), 0.68 (d, *J* = 6.7 Hz, 2H), 0.65–0.58 (m, 5H), 0.54 (d, *J* = 6.8 Hz, 1H), 0.51 (d, *J* = 6.8 Hz, 1H) ppm.

^{13}C NMR (175 MHz, DMSO-d_6, 303 K) δ = 172.1, 171.8, 171.6, 171.4, 171.2, 170.7, 170.6, 170.2, 170.1, 170.0, 167.7, 157.1, 156.1, 156.0, 137.2, 136.1, 136.0, 130.3, 129.6, 128.3, 127.7, 127.3, 127.2, 127.0, 124.1, 123.8, 123.7, 123.4, 120.8, 120.7, 118.7, 118.5, 118.2, 118.0, 117.9, 111.2, 111.1, 111.0, 110.3, 109.8, 109.7, 109.6, 105.1, 98.9, 72.3, 72.2, 72.0, 69.8, 69.7, 69.5, 68.8, 67.2, 65.2, 65.1, 63.8, 60.2, 57.2, 56.6, 55.2, 54.5, 53.8, 53.7, 53.2, 52.8, 52.0, 51.2, 50.7, 48.6, 41.2, 41.0, 40.0, 39.9, 39.8, 39.6, 39.5, 39.4, 39.3, 39.2, 38.2, 37.5, 37.4, 35.1, 32.5, 31.8, 31.4, 31.3, 31.2, 31.1, 31.0, 30.4, 29.9, 29.8, 29.7, 29.1, 29.0, 28.8, 28.7, 28.6, 28.5, 28.4, 28.0, 27.7, 27.2, 26.7, 26.6, 25.3, 25.1, 24.0, 23.1, 22.9, 22.8, 22.2, 22.1, 22.0, 21.7, 20.3, 19.9, 19.6, 19.5, 19.1, 19.0, 18.7, 18.1, 17.8, 17.6, 17.2, 15.2, 15.1, 13.9, 12.9, 12.1 ppm.

HRMS (ESI-qTOF, positive ion mode): *m/z* calcd. for $C_{54}H_{70}N_{10}O_8S$: 1018.5099 [M]; calcd. for $[M+H]^+$: 1019.5172, found: 1019.5158; calcd. for $[M+Na]^+$: 1041.4991, found: 1041.4974.

5-Orn(Cbz)-6-Trp-Lug (**120**)

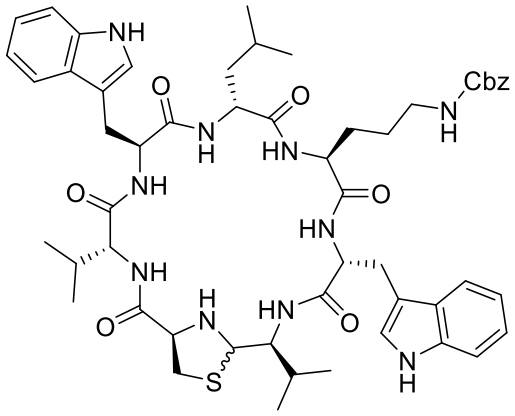

120

Yield: 98%, 34.4 mg

^{1}H NMR (700 MHz, DMSO-d_6, 303 K) δ = 10.77–10.71 (m, 2H), 8.42 (t, *J* = 7.7 Hz, 1H), 8.11–8.02 (m, 1H), 7.80 (dd, *J* = 17.6, 9.2 Hz, 1H), 7.66–7.58 (m, 2H), 7.51 (d, *J* = 7.9 Hz, 1H), 7.31 (dddd, *J* = 25.7, 11.8, 7.0, 2.6 Hz, 8H), 7.22–7.16 (m, 1H), 7.14–7.08 (m, 2H), 7.07–6.99 (m, 3H), 6.95 (tdd, *J* = 7.9, 5.6, 2.1 Hz, 3H), 5.00 (d, *J* = 3.4 Hz, 3H), 4.79–4.68 (m, 1H), 4.67 (s, 1H), 4.64 (tt, *J* = 8.5, 4.6 Hz, 1H), 4.37–4.30 (m, 2H), 4.06–3.95 (m, 1H), 3.74–3.65 (m, 1H), 3.52–3.37 (m, 14H), 3.29 (s, 2H), 3.12–3.03 (m, 2H), 3.00 (ddd, *J* = 16.9, 8.2, 3.6 Hz, 1H), 2.92 (s, 5H), 2.96–2.79 (m, 3H), 2.69 (s, 1H),

2.46 (s, 1H), 1.51–1.42 (m, 1H), 1.42–1.32 (m, 2H), 1.29 (qd, *J* = 7.4, 4.7 Hz, 1H), 1.27–1.17 (m, 2H), 1.06–0.95 (m, 3H), 0.95–0.87 (m, 1H), 0.89–0.79 (m, 4H), 0.79–0.72 (m, 3H), 0.73 (d, *J* = 9.1 Hz, 1H), 0.72–0.64 (m, 1H), 0.63–0.53 (m, 5H), 0.49 (d, *J* = 6.7 Hz, 1H) ppm.

^{13}C NMR (175 MHz, DMSO-d_6, 303 K) δ = 171.9, 171.6, 171.5, 171.3, 170.9, 170.5, 170.4, 170.2, 169.8, 158.0, 157.1, 156.1, 156.0, 137.2, 136.1, 136.0, 130.3, 128.3, 127.7, 127.3, 127.2, 127.0, 124.2, 123.9, 123.7, 123.5, 120.8, 120.7, 120.6, 118.6, 118.5, 118.1, 118.0, 111.2, 111.1, 111.0, 110.2, 109.8, 109.6, 109.3, 105.1, 98.9, 72.3, 72.2, 72.0, 69.9, 69.8, 69.7, 69.6, 69.5, 68.8, 67.2, 65.1, 65.0, 63.8, 60.2, 57.2, 57.1, 55.3, 55.2, 54.5, 53.5, 53.1, 52.7, 51.9, 51.5, 51.2, 50.8, 41.0, 40.8, 40.0, 39.9, 39.8, 39.6, 39.5, 39.4, 39.3, 39.2, 38.2, 37.5, 33.6, 32.4, 31.8, 31.4, 31.3, 31.2, 31.1, 30.7, 30.4, 29.8, 29.6, 29.5, 29.3, 28.9, 28.8, 28.7, 28.5, 28.4, 28.3, 28.1, 27.3, 26.6, 25.7, 25.4, 24.1, 24.0, 23.0, 22.9, 22.5, 22.0, 21.8, 21.7, 20.5, 19.6, 19.5, 19.1, 18.7, 18.6, 18.5, 18.0, 17.9, 17.8, 15.2, 15.0, 13.9, 13.8, 12.1, 12.0 ppm.

HRMS (ESI-qTOF, positive ion mode): *m/z* calcd. for $C_{54}H_{70}N_{10}O_8S$: 1018.5099 [M]; calcd. for $[M+H]^+$: 1019.5172, found: 1019.5167; calcd. for $[M+Na]^+$: 1041.4991, found: 1041.4979.

2,5-Di-Orn(Cbz)-6-Trp-Lug (**121**)

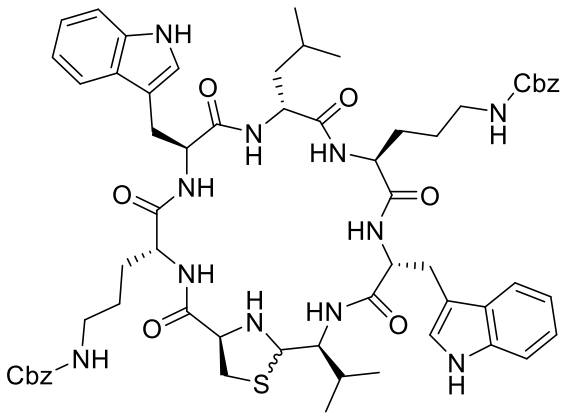

121

Yield: 81%, 40.3 mg

^{1}H NMR (700 MHz, DMSO-d_6, 303 K) δ = 10.76–10.71 (m, 5H), 8.43 (d, *J* = 8.5 Hz, 1H), 8.14–8.08 (m, 2H), 7.87 (d, *J* = 8.7 Hz, 1H), 7.81 (d, *J* = 8.1 Hz, 1H), 7.68 (d,

J = 9.5 Hz, 1H), 7.66–7.58 (m, 4H), 7.52 (d, *J* = 8.0 Hz, 1H), 7.38–7.26 (m, 35H), 7.19–7.06 (m, 7H), 7.06–6.99 (m, 5H), 6.95 (tt, *J* = 7.8, 4.2 Hz, 6H), 4.99 (dd, *J* = 8.3, 5.7 Hz, 12H), 4.78–4.69 (m, 2H), 4.69–4.61 (m, 3H), 4.33 (tdd, *J* = 12.8, 6.1, 2.1 Hz, 2H), 4.06–4.00 (m, 1H), 3.97 (tt, *J* = 7.6, 4.3 Hz, 2H), 3.64–3.58 (m, 1H), 3.51 (s, 14H), 3.52–3.48 (m, 3H), 3.30–3.23 (m, 1H), 3.09 (dd, *J* = 14.3, 7.1 Hz, 3H), 3.05–2.98 (m, 1H), 2.94 (dd, *J* = 13.3, 6.8 Hz, 1H), 2.91–2.79 (m, 5H), 1.47–1.42 (m, 2H), 1.37–1.31 (m, 4H), 1.33 (s, 6H), 1.31–1.22 (m, 2H), 1.25 (s, 13H), 1.24 (s, 3H), 1.20–1.13 (m, 3H), 1.11 (s, 2H), 1.02 (td, *J* = 5.0, 2.3 Hz, 1H), 1.01–0.94 (m, 8H), 0.96–0.88 (m, 1H), 0.85 (t, *J* = 6.9 Hz, 5H), 0.83–0.70 (m, 12H), 0.68 (t, *J* = 6.4 Hz, 3H), 0.60 (d, *J* = 6.8 Hz, 4H) ppm.

^{13}C NMR (175 MHz, DMSO-d_6, 303 K) δ = 172.0, 171.6, 171.5, 171.4, 171.2, 170.8, 170.5, 170.4, 170.2, 170.1, 157.1, 156.1, 156.0, 155.5, 137.2, 136.1, 136.0, 136.0, 130.3, 129.6, 128.3, 127.7, 127.3, 127.2, 127.1, 123.8, 123.7, 123.5, 123.3, 120.8, 120.7, 120.6, 118.6, 118.5, 118.2, 118.1, 118.0, 111.2, 111.1, 110.2, 109.8, 109.6, 109.4, 105.1, 98.9, 72.3, 72.0, 70.2, 69.8, 69.7, 69.5, 68.8, 67.2, 66.9, 65.1, 65.0, 63.8, 60.2, 57.1, 55.3, 55.2, 54.6, 53.8, 53.3, 53.2, 53.0, 52.8, 51.8, 51.5, 51.4, 51.2, 50.9, 40.9, 40.8, 40.0, 39.9, 39.8, 39.6, 39.5, 39.4, 39.3, 39.2, 38.2, 37.4, 37.2, 35.1, 33.6, 32.4, 31.8, 31.4, 31.3, 31.2, 31.1, 30.4, 29.8, 29.5, 29.4, 29.1, 29.0, 28.8, 28.7, 28.6, 28.5, 28.4, 28.3, 28.1, 27.8, 27.5, 26.7, 26.5, 25.7, 25.5, 25.4, 25.3, 25.1, 24.5, 24.0, 23.6, 23.0, 22.9, 22.5, 22.0, 21.8, 21.7, 20.8, 20.4, 19.6, 19.5, 18.0, 17.9, 17.8, 17.7, 17.6, 17.4, 17.2, 17.0, 15.2, 15.0, 13.9, 12.9, 12.5, 12.1, 12.1 ppm.

HRMS (ESI-qTOF, positive ion mode): *m/z* calcd. for $C_{62}H_{77}N_{11}O_{10}S$: 1167.5576 [M]; calcd. for $[M+H]^+$: 1168.5648, found: 1168.5631; calcd. for $[M+Na]^+$: 1190.5468, found: 1190.5447.

2,5-Di-Orn(Dde)-6-Trp-Lug (**122**)

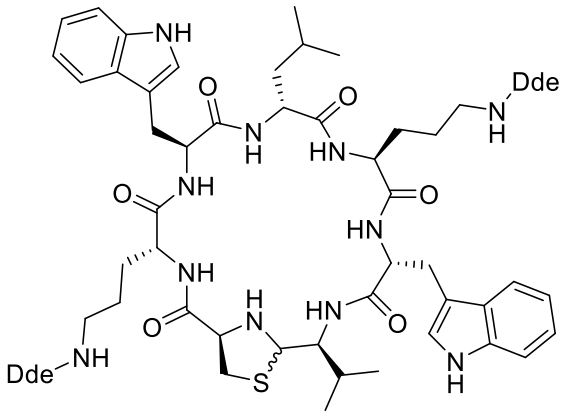

122

Yield: 91%, 38.6 mg

^{1}H NMR (700 MHz, DMSO-d_6, 303 K) δ = 10.73 (ddd, *J* = 14.0, 9.0, 2.4 Hz, 3H), 8.49 (dd, *J* = 10.0, 6.8 Hz, 1H), 7.72–7.62 (m, 3H), 7.60 (s, 5H), 7.29 (dq, *J* = 10.3, 6.9 Hz, 6H), 7.16–7.09 (m, 5H), 7.02 (dddt, *J* = 12.9, 9.5, 5.9, 2.0 Hz, 4H), 6.97–6.88 (m, 5H), 4.75–4.64 (m, 2H), 4.46–4.37 (m, 2H), 4.34 (ddt, *J* = 13.3, 8.7, 4.9 Hz, 1H), 4.09–3.98 (m, 1H), 3.51 (s, 22H), 3.52–3.44 (m, 3H), 3.28–3.16 (m, 3H), 3.16–3.05 (m, 3H), 2.93–2.85 (m, 1H), 2.41 (d, *J* = 4.5 Hz, 6H), 2.37 (s, 7H), 2.35 (s, 2H), 2.28–2.20 (m, 26H), 1.53–1.46 (m, 1H), 1.28–1.20 (m, 2H), 1.23 (s, 3H), 1.11 (s, 2H), 0.98 (t, *J* = 7.3 Hz, 5H), 0.97–0.88 (m, 39H), 0.90–0.83 (m, 3H), 0.83–0.78 (m, 2H), 0.79 (s, 2H), 0.78–0.69 (m, 7H), 0.65 (dd, *J* = 8.8, 6.7 Hz, 3H) ppm.

^{13}C NMR (175 MHz, DMSO-d_6, 303 K) δ = 172.8, 172.7, 172.6, 172.1, 171.9, 171.5, 171.4, 171.3, 170.9, 170.4, 170.1, 170.0, 169.7, 167.8, 158.0, 157.1, 139.1, 136.0, 130.3, 129.6, 127.3, 127.2, 127.1, 124.1, 123.9, 123.4, 120.8, 120.7, 118.8, 118.6, 118.3, 118.2, 118.0, 111.2, 111.1, 110.1, 109.8, 109.7, 109.5, 107.0, 106.9, 105.1, 99.0, 72.3, 71.9, 69.8, 69.7, 69.5, 68.8, 67.2, 66.9, 65.0, 63.7, 60.2, 57.0, 55.3, 55.2, 54.6, 53.6, 53.4, 53.0, 52.8, 52.3, 51.6, 51.1, 50.8, 42.2, 42.1, 42.0, 40.9, 40.8, 40.0, 39.9, 39.8, 39.6, 39.5, 39.4, 39.3, 39.2, 38.2, 37.2, 35.2, 34.4, 33.6, 32.5, 31.8, 31.4, 31.3, 31.1, 31.0, 30.4, 29.8, 29.7, 29.6, 29.1, 29.0, 28.8, 28.7, 28.5, 28.4, 28.1, 27.8, 27.6, 26.8, 25.3, 25.1, 24.7, 24.4, 24.3, 24.1, 24.0, 23.0, 22.8, 22.6, 22.4, 22.1, 21.8, 21.0, 20.5, 19.6, 17.8, 17.3, 17.2, 15.2, 15.1, 13.9, 12.1 ppm.

HRMS (ESI-qTOF, positive ion mode): *m/z* calcd. for $C_{66}H_{89}N_{11}O_{10}S$: 1227.6515 [M]; calcd. for $[M+H]^+$: 1228.6587, found: 1228.6561; calcd. for $[M+Na]^+$: 1250.6407, found: 1250.6366.

2-Orn(Cbz)-Lug (**123**)

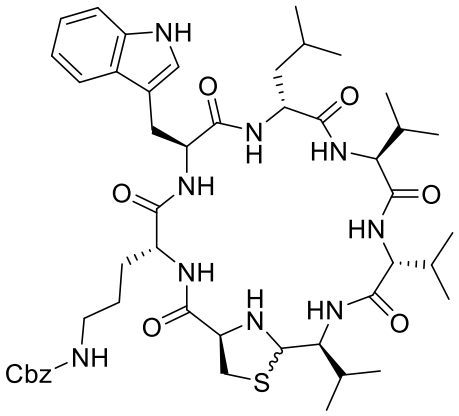

123

Yield: 84%, 27.0 mg

^{1}H NMR (600 MHz, DMSO-d_6, 303 K) δ = 10.75–10.71 (m, 2H), 8.49 (dd, *J* = 10.2, 6.7 Hz, 2H), 8.17–8.09 (m, 2H), 7.99 (dd, *J* = 15.4, 8.6 Hz, 2H), 7.71 (t, *J* = 9.3 Hz, 2H), 7.35 (tt, *J* = 8.0, 1.8 Hz, 9H), 7.34–7.26 (m, 4H), 7.11 (td, *J* = 9.3, 4.9 Hz, 4H), 7.07–6.99 (m, 3H), 6.96 (q, *J* = 6.5 Hz, 3H), 5.01 (d, *J* = 8.5 Hz, 6H), 4.54 (ddt, *J* = 10.4, 7.2, 3.6 Hz, 2H), 4.50–4.36 (m, 2H), 4.13–4.03 (m, 2H), 3.51 (s, 20H), 3.52–3.48 (m, 3H), 3.08–2.96 (m, 2H), 2.98–2.78 (m, 5H), 2.57–2.51 (m, 2H), 2.03–1.85 (m, 3H), 1.43–1.27 (m, 3H), 1.29–1.20 (m, 5H), 1.06–0.98 (m, 2H), 0.98–0.89 (m, 5H), 0.91–0.64 (m, 45H) ppm.

^{13}C NMR (151 MHz, DMSO-d_6, 303 K) δ = 171.8, 171.7, 171.5, 171.4, 171.2, 171.0, 170.9, 170.7, 170.5, 170.2, 170.1, 169.9, 167.7, 157.9, 157.1, 156.1, 156.0, 137.2, 136.0, 130.3, 129.6, 129.1, 128.3, 127.7, 127.6, 127.3, 127.1, 127.0, 123.8, 123.7, 123.4, 120.8, 120.6, 118.5, 118.2, 118.1, 118.0, 111.2, 111.1, 110.4, 109.5, 105.1, 99.0, 72.3, 72.1, 69.8, 69.7, 69.5, 68.8, 67.2, 65.3, 65.2, 65.1, 63.7, 60.2, 58.8, 57.3, 57.1, 56.9, 56.8, 55.2, 54.5, 53.9, 53.3, 52.8, 52.1, 51.4, 50.8, 41.2, 40.1, 39.9, 39.8, 39.7, 39.5, 39.4, 39.2, 39.1, 38.2, 37.7, 37.4, 36.8, 35.1, 34.4, 32.6, 31.9, 31.2, 31.1, 31.0, 30.4, 29.9, 29.8, 29.4, 29.3, 29.0, 28.9, 28.7, 28.6, 28.5, 28.1, 27.6, 26.5, 25.4, 25.3, 24.0, 23.9, 23.1, 23.0, 22.7, 22.3, 22.1, 22.0, 21.7, 21.3, 20.8, 20.5, 20.0, 19.9,

19.8, 19.7, 19.6, 19.5, 19.3, 19.2, 19.1, 18.8, 18.4, 18.3, 18.1, 18.0, 17.9, 17.8, 17.7, 17.5, 17.2, 17.0, 15.2, 13.9, 12.9, 12.0 ppm.

HRMS (ESI-qTOF, positive ion mode): *m/z* calcd. for $C_{48}H_{69}N_9O_8S$: 931.4990 [M]; calcd. for $[M+H]^+$: 932.5063, found: 932.5071; calcd. for $[M+Na]^+$: 954.4882, found: 954.4861.

5-Orn(Cbz)-Lug (**124**)

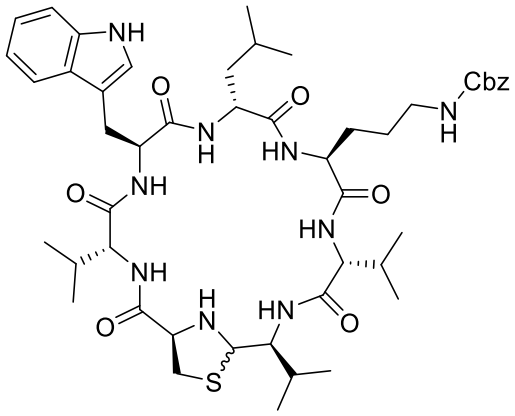

124

Yield: 78%, 25.1 mg

^{1}H NMR (700 MHz, DMSO-d_6, 303 K) δ = 10.74 (dd, *J* = 19.0, 2.4 Hz, 1H), 8.43 (dd, *J* = 12.5, 7.0 Hz, 1H), 8.16 (t, *J* = 8.0 Hz, 1H), 7.71–7.64 (m, 1H), 7.61 (s, 1H), 7.63–7.55 (m, 1H), 7.52 (d, *J* = 7.9 Hz, 1H), 7.35 (q, *J* = 7.4 Hz, 4H), 7.34–7.26 (m, 4H), 7.29 (s, 2H), 7.16–7.10 (m, 1H), 7.07–7.00 (m, 2H), 7.00–6.92 (m, 2H), 5.00 (d, *J* = 6.4 Hz, 3H), 4.77–4.67 (m, 1H), 4.64 (tt, *J* = 13.5, 6.7 Hz, 1H), 4.55 (t, *J* = 10.0 Hz, 1H), 4.50–4.42 (m, 1H), 4.18 (dt, *J* = 13.6, 8.5 Hz, 1H), 3.69 (tdt, *J* = 12.4, 9.9, 6.3 Hz, 1H), 3.51 (s, 17H), 3.51–3.47 (m, 1H), 3.43 (dt, *J* = 26.2, 5.6 Hz, 1H), 3.33 (d, *J* = 6.9 Hz, 1H), 3.08 (ddd, *J* = 30.8, 9.6, 6.2 Hz, 1H), 3.03–2.94 (m, 3H), 2.94–2.80 (m, 1H), 2.48–2.40 (m, 1H), 2.01–1.90 (m, 1H), 1.65 (dt, *J* = 13.5, 6.6 Hz, 1H), 1.42 (s, 5H), 1.42–1.28 (m, 2H), 1.24 (q, *J* = 6.9 Hz, 3H), 1.06–0.95 (m, 1H), 0.97–0.69 (m, 13H), 0.64 (t, *J* = 6.7 Hz, 2H), 0.56 (q, *J* = 8.9 Hz, 2H), 0.47 (d, *J* = 6.7 Hz, 1H) ppm.

^{13}C NMR (175 MHz, DMSO-d_6, 303 K) δ = 172.6, 171.8, 171.6, 171.3, 171.2, 171.1, 170.9, 170.6, 170.5, 169.9, 169.7, 167.7, 158.0, 157.1, 156.2, 156.0, 137.3, 137.2, 136.1, 136.0, 130.3, 129.6, 128.3, 127.7, 127.6, 127.2, 127.0, 124.2, 124.1, 123.7,

123.5, 120.8, 120.6, 118.6, 118.1, 118.0, 111.2, 111.0, 110.2, 109.6, 109.5, 108.9, 105.1, 99.0, 77.2, 75.9, 72.3, 72.2, 72.1, 70.0, 69.9, 69.8, 69.7, 69.6, 69.5, 68.8, 67.2, 65.7, 65.1, 65.0, 64.5, 63.7, 62.8, 61.2, 60.5, 60.2, 58.2, 57.6, 57.3, 57.2, 56.7, 56.5, 55.2, 54.6, 53.1, 52.8, 52.7, 52.0, 51.5, 51.3, 50.7, 41.0, 40.9, 40.1, 40.0, 39.9, 39.8, 39.6, 39.5, 39.4, 39.3, 39.2, 38.2, 38.0, 37.6, 35.1, 34.9, 34.4, 33.6, 33.5, 32.3, 31.9, 31.7, 31.2, 31.1, 30.7, 30.4, 30.2, 29.8, 29.7, 29.3, 29.1, 29.0, 28.8, 28.7, 28.5, 28.3, 28.1, 27.0, 26.7, 26.6, 26.5, 25.9, 25.7, 25.1, 24.5, 24.1, 24.0, 23.8, 23.0, 22.9, 22.5, 22.0, 21.8, 21.7, 20.9, 20.8, 20.1, 19.8, 19.6, 19.5, 19.3, 19.2, 19.1, 19.0, 18.9, 18.7, 18.5, 18.3, 18.2, 18.1, 18.0, 17.8, 17.7, 17.5, 17.2, 15.2, 15.1, 13.9, 12.9, 12.1 ppm.

HRMS (ESI-qTOF, positive ion mode): *m/z* calcd. for $C_{48}H_{69}N_9O_8S$: 931.4990 [M]; calcd. for $[M+H]^+$: 932.5063, found: 932.5036; calcd. for $[M+Na]^+$: 954.4882, found: 954.4853.

2,5-Di-Orn(Dde)-Lug (**125**)

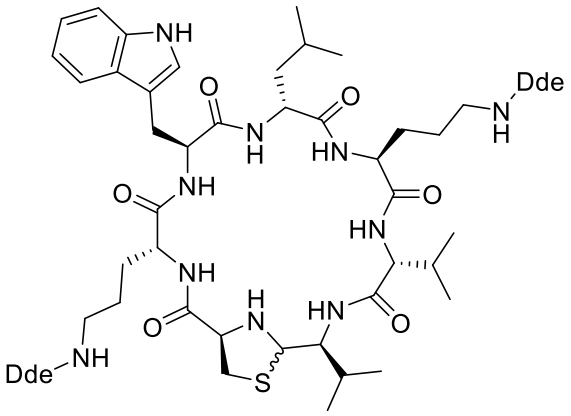

125

Yield: 88%, 34.6 mg

^{1}H NMR (700 MHz, DMSO-d_6, 303 K) δ = 10.94–10.53 (m, 1H), 8.52 (d, *J* = 8.0 Hz, 1H), 8.31–8.12 (m, 1H), 7.96–7.84 (m, 1H), 7.67 (ddd, *J* = 21.6, 11.3, 6.9 Hz, 2H), 7.53 (d, *J* = 7.9 Hz, 1H), 7.30 (dt, *J* = 15.9, 7.4 Hz, 2H), 7.12 (dd, *J* = 8.8, 2.4 Hz, 1H), 7.06–6.98 (m, 1H), 6.98–6.91 (m, 1H), 4.73 (dd, *J* = 12.9, 2.4 Hz, 1H), 4.69–4.47 (m, 1H), 4.45–4.24 (m, 1H), 4.24–4.03 (m, 1H), 3.99–3.84 (m, 1H), 3.51 (s, 12H), 3.10–2.96 (m, 2H), 2.86–2.80 (m, 1H), 2.69 (s, 1H), 2.49–2.42 (m, 8H), 2.42–2.37 (m, 4H), 2.29–2.18 (m, 15H), 0.98 (d, *J* = 7.1 Hz, 5H), 0.89–0.81 (m, 6H), 0.78–0.72 (m, 2H) ppm.

^{13}C NMR (175 MHz, DMSO-d_6, 303 K) δ = 172.8, 172.7, 171.8, 171.6, 171.5, 171.4, 170.9, 170.7, 170.5, 170.3, 170.0, 169.8, 158.0, 157.1, 136.1, 136.0, 130.4, 127.3, 127.1, 127.0, 124.1, 123.5, 120.9, 120.7, 118.6, 118.3, 118.2, 118.1, 111.2, 111.1, 110.3, 109.5, 108.7, 107.0, 106.9, 105.1, 99.0, 72.3, 72.2, 72.1, 69.9, 69.8, 69.7, 68.8, 67.2, 65.1, 63.8, 60.4, 60.2, 58.0, 57.7, 57.2, 56.9, 55.2, 54.7, 53.8, 53.2, 52.9, 52.3, 51.9, 51.5, 51.2, 51.1, 50.9, 42.3, 42.2, 42.1, 42.0, 40.9, 40.0, 39.9, 39.8, 39.6, 39.5, 39.4, 39.3, 39.2, 38.2, 37.4, 36.9, 35.1, 34.7, 32.3, 31.8, 31.3, 31.2, 30.4, 29.9, 29.8, 29.7, 29.5, 29.4, 29.0, 28.7, 28.5, 28.4, 28.1, 27.9, 27.8, 26.5, 25.1, 25.0, 24.4, 24.2, 24.1, 23.8, 23.0, 22.8, 22.5, 22.1, 21.8, 20.8, 20.6, 19.8, 19.5, 19.3, 19.2, 19.0, 18.6, 18.4, 17.9, 17.8, 17.7, 17.5, 17.3, 17.2, 15.2, 13.9, 13.8, 12.2, 12.1, 11.4 ppm.

HRMS (ESI-qTOF, positive ion mode): *m/z* calcd. for $C_{60}H_{88}N_{10}O_{10}S$: 1140.6406 [M]; calcd. for $[M+H]^+$: 1141.6478, found: 1141.6473; calcd. for $[M+Na]^+$: 1163.6298, found: 1163.6271.

3-(4-NH_2-Phe)-6-Trp-Lug (**126**)

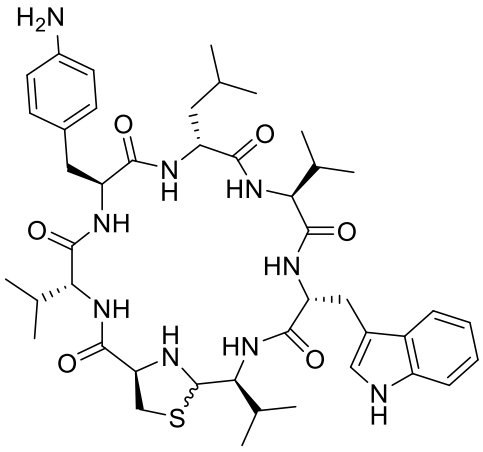

126

Yield: 9%, 0.5 mg

^{1}H NMR (600 MHz, DMSO-d_6, 303 K) δ = 10.74 (d, *J* = 16.2 Hz, 1H), 8.53 (s, 1H), 8.42 (dd, *J* = 18.6, 7.0 Hz, 1H), 8.19 (d, *J* = 7.4 Hz, 1H), 8.15–8.08 (m, 1H), 8.01 (s, 7H), 7.66 (t, *J* = 6.8 Hz, 1H), 7.28 (t, *J* = 7.5 Hz, 1H), 7.17 (d, *J* = 2.3 Hz, 4H), 7.03 (q, *J* = 6.8 Hz, 1H), 6.95 (q, *J* = 6.9 Hz, 1H), 6.89 (d, *J* = 13.2 Hz, 3H), 6.69 (s, 1H), 6.62 (s, 5H), 6.41 (t, *J* = 8.3 Hz, 1H), 5.41–5.26 (m, 4H), 4.77 (d, *J* = 12.5 Hz, 1H), 4.59 (d, *J* = 9.3 Hz, 1H), 4.23–4.11 (m, 1H), 3.98 (t, *J* = 6.6 Hz, 2H), 3.51 (s, 5H), 3.32 (d,

J = 6.5 Hz, 10H), 3.27 (s, 8H), 2.79–2.71 (m, 17H), 2.05–1.95 (m, 17H), 1.80 (s, 23H), 1.52–1.42 (m, 13H), 1.35 (s, 16H), 1.29–1.20 (m, 13H), 0.85 (td, *J* = 7.0, 1.8 Hz, 19H), 0.71–0.50 (m, 9H) ppm.

HRMS (ESI-qTOF, positive ion mode): *m/z* calcd. for $C_{44}H_{64}N_9O_6S$: 845.4622 [M]; calcd. for $[M+H]^+$: 846.4695, found: 846.4679; calcd. for $[M+Na]^+$: 868.4514, found: 868.4511.

2-Orn-6-Trp-Lug (**127**)

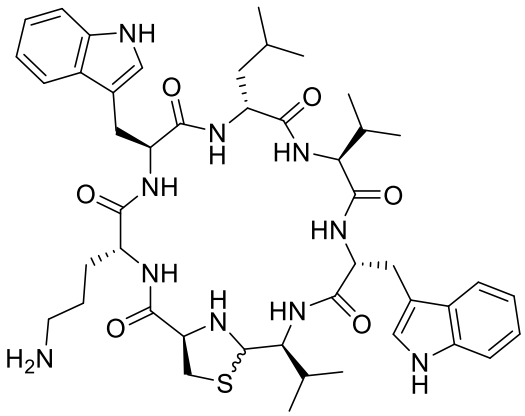

127

Yield: 95%, 12.4 mg

^{1}H NMR (600 MHz, DMSO-d_6, 303 K) δ = 10.80–10.76 (m, 5H), 8.27 (s, 1H), 8.24–8.14 (m, 4H), 7.93 (dd, *J* = 19.3, 8.4 Hz, 1H), 7.66 (d, *J* = 8.4 Hz, 1H), 7.62 (dd, *J* = 14.2, 7.7 Hz, 2H), 7.31 (t, *J* = 8.0 Hz, 6H), 7.16–7.09 (m, 4H), 7.04 (dtdd, *J* = 6.8, 5.4, 2.8, 1.2 Hz, 5H), 7.00–6.93 (m, 6H), 6.90 (s, 1H), 4.75–4.61 (m, 2H), 4.66 (s, 2H), 4.41 (s, 1H), 4.34 (td, *J* = 9.5, 5.4 Hz, 2H), 4.11–4.01 (m, 2H), 3.97 (t, *J* = 6.6 Hz, 2H), 3.51 (s, 6H), 3.14–2.98 (m, 4H), 2.97–2.79 (m, 3H), 2.74 (t, *J* = 7.4 Hz, 1H), 2.63 (s, 3H), 2.58–2.51 (m, 2H), 1.54–1.46 (m, 3H), 1.35 (s, 11H), 1.30 (s, 2H), 1.28–1.21 (m, 28H), 1.06–0.97 (m, 3H), 0.88–0.83 (m, 6H), 0.81 (d, *J* = 6.4 Hz, 2H), 0.75 (s, 33H), 0.76–0.65 (m, 8H), 0.58 (dd, *J* = 15.6, 6.8 Hz, 4H) ppm.

^{13}C NMR (150 MHz, DMSO-d_6, 303 K) δ = 172.4, 171.9, 171.8, 171.5, 171.3, 170.8, 170.5, 170.4, 170.2, 169.8, 158.1, 157.9, 157.6, 157.4, 152.0, 139.0, 136.0, 131.3, 127.3, 127.1, 124.3, 124.2, 124.1, 123.9, 123.7, 123.5, 120.7, 120.3, 118.7, 118.6, 118.5, 118.3, 118.2, 118.1, 116.3, 114.3, 111.2, 111.1, 110.1, 109.8, 109.7, 109.4,

74.6, 72.4, 71.9, 69.7, 65.1, 63.7, 57.1, 54.7, 53.3, 53.2, 53.1, 52.8, 51.5, 51.1, 50.9, 41.0, 40.7, 40.1, 39.9, 39.8, 39.7, 39.5, 39.4, 39.2, 39.1, 38.4, 38.3, 37.1, 35.5, 34.4, 34.2, 32.4, 31.2, 31.1, 30.4, 29.8, 29.4, 29.2, 29.0, 28.9, 28.8, 28.7, 28.6, 28.5, 28.2, 28.0, 27.9, 27.6, 25.3, 24.0, 23.8, 23.5, 23.3, 23.0, 22.6, 22.0, 21.7, 21.5, 20.3, 19.6, 19.5, 17.2, 15.0, 13.9 ppm.

HRMS (ESI-qTOF, positive ion mode): *m/z* calcd. for $C_{46}H_{64}N_{10}O_6S$: 884.4731 [M]; calcd. for $[M+H]^+$: 885.4804, found: 885.4818.

5-Orn-6-Trp-Lug (**128**)

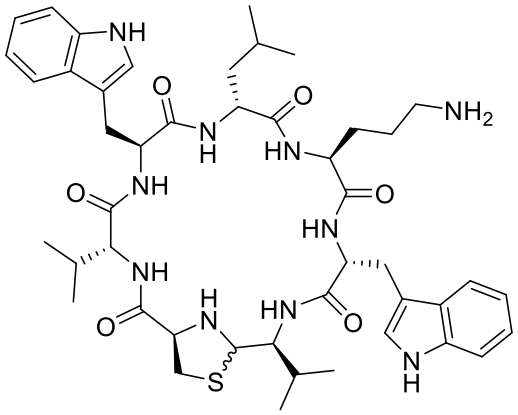

128

Yield: 90%, 11.1 mg

^{1}H NMR (700 MHz, DMSO-d_6, 303 K) δ = 10.78–10.71 (m, 2H), 7.67–7.59 (m, 1H), 7.30 (ddd, *J* = 11.3, 4.6, 2.3 Hz, 1H), 7.12 (dd, *J* = 10.3, 2.4 Hz, 1H), 7.06–7.00 (m, 2H), 6.95 (s, 2H), 4.58 (s, 1H), 3.68 (s, 1H), 3.50 (s, 12H), 3.51–3.46 (m, 1H), 3.09 (s, 1H), 2.95–2.87 (m, 1H), 2.73 (t, *J* = 7.9 Hz, 1H), 2.56–2.52 (m, 1H), 1.34 (d, *J* = 10.1 Hz, 3H), 1.34–1.26 (m, 1H), 1.28–1.21 (m, 8H), 1.19–1.13 (m, 1H), 1.04–0.77 (m, 5H), 0.79–0.70 (m, 1H), 0.54 (dd, *J* = 17.8, 6.9 Hz, 1H) ppm.

HRMS (ESI-qTOF, positive ion mode): *m/z* calcd. for $C_{46}H_{64}N_{10}O_6S$: 884.4731 [M]; calcd. for $[M+H]^+$: 885.4804, found: 885.4823; calcd. for $[M+Na]^+$: 907.4623, found: 907.4643.

2,5-Di-Orn-6-Trp-Lug (**129**)

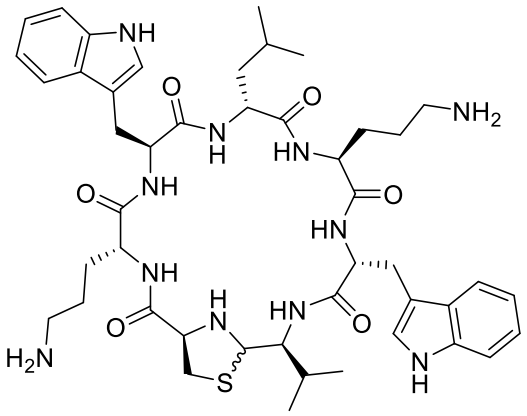

129

Yield: 49% (Dde), 7.5 mg; 20% (Cbz), 4.5 mg

^{1}H NMR (600 MHz, DMSO-d_6, 303 K) δ = 10.74 (d, *J* = 13.7 Hz, 6H), 8.51–8.41 (m, 1H), 8.29 (dd, *J* = 21.4, 8.8 Hz, 1H), 8.17–8.09 (m, 2H), 7.95 (dd, *J* = 17.4, 9.1 Hz, 1H), 7.86 (dd, *J* = 18.0, 9.2 Hz, 1H), 7.68 (dt, *J* = 19.7, 5.8 Hz, 7H), 7.61 (s, 5H), 7.53 (q, *J* = 9.1 Hz, 1H), 7.32–7.25 (m, 5H), 7.27–7.19 (m, 1H), 7.17–7.10 (m, 4H), 7.03 (tt, *J* = 9.5, 5.4 Hz, 6H), 6.99–6.92 (m, 3H), 6.94 (s, 4H), 5.00 (d, *J* = 9.7 Hz, 1H), 4.75–4.62 (m, 3H), 4.43 (s, 1H), 4.42–4.37 (m, 1H), 4.09–4.03 (m, 2H), 3.78–3.68 (m, 2H), 3.62 (s, 2H), 3.51 (s, 29H), 3.50 (s, 5H), 3.47 (dd, *J* = 20.2, 5.5 Hz, 1H), 3.42 (t, *J* = 5.3 Hz, 1H), 3.12–2.98 (m, 2H), 2.90 (dd, *J* = 15.4, 8.5 Hz, 3H), 2.89–2.78 (m, 1H), 2.06 (d, *J* = 5.7 Hz, 1H), 1.99 (dt, *J* = 21.0, 7.1 Hz, 1H), 1.70 (dq, *J* = 13.8, 6.9 Hz, 1H), 1.46 (s, 8H), 1.52–1.41 (m, 2H), 1.35 (s, 1H), 1.34–1.25 (m, 2H), 1.25 (s, 21H), 1.24 (s, 10H), 1.23 (s, 2H), 1.13 (dd, *J* = 14.6, 7.6 Hz, 1H), 0.87 (s, 13H), 0.85 (t, *J* = 7.1 Hz, 4H), 0.81–0.76 (m, 2H), 0.75 (d, *J* = 6.1 Hz, 2H), 0.70 (ddd, *J* = 13.5, 7.1, 4.4 Hz, 6H), 0.59 (tdd, *J* = 18.7, 13.9, 9.5 Hz, 7H), 0.50 (dd, *J* = 12.8, 6.7 Hz, 2H) ppm.

^{13}C NMR (150 MHz, DMSO-d_6, 303 K) δ = 172.2, 171.6, 171.2, 171.0, 170.5, 170.1, 169.9, 169.7, 143.7, 136.1, 136.0, 135.9, 129.0, 128.3, 127.7, 127.2, 127.1, 126.2, 124.1, 123.8, 123.4, 120.7, 118.2, 118.0, 117.9, 111.0, 110.1, 109.8, 109.7, 109.6, 72.3, 69.7, 60.2, 57.1, 39.9, 39.8, 39.7, 39.5, 39.4, 39.2, 39.1, 31.2, 28.9, 28.6, 26.2, 23.9, 22.9, 22.3, 22.2, 22.0, 21.7, 19.5, 19.0, 15.1, 13.9 ppm.

HRMS (ESI-qTOF, positive ion mode): *m/z* calcd. for $C_{46}H_{65}N_{11}O_6S$: 899.4731 [M]; calcd. for $[M+H]^+$: 900.4913, found: 900.4919; calcd. for $[M+Na]^+$: 922.4732, found: 922.4735.

2-Orn-Lug (**130**)

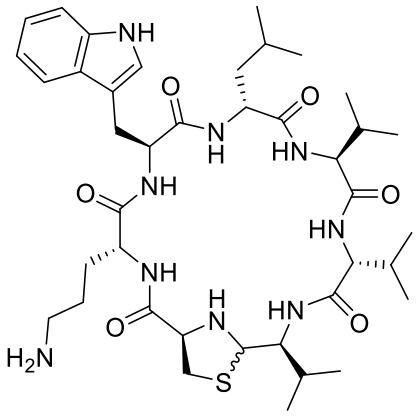

130

Yield: 92%, 11.8 mg

^{1}H NMR (700 MHz, DMSO-d_6, 303 K) δ = 10.80 (d, *J* = 8.4 Hz, 1H), 10.75 (s, 1H), 8.01 (ddt, *J* = 12.6, 8.3, 3.7 Hz, 1H), 7.83–7.70 (m, 1H), 7.56–7.49 (m, 1H), 7.39–7.25 (m, 4H), 7.15–7.10 (m, 1H), 7.07–6.92 (m, 4H), 5.05–4.97 (m, 1H), 4.47–4.41 (m, 1H), 3.78–3.68 (m, 2H), 3.67–3.58 (m, 1H), 3.51 (d, *J* = 2.3 Hz, 30H), 3.38–3.32 (m, 2H), 3.04 (dtd, *J* = 12.6, 9.9, 5.7 Hz, 2H), 2.95–2.85 (m, 2H), 2.85–2.79 (m, 2H), 2.65 (s, 1H), 2.05–1.99 (m, 1H), 2.01–1.94 (m, 2H), 1.50–1.42 (m, 1H), 1.35 (s, 5H), 1.31 (d, *J* = 12.2 Hz, 2H), 1.27 (s, 24H), 1.27–1.19 (m, 26H), 1.06–1.00 (m, 1H), 0.96 (dt, *J* = 10.9, 3.3 Hz, 1H), 0.93 (dd, *J* = 6.7, 3.3 Hz, 2H), 0.93–0.77 (m, 29H), 0.79–0.66 (m, 5H), 0.62 (td, *J* = 7.9, 4.3 Hz, 1H) ppm.

^{13}C NMR (175 MHz, DMSO-d_6, 303 K) δ = 174.2, 172.5, 171.7, 171.6, 171.5, 171.2, 170.8, 170.6, 170.2, 170.1, 169.7, 158.0, 157.8, 157.7, 157.5, 152.0, 139.1, 136.0, 131.3, 130.3, 129.6, 128.8, 128.4, 128.3, 127.7, 127.3, 127.1, 124.1, 123.9, 123.5, 120.8, 120.7, 119.9, 118.2, 116.5, 111.1, 110.2, 109.6, 105.1, 98.9, 72.3, 72.2, 72.1, 71.3, 69.8, 69.7, 69.5, 68.8, 67.2, 65.3, 63.8, 63.7, 60.2, 57.3, 57.2, 56.6, 55.2, 54.5, 52.9, 51.8, 51.1, 50.8, 41.2, 40.0, 39.9, 39.8, 39.6, 39.5, 39.4, 39.3, 39.2, 38.6, 38.2, 35.5, 35.1, 34.5, 34.4, 34.3, 33.8, 32.6, 32.0, 31.2, 31.1, 30.4, 30.1, 29.8, 29.6, 29.4, 29.3, 29.1, 29.0, 28.9, 28.8, 28.7, 28.6, 28.5, 28.2, 28.1, 26.9, 26.6, 26.5, 25.3, 25.1,

24.5, 24.0, 23.9, 23.0, 22.9, 22.3, 22.1, 22.0, 21.7, 20.8, 19.8, 19.7, 19.5, 19.4, 19.2, 19.1, 18.4, 18.1, 17.9, 17.8, 17.4, 15.2, 13.9 ppm.

HRMS (ESI-qTOF, positive ion mode): *m/z* calcd. for $C_{40}H_{63}N_9O_6S$: 797.4622 [M]; calcd. for $[M+H]^+$: 798.4695, found: 798.4703; calcd. for $[M+Na]^+$: 820.4514, found: 820.4522.

5-Orn-Lug (**131**)

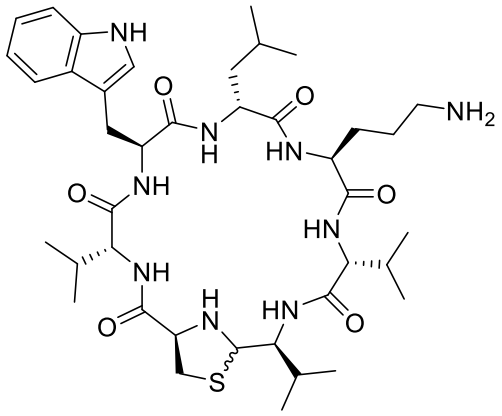

131

Yield: 93%, 11.9 mg

^{1}H NMR (700 MHz, DMSO-d_6, 303 K) δ = 10.83–10.69 (m, 1H), 8.47–8.14 (m, 1H), 7.83–7.46 (m, 7H), 7.42–7.19 (m, 3H), 7.14 (ddd, *J* = 16.9, 9.1, 2.1 Hz, 1H), 7.08–6.99 (m, 1H), 6.99–6.78 (m, 1H), 4.81–4.65 (m, 1H), 4.62–4.41 (m, 1H), 4.41–4.10 (m, 1H), 4.09–3.93 (m, 1H), 3.78–3.64 (m, 1H), 3.46–3.35 (m, 2H), 3.16–3.04 (m, 1H), 3.02–2.87 (m, 1H), 2.84–2.77 (m, 2H), 2.08–1.92 (m, 1H), 1.59–1.44 (m, 2H), 1.29–1.17 (m, 7H), 0.97–0.66 (m, 8H) ppm.

^{13}C NMR (175 MHz, DMSO-d_6, 303 K) δ = 172.5, 171.9, 171.8, 171.5, 171.5, 171.0, 170.9, 170.7, 170.5, 170.5, 169.8, 158.2, 158.0, 158.0, 157.8, 157.7, 157.1, 152.0, 139.1, 136.1, 136.0, 131.3, 130.3, 129.8, 129.2, 129.0, 128.3, 128.3, 127.6, 127.2, 127.0, 126.3, 124.3, 124.1, 124.0, 123.6, 120.8, 120.6, 119.9, 118.1, 117.9, 116.4, 111.2, 111.0, 110.2, 109.5, 105.1, 99.0, 74.6, 72.3, 72.0, 69.8, 69.5, 68.8, 67.2, 65.1, 63.7, 62.8, 60.5, 60.2, 58.2, 57.4, 57.2, 55.2, 54.7, 53.3, 52.7, 51.9, 51.0, 50.6, 41.1, 40.9, 40.0, 39.9, 39.8, 39.6, 39.5, 39.4, 39.3, 39.2, 38.5, 38.5, 38.2, 37.5, 35.6, 34.5, 34.4, 34.3, 33.6, 32.4, 32.0, 31.3, 31.1, 30.6, 30.4, 29.8, 29.3, 29.2, 29.0, 29.0, 28.9,

28.9, 28.9, 28.8, 28.8, 28.7, 28.7, 28.7, 28.5, 28.5, 28.5, 28.1, 28.0, 26.5, 25.3, 24.5, 24.1, 23.9, 23.7, 23.5, 23.4, 23.0, 23.0, 22.5, 22.1, 21.7, 21.6, 20.8, 20.7, 19.8, 19.6, 19.4, 19.3, 19.2, 19.1, 19.1, 18.7, 18.6, 18.5, 18.2, 18.2, 18.1, 18.0, 17.7, 17.5, 17.2, 17.1, 15.2, 15.1, 13.9 ppm.

HRMS (ESI-qTOF, positive ion mode): *m/z* calcd. for $C_{40}H_{63}N_9O_6S$: 797.4622 [M]; calcd. for $[M+H]^+$: 798.4695, found: 798.4707; calcd. for $[M+Na]^+$: 820.4514, found: 820.4528.

2,5-Di-Orn-Lug (**137**)

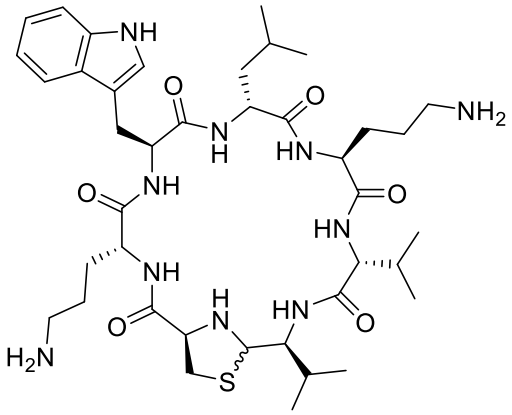

137

Yield: 55%, 8.3 mg

^{1}H NMR (700 MHz, DMSO-d_6, 303 K) δ = 10.82 (s, 2H), 8.39 (s, 5H), 8.26 (d, *J* = 8.4 Hz, 1H), 8.15 (d, *J* = 8.6 Hz, 1H), 7.67 (s, 1H), 7.30 (dd, *J* = 12.9, 8.1 Hz, 3H), 7.18 (d, *J* = 7.9 Hz, 1H), 7.11 (s, 1H), 7.07–7.01 (m, 3H), 6.96 (q, *J* = 7.5 Hz, 3H), 6.90 (s, 1H), 4.74 (dd, *J* = 12.7, 2.1 Hz, 1H), 4.66 (q, *J* = 7.7 Hz, 1H), 4.50 (t, *J* = 9.9 Hz, 1H), 4.17 (t, *J* = 8.2 Hz, 1H), 4.04 (t, *J* = 8.8 Hz, 1H), 3.97 (t, *J* = 6.6 Hz, 1H), 3.93–3.88 (m, 1H), 3.74–3.68 (m, 1H), 3.51 (s, 2H), 3.17 (s, 2H), 3.07 (dd, *J* = 23.6, 7.3 Hz, 1H), 3.06–3.02 (m, 1H), 3.04–2.98 (m, 1H), 2.71 (dt, *J* = 31.5, 7.3 Hz, 3H), 2.54 (t, *J* = 7.5 Hz, 1H), 1.94 (s, 3H), 1.89 (s, 1H), 1.55–1.49 (m, 1H), 1.41 (s, 2H), 1.45–1.36 (m, 1H), 1.35 (s, 8H), 1.30 (s, 2H), 1.27–1.22 (m, 18H), 1.19–1.12 (m, 2H), 1.07–0.99 (m, 3H), 0.96 (q, *J* = 4.2 Hz, 1H), 0.92 (d, *J* = 6.7 Hz, 2H), 0.89–0.82 (m, 13H), 0.81 (q, *J* = 6.8 Hz, 3H), 0.77 (dd, *J* = 11.9, 6.5 Hz, 4H), 0.70 (d, *J* = 6.9 Hz, 2H).

HRMS (ESI-qTOF, positive ion mode): *m/z* calcd. for $C_{40}H_{64}N_{10}O_6S$: 812.4731 [M]; calcd. for $[M+H]^+$: 813.4804, found: 813.4804; calcd. for $[M+Na]^+$: 835.4623, found: 835.4622.

6.6. Minimum inhibitory concentration (MIC) assays

Antimicrobial activity for MCA17-1 (**30**, dissolved in DMSO, 10 $mg \cdot mL^{-1}$) against ESKAPE pathogens, *B. subtilis*, *S. aureus* and *E. coli* was determined by JAN STRAETNER in accordance to the guidelines of the Clinical and Laboratory Standards Institute (CLSI) and as described in *ACS Chemical Biology* on a microtiter plate.[184] The MIC was determined as the lowest concentration of test compound that inhibited visible bacterial growth. The following compounds were used as controls: Doxycyclin, vancomycin and daptomycin (10 $mg \cdot mL^{-1}$ stocks in DMSO).

Table 5: MIC values for MCA17-1 (**30**) against ESKAPE pathogens.

Strain	MIC [$\mu g \cdot mL^{-1}$]
E. faecium BM4147-1	>64
S. aureus ATCC29213	>64
K. pneumoniae ATCC12657	>64
A. baumannii 09987	>64
P. aeruginosa ATCC27853	>64
E. aerogenes ATCC13048	>64
E. coli ATCC25922	>64
B. subtilis 168	>64

MIC assays against *S. aureus* USA300 LAC and *E. coli* DC10B were carried out by B. KRISMER as previously described in *Nature* on a microtiter plate.[32] The following compounds were used as controls: Daptomycin (10 mg·mL^{-1} in DMSO), vancomycin (10 mg·mL^{-1} in DMSO), Lugdunin (10 mg·mL^{-1} in DMSO) and DMSO (negative control).

Table 6: MIC values for lugdunin derivatives against *S. aureus* USA300 LAC.

Compound	MIC [µg·mL^{-1}]	Compound	MIC [µg·mL^{-1}]
109	>100	**123**	6.25
110	>100	**124**	>100
111	>100	**125**	>100
112	>100	**126**	>100
113	>100	**127**	100
115	>100	**128**	50
118	>100	**129**	50
119	>100	**130**	50
120	>100	**131**	50
121	>100	**137**	>100
122	>100	Crude mixture of **129**, **132**, **133** and **134**	12.5

Table 7: MIC values for lugdunin derivatives against *E. coli* DC10B.

Compound	MIC [µg·mL^{-1}]
127	50
128	>100
129	>100
130	>100
131	>100
137	50

MIC assays of lugdunin (**6**) against *E. coli* strains with polymyxin B nonapeptide (**117**, 10 mg·mL^{-1} stock in DMSO) as additive were carried out by A. BERSCHEID and JAN STRAETNER as previously described in *Antimicrobial Agents and Chemotherapy*.[185]

Table 8: MIC values for lugdunin (**6**) against selected *E. coli* strains with and without polymyxin B nonapeptide (PMBN, **117**).

Strain	Additive	MIC [µg·mL^{-1}]
E. coli ATCC25922	no additives	>50
	15 µg·mL^{-1} PMBN (**117**)	50
E. coli BW25113	no additives	>50
	15 µg·mL^{-1} PMBN (**117**)	25
E. coli BW25113 Δ*acrA*	no additives	>50
	15 µg·mL^{-1} PMBN (**117**)	12.5
E. coli BW25113 Δ*tolC*	no additives	>50
	15 µg·mL^{-1} PMBN (**117**)	6.25

6.7. Inhibitory concentration (IC) assay on human MRC5 cells

Cytotoxicity evaluation for epifadin (**24**) and MCA17-1 (**30**) was performed by JAN STRAETNER as previously described in *ACS Chemical Biology*.[184]

Table 9: IC_{50} values of epifadin (**24**) and MCA17-1 (**30**) on MRC5 cells.

Compound	IC_{50} [µg·mL^{-1}]
Epifadin (**24**)	>64
MCA17-1 (**30**)	>64

7 References

[1] C. L. Ventola, *P T* **2015**, *40*, 277-283.
[2] A. R. Coates, G. Halls, Y. Hu, *Br J Pharmacol* **2011**, *163*, 184-194.
[3] G. Kapoor, S. Saigal, A. Elongavan, *J Anaesthesiol Clin Pharmacol* **2017**, *33*, 300-305.
[4] R. R. Yocum, J. R. Rasmussen, J. L. Strominger, *J Biol Chem* **1980**, *255*, 3977-3986.
[5] K. Bush, P. A. Bradford, *Cold Spring Harb Perspect Med* **2016**, *6*.
[6] I. Chopra, M. Roberts, *Microbiol Mol Biol Rev* **2001**, *65*, 232-260.
[7] D. C. Hooper, G. A. Jacoby, *Cold Spring Harb Perspect Med* **2016**, *6*.
[8] A. Rusu, I. A. Lungu, O. L. Moldovan, C. Tanase, G. Hancu, *Pharmaceutics* **2021**, *13*.
[9] CDC, Atlanta, GA: U.S. Department of Health and Human Services, **2019**.
[10] F. C. Tenover, *Am J Med* **2006**, *119*, 3-10.
[11] P. A. Lambert, *J R Soc Med* **2002**, *95*, 22-26.
[12] H. Grundmann, M. Aires-de-Sousa, J. Boyce, E. Tiemersma, *Lancet* **2006**, *368*, 874-885.
[13] G. A. Jacoby, *Clin Infect Dis* **2005**, *41*, 120-126.
[14] C. L. Tooke, P. Hinchliffe, E. C. Bragginton, C. K. Colenso, V. H. A. Hirvonen, Y. Takebayashi, J. Spencer, *J Mol Biol* **2019**, *431*, 3472-3500.
[15] T. Naas, S. Oueslati, R. A. Bonnin, M. L. Dabos, A. Zavala, L. Dortet, P. Retailleau, B. I. Iorga, *J Enzyme Inhib Med Chem* **2017**, *32*, 917-919.
[16] J. O'Neill, *Rev Antimicrob Resist* **2014**.
[17] J. O'Neill, *Rev Antimicrob Resist* **2016**.
[18] H. Y. Mahmood, S. Jamshidi, J. M. Sutton, K. M. Rahman, *Curr Med Chem* **2016**, *23*, 1062-1081.
[19] C. J. L. Murray, K. S. Ikuta, F. Sharara, L. Swetschinski, G. Robles Aguilar, A. Gray, C. Han, C. Bisignano, P. Rao, E. Wool, S. C. Johnson, A. J. Browne, M. G. Chipeta, F. Fell, S. Hackett, G. Haines-Woodhouse, B. H. Kashef Hamadani, E. A. P. Kumaran, B. McManigal, S. Achalapong, R. Agarwal, S. Akech, S. Albertson, J. Amuasi, J. Andrews, A. Aravkin, E. Ashley, F.-X. Babin, F. Bailey, S. Baker, B. Basnyat, A. Bekker, R. Bender, J. A. Berkley, A. Bethou, J. Bielicki, S. Boonkasidecha, J. Bukosia, C. Carvalheiro, C. Castañeda-Orjuela, V. Chansamouth, S. Chaurasia, S. Chiurchiù, F. Chowdhury, R. Clotaire Donatien, A. J. Cook, B. Cooper, T. R. Cressey, E. Criollo-Mora, M. Cunningham, S. Darboe, N. P. J. Day, M. De Luca, K. Dokova, A. Dramowski, S. J. Dunachie, T. Duong Bich, T. Eckmanns, D. Eibach, A. Emami, N. Feasey, N. Fisher-Pearson, K. Forrest, C. Garcia, D. Garrett, P. Gastmeier, A. Z. Giref, R. C. Greer, V. Gupta, S. Haller, A. Haselbeck, S. I. Hay, M. Holm, S. Hopkins, Y. Hsia, K. C. Iregbu, J. Jacobs, D. Jarovsky, F. Javanmardi, A. W. J. Jenney, M. Khorana, S. Khusuwan, N. Kissoon, E. Kobeissi, T. Kostyanev, F. Krapp, R. Krumkamp, A. Kumar, H. H. Kyu, C. Lim, K. Lim, D. Limmathurotsakul, M. J. Loftus, M. Lunn, J. Ma, A. Manoharan, F. Marks, J. May, M. Mayxay, N. Mturi, T. Munera-Huertas, P. Musicha, L. A. Musila, M. M. Mussi-Pinhata, R. N. Naidu, T. Nakamura, R. Nanavati, S. Nangia, P. Newton, C. Ngoun, A. Novotney, D. Nwakanma, C. W. Obiero, T. J. Ochoa, A. Olivas-Martinez, P. Olliaro, E. Ooko, E. Ortiz-Brizuela, P. Ounchanum, G. D. Pak, J. L. Paredes, A. Y. Peleg, C. Perrone, T. Phe, K. Phommasone, N. Plakkal, A. Ponce-de-Leon, M. Raad, T. Ramdin, S. Rattanavong, A. Riddell, T. Roberts, J. V. Robotham, A. Roca, V. D.

Rosenthal, K. E. Rudd, N. Russell, H. S. Sader, W. Saengchan, J. Schnall, J. A. G. Scott, S. Seekaew, M. Sharland, M. Shivamallappa, J. Sifuentes-Osornio, A. J. Simpson, N. Steenkeste, A. J. Stewardson, T. Stoeva, N. Tasak, A. Thaiprakong, G. Thwaites, C. Tigoi, C. Turner, P. Turner, H. R. van Doorn, S. Velaphi, A. Vongpradith, M. Vongsouvath, H. Vu, T. Walsh, J. L. Walson, S. Waner, T. Wangrangsimakul, P. Wannapinij, T. Wozniak, T. E. M. W. Young Sharma, K. C. Yu, P. Zheng, B. Sartorius, A. D. Lopez, A. Stergachis, C. Moore, C. Dolecek, M. Naghavi, *The Lancet* **2022**, *399*, 629-655.

[20] H. B. Bode, B. Bethe, R. Höfs, A. Zeeck, *ChemBioChem* **2002**, *3*, 619-627.

[21] D. Jones, H. J. Metzger, A. Schatz, S. A. Waksman, *Science* **1944**, *100*, 103-105.

[22] R. E. de Lima Procópio, I. R. da Silva, M. K. Martins, J. L. de Azevedo, J. M. de Araújo, *Braz J Infect Dis* **2012**, *16*, 466-471.

[23] E. Fjærvik, S. B. Zotchev, *Appl Microbiol Biotechnol* **2005**, *67*, 436-443.

[24] P. Caffrey, S. Lynch, E. Flood, S. Finnan, M. Oliynyk, *Chem Biol* **2001**, *8*, 713-723.

[25] J. F. Aparicio, E. G. Barreales, T. D. Payero, C. M. Vicente, A. de Pedro, J. Santos-Aberturas, *Appl Microbiol Biotechnol* **2016**, *100*, 61-78.

[26] T. Kino, H. Hatanaka, M. Hashimoto, M. Nishiyama, T. Goto, M. Okuhara, M. Kohsaka, H. Aoki, H. Imanaka, *J Antibiot (Tokyo)* **1987**, *40*, 1249-1255.

[27] S. N. Sehgal, H. Baker, C. Vézina, *J Antibiot* **1975**, *28*, 727-732.

[28] K. Iskandar, J. Murugaiyan, D. Hammoudi Halat, S. E. Hage, V. Chibabhai, S. Adukkadukkam, C. Roques, L. Molinier, P. Salameh, M. Van Dongen, *Antibiotics* **2022**, *11*, 182.

[29] L. L. Silver, *Clin Microbiol Rev* **2011**, *24*, 71-109.

[30] L. Chen, S. Kumar, H. Wu, *Arch Microbiol* **2023**, *205*, 356.

[31] N. Shahsavari, B. Wang, Y. Imai, M. Mori, S. Son, L. Liang, N. Böhringer, S. Manuse, M. F. Gates, M. Morrissette, R. Corsetti, J. L. Espinoza, C. L. Dupont, M. T. Laub, K. Lewis, *mBio* **2022**, *13*, e00700-00722.

[32] A. Zipperer, M. C. Konnerth, C. Laux, A. Berscheid, D. Janek, C. Weidenmaier, M. Burian, N. A. Schilling, C. Slavetinsky, M. Marschal, M. Willmann, H. Kalbacher, B. Schittek, H. Brötz-Oesterhelt, S. Grond, A. Peschel, B. Krismer, *Nature* **2016**, *535*, 511-516.

[33] S. Heilbronner, B. Krismer, H. Brötz-Oesterhelt, A. Peschel, *Nat Rev Microbiol* **2021**, *19*, 726-739.

[34] E. Garcia-Gutierrez, M. J. Mayer, P. D. Cotter, A. Narbad, *Gut Microbes* **2019**, *10*, 1-21.

[35] B. O. Torres Salazar, S. Heilbronner, A. Peschel, B. Krismer, *Microb Physiol* **2021**, *31*, 198-216.

[36] R. Sender, S. Fuchs, R. Milo, *PLoS Biol* **2016**, *14*, e1002533.

[37] K. Hou, Z.-X. Wu, X.-Y. Chen, J.-Q. Wang, D. Zhang, C. Xiao, D. Zhu, J. B. Koya, L. Wei, J. Li, Z.-S. Chen, *Signal Transduct Target Ther* **2022**, *7*, 135.

[38] A. B. Shreiner, J. Y. Kao, V. B. Young, *Curr Opin Gastroenterol* **2015**, *31*, 69-75.

[39] E. A. Grice, J. A. Segre, *Annu Rev Genom Hum Genet* **2012**, *13*, 151-170.

[40] N. A. Schilling, A. Berscheid, J. Schumacher, J. S. Saur, M. C. Konnerth, S. N. Wirtz, J. M. Beltrán-Beleña, A. Zipperer, B. Krismer, A. Peschel, H. Kalbacher, H. Brötz-Oesterhelt, C. Steinem, S. Grond, *Angew Chem Int Ed* **2019**, *58*, 9234-9238.

[41] S. A. Samel, B. Wagner, M. A. Marahiel, L.-O. Essen, *J Mol Biol* **2006**, *359*, 876-889.
[42] P. Piewngam, Y. Zheng, T. H. Nguyen, S. W. Dickey, H.-S. Joo, A. E. Villaruz, K. A. Glose, E. L. Fisher, R. L. Hunt, B. Li, J. Chiou, S. Pharkjaksu, S. Khongthong, G. Y. C. Cheung, P. Kiratisin, M. Otto, *Nature* **2018**, *562*, 532-537.
[43] X. Tang, Y. Kudo, J. L. Baker, S. LaBonte, P. A. Jordan, S. M. K. McKinnie, J. Guo, T. Huan, B. S. Moore, A. Edlund, *ACS Infect Dis* **2020**, *6*, 563-571.
[44] M. G. Gänzle, R. F. Vogel, *Appl Environ Microbiol* **2003**, *69*, 1305-1307.
[45] H. Do, Z.-R. Li, P. K. Tripathi, S. Mitra, S. Guerra, A. Dash, D. Weerasekera, N. Makthal, S. Shams, S. Aggarwal, B. B. Singh, D. Gu, Y. Du, R. J. Olsen, C. LaRock, W. Zhang, M. Kumaraswami, *Nat Microbiol* **2024**, *9*, 502-513.
[46] J. S. Saur, S. N. Wirtz, N. A. Schilling, B. Krismer, A. Peschel, S. Grond, *J Med Chem* **2021**, *64*, 4034-4058.
[47] H. C. Gram, *Fortschr Med* **1884**, *2*, 185-189.
[48] T. J. Silhavy, D. Kahne, S. Walker, *Cold Spring Harb Perspect Biol* **2010**, 2:a000414.
[49] Z. Si, K. Pethe, M. B. Chan-Park, *JACS Au* **2023**, *3*, 276-292.
[50] M. M. Dwarikadhish Kaushik, Dhammraj M Borade, Onkar C Swami, *J Clin Diagn Res* **2014**, *8*, ME01-ME03.
[51] P. A. Smith, M. F. T. Koehler, H. S. Girgis, D. Yan, Y. Chen, Y. Chen, J. J. Crawford, M. R. Durk, R. I. Higuchi, J. Kang, J. Murray, P. Paraselli, S. Park, W. Phung, J. G. Quinn, T. C. Roberts, L. Rougé, J. B. Schwarz, E. Skippington, J. Wai, M. Xu, Z. Yu, H. Zhang, M.-W. Tan, C. E. Heise, *Nature* **2018**, *561*, 189-194.
[52] M. F. Richter, P. J. Hergenrother, *Ann NY Acad Sci* **2019**, *1435*, 18-38.
[53] M. F. Richter, B. S. Drown, A. P. Riley, A. Garcia, T. Shirai, R. L. Svec, P. J. Hergenrother, *Nature* **2017**, *545*, 299-304.
[54] E. N. Parker, B. S. Drown, E. J. Geddes, H. Y. Lee, N. Ismail, G. W. Lau, P. J. Hergenrother, *Nat Microbiol* **2020**, *5*, 67-75.
[55] S. E. Motika, R. J. Ulrich, E. J. Geddes, H. Y. Lee, G. W. Lau, P. J. Hergenrother, *J Am Chem Soc* **2020**, *142*, 10856-10862.
[56] H. Wang, P. A. Mann, L. Xiao, C. Gill, A. M. Galgoci, J. A. Howe, A. Villafania, C. M. Barbieri, J. C. Malinverni, X. Sher, T. Mayhood, M. D. McCurry, N. Murgolo, A. Flattery, M. Mack, T. Roemer, *Cell Chem Biol* **2017**, *24*, 576-588.e576.
[57] K. A. Muñoz, P. J. Hergenrother, *Acc Chem Res* **2021**, *54*, 1322-1333.
[58] S. J. Perlmutter, E. J. Geddes, B. S. Drown, S. E. Motika, M. R. Lee, P. J. Hergenrother, *ACS Infect Dis* **2021**, *7*, 162-173.
[59] *Nat Chem Biol* **2007**, *3*, 351-351.
[60] M. R. Seyedsayamdost, *J Ind Microbiol Biotechnol* **2019**, *46*, 301-311.
[61] M. A. Fischbach, C. T. Walsh, *Chem Rev* **2006**, *106*, 3468-3496.
[62] L. Du, L. Lou, *Nat Prod Rep* **2010**, *27*, 255-278.
[63] B. S. Evans, S. J. Robinson, N. L. Kelleher, *Fungal Genet Biol* **2011**, *48*, 49-61.
[64] K. M. Fisch, *RSC Advances* **2013**, *3*, 18228-18247.
[65] E. J. N. Helfrich, J. Piel, *Nat Prod Rep* **2016**, *33*, 231-316.
[66] E. J. N. Helfrich, R. Ueoka, A. Dolev, M. Rust, R. A. Meoded, A. Bhushan, G. Califano, R. Costa, M. Gugger, C. Steinbeck, P. Moreno, J. Piel, *Nat Chem Biol* **2019**, *15*, 813-821.

[67] K. Blin, S. Shaw, H. E. Augustijn, Z. L. Reitz, F. Biermann, M. Alanjary, A. Fetter, B. R. Terlouw, W. W. Metcalf, E. J. N. Helfrich, G. P. van Wezel, M. H. Medema, T. Weber, *Nucleic Acids Res* **2023**, *51*, W46-W50.
[68] K. Blin, S. Shaw, A. M. Kloosterman, Z. Charlop-Powers, G. P. van Wezel, Marnix H. Medema, T. Weber, *Nucleic Acids Res* **2021**, *49*, W29-W35.
[69] K. Blin, S. Shaw, K. Steinke, R. Villebro, N. Ziemert, S. Y. Lee, M. H. Medema, T. Weber, *Nucleic Acids Res* **2019**, *47*, W81-W87.
[70] V. Miao, M.-F. Coëffet-LeGal, P. Brian, R. Brost, J. Penn, A. Whiting, S. Martin, R. Ford, I. Parr, M. Bouchard, C. J. Silva, S. K. Wrigley, R. H. Baltz, *Microbiology* **2005**, *151*, 1507-1523.
[71] S. R. Park, Y. J. Yoo, Y.-H. Ban, Y. J. Yoon, *J Antibiot* **2010**, *63*, 434-441.
[72] K. M. Hoyer, C. Mahlert, M. A. Marahiel, *Chem Biol* **2007**, *14*, 13-22.
[73] P. S. Patel, S. Huang, S. Fisher, D. Pirnik, C. Aklonis, L. Dean, E. Meyers, P. Fernandes, F. Mayerl, *J Antibiot (Tokyo)* **1995**, *48*, 997-1003.
[74] J. Moldenhauer, X.-H. Chen, R. Borriss, J. Piel, *Angew Chem Int Ed* **2007**, *46*, 8195-8197.
[75] M. Kawada, Y. Yoshimoto, H. Kumagai, T. Someno, I. Momose, N. Kawamura, K. Isshiki, D. Ikeda, *J Antibiot (Tokyo)* **2004**, *57*, 235-237.
[76] F. Vinale, M. Nigro, K. Sivasithamparam, G. Flematti, E. L. Ghisalberti, M. Ruocco, R. Varlese, R. Marra, S. Lanzuise, A. Eid, S. L. Woo, M. Lorito, *FEMS Microbiol Lett* **2013**, *347*, 123-129.
[77] S. Gatenbeck, J. Sierankiewicz, *Antimicrob Agents Chemother* **1973**, *3*, 308-309.
[78] B. J. C. Law, Y. Zhuo, M. Winn, D. Francis, Y. Zhang, M. Samborskyy, A. Murphy, L. Ren, P. F. Leadlay, J. Micklefield, *Nat Catal* **2018**, *1*, 977-984.
[79] B. Kunze, K. Schabacher, H. Zähner, A. Zeeck, *Arch Mikrobiol* **1972**, *86*, 147-174.
[80] J.-T. Cheng, H.-M. Wang, J.-H. Yu, C.-F. Sun, F. Cao, X.-H. Jiang, X.-A. Chen, Q.-W. Zhao, L.-S. Gan, R.-R. Xie, S.-L. Wang, J. Li, Y. Zang, X.-M. Mao, *J Agric Food Chem* **2021**, *69*, 11303-11310.
[81] R. F. Vesonder, L. W. Tjarks, W. K. Rohwedder, H. R. Burmeister, J. A. Laugal, *J Antibiot (Tokyo)* **1979**, *32*, 759-761.
[82] V. Hellwig, T. Grothe, A. Mayer-Bartschmid, R. Endermann, F. U. Geschke, T. Henkel, M. Stadler, *J Antibiot (Tokyo)* **2002**, *55*, 881-892.
[83] J. A. V. Blodgett, D.-C. Oh, S. Cao, C. R. Currie, R. Kolter, J. Clardy, *Proc Natl Acad Sci U S A* **2010**, *107*, 11692-11697.
[84] Y. Asami, H. Kakeya, R. Onose, A. Yoshida, H. Matsuzaki, H. Osada, *Org Lett* **2002**, *4*, 2845-2848.
[85] J. G. Batelaan, J. W. F. K. Barnick, J. L. van der Baan, F. Bickelhaupt, *Tetrahedron Lett* **1972**, *13*, 3103-3106.
[86] J. L. Van Der Baan, J. W. F. K. Barnick, F. Bickelhaupt, *Tetrahedron* **1978**, *34*, 223-231.
[87] F. Yu, K. Zaleta-Rivera, X. Zhu, J. Huffman, J. C. Millet, S. D. Harris, G. Yuen, X.-C. Li, L. Du, *Antimicrob Agents Chemother* **2007**, *51*, 64-72.
[88] N. A. Schilling, PhD thesis, Eberhard Karls Universität Tübingen (DE) **2018**.
[89] R. P. Daniele, S. K. Holian, *Proc Natl Acad Sci U S A* **1976**, *73*, 3599-3602.
[90] A. G. dos Santos, J. T. Marquês, A. C. Carreira, I. R. Castro, A. S. Viana, M. P. Mingeot-Leclercq, R. F. M. de Almeida, L. C. Silva, *Phys Chem Chem Phys* **2017**, *19*, 30078-30088.

[91] B. Krismer, M. Liebeke, D. Janek, M. Nega, M. Rautenberg, G. Hornig, C. Unger, C. Weidenmaier, M. Lalk, A. Peschel, *PLoS Pathog* **2014**, *10*, e1003862.
[92] D. Janek, A. Zipperer, A. Kulik, B. Krismer, A. Peschel, *PLoS Pathog* **2016**, *12*, e1005812.
[93] B. O. T. Salazar, PhD thesis, Eberhard Karls Universität Tübingen (DE) **2021**.
[94] B. O. Torres Salazar, T. Dema, N. A. Schilling, D. Janek, J. Bornikoel, A. Berscheid, A. M. A. Elsherbini, S. Krauss, S. J. Jaag, M. Lämmerhofer, M. Li, N. Alqahtani, M. J. Horsburgh, T. Weber, J. M. Beltrán-Beleña, H. Brötz-Oesterhelt, S. Grond, B. Krismer, A. Peschel, *Nat Microbiol* **2024**, *9*, 200-213.
[95] M. d. l. A. Garavagno, R. Holland, M. A. H. Khan, A. J. Orr-Ewing, D. E. Shallcross, *Sustainability* **2024**, *16*, 2382.
[96] I. Fleming, D. Williams, in *Spectroscopic Methods in Organic Chemistry*, Springer International Publishing, Cham, **2019**, pp. 55-83.
[97] C. Hazra, T. Samanta, V. Mahalingam, *J Mater Chem C* **2014**, *2*, 10157-10163.
[98] E. J. Han, M. R. Seyedsayamdost, *Curr Opin Chem Biol* **2024**, *81*, 102481.
[99] K. M. Guzman, K. P. Yuet, S. R. Lynch, C. W. Liu, C. Khosla, *J Org Chem* **2021**, *86*, 11100-11106.
[100] T. Weber, K. J. Laiple, E. K. Pross, A. Textor, S. Grond, K. Welzel, S. Pelzer, A. Vente, W. Wohlleben, *Chem Biol* **2008**, *15*, 175-188.
[101] R. A. Butcher, F. C. Schroeder, M. A. Fischbach, P. D. Straight, R. Kolter, C. T. Walsh, J. Clardy, *Proc Natl Acad Sci U S A* **2007**, *104*, 1506.
[102] A. S. Edison, F. C. Schroeder, in *Comprehensive Natural Products II* (Eds.: H.-W. Liu, L. Mander), Elsevier, Oxford, **2010**, pp. 169-196.
[103] C. Drescher, M. Keller, O. Potterat, M. Hamburger, R. Brückner, *Org Lett* **2020**, *22*, 2559-2563.
[104] V. M. Csizmadia, K. M. Koshy, K. C. M. Lau, R. A. McClelland, V. J. Nowlan, T. T. Tidwell, *J Am Chem Soc* **1979**, *101*, 974-979.
[105] Margarita Petroliagi, Olga Igglessi-Maikopoulou, John Markopoulos, *Heterocycl Commun* **2000**, *6*, 157-164.
[106] E. Nicolás, E. Pedroso, E. Girald, *Tetrahedron Lett* **1989**, *30*, 497-500.
[107] R. Dölling, M. Beyermann, J. Haenel, F. Kernchen, E. Krause, P. Franke, M. Brudel, M. Bienert, *J Chem Soc, Chem Commun* **1994**, 853-854.
[108] Y. Yang, W. V. Sweeney, K. Schneider, S. Thörnqvist, B. T. Chait, J. P. Tam, *Tetrahedron Lett* **1994**, *35*, 9689-9692.
[109] J. L. Lauer, C. G. Fields, G. B. Fields, *Lett Pept Sci* **1995**, *1*, 197-205.
[110] I. Schön, T. Szirtes, A. Rill, G. Balogh, Z. Vadász, J. Seprődi, I. Teplán, N. Chino, K. Y. Kumogaye, S. Sakakibara, *J Chem Soc, Perkin Trans 1* **1991**, 3213-3223.
[111] R. Behrendt, S. Huber, P. White, *J Pept Sci* **2016**, *22*, 92-97.
[112] K. Neumann, J. Farnung, S. Baldauf, J. W. Bode, *Nat Commun* **2020**, *11*, 982.
[113] H. Gerhardt, A. Sievers-Engler, G. Jahanshah, Z. Pataj, F. Ianni, H. Gross, W. Lindner, M. Lämmerhofer, *J Chromatogr A* **2016**, *1428*, 280-291.
[114] T. Zhang, E. Holder, P. Franco, M. Lämmerhofer, A. Sievers-Engler, H. Gerhardt, H. Gross, W. Lindner, *LCGC Europe* **2016**, *29*, 112-128.
[115] M. L. Hofferberth, R. Brückner, *Angew Chem Int Ed* **2014**, *53*, 7328-7334.
[116] C. Drescher, R. Brückner, *Org Lett* **2021**, *23*, 6194-6199.
[117] C. Drescher, R. Brückner, *Eur J Org Chem* **2022**, *2022*, e202101053.
[118] A. Sorg, K. Siegel, R. Brückner, *Chem Eur J* **2005**, *11*, 1610-1624.
[119] W. A. Henderson, Jr., C. J. Schultz, *J Org Chem* **1962**, *27*, 4643-4646.

[120] T. Yoshinari, K. Ohmori, M. G. Schrems, A. Pfaltz, K. Suzuki, *Angew Chem Int Ed* **2010**, *49*, 881-885.
[121] T. Okazoe, K. Takai, K. Utimoto, *J Am Chem Soc* **1987**, *109*, 951-953.
[122] D. M. Hodgson, L. T. Boulton, G. N. Maw, *Tetrahedron* **1995**, *51*, 3713-3724.
[123] S. Prasad, K. K. Yadav, S. Kumar, N. Gupta, M. M. S. Cabral-Pinto, S. Rezania, N. Radwan, J. Alam, *J Environ Manage* **2021**, *285*, 112174.
[124] L. D. Bergelson, M. M. Shemyakin, *Angew Chem Int Ed Engl* **1964**, *3*, 250-260.
[125] M. Schlosser, K. F. Christmann, *Angew Chem, Int Ed Engl* **1966**, *5*, 126.
[126] G. R. W. Pitt, PhD thesis, University of Southampton (GB) **2008**.
[127] A. Illigmann, Y. Thoma, S. Pan, L. Reinhardt, H. Brötz-Oesterhelt, *Microb Physiol* **2021**, *31*, 260-279.
[128] T. Böttcher, S. A. Sieber, *Angew Chem Int Ed* **2008**, *47*, 4600-4603.
[129] D. Frees, S. N. A. Qazi, P. J. Hill, H. Ingmer, *Mol Microbiol* **2003**, *48*, 1565-1578.
[130] J. Schelin, M. T. Cohn, B. Frisk, D. Frees, *Toxins (Basel)* **2020**, *12*, 553.
[131] M. Lakemeyer, W. Zhao, F. A. Mandl, P. Hammann, S. A. Sieber, *Angew Chem Int Ed* **2018**, *57*, 14440-14475.
[132] J. H. Seo, D. B. Rivadeneira, M. C. Caino, Y. C. Chae, D. W. Speicher, H.-Y. Tang, V. Vaira, S. Bosari, A. Palleschi, P. Rampini, A. V. Kossenkov, L. R. Languino, D. C. Altieri, *PLoS Biol* **2016**, *14*, e1002507.
[133] A. Cole, Z. Wang, E. Coyaud, V. Voisin, M. Gronda, Y. Jitkova, R. Mattson, R. Hurren, S. Babovic, N. Maclean, I. Restall, X. Wang, Danny V. Jeyaraju, Mahadeo A. Sukhai, S. Prabha, S. Bashir, A. Ramakrishnan, E. Leung, Yi H. Qia, N. Zhang, Kevin R. Combes, T. Ketela, F. Lin, Walid A. Houry, A. Aman, R. Al-awar, W. Zheng, E. Wienholds, Chang J. Xu, J. Dick, Jean C. Y. Wang, J. Moffat, Mark D. Minden, Connie J. Eaves, Gary D. Bader, Z. Hao, Steven M. Kornblau, B. Raught, Aaron D. Schimmer, *Cancer Cell* **2015**, *27*, 864-876.
[134] H. Brötz-Oesterhelt, D. Beyer, H.-P. Kroll, R. Endermann, C. Ladel, W. Schroeder, B. Hinzen, S. Raddatz, H. Paulsen, K. Henninger, J. E. Bandow, H.-G. Sahl, H. Labischinski, *Nat Med* **2005**, *11*, 1082-1087.
[135] M. W. Hackl, M. Lakemeyer, M. Dahmen, M. Glaser, A. Pahl, K. Lorenz-Baath, T. Menzel, S. Sievers, T. Böttcher, I. Antes, H. Waldmann, S. A. Sieber, *J Am Chem Soc* **2015**, *137*, 8475-8483.
[136] N. P. Lavey, J. A. Coker, E. A. Ruben, A. S. Duerfeldt, *J Nat Prod* **2016**, *79*, 1193-1197.
[137] B. P. Conlon, E. S. Nakayasu, L. E. Fleck, M. D. LaFleur, V. M. Isabella, K. Coleman, S. N. Leonard, R. D. Smith, J. N. Adkins, K. Lewis, *Nature* **2013**, *503*, 365-370.
[138] K. A. Gill, F. Berrué, J. C. Arens, G. Carr, R. G. Kerr, *J Nat Prod* **2015**, *78*, 822-826.
[139] A. Illigmann, M.-T. Vielberg, M. Lakemeyer, F. Wolf, T. Dema, P. Stange, W. Kuttenlochner, E. Liebhart, A. Kulik, N. D. Staudt, I. Malik, S. Grond, S. A. Sieber, L. Kaysser, M. Groll, H. Brötz-Oesterhelt, *Angew Chem Int Ed* **2024**, *63*, e202314028.
[140] H. Brötz-Oesterhelt, A. Vorbach, *Front Mol Biosci* **2021**, *8*, 690902.
[141] V. Bhandari, K. S. Wong, J. L. Zhou, M. F. Mabanglo, R. A. Batey, W. A. Houry, *ACS Chem Biol* **2018**, *13*, 1413-1425.
[142] R. M. Freidinger, J. S. Hinkle, D. S. Perlow, *J Org Chem* **1983**, *48*, 77-81.
[143] T. Fukuyama, C.-K. Jow, M. Cheung, *Tetrahedron Lett* **1995**, *36*, 6373-6374.

[144] S. T. Cheung, N. L. Benoiton, *Can J Chem* **1977**, *55*, 906-910.
[145] E. Biron, H. Kessler, *J Org Chem* **2005**, *70*, 5183-5189.
[146] S. C. Miller, T. S. Scanlan, *J Am Chem Soc* **1997**, *119*, 2301-2302.
[147] E. Biron, J. Chatterjee, H. Kessler, *J Pept Sci* **2006**, *12*, 213-219.
[148] J. Chatterjee, B. Laufer, H. Kessler, *Nat Protoc* **2012**, *7*, 432-444.
[149] X. Li, N. Wang, Y. Liu, W. Li, X. Bai, P. Liu, C.-Y. He, *Bioorg Chem* **2023**, *141*, 106892.
[150] E. Biron, J. Chatterjee, O. Ovadia, D. Langenegger, J. Brueggen, D. Hoyer, H. A. Schmid, R. Jelinek, C. Gilon, A. Hoffman, H. Kessler, *Angew Chem Int Ed* **2008**, *47*, 2595-2599.
[151] D. Ruppelt, M. F. W. Trollmann, T. Dema, S. N. Wirtz, H. Flegel, S. Mönnikes, S. Grond, R. A. Böckmann, C. Steinem, *Nat Commun* **2024**, *15*, 3521.
[152] A. S. Ladokhin, in *Encyclopedia of Analytical Chemistry*.
[153] G. Beschiaschvili, J. Seelig, *Biochim Biophys Acta* **1991**, *1061*, 78-84.
[154] C. Mollay, G. Krell, *Biochim Biophys Acta* **1973**, *316*, 196-203.
[155] H. Zhao, P. K. J. Kinnunen, *J Biol Chem* **2002**, *277*, 25170-25177.
[156] N. G. Park, U. Silphaduang, H. S. Moon, J. K. Seo, J. Corrales, E. J. Noga, *Biochemistry* **2011**, *50*, 3288-3299.
[157] R. F. Epand, P. B. Savage, R. M. Epand, *Biochim Biophys Acta* **2007**, *1768*, 2500-2509.
[158] G. van Meer, D. R. Voelker, G. W. Feigenson, *Nat Rev Mol Cell Biol* **2008**, *9*, 112-124.
[159] S. A. Tatulian, *Biochemistry* **2003**, *42*, 11898-11907.
[160] B. Claro, E. González-Freire, M. Calvelo, L. J. Bessa, E. Goormaghtigh, M. Amorín, J. R. Granja, R. Garcia-Fandiño, M. Bastos, *Colloids Surf B Biointerfaces* **2020**, *196*, 111349.
[161] A. Barth, C. Zscherp, *Q Rev Biophys* **2002**, *35*, 369-430.
[162] J. Montenegro, M. R. Ghadiri, J. R. Granja, *Acc Chem Res* **2013**, *46*, 2955-2965.
[163] Y. Zhao, L. J. Leman, D. J. Search, R. A. Garcia, D. A. Gordon, B. E. Maryanoff, M. R. Ghadiri, *ACS Cent Sci* **2017**, *3*, 639-646.
[164] B. Claro, A. Peón, E. González-Freire, E. Goormaghtigh, M. Amorín, J. R. Granja, R. Garcia-Fandiño, M. Bastos, *Colloids Surf B Biointerfaces* **2021**, *208*, 112086.
[165] D. A. Kelkar, A. Chattopadhyay, *Biochim Biophys Acta* **2007**, *1768*, 2011-2025.
[166] P. Viljanen, M. Vaara, *Antimicrob Agents Chemother* **1984**, *25*, 701-705.
[167] N. Thieriet, J. Alsina, E. Giralt, F. Guibé, F. Albericio, *Tetrahedron Lett* **1997**, *38*, 7275-7278.
[168] K. Augustyns, W. Kraas, G. Jung, *J Pept Res* **1998**, *51*, 127-133.
[169] T. W. Greene, P. G. M. Wuts, in *Protective Groups in Organic Synthesis*, **1999**, pp. 494-653.
[170] T. W. Greene, P. G. M. Wuts, in *Protective Groups in Organic Synthesis*, **1999**, pp. 701-748.
[171] P. Lott, M. Eck, D. E. Doronkin, A. Zimina, S. Tischer, R. Popescu, S. Belin, V. Briois, M. Casapu, J.-D. Grunwaldt, O. Deutschmann, *Appl Catal B: Environ* **2020**, *278*, 119244.
[172] L. J. Hoyos, M. Primet, H. Praliaud, *J Chem Soc, Faraday Trans* **1992**, *88*, 113-119.
[173] Y. Kiso, K. Ukawa, S. Nakamura, K. Ito, T. Akita, *Chem Pharm Bull (Tokyo)* **1980**, *28*, 673-676.

[174] I. Mutanda, J. Sun, J. Jiang, D. Zhu, *Biotechnol Adv* **2022**, *59*, 107952.
[175] Y. Luo, Y. Song, *Int J Mol Sci* **2021**, *22*, 11401.
[176] E. Kamble, P. Sanghvi, K. Pardesi, *Biofilm* **2022**, *4*, 100068.
[177] Y. Zhou, Y. Peng, *Exp Ther Med* **2013**, *6*, 1000-1004.
[178] M. de Boer, C. Heuer, H. Hussein, S. McDougall, *J Dairy Sci* **2015**, *98*, 4427-4438.
[179] T. Sato, R. Ito, M. Kawamura, S. Fujimura, *Infect Drug Resist* **2023**, *16*, 6357-6366.
[180] J. M. A. Blair, G. E. Richmond, L. J. V. Piddock, *Future Microbiol* **2014**, *9*, 1165-1177.
[181] K. M. Zack, T. Sorenson, S. G. Joshi, *Pathogens* **2024**, *13*, 197.
[182] A. Sharma, V. K. Gupta, R. Pathania, *Indian J Med Res* **2019**, *149*, 129-145.
[183] G. R. Fulmer, A. J. M. Miller, N. H. Sherden, H. E. Gottlieb, A. Nudelman, B. M. Stoltz, J. E. Bercaw, K. I. Goldberg, *Organometallics* **2010**, *29*, 2176-2179.
[184] G. Castro-Falcón, J. Straetener, J. Bornikoel, D. Reimer, T. N. Purdy, A. Berscheid, F. M. Schempp, D. Y. Liu, R. G. Linington, H. Brötz-Oesterhelt, C. C. Hughes, *ACS Chem Biol* **2024**, *19*, 743-752.
[185] D. Hörömpöli, C. Ciglia, K.-H. Glüsenkamp, L. O. Haustedt, H. Falkenstein-Paul, G. Bendas, A. Berscheid, H. Brötz-Oesterhelt, *Antimicrob Agents Chemother* **2021**, *65*, 10.1128/aac.00986-00920.

C. INDEX OF ABREVIATIONS

2-TMS-EtOH	2-(Trimethylsilyl)ethanol
AA	Amino acid
Ac_2O	Acetic anhydride
AcOH	Acetic acid
ACP	Acyl carrier protein
ADEP	Acyldepsipeptide
A-domain	Adenylation domain
Alloc	Allyloxycarbonyl
Asn	Asparagine
Asp	Aspartic acid
AT	Acyltransferase
ATP	Adenosine triphosphate
ATR-IR	Attenuated total reflection infrared spectroscopy
BGC	Biosynthetic gene cluster
Boc	*tert*-Butyloxycarbonyl
BPC	Base peak chromatogram
CAP	Covalently attached protein
Cbz	Benzyloxycarbonyl
C-domain	Condensation-domain
CL	Cardiolipin
ClpP	Caseinolytic protease P
CoA	Coenzyme A
COSY	Correlation spectroscopy
Da	Dalton
DAD	Diode array detector
dba	Dibenzylideneacetone
DBU	2,3,4,6,7,8,9,10-Octahydropyrimido[1,2-*a*]azepine
DCC	*N*,*N*′-Dicyclohexylcarbodiimide
DCM	Dichloromethane

Dde	1-(4,4-dimethyl-2,6-dioxocyclohex-1-ylidene)ethyl
DH	Dehydratase
DIPEA	*N*,*N*-Diisopropylethylamine
DMAP	4-Dimethylaminopyridine
DMB	2,4-Dimethoxybenzyl
DMF	*N*,*N*-Dimethylformamid
DMPC	1,2-dimyristol-*sn*-glycero-3-phosphocholine
DMSO	Dimethyl sulfoxide
DNA	Deoxyribonucleic acid
DOPC	1,2-dioleoyl-*sn*-glycero-3-phosphocholine
E-domain	Epimerization-domain
EIC	Extracted ion chromatogram
eq	Equivalents
ER	Enoylreductase
ESI	Electrospray ionization
EtOAc	Ethyl acetate
FA	Formic acid
Fmoc	Fluorenylmethyloxycarbonyl
Gal	D-Galactose
GISA	Glycopeptide resistant *S. aureus*
Glc	D-Glucose
HATU	1-[Bis(dimethylamino)methylene]-1*H*-1,2,3-triazolo[4,5-*b*]pyridinium 3-oxide hexafluorophosphate
Hep	L-*Glycero*-D-*manno*-heptose
HMBC	Heteronuclear multiple-bond correlation spectroscopy
HOAt	3*H*-[1,2,3]Triazolo[4,5-*b*]pyridin-3-ol
HOBt	1*H*-1,2,3-Benzotriazol-1-ol
HPLC	High-performance liquid chromatography
HRMS	High resolution mass spectrometry
HSQC	Heteronuclear single quantum correlation
IC_{50}	Half maximal inhibitory concentration

IMP	Integral membrane protein
IPA	Isopropyl alcohol
Kdo	3-deoxy-D-*manno*-oct-2-ulosonic acid
KR	Ketoreductase
KS	Ketosynthase
LC	Liquid chromatography
Leu	Leucine
LP	Lipoprotein
LPS	Lipopolysaccharide
LTA	Lipoteichoic acid
MeOH	Methanol
MIC	Minimum inhibitory concentration
MPLC	Medium-pressure liquid chromatography
MRSA	Methicillin-resistant S. aureus
MS	Mass spectrometry
mTBD	1-Methyl-2,3,4,6,7,8-hexahydro-1*H*-pyrimido[1,2-*a*]pyrimidine
NMM	4-Methylmorpholine
NMP	1-Methylpyrrolidin-2-one
NMR	Nuclear magnetic resonance
NOE	Nuclear Overhauser effect
NOESY	Nuclear Overhauser effect spectroscopy
NRPS	Non-ribosomal peptide synthase
OM	Outer membrane
OMP	Outer membrane protein
oNBS	2-Nitrobenzenesulfonyl
OSMAC	One Strain-Many Compounds
PCP-domain	Peptidyl-carrier-protein domain/thiolation domain
Phe	Phenylalanine
PKS	Polyketide synthase
PMBN	Polymyxin B nonapeptide
POPC	1-palmitoyl-2-oleoyl-*sn*-glycero-3-phosphocholine

POPG	1-Palmitoyl-2-oleoyl-*sn*-glycero-3-phospho(1'-*rac*-glycerol)
qTOF	Quadrupol-Time-of-Flight
RAM	Rink Amide
RNA	Ribonucleic acid
ROESY	Rotating Frame Overhauser Enhancement Spectroscopy
RP	Reversed phase
Rt	Retention time
rt	Room temperature
SPPS	Solid-phase peptide synthesis
TBAF	Tetra-*n*-butylammonium fluoride
*t*Bu	*tert*-Butyl
TE	Thioesterase
TFA	Trifluoroacetic acid
TG S RAM	TentaGel S Rink Amide
THF	Tetrahydrofuran
Thz	Thiazolidine
TIPS	Triisopropylsilane
TMSE	2-Trimethylsilylethyl
tRNA	Transfer RNA
Trp	Tryptophan
Trt	Trityl
UV	Ultraviolet
Val	Valine
VRE	Vancomycin-resistant *Enterococcus*
WT	Wild type
WTA	Wall teichoic acid
xs	excess